Investigating the metabolomics of treatment response in patients with inflammatory rheumatic diseases

Cameron George Best, MSci.

Thesis submitted in fulfilment of the requirements for the degree of

Doctor of Philosophy

College of Medical, Veterinary and Life Sciences

School of Infection and Immunity

University of Glasgow

May 2023

Abstract

Background

Rheumatic and musculoskeletal diseases (RMDs) are autoimmune-mediated chronic diseases affecting the joints around the body, involving an inappropriate immune response being launched against the tissues of the joint. These devastating diseases include rheumatoid arthritis (RA) and psoriatic arthritis (PsA). If insufficiently managed – or indeed in severe cases – these diseases can substantially impact a patient's quality of life, leading to joint damage, dysfunction, and disability. However, numerous treatments exist for these diseases that control the immune-mediated factors driving disease, described as disease modifying anti-rheumatic drugs (DMARDs). Despite the success of these drugs for patients in achieving remission, they are not effective in all patients, and those who do not respond well to first-line treatments will typically be given an alternative drug on a trial-and-error basis until they respond successfully. Given the rapid and irreversible damage these diseases can induce even in the early stages, the need for early and aggressive treatment is fundamental for reaching a good outcome for the patient. Biomarkers can be employed to identify the most suitable drug to administer on a patient-to-patient basis, using these to predict who will respond to which drug. Incorporating biomarkers into the clinical management of these diseases is expected to be fundamental for precision medicine. These may come from multiple molecular sources. For example, currently used biomarkers include autoantibodies while this project primarily focuses on discovering biomarkers from the metabolome.

Methodology

This project involved the secondary analyses of metabolomic and transcriptomic datasets generated from patients enrolled on multiple clinical studies. These include data from the Targeting Synovitis in Early Rheumatoid Arthritis (TaSER) (n=72), Treatment in the Rotterdam Early Arthritis Cohort (tREACH) (n=82), Characterising the Centralised Pain Phenotype in Chronic Rheumatic Disease (CENTAUR) (n=50) and Mayo Clinic - Hur et al. (2021) (n=64) – cohorts. The

metabolic findings' translatability across cohorts was evaluated by incorporating datasets from various regions, including the United Kingdom, the Netherlands, and the United States of America.

These multi-omic datasets were analysed using an in-house workflow developed throughout this project's duration, involving the use of the R environment to perform exploratory data analysis, supervised machine learning and an investigation of the biological relevance of the findings. Other methods were also employed, notably an exploration and evaluation of data integration methods.

Supervised machine learning was included to generate molecular profiles of treatment responses from multiple datasets. Doing so showed the value of combining multiple weakly-associated analytes in a model that could predict patient responses. However, an important component, the validation of these models, could not be performed in this work, although suggestions were made throughout of possible next steps.

Results and Discussion

The analysis of the TaSER metabolomic data showed metabolites associated with methotrexate response after 3 months of treatment. Tryptophan and arginine-related metabolites were included in the metabolic model predictive of the 3-month response. While the model was not directly validated using subsequent datasets, including the tREACH and Mayo Clinic cohorts, additional features from these pathways were associated with treatment response. Included across cohorts were several tryptophan metabolites, including those derived from indole. Since these are largely produced via the gut microbiome it was suggested that the gut microbiome may influence the effectiveness of RMD treatments. Since RA and PsA were considered in this work as two archetypal RMDs, part of the project intended to investigate whether there were shared metabolic features found in association to treatment response in both diseases. These common metabolites were not clearly identified, although arginine-related metabolites were observed in models generated from the TaSER and CENTAUR cohorts in association with response to treatment in both conditions.

Owing to the limitations of the untargeted metabolomic approach, this work was expected to provide an initial step in understanding the involvement of arginine and tryptophan related pathways in influencing treatment response in RMDs. Not performed in this work, it was expected that targeted metabolomics would provide clearer insights into these metabolites, providing absolute quantification with the identification of these features of interest in the patient samples. It was expected that expanding the cohort sizes and incorporating other omics platforms would provide a greater understanding of the mechanisms of the resolution of RMDs and inform future therapeutic targets.

An important output from this project was the analytical pipeline developed and employed throughout for the omics analysis to inform biomarker discovery. Later work will involve generating a package in the R environment called *markerHuntR*. The R scripts for the functions with example datasets can be found at https://github.com/cambest202/markerHuntR.git. It is anticipated that the package will soon be described in more detail in a publication. The package will be available for researchers familiar with R to perform similar analyses as those described in this work.

Table of Contents

Acknowledgements

Firstly, I would like to thank my primary supervisor, Professor Mike Barrett. I'm incredibly grateful for his encouragement, inspiration, and guidance over the last four years. His excitement for metabolomics has been contagious and I am truly thankful for his enthusiasm for this project. I would also like to thank Professor Iain McInnes, Dr Simon Rogers, and Professor Mick Watson as supervisors as well as Professors Jill Pell, Carl Goodyear, Stefan Siebert and Neil Basu for their support throughout the project and for my own development. I also thank everyone in the MRC DTP in Precision Medicine programme for their help and engagement.

Thanks to John, Gavin and Ronan who got me up and running with the computational work at the start of the pandemic. I would not have progressed very far without them! Thank you to James Dale and Flavia Sunzini, who very kindly shared the TaSER and CENTAUR metabolomic datasets with me, along with Professor Robert de Jonge for the tREACH dataset and Professor Jaeyun Sung for the support of the analysis of the data from the Mayo Clinic.

Thank you to past and present members of the Barrett Lab: Ryan, Lesley, Matt, Emily, Supriya, Victoria, Wendy and Connor. Thanks also to the members of the Goodyear lab. A big thanks to Federica, Dagmara, Marianne, Carla, and Chess for all of the support, advice, coffee and cakes provided over the years.

Thank you to my close friends who have supported me throughout the project and beyond: to Jack, Steven, Thomas, Craig, Andrew, Ross, Nicky, Ruaridh and Scott; to Mark and Sarah, Dave and Cat, Chris and Steph, Jon and Beth, Paul and Natalie, Rob and Lisa, for their friendship during these years; to my house group and Kirkintilloch Baptist Church for their kindness, fellowship, and prayers.

Thanks to Mum, Dad, Gordon and Joanna; to Gran and Grandad; and to Joy, Sandy and Katie. Their love and support have been greatly cherished.

Most of all, I thank my wife Eilidh, for her love, faith, encouragement, patience, and confidence in me during the highs and lows. She has been my greatest support and I'm endlessly grateful.

Author's Declaration

I declare that this thesis is the result of my own work. No part of this thesis has been submitted for any other degree at The University of Glasgow, or any other institution.

Signature: Printed name: Cameron G Best

Abbreviations

A	ACP	Anti-citrullinated protein
	ACMSD	Aminocarboxymuconate semialdehyde decarboxylase
	ACPA	Anti-citrullinated protein antibodies
	ACR	American College of Rheumatology
	ADA	Adenine deaminase
	ADAR	Adenosine deaminase RNA specific
	AGAT	Arginine glycine amidinotransferase
	AhR	Aryl hydroxarbon receptor
	AICAR	5-Aminoimidazole 4-carboximde ribonucleotide
	ALE	Accumulated local effects
	AMP	Adenosine monophosphate
	AMPA	Anti-modified peptide antibodies
	AMPDA	AMP deaminase
	APR	Acute phase reactant
	ARG	Arginase
	ASL	Argininosuccinate lyase
	ASS	Argininosuccinate synthase 1
	ATIC	AICAR transformylase
	AUC	Area under the curve
	AUC-PR	Area under the precision recall curve
	AUC-ROC	Area under the receiver operating characteristic curve
	ax-SpA	Axial spondyloarthrits
B	BAPX1	Bagpipe homeobox homolog 1
	BATF2	Basic leucine zipper ATF-like transcription factor 2
	BER	Balanced error rate
	BH	Benjamini Hochberg
	BMD	Bone mineral density
	BMI	Body mass index
	BSR	British Society of Rheumatology
	BST2	Bone marrow stromal cell antigen 2
C	CASPAR	Classification criteria for Psoriatic Arthritis
	CCL2	Monocyte chemoattractant protein -1 (MCP-1)
	CD	Cluster of differentiation
	CDAI	Clinical disease activity index
	CE	Capillary electrophoresis

	CENTAUR	Characterising Centralised Pain Phenotype in Chronic Rheumatic Disease
	CIA	Collagen induced arthritis model
	CIITA	Class II major histocompatibility complex transactivator
	CR	Conventional radiography
	CRP	C-reative protein
	csDMARD	Conventional synthetic DMARD
	CSF	Cerebrospinal fluid
	CTLA4	Cytotoxic T-lymphocyte associated protein 4
	CV	Cardiovascular
D	DA	Disease activity
	DAPSA	DIsease activity in psoriatic arthritis
	DAS28	Disease activity score across 28 joints
	DAS44	Disease activity score across 44 joints
	DHFR	Dihydrofolate reductase
	DIABLO	Data integration analysis for biomarker discovery using latent variable approaches for omics studies
	DKK1	Dickkopf wnt signaling pathway inhibitor 1
	DMARDs	Disease modifying anti-rheumatic drugs
E	ECGF1	Endothelial cell growth factor 1
	ER	Error rate
	ESI	Electrospray ionisation
	ESR	Erythrocyte sedimentation rate
	EULAR	European Alliance of Associations for Rheumatology
F	FAICAR	Formyl AICAR
	FAM57A	Family with sequence similarity 57 member A
	FDR	False discovery rate
	FLS	Fibroblast like synoviocytes
	FM	Fibromyalgia
	FN	False negative
	FOXD4L4	Forkhead box D4 like 4
	FP	False positive
	FPR	False positive rate
	FRMD3	FERM domain containing 3
G	GA	Guanidinoacetate
	GATM	Glycine amidinotransferase
	GC	Gas chromatography
	GCCA	Generalised canonical correlation analysis

	GCN	Graph convolutional network
	GDP	Guanosine diphosphate
	GHVAS	Patient general health assessment
	GLM	Logistic regression
	GLMB	Boosted logistic regression
	GRACE	GRAPPA composite score
	GRAPPA	Group for research and assessment of psoriasis and psoriatic arthritis
	GRZB	Granzyme B
H	HA	Homoarginine
	HAQ	Health assessment questionnaire
	HBA1	Haemoglobin subunit alpha 1
	HDA	High disease activity
	HILIC	Hydrophilic interaction liquid chromatography
	HLA-B/C	Histocompatibility leukocyte antigen B or C
	HLA-DRB1	Histocompatibility leukocyte antigen DRB1
	HM	Half minimum
	HMDB	Human Metabolome Database
	HTRA1	High temperature requirement A serine peptidase 1
I	IBD	Inflammatory bowel disease
	IDO	Indoleamine 2,3-dioxygenase
	IFI35	IFN induced protein 35
	IFN	Interferon
	IFNLR1	IFN lambda receptor 1
	IKBKE	Inhibitor of NFκB subunit epsilon
	IL	Interleukin
	IL1R	IL-1 receptor
	IL1RA	IL1R antagonist
	IMP	Inosine monophosphate
	INDO	Indole 2,3-dioxygenase 1 gene
	IPA	Indolepropionic acid
	IRAK	IL-1 receptor associated kinase
	IRF9	IFN regulatory factor 9
	IRG1	Immunoresponsive gene 1
	ISG15	IFN stimulated gene 15
K	KEAP1	Kelch-like ECH-associated protein 1
	KEGG	Kyoto Encyclopedia of Genes and Genomes
	KMO	Kynurenine 3-monooxygenase

	KNN	K-nearest neighbour
	KYNU	Kynureninase
J	JAK	Janus kinase
L	LASS3	Longevity assurance homologue 3
	LC	Liquid chromatography
	LC-MS	Liquid chromatography mass spectrometry
	LDA	Low disease activity
	LOESS	Locally weighted scatterplot smoothing
	LOQ	Limit of quantification
	LPS	Lipopolysaccharide
M	m/z	Mass to charge
	MCC	Matthews Correlation Coefficient
	MDA	Minimal disease activity
	MerTK	Mer Tyrosine Kinase
	MHC	Major histocompatibility complex
	MHC2TA	MHC class II transactivator
	MMP	Matrix metalloproteinases
	MNAR	Missing not at random
	MS	Mass spectrometry
	MSEA	Metabolite set enrichment analysis
	MSUS	Musculoskeletal ultrasound
	MTHFR	Methylenetetrahydrofolate reductase
	MTX	Methotrexate
	MX1	IFN induced GTP binding protein
N	NB	Naïve Bayes
	NCKAP1	Nck associated protein 1
	NICE	National Institute for Health and Care Excellence
	NFκB	Nuclear factor of kappa light chain enhancer of activated B-cells
	NFKBIE	NFKB inhibitor epsilon
	NLRP	NLR family pyrin domain containing
	NMR	Nuclear magnetic resonance
	NOS	Nitric oxide synthase
	NRF2	Nuclear factor erythroid 2–related factor 2
O	OAS1	2'-5'-Oligoadenylate Synthetase 1
	OPLS-DA	Orthogonal PLS-DA
	ORA	Overrepresentation analysis
P	P4HA2	Prolyl 4-hydroxylase subunit alpha 2

	PADI4	Protein arginine deiminase type 4
	P/MAMP	Pathogen/microbial associated molecular patterns
	PAS-II	Patient activity scale II
	PASDAS	Psoriatic arthritis disease activity score
	PBMC	Peripheral blood mononuclear cells
	PC	Principal component
	PCA	Principal components analysis
	PDHA2	Pyruvate dehydrogenase E1 subunit alpha 2
	PDP	Partial dependence plot
	PDE	Phosphodiesterase
	PGE	Prostaglandin E
	PLS-DA	Partial least squares discriminant analysis
	POC	Point of care
	ppm	Parts per million
	PQN	Probabilistic quotient normalisation
	PsA	Psoriatic arthritis
	PSA	Polysaccharide
	PTPN22	Protein tyrosine phosphatase non-receptor type 22
	PVAS	Pain visual analogue scale
Q	QRILC	Quantile regression imputation of left-centred data
R	R5P	Ribose 5 phosphate
	RA	Rheumatoid arthritis
	RAI	Rheumatology attitudes index
	RAPID3	Routine assessment of patient index data with 3 measures
	RhF	Rheumatoid factor
	RF	Random forest
	RFC1	Transmembrane reduced folate carrier 1
	RFE	Recursive feature elimination
	RGCCA	Regularised GCCA
	RIG-I	Retinoic acid inducible gene I
	RMD	Rheumatic and musculoskeletal diseases
	ROC	Receiver operating characteristic
	ROS	Reactive oxygen species
	RSAD2	Radical S-adenosyl methionine domain containing 2
	RT	Retention time
S	SCFA	Short chain fatty acid
	SCO2	Synthesis of cytochrome C oxidase 2

	scRNAseq	Single-cell RNA sequencing
	SDAI	Simplified disease activity index
	SDH	Succinate dehydrogenase
	SF	Synovial fibroblasts
	sGCCA	Sparse GCCA
	SHAP	Shapley additive explanation
	SJC	Swollen joint count
	SLC	Solute carrier
	SLE	Systemic lupus erythematosus
	SPAG	Sperm associated antigen
	sPLS-DA	Sparse PLS-DA
	STAT	Signal transducer and activator of transcription
	SVM	Support vector machine
	SWPDB	Small molecule pathway database
T	TaSER	Targeting Synovitis in Early Rheumatoid Arthritis
	TCA	Tricarboxylic acid
	TDO	Tryptophan 2,3-dioxygenase
	T_H cells	Helper T cells
	TJC	Tender joint count
	TN	True negative
	TNF	Tumour necrosis factor
	TNFAIP	TNF alpha induced protein
	TNIP2	TNFAIP3-interacting protein 2
	TP	True positive
	TPR	True positive rate
	TRAF	Tumour necrosis factor receptor associated factor
	tREACH	Treatment in the Rotterdam Early Arthritis Cohort
	TREM	Triggering receptor expressed on myeloid cells
	T_{reg} cells	Regulatory T cells
	tsDMARD	Targeted synthetic DMARD
	TTT	Treat to target
	TYMS	Thymidylate synthase
U	UBA1	Ubiquitin like modifier activating enzyme 1
	UPLC-MS/MS	Ultra high-performance LC-MS/MS
	US	Ultrasound
	UTP	Uridine triphosphate
V	VAS	Visual analogue score

	VAX1	Ventral anterior homeobox 1
	VEGF	Vascular endothelial growth factor
	VLDA	Very low disease activity
X	XGB	Extreme gradient boosting

List of Tables

List of Figures

1. Introduction

1.1. Project Overview

Rheumatic and musculoskeletal diseases (RMDs) encompass clinically related conditions, including rheumatoid arthritis (RA), psoriatic arthritis (PsA), axial spondyloarthrits (ax-SpA), systemic lupus erythematosus (SLE) and gout (Saas, Toussirot and Bogunia-Kubik, 2022). RA and PsA are archetypal RMDs and are characterised by chronic inflammation targeting the tissue of the musculoskeletal system, including bone and cartilage, ultimately leading to joint damage and disability if the disease is not managed (Smolen *et al.*, 2018; Coates *et al.*, 2022). Patients suffering from RMDs may also experience extra-articular effects, including inflammatory bowel disease (IBD), pericarditis, vasculitis, neuropathies, pulmonary fibrosis and peripheral nodules developing in various locations, with patients at higher risk of early death, typically due to cardiovascular (CV) disease (Turesson *et al.*, 2003). Psychologic and systemic bone diseases are also more common.

While many treatments are available for patients with RMDs, these are developed based on group trial designs, thus, identifying the optimal treatment for an individual patient is challenging. The current convention involves a trial-and-error-based approach which may ultimately be detrimental to the patient (Heutz and Jong, 2021). Patients may experience a poor long-term outcome due to the delay in receiving early disease management, leading to progressive joint damage, or accelerated co-morbidities. Determining the optimal treatment for the patient remains a fundamental challenge in rheumatology, where the ability to design a treatment strategy based on an individual's needs would provide the best outcome. This thesis describes an approach to identify panels of molecules associated with successful treatment outcomes in patients with RA and PsA. The unearthing of these molecules, mainly derived from the metabolome, was expected to inform the discovery of biomarkers capable of predicting patient responses to treatment, thus, guiding optimal disease management and help develop the understanding of the molecular mechanisms involved in the resolution of inflammation.

It was anticipated that incorporating multiple omic datatypes into the analysis will expand the understanding of mechanisms of disease resolution owing to the richness of the molecular data and the mechanistic insights obtained through their interrogation. There has been considerable development in the technology and methods of data collection and processing which has provided the opportunity to more readily compile a multi-omic profile for the patient (Hasin, Seldin and Lusis, 2017; Menyhárt and Győrffy, 2021; Fan *et al.*, 2022; Xiao *et al.*, 2022). Since the different omics platforms provide alternative views of the molecular processes that contribute to the phenotype, such as the transcriptome and the metabolome, their integration may enable a comprehensive perspective of these processes where a single approach may be limited (Hasin, Seldin and Lusis, 2017).

By analysing metabolomic, transcriptomic and cytokine-derived data from patient samples, the influence of upstream and downstream processes on the mechanisms leading to changes in inflammation can be explored. For example, changes in the expression of genes encoding enzymes that modulate metabolic pathways may be uncovered, demonstrating pathway-wide perturbations that may offer novel therapeutic targets. Moreover, associations between cytokines and metabolites may indicate immunomodulatory effects of metabolites, thus revealing how alterations to metabolite levels may lead to perturbations in downstream inflammatory processes.

1.2. Rheumatoid Arthritis

Rheumatoid arthritis (RA) is one of the most common autoimmune diseases, affecting 0.5-1% of the UK's population (McInnes and Schett, 2017). It is a complicated, inflammatory disease causing progressive, pervasive damage to synovial joints, leading to disability in severe/poorly managed disease (Smolen et al., 2018). Characteristic events in established RA include localised inflammation, cartilage and bone damage, synovium hyperplasia, soft tissue swelling and pain, as depicted in Figure 1.1. In addition, life-limiting extra-articular symptoms can occur, including fibrotic diseases, atherosclerosis, lung disease, fatigue, cognitive impairment and depression, as well as an increased risk of developing certain kinds of cancer (Arts et al., 2017; Guo et al., 2018).

An inflammatory response against cells and tissues of synovial joints is mediated by the release of pro-inflammatory signalling molecules from immune cells, which migrate to the joint (Arango Duque and Descoteaux, 2014; Guo *et al.*, 2018). The presence of autoantibodies in RA has been well described in the literature, including rheumatoid factor (RhF) and anti-citrullinated protein (ACP) antibodies (ACPAs), reflecting the autoimmune component of the disease (Derksen et al., 2017; Guo *et al.*, 2018; Waaler, 1940). Autoreactive specificities also develop against carbamylated and acetylated self-proteins suggesting a fundamental breakdown in tolerance to post-translationally modified self-proteins. Collectively these are termed as AMPAs (anti-modified peptide antibodies) (Volkov *et al.*, 2021).

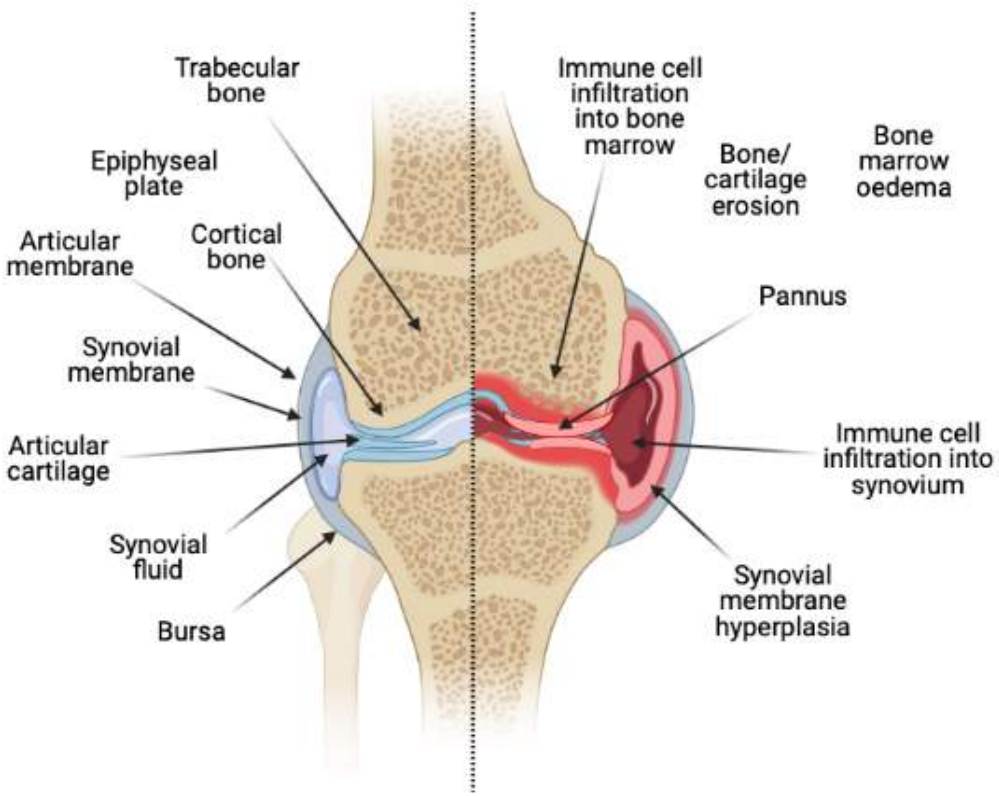

Figure 1.1. Characteristics of an inflamed synovial joint in a patient with rheumatoid arthritis. Adapted from (Akram et al*., 2021).*

Though the clinical presentation of RA has been well-characterised, there is no current cure for the disease (Guo et al., 2018). This is partly because RA is highly heterogeneous in its clinical manifestation, molecular composition, and response to treatment (Cherlin et al., 2018). Notably, several molecules associated with the

disease, including AMPAs, can be detected years before symptoms emerge (de Brito Rocha et al., 2019). ACPAs are produced at mucosal sites distant from the synovial joints, including the lungs, gut and mouth (Guo *et al.*, 2018). This finding may be significant as the exposure of such tissues to environmental factors, including smoke and silica dust, has been suggested to drive post-translational modifications, such as citrullination, ultimately leading to chronic joint inflammation as a critical step towards breaking immunotolerance owing to these protein modifications (Stolt et al., 2010).

ACPA and RhF are associated with disease progression and severity and thus have been marked as prognostic biomarkers (albeit with variable clinical success) (Smolen *et al.*, 2018). Indeed, ACPA-positive and RhF-positive patients were generally found to have higher disease activity and elevated levels of inflammatory cytokines (Sokolove *et al.*, 2014). However, the association of ACPA with disease activity was disputed. It was reported that RhF was more strongly associated with disease activity as the ACPA titre did not appear to be associated with disease activity at baseline (Aletaha, Alasti and Smolen, 2015). Patients with RA may be seropositive or seronegative for these proteins, indicating the need for more robust biomarkers to characterise the disease and its subgroups.

1.2.1. Joint Pathology

While RA is now understood to be a systemic autoimmune disease reflected by elevated levels of circulating autoantibodies, immune cells and pro-inflammatory cytokines, the main focus of the disease is the synovial joints (McInnes and Schett, 2007; Smolen et al., 2018). The synovium (synovial membrane) consists of soft tissue within the articular joint, enclosing the synovial cavity and extending to the tendon sheath. It contains synovial fluid — a yolk-like liquid rich in hyaluronic acid — which functions to lubricate the articular cartilage to reduce friction which would otherwise be damaging and also provides a blood supply to the poorly vascularised tissue within the joint, including the cartilage itself (Narvaez et al., 2010).

An important clinical feature of RA is synovitis (synovium inflammation) accompanied by pain and swelling (Alivernini, Firestein and McInnes, 2022). The

development of synovitis is an important event which drives RA pathology through the infiltration of lymphoid and myeloid cells into the synovium and the induction of osteoclasts from the bone, which play a critical role in bone resorption and erosion (Boutet et al., 2021). The synovial inflammation is reflected through the infiltration of leukocytes into the synovium. This is first seen with an increasing density of cells in the subintimal lining of the synovium, including memory $CD4^+$ T cells, a small number of $CD8^+$ T cells and antigen-presenting innate cells, such as macrophages, mast cells and dendritic cells. Accompanying the immune cell infiltration is angiogenesis, allowing the delivery of more cells into a usually immune cell-sparse tissue (McInnes and Schett, 2011; Narvaez et al., 2010; Orr et al., 2017). In addition, the intimal lining of the synovium begins to swell with the increasing number of synoviocytes (including FLS and macrophages), with an increasingly diverse population of cell subtypes (Culemann *et al.*, 2019; Boutet *et al.*, 2021; Kurowska-Stolarska and Alivernini, 2022).

Single cell omics technologies have revealed new insights of distinct cell types in the synovium and the mechanisms contributing to the pathogenesis of RA (Boutet *et al.*, 2021; Schonfeldova, Zec and Udalova, 2022). Moreover, these approaches have underlined the highly heterogeneous cell populations and subtypes found in the synovium, notably including macrophages, T cells and synovial fibroblasts (SFs) (Schonfeldova, Zec and Udalova, 2022). For example, using single-cell RNA sequencing (scRNAseq) on synovial tissue from patients with RA showed the involvement of subtypes of SFs in driving disease, with the increased expression of matrix metalloproteases (MMPs) being observed in a subtype of RA that correlated with disease activity (Micheroli *et al.*, 2022). Other synovial tissue resident macrophage populations were characterised and play a role in healthy joint homeostasis, being linked to the resolution of inflammation in patients with RA (Alivernini *et al.*, 2020). This subpopulation included cells expressing MerTK, CD206 and TREM2 ($TREM2^{pos}$ $MerTK^{pos}$ $CD206^{pos}$). $MerTK^{neg}$ cells were found to be increased in the synovium of patients with active RA with $MerTK^{neg}$ $CD206^{neg}$ cells representing tissue-infiltrating macrophages which were involved in driving inflammation (Kurowska-Stolarska and Alivernini, 2022). The $MerTK^{pos}$ $CD206^{pos}$ cells also had differences in their lipid metabolism profiles, with increased expression of genes encoding enzymes that produce anti-inflammatory mediators.

These findings from scRNAseq underline the advancements made in characterising the cell populations in the synovium and understanding the mechanisms that modulate inflammation. Since macrophages undergo metabolic reprogramming based on their activation state, it is likely that cell population differences in the synovium will be linked to metabolomic differences across patients.

The infiltration of immune cells into the synovium is accompanied by an increased release of pro-inflammatory cytokines, including IL-1, IL-6 and TNF, as well as proteases, for example, MMPs, which are effectors in damaging the cartilage and bone tissue (Orr *et al.*, 2017). The release of MMPs, along with mediators of inflammation (including various eicosanoids), is characteristic of fibroblast-like synoviocytes (FLSs), a driver of joint damage in RA (Bartok and Firestein, 2010).

The formation of the pannus represents an important event in established RA. The pannus is considered an extension of the synovial tissue which attaches to the surface of the articular cartilage and bone, spearheading the degradation of the tissue through the action of bone-resorbing osteoclasts, stimulated by pro-inflammatory cytokines by macrophages and FLS (Pettit et al., 2006). The ability of the pannus to drive pathology in RA is compared to a localised tumour, invading and destroying the healthy tissue it comes in contact with (Bartok and Firestein, 2010).

In severe disease, degradation of cartilage and bone can lead to impaired joint mobility. However, current approaches to disease management allow many patients to avoid disease-related disability (Smolen *et al.*, 2018). Nevertheless, the impact on quality of life remains an issue for patients, where symptoms can emerge rapidly, involving pain, swelling and tenderness of the joints even in early RA (Grassi et al., 1998). In RA, joints that are generally impacted include those of the hands (metacarpophalangeal/proximal interphalangeal joints) and feet, along with the wrists, ankles, knees, elbows, shoulders and hips (Smolen *et al.*, 2018).

1.2.2. Disease Activity Measurements

The diagnosis of RA is complicated by the similarity of the clinical symptoms of the disease with other musculoskeletal disorders, including Lyme arthritis, osteoarthritis, metabolic diseases, viral arthritis, psoriatic arthritis and peripheral

spondyloarthrits (Smolen *et al.*, 2018). Moreover, due to the progressive nature of RA, clinical outcomes for patients are greatly improved when they receive an early diagnosis and are given treatment rapidly, highlighting the vital need for early diagnosis to ensure optimal patient outcome (Emery *et al.*, 2002; Aletaha and Smolen, 2018). Yet, because RA is highly heterogenous in its clinical presentation and patient outcomes, no current diagnostic tool embodies the entirety of manifestations of the disease (Aggarwal et al., 2015). This has meant that patient diagnosis requires a case-by-case approach involving a rheumatologist guiding the diagnosis and subsequent management of the disease based on their examination of the individual patient (Aletaha et al., 2016; Smolen *et al.*, 2018).

While classification criteria exist for RA, these are generally designed to define homogenous populations of patients in clinical research, allowing for groups of patients with similar clinical characteristics to be compared. As such, while classification criteria can help guide the "diagnosis" of patients, they may result in patients being incorrectly diagnosed due to variations between groups of patients. This was demonstrated when the 1990 American College of Rheumatology (ACR) classification criteria for vasculitis was compared to the reference diagnoses by a physician of vasculitis, where the requirements only matched the reference diagnoses in 75% of cases (Rao et al., 1998).

Despite the limitations of using classification criteria, providing measurable markers in patients with a given set of musculoskeletal symptoms, these may still be informative for characterising disease. The 2010 ACR/European Alliance of Associations for Rheumatology (EULAR) classification criteria included the following:

- At least one joint is involved based on a physical exam or imaging revealing synovitis.
- RA-associated autoantibodies (RhF and ACPAs) detected from serology.
- Elevated acute phase reactant (APR) response, including C-reactive protein (CRP) or erythrocyte sedimentation rate (ESR).
- Symptoms last longer than six weeks.
- There is no alternative diagnosis to explain synovitis (Aletaha et al., 2010).

Following diagnosis, measuring patient progression is typically done using composite disease activity (DA) measures. Composite measures arguably provide the greatest insight into pathological changes in a single score by combining different elements contributing to the pathology of disease (Aletaha and Smolen, 2018). Recently, five composite measures of DA were recommended for clinical use by the American College of Rheumatology, which are summarised in Table 1.1 along with the DAS44 measure, which was included in the Targeting Synovitis in Early Rheumatoid Arthritis (TaSER) trial (Dale *et al.*, 2016; England *et al.*, 2019).

Table 1.1. Summary of composite scoring systems for rheumatoid arthritis.*

Disease Measure	Formula	Joint Count	Lab Requirement	Administration Approach
DAS28-ESR/CRP	$0.56\ x\ \sqrt{28TJC} + 0.28\ x\ \sqrt{28SJC} + 0.7\ x\ ln(ESR\ or\ CRP) + 0.014\ x\ patient\ global\ VAS$	Yes	Yes	Patient, physician and laboratory tools
DAS44	$0.54\ x\ \sqrt{RAI} + 0.65\ x\ 44SJC + 0.33\ X\ ln(ESR\ or\ CRP) + 0.00722\ x\ patient\ global\ VAS$	Yes	Yes	Patient, physician and laboratory tools
CDAI	$28TJC + 28SJC + patient\ global\ VAS + physician\ VAS$	Yes	No	Patient and physican tools
SDAI	$28TJC + 28\ SJC + patient\ global\ VAS + physician\ VAS + CRP$	Yes	Yes	Patient, physician and laboratory tools
RAPID3	$1/3(3.33(MD - HAQ) + pain\ VAS + patient\ global\ VAS$	No	No	Patient-driven
PAS-II	1/3(3.33(HAQ) + pain VAS + patient global VAS	No	No	Patient-driven

* DAS28- disease activity score across 28 joints; ESR- erythrocyte sedimentation rate; CRP- C-reactive protein; TJC- tender joint count; SJC- swollen joint count; VAS- visual analogue scale; CDAI- Clinical Disease Activity Index; SDAI- Simplified Disease Activity Index; RAPID3- Routine Assessment of Patient Index Data with 3 measures; HAQ- Health Assessment Questionnaire; PAS- Patient Activity Scale.

The DAS28 is a composite score considering the tender joint count (TJC), swollen joint count (SJC), the patient global visual analogue score and the ESR/CRP level,

providing a score between 0 and 9.4. Remission, low disease activity (LDA) and high disease activity (HDA) can be defined using this score. The DAS44, which predates the DAS28 score, involves measures taken across 44 joints, providing wider coverage of the disease status. However, the incorporation of joints in the feet and ankles may increase the variance of the scoring, owing to the reduced sensitivity typically experienced at these joints compared to those, for example, in the hands. Additionally, the DAS28 is used extensively in research and the clinic, mainly due to its ease of measurement with fewer joints considered. It is thus considered the benchmark of scoring systems in RA, used widely in clinical management of disease (Wells *et al.*, 2009). However, the reliance of the DAS28 score on acute phase reactants (APRs) – including CRP and ESR – may lead to inaccuracies in reporting changes in disease activity since they do not necessarily reflect articular disease (Kay *et al.*, 2014; Orr *et al.*, 2018; Felson *et al.*, 2021). Since treatments for RMDs target different mechanisms, the use of DAS28 involving APRs may show overly optimistic results for drugs targeting inflammatory mechanisms, such as drugs that block IL-6 (for example, toclizumab) or TNF (for example, etanercept). As a result, alternative composite measures, demonstrated by the CDAI score, may be favourable since they does not rely on APRs and laboratory measures. Instead, the CDAI score captures joint counts and extra-articular symptoms through global and physician VAS scores, thus providing a comprehensive measure of disease activity that is not influenced by APRs (Janke *et al.*, 2022).

1.2.3. Detecting Joint Inflammation and Damage

In addition to the composite measures of disease, imaging techniques can provide insights into the structural and functional changes that take place during the course of RA disease progression in the joint, including magnetic resonance imaging (MRI), conventional radiography (CR) and ultrasound (US) (Baker et al., 2017; Jimenez-Boj et al., 2007; Sudoł-Szopińska et al., 2017). Indeed, CR is recommended as the initial approach for imaging joint damage, where it can reveal structural changes associated with joint damage such as joint space narrowing (Sudoł-Szopińska et al., 2017). However, CR is limited in that it can only detect erosions after ~20% of the bone has been removed, and so more sensitive

techniques – including MRI and US – are required to detect lower degrees of erosion (Ejbjerg *et al.*, 2006; Kgoebane *et al.*, 2018).

1.3. Psoriatic Arthritis

Psoriatic arthritis (PsA) is a chronic inflammatory disease that similarly involves the immune system causing damage to joint tissue, affecting approximately 1% of the population (Veale and Fearon, 2018). As a heterogeneous disease, patients with PsA can experience lasting mild symptoms, while others may initially have mild inflammation of the joints but progress towards joint damage and dysfunction. Patients might also experience the emergence of extra-articular effects, with sites including the eye (uveitis), nail and skin (psoriasis), and the bowel (IBD) (Fraga *et al.*, 2012; Coates and Helliwell, 2017; Bengtsson *et al.*, 2021). It is a complex disease involving articular and non-articular symptoms, with severe or poorly managed disease leading to an increased risk of early death, typically through CV disease (Coates and Helliwell, 2017). The complexity of PsA comes from the varied presentation of symptoms and difficulty in differentiating the disease from other RMDs including RA (Gossec *et al.*, 2016).

Up to one-third of patients with psoriasis develop PsA, indicating a strong link between these conditions (Scher *et al.*, 2019). The following symptoms are typical in patients suffering from PsA with the severity ranging across patients:

- Joint tenderness, stiffness, dysfunction, and deformity
- Enthesitis (inflammation of tendon/ligament attachment site to bone)
- Synovitis (inflammation of synovial tissue)
- Osteitis (inflammation of the bone)
- Dactylitis (inflammation of finger/toe)
- Psoriasis (inflammation of the skin)
- Nail changes
- Uveitis (inflammation of the eye)
- Bone oedema
- Fatigue

Like other arthritis diseases, PsA substantially impacts a patient's quality of life, affecting their motion, energy levels, and mental health. Patients may experience comorbidities, including obesity, CV disease, depression, and anxiety (S. Gupta *et al.*, 2021). In a recent systematic review, it was found that 33% (95% CI: 17-53%) of patients with PsA suffered from anxiety, while 20% (95% CI: 8-35%) suffered from depression (Zhao *et al.*, 2020).

1.3.1. Diagnosing PsA

The diagnosis of PsA relies on clinical examination by a rheumatologist and the identification of signs of inflammatory arthritis or enthesitis, including joint/enthesial tenderness and pain, supported by markers of inflammation such as ESR and CRP – although these may remain at normal levels in a significant proportion of patients (FitzGerald *et al.*, 2021; Houttekiet *et al.*, 2022). Like RA, no diagnostic test is available for PsA.

Determining the type of arthritis can be done using several criteria, including observing the joints affected since there are differences in the pattern of joints affected in RA and PsA (Veale and Fearon, 2015). While patients with RA often have symmetric joint involvement, there is usually an asymmetry in the joints involved in PsA (Merola, Espinoza and Fleischmann, 2018). Diagnosing PsA relies on the patient experiencing joint inflammation and typically involves detecting psoriasis and eliminating other conditions that may lead to related symptoms, including RA. Classification criteria are generally only used in research to select patients with diagnosed PsA for clinical trials, meaning these criteria are not necessarily helpful in the initial diagnosis.

The Classification criteria for Psoriatic Arthritis (CASPAR) advanced a classification system for PsA developed on the system laid out in the 1970s (Moll and Wright, 1973; Taylor *et al.*, 2006). While still used in the field, the Moll and Wright criteria were largely considered inadequate in their ability to distinguish PsA from RA, where the classification was based on the presence of inflammatory arthritis, a negative test for RhF, and pre-existing psoriasis in patients (Moll and Wright, 1973; Helliwell and Taylor, 2005).

In classifying PsA patients for trials, the CASPAR criteria have limitations in differentiating arthropathies for several reasons. Firstly, patients with RA are not all seropositive for RhF. In contrast, 5-13% of patients with PsA may be seropositive for RhF and APCA, albeit with a typically lower titre of autoantibody than RA (Punzi *et al.*, 2007; Merola, Espinoza and Fleischmann, 2018). Additionally, since the classification depends on the presence of psoriasis, patients may be misclassified where psoriasis may be missed in hidden areas, such as in the hairline or the navel (Helliwell and Taylor, 2005). Another important limitation of the CASPAR classification is that the cohort from which it was generated included a small proportion of patients (<10%) with early PsA, defined as symptoms having emerged within two years. This means that the classification is most helpful with established PsA, and so the challenge persists when differentiating patients with early disease (Van den Bosch and Coates, 2018).

1.3.2. Differentiating Psoriatic and Rheumatoid Arthropathies

While sharing features as inflammatory arthropathies, PsA and RA differ in terms of their clinical, molecular and therapeutic aspects (Veale and Fearon, 2015). These differences are summarised in Table 1.2, with examples of treatments available for both conditions in the lowest panel.

PsA and RA share inflammatory joint features, although these are now understood to vary, for example, in joint and tissue involvement. Moreover, further differences have been uncovered on a genetic and molecular level. For example, the main genetic risk factor for RA is the HLA-DRB1 alleles, while HLA-B/C-related alleles are associated with PsA features (particularly those with spinal involvement) (McInnes and Schett, 2011; Winchester *et al.*, 2012; Mc Ardle *et al.*, 2015). Numerous additional polymorphisms have been found associated with PsA and RA, largely relating to the immune system and some of these are noted in Table 1.2 (Shi *et al.*, 2020; Akhtar *et al.*, 2021).

The joint inflammation characterising these diseases was previously considered homogeneous, involving the same contribution of immune cells, chemokines and cytokines (Veale and Fearon, 2015). However, the differences in circulating

inflammatory markers between the diseases, including CRP, indicate that the inflammatory profile of each is not necessarily the same (Cunnane *et al.*, 2000).

Table 1.2. Comparison of PsA and RA. Adapted from Veale and Fearon (2014), Merola et al. (2018) and Ben Mrid et al. (2022).

Features	Psoriatic Arthritis	Rheumatoid Arthritis
Clinical	• Psoriasis • Asymmetrical joint involvement • Enthesitis, dactylitis • Distal interphalangeal and axial spine involvement • Nail dystrophy • Bone proliferation	• Largely symmetrical joint involvement • Cervical spine involvement • Bone erosion
Genetic	• HLA-B/C-related alleles • Other associated genes: IL23R, IFNLR1, PTPN22, P4HA2, TNIP1, IL12B, TRAF3IP2, STAT2, IL23A	• HLA-DRB1 • Other associated genes: PTPN22, PAD14, CTLA4,IL2RA, DKK1, GRZB, MMP9, SPAG16 TNFAIP3, IRAK1, IL6R, NFKBIE
Molecular	• Low (if any) RhF and ACPA • Low CRP and ESR • Elevated vascular growth factor expression in early disease • Elevated IL-17A, IL-12/23 and TNFα	• Often high RhF and ACPA in circulation • Elevated CRP and ESR • Elevated vascular growth factor expression in late disease • Elevated IL-6 and TNFα
Responses to Treatment	• csDMARDs (e.g. MTX) • TNF inhibitors (e.g. etanercept, infliximab, adalimumab) • Abatacept (T cell inhibitor) • Ustekinumab (IL-12/23 inhibitor) • Secukinumab (IL-17 inhibitor) • Apremilast (PDE-4 inhibitor) • Tofacitinib (JAK1/3 inhibitor)	• csDMARDs (e.g. MTX, sulfasalazine, leflunomide) • TNF inhibitors (e.g. etanercept, infliximab, adalimumab) • Abatacept (T cell inhibitor) • Rituximab (CD20 inhibitor) • Tocilizumab (IL-6 inhibitor) • Baricitinib (JAK-STAT inhibitor) • Iguratimod (NF-κB pathway inhibitor)

The different immune cell environments involved in each disease can be highlighted by the success of therapies that target different immune features, as described in Table 1.2. For example, the increased type-17 cells (encompassing those that produce IL-17A and IL-17F, TNF and CCL20, including T_H17, natural killer cells and neutrophils) in the circulation of patients with PsA led to the testing of previously developed drugs that targeted the IL-23/IL-17 axis in psoriasis (Cua and Tato, 2010; McInnes *et al.*, 2013; Boutet *et al.*, 2018).

Additionally, ustekinumab, secukinumab, izekizumab, sonelokumab and brodalumab have either proven efficacy against PsA or are being tested for PsA treatment, having been used in clinical practice/being tested in patients with psoriasis (McInnes *et al.*, 2013; Lebwohl *et al.*, 2015; Philip J Mease *et al.*, 2017; Mease *et al.*, 2018; Boutet *et al.*, 2018). The resulting decrease in IL-17R stimulation can lead to reduced pro-inflammatory effects, including the activation of FLS, osteoclasts, neutrophils and monocytes, which contribute to joint damage by increasing inflammatory cytokine release and bone resorption (Kotake *et al.*, 1999; Hwang *et al.*, 2004; Raychaudhuri, Raychaudhuri and Genovese, 2012).

It is important to note the involvement of multiple tissue domains in PsA, whereby the disease manifests differently across affected tissues, including skin, peripheral and axial joints, and enthesis (Coates *et al.*, 2022). Given the prevalence of different cell types in the skin, synovial joints, and enthesis there is evidence of unique tissue-specific immunological profiles consisting of different proportions of innate and adaptive immune cells and chemokines/cytokines (Cheung *et al.*, 2019; Najm *et al.*, 2023).

1.3.3. Management of PsA

Since a treat-to-target (TTT) approach is increasingly used for treating PsA, quantifying the response to treatment is paramount for successfully managing the disease (Dures *et al.*, 2020). There are multiple disease activity measures in use for PsA, either focusing on a single domain such as skin or joint disease or as composite scores, including the following: Disease Activity in Psoriatic Arthritis (DAPSA); PsA Disease Activity Score (PASDAS), the Composite Disease Activity Index in PsA (CDAI), and the Group for Research and Assessment of Psoriasis and Psoriatic Arthritis (GRAPPA) composite score (GRACE) (Coates and Helliwell, 2016; Schoels *et al.*, 2016; Dures *et al.*, 2020; Helliwell *et al.*, 2020). Considering the aims of managing PsA, the ultimate aim is for patients to reach the lowest state of disease across each of the domains of disease, including peripheral/axial arthritis, enthesitis, dactylitis and skin psoriasis (Coates *et al.*, 2022). Part of this involves ensuring the maximum quality of life possible, retaining functionality and structural health where possible. Since patients with PsA may also have comorbidities, these also ought to be considered as part of the management of

disease, incorporating other specialists alongside rheumatologists as part of the clinical care team.

The PASDAS and CDAI are composite measures of disease considering the articular and extra-articular components of PsA. Meanwhile, DAPSA focuses on joint disease, making it a more limited measure (Wervers *et al.*, 2018). Since PsA has multiple domains, such as joint, skin, spine and entheseal involvement, fatigue, and quality of life measures, finding a composite measure that incorporates each has proven difficult (Mease *et al.*, 2005; Coates *et al.*, 2020). Nevertheless, the DAPSA remains useful where the treatment of PsA largely focuses on resolving joint symptoms, where the extra-articular symptoms are typically secondary targets (Wervers *et al.*, 2018).

Another composite measure, the Minimal Disease Activity (MDA) score, was reported as a more stringent treatment target for patients with PsA compared with the DAPSA-defined remission in a recent study (Coates, Fransen and Helliwell, 2010; Coates *et al.*, 2020). To achieve MDA, patients must satisfy five of the seven criteria in Table 1.3.

Table 1.3. PsA disease activity criteria for Minimal Disease Activity (MDA).

Remission Criteria	**Score Required**
Tender Joint Count	≤ 1
Swollen Joint Count	≤ 1
Psoriasis Area and Severity Score	< 1
Patient Pain Visual Analogue Score	≤ 15
Patient Global Disease Activity	≤ 20
Health Assessment Questionnaire	≤ 0.5
Tender Entheseal Points	≤ 1

Patients who meet all seven of these criteria are graded as having Very Low Disease Activity (VLDA). Compared with the DAPSA-defined remission and low

disease activity (LDA) it was found that VLDA and MDA were less commonly met as treatment goals, where patients meeting DAPSA-defined goals typically had higher levels of residual disease, likely owing to the extra-articular domains not considered in this measure (Coates *et al.*, 2020).

1.4. Treating RMDs: Precision Medicine

Patients with RMDs are generally treated with combinations of glucocorticoids and DMARDs, such as methotrexate (MTX), sulfasalazine and thereafter with biologic and targeted synthetic DMARDs (tsDMARDs) (Smolen *et al.*, 2023). These are often successful in driving patients towards remission. For many patients, especially those with early disease, remission can be achieved using a combination of drugs in an aggressive and tailored treatment strategy for the individual (Aletaha, Alasti and Smolen, 2016). This typically involves a stepwise escalation of these drugs to achieve the treatment target, for example, adding further DMARDs to the cocktail where the first-line drugs may fail to induce a satisfactory disease resolution. Such a strategy describes the TTT approach, described in the literature as favourable for patients' long-term quality of life (Möttönen et al., 2002; Verstappen et al., 2007; Smolen et al., 2016).

The TTT approach has several principles, including defining the target the treatment aims to achieve, often remission for patients with early RA (Smolen et al., 2016). With various drugs available, the aim is to treat the patient aggressively until the target is met, altering the course of treatment until the patient reaches this disease activity target.

In RMDs, the failure to manage the disease with an early and aggressive campaign of treatment generally leads to a worse outcome for the patient due to progressive and irreversible damage to the joints and the risk of developing comorbidities, including CV disease and cancer (Turesson and Matteson, 2013; McInnes and Schett, 2017; Buleu *et al.*, 2019). Patients with RA and PsA often receive MTX as a first-line treatment, a mainstay of RMD treatment (Cronstein and Aune, 2020). However, up to 40% of patients with RA treated with MTX do not respond successfully or experience intolerable side effects, and so require alternative treatments (Nam *et al.*, 2017; Maciejewski *et al.*, 2021). As a result, these patients

experience a delay in receiving successful treatment, which can be detrimental to their long-term outcome due to the progressing joint damage that may occur during the period of ineffective treatment.

Incorporating a precision medicine approach into treating patients with RMDs holds great potential to improve patient outcomes. As a highly heterogeneous disease, RA, representing RMDs, may comprise a variety of distinct diseases, characterised increasingly on a clinical and molecular level, which, as a result, may require the establishment of disease subgroup-specific treatments (Heutz and Jong, 2021). Given the ability to categorise subtypes of RA and the variety of treatments available, the potential for precision medicine in RA is considerable.

Biological markers (biomarkers) play an important role in precision medicine and are largely driving precision medicine since they can be used for numerous purposes for the benefit of the patient (Vargas and Harris, 2016). Biomarkers may be used for several purposes: to characterise and understand disease on a molecular level; to follow the progression of disease; to diagnose patients early before symptoms arise; to predict patients' prognoses; and to predict their responses to the available treatments (Gibson *et al.*, 2012). It is feasible that a patient may go to the clinic with symptoms of RA, and a panel of biomarkers are measured from their blood, providing the clinician with an understanding of their specific subtype of RA and, therefore, what treatment would be most appropriate for their individual molecular needs.

There is great potential in using biomarkers to improve how patients with RMDs are treated. Moreover, it was anticipated that in highly heterogeneous diseases like RA and PsA, the true power of precision medicine could be demonstrated. With the ability to characterise patient subgroups on a molecular level, it was expected that novel insights into the mechanisms of disease emergence, progression and resolution might be uncovered. Such mechanisms may point towards potential therapeutic targets and direct the development of a new generation of treatments informed by biomarker discovery.

1.5. Methotrexate: First-Line Treatment and a Precision Medicine Opportunity

MTX is a conventional synthetic DMARD (csDMARD) that entered trials for treating RA in the early 1980s, with earlier studies indicating positive results with low doses compared to that typically used to treat cancers (Black et al., 1964; Hoffmeister, 1972; Willkens, Watson and Paxson, 1980; Willkens and Watson, 1982). Since then, it has been a first-line treatment for RA for over 40 years (Weinblatt, 2013). MTX is an especially complicated drug, inducing its anti-inflammatory effects at a low dose compared to its anti-cancer effects, which occur at doses up to 1000 times greater than for its anti-inflammatory effects (Cronstein and Aune, 2020). However, where the anti-cancer effects of MTX arise due to reduced leukocyte proliferation as a result of anti-folate effects, this is not believed to be a main mechanism of the anti-inflammatory effects of MTX since the administration of folic acid to patients with RMDs does not result in a reduction of the therapeutic effects of the drug (Cronstein and Aune, 2020). Other mechanisms are at play when treating RMDs using MTX, reflecting its ability to target multiple mechanisms to achieve a beneficial therapeutic effect.

MTX can be administered orally or parenterally for RA. The drug is found in a monoglutamated form upon administration, which is then converted to its more potent polyglutamated form within the cell (Cronstein and Aune, 2020). The monoglutamated MTX enters the cell via the transmembrane reduced folate carrier 1 (RFC1), which transports folate and its derivatives across the membrane (Wang *et al.*, 2001; Drozdzik *et al.*, 2007). The polyglutamated MTX accumulates within the cell, potentially explaining the delay in its therapeutic effect in patients as the intracellular concentration of the active drug increases over time (Cronstein and Aune, 2020).

Polyglutamated MTX is a potent inhibitor of several intracellular enzymes, including dihydrofolate reductase (DHFR), 5-aminoimidazole-4-carboxamide ribonucleotide (AICAR) transformylase (ATIC), methylenetetrahydrofolate reductase (MTHFR) and thymidylate synthase (TYMS). It is thought that inhibiting these enzymes leads to several immunomodulatory effects, as summarised in Figure 1.2, along with the induction of long intergenic non-coding RNA-p21.

Perhaps the most important immunomodulatory mechanism of MTX involves the inhibition of the ATIC enzyme, which leads to an increase in the extracellular adenosine levels (Friedman and Cronstein, 2019).

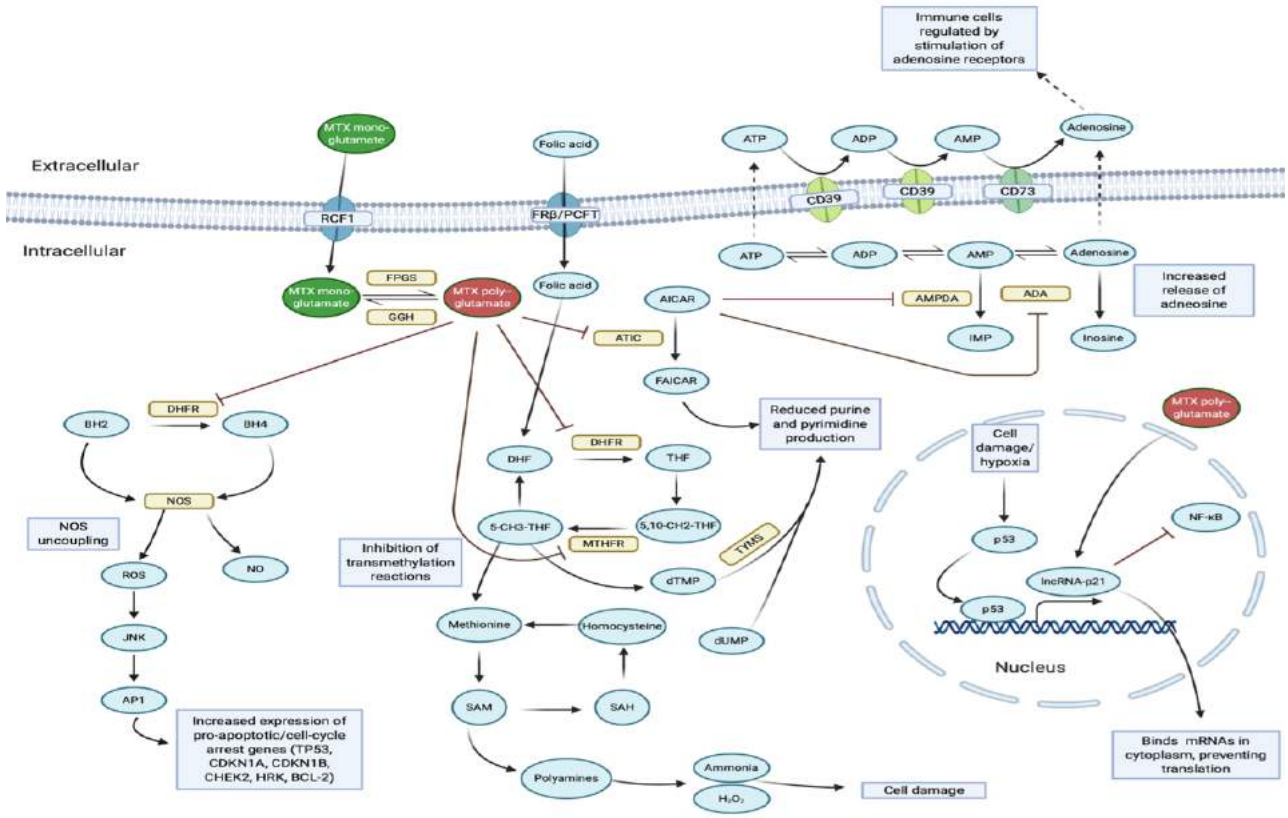

Figure 1.2. Proposed mechanisms of methotrexate on modulating immune cells. Adapted from Cronstein and Aune (2020).

Since the ATIC enzyme mediates the conversion of AICAR to its metabolic product, formyl AICAR (FAICAR), the resulting increased levels of AICAR cause the inhibition of AMP deaminase (AMPDA) and adenine deaminase (ADA), leading to increased AMP and adenosine (Cronstein and Aune, 2020). The increased intracellular adenosine can then be released from the cell and act upon its receptors (Friedman and Cronstein, 2019).

The increased extracellular adenosine is believed to induce a primarily regulatory effect by stimulating its four main receptors — A1, A2A, A2B and A3 — across a multitude of immune cells, including monocytes, macrophages, fibroblasts, neutrophils, dendritic cells, T cells subtypes and B cells (Antonioli *et al.*, 2019). The A2A receptor has immunomodulatory effects across immune cells, including

macrophages, neutrophils and T-cells, as demonstrated by the increased production of the anti-inflammatory cytokine, IL-10, in immune cells following the A2A receptor activation (Haskó *et al.*, 2008). Additionally, the stimulation of murine macrophages with adenosine resulted in a reduced release of the inflammatory cytokine, IL-12, which was similarly reduced when the adenosine uptake inhibitor, dipyridamole, was used (Haskó *et al.*, 2000). Using a synthetic A2A receptor agonist reduced the release of TNFα from LPS-induced THP-1 cells, indicating an anti-inflammatory effect that was reversed with the pharmacological inhibition of the A2A receptor (Bshesh *et al.*, 2002). The increased A2A receptor mRNA in activated murine CD4+ T cells was also associated with a decrease in the release of the pro-inflammatory IFN-γ (Lappas, Rieger and Linden, 2005). In addition, adenosine can induce the anti-inflammatory M2-like, or tissue resolving, macrophage phenotype while increasing the production of further anti-inflammatory cytokines, including VEGF, and reducing TNF, IFN-γ, IL-4 and IL-12 from CD4+ T-cells, known to be pro-inflammatory cytokines (Bshesh *et al.*, 2002; Cronstein and Sitkovsky, 2017).

The complexity of MTX's mechanisms is partly reflected by the difficulty in developing biomarkers to predict how patients will respond to the drug. Recent work has aimed to discriminate treatment responses using measurements of cytokines, such as IL-1ß, IL-4, IL-6 and TNF-α where these pro-inflammatory cytokines play an important role in driving the inflammation behind RMDs (Seitz, Zwicker and Villiger, 2003; Dervieux *et al.*, 2006; Maillefert *et al.*, 2010; Halilova *et al.*, 2012). For example, high levels of cytokines, including TNF-α, may reflect a more severe inflammatory phenotype in patients, where TNF-α levels above 20.1pg/ml were associated with a negative response after 6 months of treatment with MTX in a cohort of patients with active RA (Maillefert *et al.*, 2010).

1.6. Introducing Metabolomics

Biomarkers that predict patient responses may be obtained from various omics platforms, including the metabolome (Puentes-Osorio *et al.*, 2021). The metabolome describes the entirety of small molecules that can be measured in a biofluid, representing an advanced stage in the biochemical journey from the genome to the phenotype (Wishart, 2016). Due to the proximity of the

metabolome to the phenotype, it is an especially useful platform for understanding the interactions between the environment and the biochemicals modulating the phenotype (Rattray *et al.*, 2018).

The metabolome reflects a heterogeneous collection of compounds, including amino acids, small peptides, steroids, nucleotides, fatty acids, sugars, and xenobiotics derived from food and drug-products (Turi *et al.*, 2018). For this reason, no single analytical technology can measure the entire metabolome. In fact, the complete set of metabolites found in the human body has yet to be fully discovered (Lu *et al.*, 2017). This marks an important limitation of metabolomics, where the analysis of a given sample may include numerous unidentified/unmapped metabolites, sometimes termed the “dark matter” of the metabolome, including both biologically relevant and irrelevant compounds (da Silva, Dorrestein and Quinn, 2015). This is an essential consideration for untargeted metabolomics, which is the unbiased study of the detectable metabolites within a sample, including those not yet identified. Targeted metabolomics describes the pre-selection of known metabolites and their measurement, often involving the generation of standard curves using exogenous reference compounds to allow absolute quantification of the metabolites of interest (Roberts *et al.*, 2012).

1.6.1. Generating the Metabolome

Due to the biochemical/physical diversity of metabolites in any given sample, there are many options available for their measurement, including variants of nuclear magnetic resonance (NMR) spectroscopy and mass spectrometry (MS) (Miggiels *et al.*, 2019). In untargeted and targeted metabolomics, the MS is typically coupled with another device to support the separation of the metabolites, involving a chromatography column, many types of which can be used. These include liquid chromatography (LC), gas chromatography (GC) and capillary electrophoresis (CE) (Gowda and Djukovic, 2014). Of these, the LC-MS method is commonly used in metabolomics studies.

Incorporating chromatography can improve the analyte separation of metabolomics approaches, including the hypothesis generating untargeted methods and

hypothesis testing targeted methods. Doing so allows the measurement of a wide range of metabolites, including polar and non-polar compounds, depending on the type of chromatography column used. For example, non-polar compounds, such as lipids and many fatty acids, are most easily separated using the reverse phase column. Highly polar compounds can be separated using hydrophilic interaction liquid chromatography (HILIC) columns (Bajad *et al.*, 2006; Gowda and Djukovic, 2014). As a result, several chromatographic columns are required to measure all detectable metabolites. The samples may need to be analysed multiple times which generates a sizeable expense, reflecting one of the major limitations in generating a complete metabolome.

Given the differences in the physicochemical properties of the metabolites, these elute from the chromatography columns at different rates, reflected as their retention time (RT). Once separated chromatographically, the compounds need to be ionised to be detected, typically done using an electrospray ionisation (ESI) source, producing ionised compounds that are passed through a magnetic field to the mass analyser, which then differentiates the compounds based on their mass: charge (m/z) ratio. Following the separation of these ionised compounds, they are passed through to a detector which then provides a mass spectrum, showing the intensities of the ions across the range of detected m/z ratios (Nash and Dunn, 2019). In addition to the peaks representing biologically relevant metabolites, many of the peaks will include adducts and fragments produced due to the ionisation process, which may confound the metabolite identification (Chen *et al.*, 2021). Metabolite annotation is of great importance and is a research field in and of itself, with numerous computational methods having been developed to attempt to expedite and improve the process (Creek *et al.*, 2012; Zhu, Liu and Hassoun, 2020; Young, Wang and Röst, 2021; Bach, Schymanski and Rousu, 2022; Ebbels *et al.*, 2023; Wandy *et al.*, 2023).

Using an LC-MS approach for metabolome generation, each compound has two primary measurements for identification and quantification: the RT and the m/z ratio. However, using untargeted metabolomics, only a relative quantitative measurement of the metabolites is provided, given the need for standard curves generated for each metabolite. The metabolite measurements are provided as an

abundance or peak intensity, with the peak intensity typically determined relative to the total ion count. Given the different efficiencies of the ionisation processes and the possible instrumentation differences, the metabolite measures may vary drastically across studies using different variations of the LC-MS platform (Lu *et al.*, 2017).

1.6.2. Immunometabolism

While metabolites were once considered to be mere by-products of cellular processes, they are increasingly understood to be important modulators of, for example, immune processes (Murakami *et al.*, 2013; Mills *et al.*, 2016; Wirthgen *et al.*, 2018; O'Neill and Artyomov, 2019; Pucino *et al.*, 2019; Pålsson-McDermott and O'Neill, 2020). In RMDs, where an inappropriate immune response against the tissue of the joints drives the pathology, the immunomodulatory effects of metabolites may offer clues as to the mechanisms of pathogenesis and resolution of inflammation in response to treatment.

A prime example may be itaconate, a derivative of the TCA cycle with immunomodulatory effects and specifically harnessed by macrophages undergoing a shift in their inflammatory profile (O'Neill and Artyomov, 2019). Itaconate was found to have anti-inflammatory effects in LPS-stimulated macrophages via multiple mechanisms, including the inhibition of succinate dehydrogenase (SDH) which blocks succinate oxidation and the formation of reactive oxygen species (ROS) and the pro-inflammatory cytokine, IL-1ß, along with promoting the activation of the anti-inflammation transcription factor, NRF2, by inhibiting the NRF2-regulating KEAP1 protein (Tannahill *et al.*, 2013; Lampropoulou *et al.*, 2016; Mills *et al.*, 2018). Since an increase in itaconate in plasma samples from patients with RA during treatment was associated with a reduced DAS44 score, itaconate may be a useful biomarker of treatment response and have clinically relevant immunomodulatory effects (Daly *et al.*, 2020).

Metabolic changes in patients with RA and other inflammatory diseases may shed light on the mechanisms that modulate the disease activity, potentially offering opportunities for novel targets. Numerous studies have been performed to investigate the metabolic associations with disease state and treatment response

across inflammatory diseases (Cuppen *et al.*, 2016; Bao *et al.*, 2017; Anderson *et al.*, 2018; Ren *et al.*, 2019; Cussotto *et al.*, 2020; Ge *et al.*, 2020). For example, tryptophan metabolism may be perturbed across various diseases, including sepsis, cancer, obesity and other inflammatory diseases, such as RA (Changsirivathanathamrong *et al.*, 2011; Wirthgen *et al.*, 2018; Cussotto *et al.*, 2020; Lanser *et al.*, 2020).

The association of tryptophan metabolism to these diseases may relate to the increased activity of indoleamine-2,3-dioxygenase (IDO) during inflammation, specifically via the cytokine interferon-γ (IFN-γ), which gives rise to the anti-inflammatory metabolite, kynurenine and its downstream products (Brown *et al.*, 1991). Novel therapeutics or treatment strategies may arise from a series of steps. Beginning with exploring metabolic changes in disease, subsequent steps then include understanding the mechanism by which such changes occur and how they may influence disease. This may be followed by discovering methods of exploiting these mechanisms. For example, immunomodulation may be achieved by increasing the production of tryptophan metabolites by blocking IDO, leading to the production of non-IDO-mediated intermediates. New drugs are emerging, including indoximod which is producing promising results in in clinical trials for various cancers (Liu *et al.*, 2018; Zakharia *et al.*, 2021).

Metabolites at baseline that were found to be associated with treatment response may reveal molecular conditions that promote treatment efficacy, which could be harnessed across the patient population to improve global responses. This may involve, for example, therapeutically targeting key metabolic pathways using pharmacological inhibitors or supplementing patients with exogenous metabolites, such as in the management of osteoarthritis pain and joint injury in athletes with glucosamine (Reichelt *et al.*, 1994; Ostojic *et al.*, 2007).

An important consideration when dealing with blood-based metabolite biomarkers is that there may be homeostatic processes that modulate the levels of the analyte other than those occurring in the local disease site. For this reason, it is difficult to know the source and influence of the metabolites detected in the circulation, yielding uncertainty around their clinical importance. Nevertheless, a robust association of a blood-derived metabolite with a changing disease state in response

to treatment may still provide an invaluable biomarker and point towards targetable mechanisms that were historically elusive (Bartikoski *et al.*, 2022).

1.6.3. Current Metabolomic Markers of Treatment Response

Given the connection between the immune response and the metabolome, identifying predictive biomarkers from the metabolome may indicate possible immunomodulatory mechanisms. Using various statistical methods, several candidate predictive biomarkers for a number of therapies have been reported in the RA literature, as summarised in Table 1.4.

Table 1.4. Review of candidate metabolic biomarkers of treatment response across studies in patients with RA.

Metabolite	Method of Association	Sample Type	Treatment	Platform	Study
6-bromotryptophan; bilirubin; biliverdin; glucuronate; N-acetyltryptophan; N-acetyltyrosine; serine; trigonelline	• Differentially abundant across high and low DAS28-CRP groups • Correlations with DAS28-CRP	Plasma	Various	LC-MS	Hur et al. (2021)
Homocysteine; taurine; ATP; GDP; uric acid; 1,3-diphosphoglyceric acid; 2,3-diphosphoglyceric acid; glycerol-3-phosphate	• Differentially abundant at baseline across high and low disease activity after 3 months • Multivariate logistic regression model	Plasma	MTX	LC-MS	Gosselt et al. (2020)
Ethanolamine; lysine; sn-1-LPC(18:3-ω3/ω6); sn-1-LPC(15:0)	• Multivariate logistic regression model	Serum	TNF inhibitors	LC-MS	Cuppen et al. (2016)
Uric acid; taurine; uracil; TMAO; tryptophan; glycine; histidine; hypoxanthine; methionine; aspartate; 2-oxoglutarate	• Partial least squares discriminant analysis (PLS-DA)	Serum	MTX	^{1}H NMR	Wang et al. (2012)
Lysine; proline; 3-methylhistidine; PGE2; pipecolic acid; histamine	• PLS-DA	Serum	MTX and tocilizumab	MS	Teitsma et al. (2018)
Histamine; glutamine; xanthurenic acid; ethanolamine; phosphocreatinine; thymine; creatinine; phenylactic acid; xanthine	• PLS regression • PLS-DA	Urine	TNF inhibitors	^{1}H NMR	Kapoor et al. (2013)
Isobutyrate; 3-hydroxybutyrate; lysine; phenylalanine; sn-glyco-3-phosphocholine; tryptophan; tyrosine	• Orthogonal partial least square discriminant analysis (OPLS-DA)	Plasma	Tocilixumab	^{1}H NMR	Murillo-Saich et al. (2021)
Betonicine; glycerol-3-phosphate; N-acetylalanine; hexanoic acid; taurine	• OPLS-DA	Serum	TNF inhibitors	CE-MS	Takahani et al. (2019)
N-ethylisoleucine; 2,3-dihydrobutanoic acid; nornicotine	• Correlation with DAS28	Plasma	MTX	GC/LC-MS	Medcalf et al. (2021)

While other studies certainly exist whose results were not included in Table 1.4., the fact that there were few metabolites that consistently appeared across this sample of studies involving biomarkers associated with treatment response was noteworthy. However, there were some notable exceptions to this, including tryptophan and its derivatives, uric acid, histamine and taurine, which appeared in

more than one of these studies (Wang *et al.*, 2012; Kapoor *et al.*, 2013; Teitsma, Yang, *et al.*, 2018; Gosselt *et al.*, 2020; Takahashi *et al.*, 2020; Murillo-Saich *et al.*, 2021). Another important consideration is that semi-targeted metabolomics was performed in two of these studies, mentioned by Gosselt et al. (2020) and Medcalf et al. (2021), thereby limiting the number of metabolites being included in the analysis. The biomarkers described in Table 1.4. only include those for RA, while considerably fewer studies at the time of writing reported candidate predictive biomarkers in PsA and other RMDs.

1.7. Gaps in the existing research

While numerous metabolites are offered as candidate predictive biomarkers for treatment response in RMDs, as reflected by historical results in Table 1.4., very few validation studies have been performed to support their clinical use (Gibson *et al.*, 2012). It was apparent that throughout this project, care ought to be taken when considering whether the supposed biomarkers of treatment response were indeed found to be similarly associated elsewhere. Doing so would provide evidence of some degree of robustness of the metabolites, supporting their development as biomarkers and clinically useful tools. The metabolome is especially sensitive to changes in lifestyle factors, such as diet, smoking status, exercise and age (Beuchel *et al.*, 2019; Chen *et al.*, 2022). As a result, it was important to deliberate on whether the biomarkers considered throughout this thesis were strongly associated enough with the response to treatment across demographics. Moreover, the relative quantitation used in many of the MS-based studies meant that the metabolite measurements were likely to be substantially influenced by differences in instrumentation factors, such as ionisation source, ionisation efficiency, chromatography column type, and chromatography column state.

1.8. Aims

This project sought new biomarkers to predict the responses of patients with RMDs to commonly used treatments. In particular, biomarkers that predict how patients with RA respond to the first-line treatment, MTX, were explored throughout this thesis. Since other drugs are often used alongside MTX, a search for biomarkers

that could predict a general treatment response was also performed. Thus, a secondary aim was to explore the molecules that may modulate the inflammatory environment favouring successful patient treatment, pointing to opportunities for developing treatment-supplementary agents.

Potential biomarkers that could be used to predict responses in PsA were also investigated. It was anticipated that where RMDs, including RA and PsA, are distinct diseases, the shared resolution of inflammation that characterises the response to treatment may point towards similar molecular pathways being implicated, showing shared mechanisms that may modulate how inflammation is alleviated across diseases.

When considering the potential metabolic biomarkers in this work, part of the aim was to compare the findings with related studies. This was an especially important feature of the analysis owing to the apparent difficulties in translating the metabolites across studies performed in other research centres.

2. Methodology

2.1. Datasets

Secondary analyses were performed on metabolomic and transcriptomic datasets from clinical studies performed at multiple research centres. These datasets are detailed in Table 2.1, having been obtained from the University of Glasgow, Amsterdam University Medical Centre and the Mayo Clinic. All data were generated as part of studies that were performed in accordance with the Declaration of Helsinki and were approved by the respective ethics committees at each research centre (Dale *et al.*, 2016; Gosselt *et al.*, 2020; Hur *et al.*, 2021).

Table 2.1. Summary of datasets analysed throughout project.

Description	TaSER Metabolomics	TaSER Transcriptomics	tREACH Metabolomics	Mayo Clinic (Hur et al.) Metabolomics	CENTAUR Metabolomics
Data Type	Untargeted metabolomics	Transcriptomics	Semi-targeted metabolomics	Untargeted metabolomics	Untargeted metabolomics
Research Institute	University of Glasgow	University of Glasgow	Amsterdam University Medical Centre	Mayo Clinic	University of Glasgow
Inflammatory Rheumatic Disease	Rheumatoid arthritis	Rheumatoid arthritis	Rheumatoid arthritis	Rheumatoid arthritis	Psoriatic arthritis
Analytical Platform	LC-MS (pHILIC column and Orbitrap Exactive mass spectrometer)	Illumina HumanHT-12v4 Beadchip Microarray	UPLC-MS (cHILIC column and Bruker Impact II™ Ultra-High Resolution Qq-Time of Flight mass spectrometer)	UPLC-MS/MS (Waters ACQUITY and Q-Exactive mass spectrometer and Orbitrap mass analyser)	LC-MS (pHILIC column and Orbitrap Exactive mass spectrometer)
Sample Size	72	72	82	64	50
Sample Type	Plasma	Whole blood	Plasma	Plasma	Serum

The metabolomic data from the University of Glasgow studies were generated at the Glasgow Polyomics facility. These included the TaSER and CENTAUR metabolomic data, while the TaSER transcriptomic data were generated at the School of Cardiovascular and Medical Science, University of Glasgow. These data were kindly made available by Dr James Dale (TaSER), Dr Flavia Sunzini, and Dr

Neil Basu (CENTAUR), who supported and helped direct the project aims throughout the analyses of these data.

The metabolomic data from the tREACH trial from Amsterdam UMC was kindly shared as part of a data transfer agreement with Professor Robert de Jonge following his laboratory's recent publication (Gosselt *et al.*, 2020).

The study from the Mayo Clinic (MA, USA) was identified using an advanced search on PubMed with the following search terms: *(plasma)) AND (rheumatoid arthritis)) AND (metabolome) AND (treatment response)*. The search revealed 17 articles, which were checked for data availability, study design and the inclusion of MTX as a patient treatment. Of these articles, the work by Hur et al. (2021) included openly available metabolomic data. Importantly, the clinical dataset was evaluated to ensure it was appropriate to include in this project based on the following criteria:

- It included MTX-treated patients for an RMD, either RA or PsA
- Metabolomic data was generated from blood (either serum or plasma) using a mass spectrometry platform, preferably, LC-MS.
- It included baseline features measured before administering a new DMARD treatment for patients.
- Disease activity was measured at an appropriate time point after the initiation of treatment, whereby a response in terms of changed disease activity could be quantified.
- Disease activity was measured using DAS28-ESR/CRP.

Professor Jaeyun Sung from the Mayo Clinic kindly supported the inclusion of their data in this project.

2.2. Data Generation

Since this project involved the secondary analysis of data generated from multiple studies, the analytical platform, study design, and processing steps used to generate the available data were evaluated. This helped support the comparison of the findings from each dataset and determine where translation of the results could be made. Additional details can be found in the associated articles mentioned in the following sections. For example, this work did not provide a complete description of the generation of the transcriptomic dataset that

contributed to the analysis in Sections 4 and 5. The original study was cited where complete details could be obtained. In particular, the generation and processing of the transcriptomic data was comprehensively described in Dr James Dale's thesis (Dale, 2014).

2.2.1. TaSER and CENTAUR Studies Metabolomic Data

The metabolomic data from the TaSER and CENTAUR studies was generated from Glasgow Polyomics (University of Glasgow, UK) and were analysed using liquid-chromatography mass spectrometry (LC-MS) (UltiMate 3000 RSLC (Thermo Fisher, San Jose, CA, USA)), using a type of hydrophilic interaction liquid chromatography (HILIC) known as a ZIC-pHILIC column (Merck SeQuant, Umea, Sweden) with an Orbitrap Exactive detection analyser (Thermo Fisher, San Jose, CA, USA). Both negative and positive electrospray ionisation (ESI) modes were used to generate the data and were combined. Further work that describes these methods in more detail can be found in Daly et al. (2020) and Blackburn et al. (2020). These datasets were generated at different times, meaning that further comparative analysis across these datasets was limited, owing to the relative quantitative measurement of the metabolites.

The raw data were pre-processed, a necessary step due to the inherent challenges in handling the LC-MS-derived data. The pre-processing was performed by Dr Gavin Blackburn and Dr Ronan Daly at Glasgow Polyomics. Such steps included correcting for background noise, filtering poor-quality peaks (due to low signal intensity or a low number of detections across samples) and determining actual metabolite signals. The raw LC-MS files were previously converted to mzXML open format using MSConvert from the Proteowizard pipeline (Holman, Tabb and Mallick, 2014). The m/z data was centroided, and the centwave detection algorithm was used to extract unique chromatographic peaks from the mzXML files. The subsequent PeakML files were filtered with peaks that could not be reproducibly detected across filtered samples. These files were combined based on their m/z ratio and RTs using mzMatch.R. The combined PeakML files were then subjected to additional intensity filtering, noise filtering and gap-filling to produce a set of reproducible peaks. Instrumental drift was corrected using a Gaussian process regression algorithm modelled on the pooled samples developed and applied by Dr

Ronan Daly and Dr Gavin Blackburn, respectively, at Glasgow Polyomics. Peaks were manually checked for consistency and integrated using QuanBrowser (Thermo Fisher, San Jose, CA, USA) where appropriate. Tentative identifications were based on the Metabolomics Standards Initiative proposed minimum reporting standards, based on mass alone (Fiehn *et al.*, 2007). Metabolite identifications were made where authentic reference standards were provided with matching RT and m/z ratios to the features detected.

The peak set was then converted to mzML files and further analysed using IDEOM v8 (Creek *et al.*, 2012). The output from the IDEOM analysis was used as the basis for the subsequent analysis performed in R versions 3.6.1-4.2.3 (R Core Team, 2022),

Identification of the metabolites was based on matching the m/z ratio and RT with the authentic reference standards provided by Glasgow Polyomics. Mass was determined with an accuracy within 3 ppm. Since most metabolites do not have a reference standard, many of the metabolites were only tentatively identified based on mass alone. The monoisotopic formula was estimated using the m/z ratio from peak signals that were likely to represent whole metabolites rather than adducts or fragments based on the mass spectrum generated. This was done by visual evaluation of the peaks using the *PeakML Viewer*. From this, multiple molecules with matching formula are often found. The most likely identity was subjectively determined using HMDB to guide the identification with known biological metabolites. The identification was therefore limited owing to this subjectivity, since only a fraction of metabolites had matching reference standards and fragmentation patterns were not widely observed.

The peak signals from the mass spectrometer were also analysed for their quality, whereby the signal components were evaluated from the mass spectrum, including the peak shape, resolution, and signal-to-noise ratio. Problematic signals may occur owing to various factors, including ion suppression, co-elution of compounds, a saturation of the detector and also due to matrix interference, typically experienced with complex matrices, such as plasma or serum (An *et al.*, 2020).

Where internal standards were not available, metabolite annotations were made based on the mass alone of the feature, described as a putative identification at

Level 2 of the Metabolomics Standards Initiative (Fiehn et al., 2007). Metabolites that were identified using matching RT and mass to internal standards could be identified more accurately at Level 1 of the Metabolomics Standards Initiative.

2.2.2. tREACH Study Metabolomic Data

The metabolomic data from the tREACH study were obtained as a CSV file from Professor Robert de Jonge from Amsterdam UMC. The data were originally generated using a SeQuant cHILIC column (Merck, Darmstadt, Germany) coupled with a Quadrupole Time of Flight mass spectrometer (Bruker Daltoniks), with the positive and negative ESI modes being used. The raw files were analysed using the Bruker TASQ software version 2.1.22.3, described by Gosselt et al. (2021). These files were shared, although processing the files required the proprietary software which was not available. As such, only the identified metabolites from the tREACH metabolomic data were included. These consisted of features identified using the Small Molecule Pathway Database (SMPDB) (Jewison *et al.*, 2014).

2.2.3. Hur Study Metabolomic Data

The metabolomic data from the Hur et al. (2021) study were generated from patient plasma samples using the ultra-high performance liquid chromatography-tandem mass spectrometer (UPLC-MS/MS). The study was led by researchers at the Mayo Clinic (MA, USA). The LC-MS platform incorporated a Waters ACQUITY UPLC HILIC column and an Orbitrap Exactive detection analyser (Thermo Fisher, San Jose, CA, USA). Positive and negative ion modes were generated using a heated ESI source.

As reported in the original publication, the raw data were pre-processed using Metabolon Inc's (Durham, NC, USA) software (Hur *et al.*, 2021) The metabolites were identified based on their m/z ratioand RT match to Metabolon Inc's library of authentic standards. This consisted of 3,300 commercially available compounds at the time of data generation. The RT index was principally used in identification. The mass accuracy was determined with a match within 10 ppm of the standards. This was compared to the more stringent threshold of 3 ppm for the m/z ratio being calculated at Glasgow Polyomics, which provided greater confidence in identifying the metabolites. However, a mass accuracy error of 5-10 ppm in

untargeted metabolomics is typical in the literature (Brenton and Godfrey, 2010; Hao *et al.*, 2018).

2.2.4. Bulk Transcriptomic Data Generation from the TaSER Study

Dr James Dale kindly shared the transcriptomic data generated from the whole blood RNA samples. Initially, including 79 patient samples, this was reduced to 72 to allow the pairing of the samples with those that also provided a plasma sample for the metabolomic analysis, thereby providing the opportunity to perform a multi-omic integration of the data for the same samples. Given the growing interest in the integration of omic platforms, the method for the integration was explored in later chapters to provide a more comprehensive view of the molecular features associated with treatment response.

The whole blood sample preparation was reported previously, involving a standardised Illumina TotalPrep RNA Amplification procedure (Dale, 2014). The analysis used Illumina HumanHT-12v4.0 Beadchip microarray chips (Illumina Inc, San Diego, California, USA). The PAXgene-collected RNA samples were processed using the method described by the manufacturer (Preanalytix, Qiagen Group, Becton, Dickinson and Company, Franklin Lakes, New Jersey, USA).

Using the Illumina Beadchip microarray technology allowed 25,400 genes to be picked up with the 47,321 probes on the microarray. Since single genes could be detected and quantified over multiple probes, it was likely that multiple isoforms of the genes were detected. This may be observed in genes with multiple alleles, such as the HLA-DRB1 alleles associated with RA-associated autoantibodies, such as ACPA (Balandraud et al., 2013). However, using RNA sequencing would provide a more complete list of genes and isoforms than the microarray technology used in this work.

2.3. Data Processing

2.3.1. Missing Values

Across the multi-omics data, missing values were found when signals were not detected or quantified within the analytical limitations of the instrumentation

used. This can occur due to poor signal quality — for example, when pre-processing steps fail to remove incomplete signals, such as split signals in metabolomics. Values that were missing not at random (MNAR) may also arise when signals are below the lower limit of quantification (LOQ) (Wei *et al.*, 2018). These signals may remain informative of low metabolite levels, so their substitution with very low values may deal with these missing values. However, this may skew the analysis with a distribution and standard deviation leaning closer towards zero. In this work, missing values were imputed using the half-minimum (HM) method, an approach taken by the MetaboAnalyst toolkit where the smallest values for each feature in the data were halved to impute for these missing values (Grace and Hudson, 2016; Wei *et al.*, 2018). However, other methods, such as quantile regression imputation of left-censored data (QRILC) or random forest (RF) imputation, may also be favourable. The HM and QRILC methods are often used when the missing values are MNAR, meaning that the compound being detected may still exist within the sample but at a level that cannot be detected by the technology at hand, while RF imputation may be better employed when the missing values occur at random, owing to either technical or biological explanations (Karpievitch, Dabney and Smith, 2012; Wei *et al.*, 2018). Features were removed from the analysis if they had missing values in >20% samples (Bijlsma *et al.*, 2006). A representative script showing the code for the processing and analysis of the data was included in the Appendix.

2.3.2. Normalisation

Often with omics data, non-biological factors may cause an unmanageable degree of heterogeneity across features within the dataset, including batch effects and differences in sample concentrations (Sysi-Aho *et al.*, 2007). Normalising the data is fundamental in preventing such factors from biasing the analysis. Since the aim of analysing these data was to compare the samples found in a dataset, the normalisation allowed the features to be distributed on a common range and let comparisons be made. When analysing the data, the varying ranges of values for the features can cause problems, introducing biases when important features have altogether different ranges of values from the other features. In metabolomics, such factors can include differences in the chromatography columns used,

different technicians/operators, and technical differences, such as ionisation efficiencies (Karpievitch, Dabney and Smith, 2012). In addition, biological differences ought to be considered. For example, a small difference in the concentration of one feature may be biologically meaningful, but the same difference in another was not. Normalising the data helps to extract these meaningful differences by applying the same range to each feature.

The datasets were normalised on a case-by-case basis after visual inspection of the distribution of the abundance/expression of the features across the samples. Prior to the normalisation, the data typically underwent a logarithmic transformation (Ejigu *et al.*, 2013; Cook, Ma and Gamagedara, 2020).

2.3.3. Comparison of Normalisation Methods

The *normalizeCyclicLoess* function from the limma package was used where normalisation was required. The cyclic loess function was reported to reduce the variability consistently in a study comparing different methods for normalising metabolomic data, along with quantile normalisation and probabilistic quotient normalisation (PQN) (Li *et al.*, 2016).

The cyclic loess normalisation method extends the locally weighted scatterplot smoothing (loess) method. To understand this, when considering two samples, an MA plot can be generated to depict the differences of the features across two samples, plotting these in terms of the log fold change (y-axis) and the mean log expression (x-axis) of the features, as shown in Figure 2.1A using an artificially generated dataset. A curve can be fitted to these data, shown as a red line in Figure 2.1A, which shows the skewness of the data, reflecting the samples being assessed having varying distributions. The loess process smooths this curve in the MA plot by applying an adjustment to scale the points towards zero. Where only two samples are depicted in

Figure 2.1, this process is repeated where the cyclic loess function cycles through every combination of samples and computes an adjustment for each pair. A final adjustment is applied across all samples, bringing the samples' distributions to a

common range (Dudoit *et al.*, 2002). For the two samples, the result of the normalisation is apparent in

Figure 2.1B-C, where the MA plot is centred to zero following the cyclic loess and quantile normalisation process.

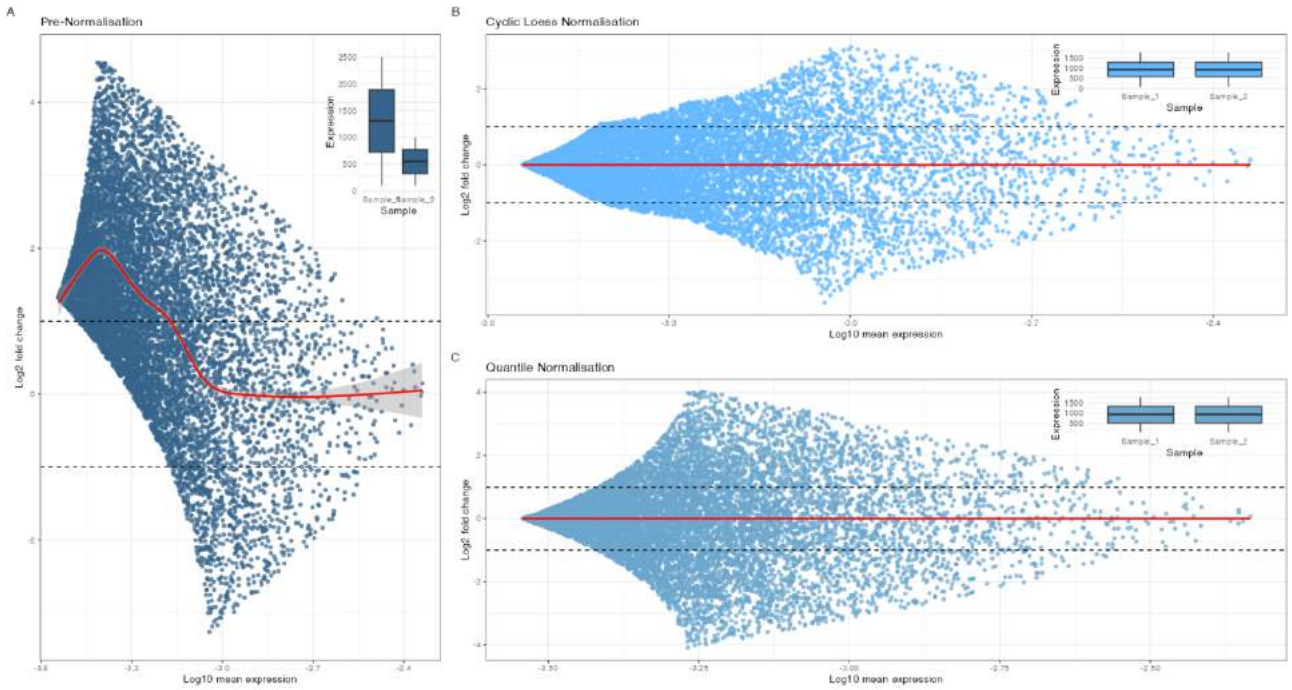

Figure 2.1. MA plots and the evaluation of the normalisation methods and their effects on the distribution of features in an example dataset that the author artificially generated. Embedded within each plot is a boxplot reflecting the overall feature distribution and levels across the samples. Red lines are plotted to show the fitting of a smoothing curve to highlight the differences of the samples across their shared features. The deviation of the red line along the y-axis shows the skewness of the data and the magnitude of the difference between samples. A. Pre-normalisation MA plot with red line reflecting deviance between samples with boxplot showing difference between artificial samples. B. Post-cyclic loess normalisation MA plot, with the red line showing the effect of the loess algorithm in adjusting the differences between the samples to zero. C. Post-quantile normalisation MA plot. Similarly, the red line shows the difference across features between samples to be zero. The boxplots show the result of the normalisation across the two samples.

The quantile normalisation process applies a more stringent but simpler method. Where the samples in a dataset have different distributions, the quantile normalisation process adjusts each sample to have the same quantiles and median values. Quantile normalisation involves taking the original data and ranking

features based on their values within each sample. The average of the features is then calculated, and the actual feature values are then replaced by this average within the rank-defined space (Zhao, Wong and Goh, 2020). The distributions of the samples for the respective methods are comparable, as shown in the top right panel.

The cyclic loess method was selected after being evaluated in a preliminary analysis of the TaSER metabolomic data. The literature also supports the use of this method, although others were also evaluated as candidate methods with only marginal differences being observed (Cook, Ma and Gamagedara, 2020).

2.4. Analysis

A standard analytical workflow was established using the TaSER metabolomic dataset. This was used to analyse the additional datasets, producing results that could be compared. The steps involved in the workflow are described in the following section. The *tidyverse and ggplot2* packages and base R functions were used throughout the project for data transformation, visualisation and analysis (Kuhn and Wickham, 2020). The workflow included multivariate analysis, univariate analyses, supervised machine learning methods and feature interpretation.

2.4.1. Multivariate Analysis of Whole Omics-Dataset

Multivariate analysis was performed using principal component analysis (PCA) to investigate the variance across the samples based on the omics data. This was performed using the *stats* package in the R environment (R Core Team, 2020). Any effects on unsupervised clustering of the samples in the PCA by patient factors, including age, sex, smoking status, and the response to treatment, were assessed by labelling the samples based on these factors within the PCA plot.

Through this approach, batch effects could also be assessed that may arise due to sample handling or processing. These were corrected using the *limma* package and the *removeBatchEffect* function prior to the normalisation (Ritchie *et al.*, 2015).

2.4.2. Differential Expression/Abundance

Univariate analyses were performed across the datasets to explore the association of the omic features with treatment-mediated states of inflammation resolution in patients. This was done through several methods, including differential analysis of these features across clinically relevant classes, such as identifying significantly different metabolites among patients with RA who have a good response to MTX.

The differential analysis was performed using the *limma* package in R, initially designed to generate linear models for microarray data but also used for analysing other datatypes, including metabolomics (Ritchie *et al.*, 2015). The *limma* package uses an empirical Bayes method, comparing the pre-designated groups of samples to produce a t-statistic to indicate which peaks change most substantially between the groups. Due to the increased prevalence of false positives through multiple testing, the false discovery rate (FDR) for the p-values was calculated by using the Benjamini-Hochberg (BH) adjustment, producing adjusted p-values that were used to guide the selection of features that were significantly different across the conditions of interest (Benjamini and Hochberg, 1995). The differential analysis of features of interest was largely performed using non-parametric testing due to the non-normal distributions of many of the features being investigated. This was mainly done using the Wilcoxon test, which provided a p-value to determine whether the difference in the abundance/expression of the features was due to chance.

2.4.3. Correlation Analysis

The features found to be differentially abundant/expressed were assessed for their correlations with disease activity using the *corrplot* and *ggstatsplot* packages in R (Patil, 2021; Wei and Simko, 2022). Since the data were generally not normally distributed, a non-parametric method was used for the correlation analysis which involved calculating the Spearman correlation coefficient. This uses a rank-based analysis rather than the absolute values of the two variables in the Pearson correlation.

While correlation analysis helps explain the relationship between the features and the disease measures and the potential associations between the features,

additional statistical tools were used to understand the interactions between the features and the disease measures. For example, simple linear models were generated, regressing the disease measures (reflecting treatment response) to the baseline feature levels. These models were generated to investigate whether differences in the features at baseline impacted the disease activity in response t a treatment period. This was done using the *lm* function from the *stats* package and the *purrr* package in R (Henry and Wickham, 2020; Kuhn and Wickham, 2020; R Core Team, 2022). These tools helped to quantify the relationship between the variables with a p-value statistic and effect size (R-score) being generated. Due to the number of assessed features, the p-values were used to control for false positives by adjusting with the BH correction (Benjamini and Hochberg, 1995). An adjusted p-value cut-off of < 0.05 was used to determine the significant relationships between features and the disease measures.

2.4.4. Explaining the Influence of Patient Factors on Feature Variance

The influence of clinical factors on the variance across the features in each dataset was explored using the *variancePartition* package in R (Hoffman and Schadt, 2016). This involved a linear mixed model being generated for each dataset for the features of interest, which can help to understand the factors that impact the variation of the features.

As shown in Figure 2.2, an example dataset was generated to demonstrate the value of the *variancePartition* tool. This involved a dataset of artificially generated *p* features and *x* samples, with patient factors, including sex, smoking status, age and BMI. By fitting a linear mixed model, *variancePartition* can explain the influence of the different patient factors on the overall variance of each feature (Figure 2.2A) and the overall variance across all features (Figure 2.2B) (Hoffman and Schadt, 2016). This was done by generating a multiple regression model and designating the factors to be included.

For example, in Figure 2.2A, sex, BMI, and age explained much of the variance of features 1 and 2, while other factors were at play in explaining most of the variance of features 3-5. Across the five features, the boxplot in Figure 2.2B shows

that sex explained a median of ~15% of the variation observed. This is the case after the model corrected for the other factors. As a factor, BMI explained ~10% of the variance of the features after correcting for sex, age and smoking status.

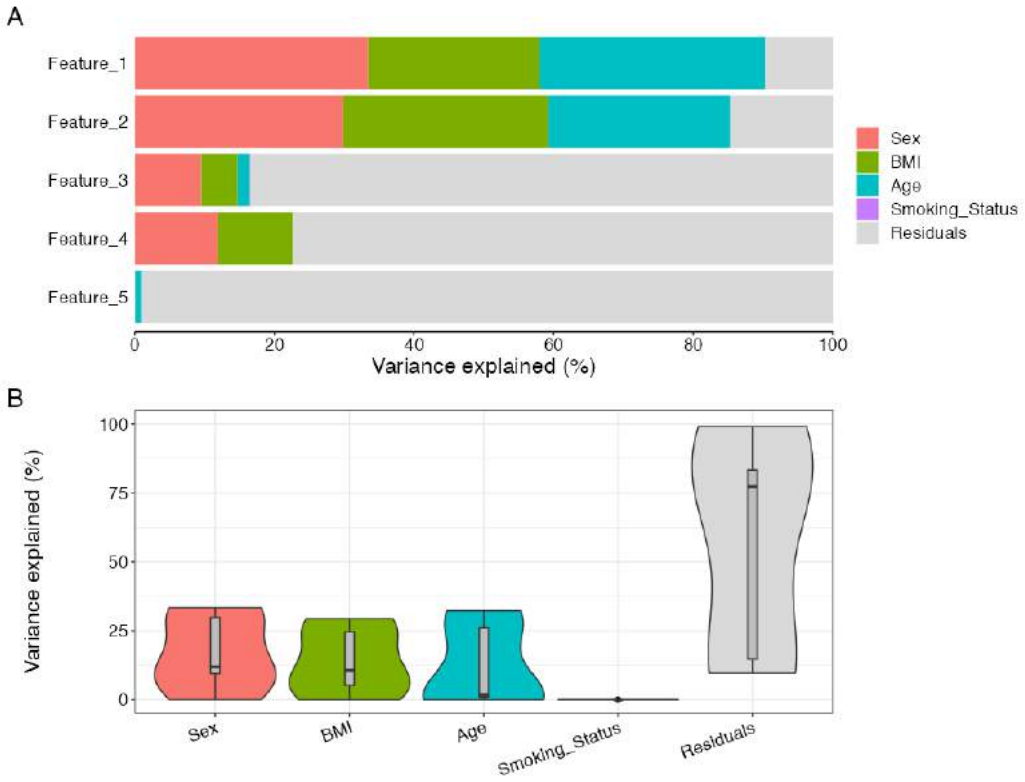

Figure 2.2. Explaining the variance of the features by patient factors. Example data generated by author. A. Bar plot showing each feature and proportional variance explained by factors. B. Boxplots depicting the average variance explained across features by the example factors.

2.5. Pathway Analysis

Pathway analysis was used as an additional tool to investigate the biological context of the treatment-associated features throughout this project. This involved investigating the overrepresentation of a pathway by its components, whether through differences in gene expression, cell abundances or metabolite production (Chicco and Agapito, 2022). Pathway analysis tools typically offer statistical methods that allow an analysis of whether the pathway was truly enriched or was overrepresented by chance. The features included in the pathway were mapped using databases, such as KEGG (Kanehisa and Goto, 2000; Chicco and

Agapito, 2022). An important consideration with pathway analysis for a metabolomic dataset is that it was designed for targeted metabolomics, whereby the identities of the metabolites were previously ascertained (Lu et al., 2023). The identities of metabolites need to be provided, which was only tentative for many of the metabolites in this work, thus limiting the overall value of this approach.

The overrepresentation analysis (ORA) tool from Metaboanalyst was used for the metabolomics analysis in this work, specifically using the metabolite set enrichment analysis (MSEA) (Xia & Wishart, 2010; Chong et al., 2019). ORA often relies on features selected through differential analysis across conditions of interest. The list is then compared with the biological database, including all the known features across pathways. The comparison involves a statistical test to determine whether the list's features are found across a pathway more than that expected simply by chance alone (Cavill *et al.*, 2011). This involves the calculation of the enrichment ratio, with a reference metabolome provided to measure the pathway enrichment. From this, the pathways most enriched were ranked, with the number of features mapped to the pathway and the p-value and FDR calculated for each pathway.

In addition, ShinyGO v0.77 was used for gene enrichment analysis as part of the transcriptomics analysis in Chapters 4 and 5 (Ge, Jung and Yao, 2020). The over-representation of the pathways was determined by calculating the fold enrichment, taking the percentage of the list of genes from the differential analysis that was found in the pathway and dividing this by the percentage of genes found in the background list, thereby providing an effect size. A hypergeometric test was used to calculate a p-value distribution for the pathway analysis in ShinyGo, and the p-values were corrected using the FDR.

2.6. Supervised Machine Learning

This project aimed to identify molecules from multi-omic platforms that could be used as biomarkers to predict how patients with RMDs respond to first-line treatments. By incorporating a supervised machine learning approach into the workflow, the analytes weakly associated with treatment response could be combined within a predictive model where the sum of its parts was expected to be

more powerful than its constituent features. Rather than depending on just one or two biomarkers, this approach may provide a more robust clinical tool that gives insights into the different omics features and processes that may contribute towards the resolution of inflammation. The process involved specifying binary responses to treatment (Y), usually the DAS28 or DAPSA at 3 months, with the omics features being the predictors (X), shown in Figure 2.3.

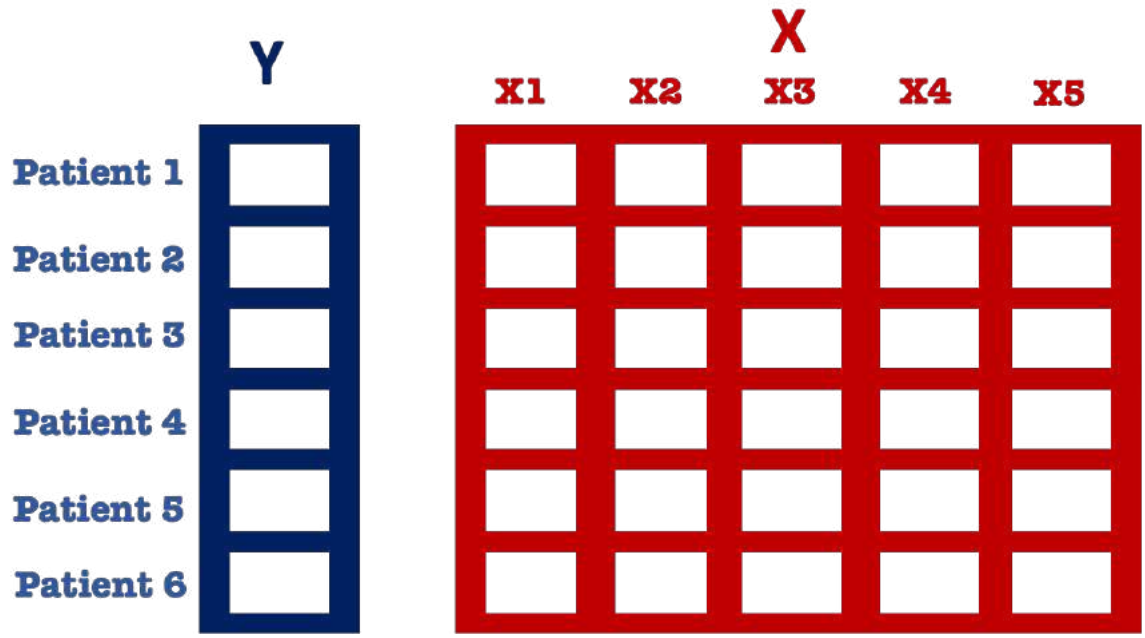

Figure 2.3. Overview of supervised machine learning structures, with each patient's label (Y) being predicted using the features (X) in the data.

For example, in the TaSER trial, patients were categorised as either being in remission or having a good or poor response to treatment based on their DAS28-based outcome after 3 months (Colebatch *et al.*, 2013; Dale *et al.*, 2016). The project aimed to develop models consisting of a panel of molecules associated with treatment response that was representative of the population of patients with RMDs. As such, the models were generated and tuned using subsets of the original data, thereby avoiding the overfitting of the models to the data they were trained on which was expected to make them reproducible across cohorts. This was done in different ways, with the size of the dataset being the main factor in deciding the method. For example, repeated k-fold cross-validation is usually used to evaluate the model generated using small datasets, where the samples need to be

used efficiently. In contrast, a train/test split (hold-out) can be used where many samples are included in the dataset.

However, using various splits of a single dataset was not expected to be as rigorous a validation method compared with evaluating the model in an independent dataset. This was an additional approach explored throughout this thesis.

2.6.1. Train/Test Split (Hold-Out)

Using the hold-out method, the original data is split into training and testing subsets and the models can be generated in the former and evaluated in the latter. While there is no consensus on the ratio used for the split, it is often a 67:33, 70:30 or 80:20 that is used, reflecting the bias-variance trade-off. For example, the TaSER metabolome was split using the *caret* package with a 70:30 ratio for the training and testing subsets (Kuhn, 2019).

The *createDataPartition* function from the *caret* package was used to perform each split, applying random sampling in each binary response category being predicted to allow the training and testing subsets to be similarly balanced for these categories (Kuhn, 2019). For each split, a random seed was set using the *set.seed* function to fix these sample subsets. The model generated on the training subset was subject to k-fold cross-validation, which will be described in the subsequent section. This provided an additional layer of protection against overfitting the model to the data.

2.6.2. Repeated K-Fold Cross-Validation

Repeated k-fold cross-validation is another method to evaluate the performance of a model trained on multiple, limited subsets of the available data, as demonstrated in Figure 2.4. This involves multiple models being created across groups ('folds') of the data, and an average of the models across the k groups can be calculated. After splitting the data into k groups, a model is trained to each minus one (where the last fold is used as an evaluation subset). Here, the light blue portion shows the data in each split used to train the model, while the dark portion shows the 'testing' data. The metrics were averaged upon testing the

models from each split, and the final model's performance can be determined across these groups.

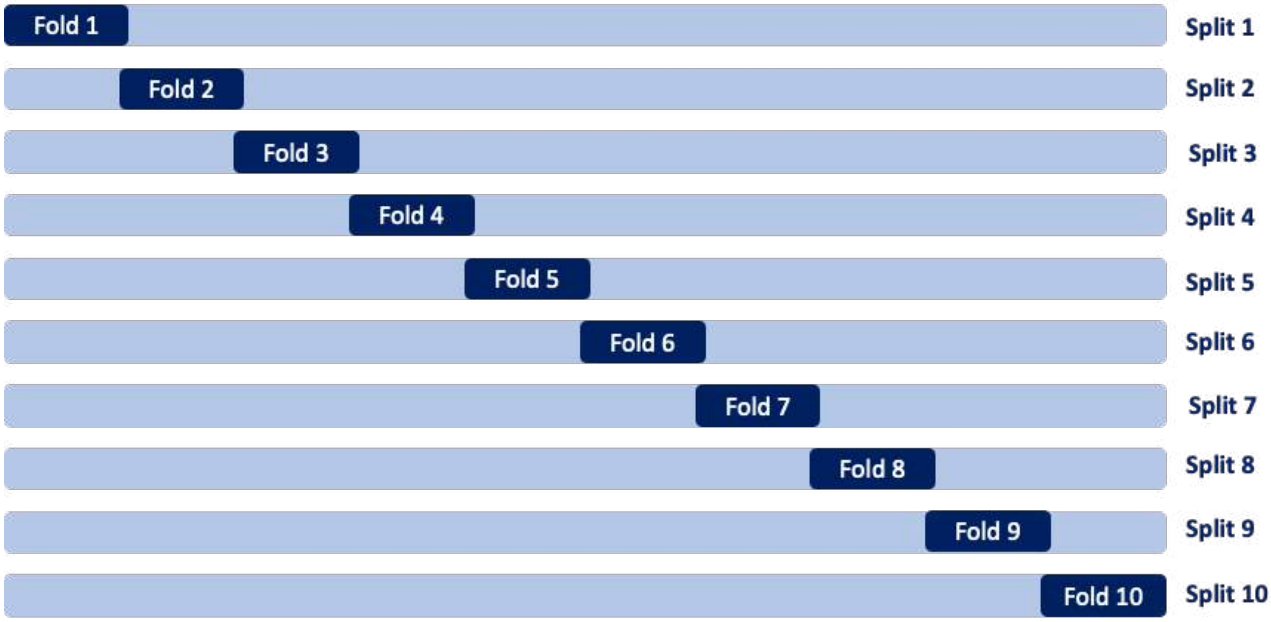

Figure 2.4. Illustrating k-fold cross-validation. The dataset is split into k groups or 'folds', and a model is generated on the fold *k* minus one and evaluated on the fold *k*. New models are generated for each fold *k* created in the data splitting, and the model's performance is determined by taking the mean across the folds.

It is common for a value of 10 to be used for the k parameter (Kim, 2009). To provide a more robust model, albeit more computationally expensive, the 10-fold cross-validation was repeated 10 times during the model tuning and 100 times during the final model generation.

In essence, the repeated k-fold cross-validation helps to protect the models against generating rules to discriminate samples based on the noise in the data; instead, by incorporating this method, it was expected that only meaningful biologically/clinically relevant feature events were used. Using the repeated k-fold cross-validation method, the model could be trained and tested on the entirety of the dataset with increased confidence of its reproducibility in other cohorts. However, no method can guard against poor-quality data and so the following results chapters that used these methods may still include overfitted models and be influenced by noisy data.

2.6.3. Feature Selection

Feature selection was performed on each dataset to determine the most influential features in predicting patient responses. These features were taken forward in the model development, removing redundant features that would not add to the model's predictive ability. Using feature selection reduced the number of features incorporated into the model, providing a more efficient, less computationally expensive, and more pragmatic model. Reducing the number of features to only those most relevant in the model was expected to provide a more practical tool for predicting responses in the clinic and indicate the molecules potentially involved in modulating the inflammatory processes.

There are several ways of performing feature selection. The recursive feature elimination (RFE) algorithm was used in this work since it is a robust method across datatypes and performs well compared to other simpler methods, at the cost of being computationally expensive (Pudjihartono *et al.*, 2022). The RFE algorithm is described as a wrapper-type algorithm. Briefly, as a wrapper-type algorithm, the RFE uses another machine learning model — for example, a random forest (RF) algorithm. This algorithm recursively generates a model from the features in the dataset and ranks these based on their relative importance in the classification. The lowest ranked features are removed, and the model is regenerated from the remaining features, which is repeated until the optimal features remain (Guyon *et al.*, 2002). The user can also designate this number. Like other hyperparameters in a model, this number goes through a tuning process. The number of features retained is selected based on the model's classification accuracy using that subset of features.

Repeated k-fold cross-validation, a method of resampling described in the previous section, was used as part of the RFE feature selection process to reduce the risk of overfitting the model to the data. This was done by applying a 10-fold cross-validation repeated 50 times. The RFE process was repeated 10 times, with different seeds being applied in each iteration to introduce variation into the process. The results from each iteration of the RFE process were then aggregated, and the features that appeared in at least half of these were kept, increasing the robustness of the results.

The *rfe* function from the *caret* packages was used for the feature selection in the R environment (Kuhn, 2019). Following the initial feature selection procedure, a filtering method was performed based on the coefficients calculated when the features were correlated to remove any redundant features (Grissa *et al.*, 2016). Features that strongly correlated (correlation coefficient > 0.7) were assessed, and those with matching RTs were investigated further since these were likely different signals for the same feature. To reduce redundancy, one of the correlating features was removed based on its lower relative importance score.

The number of features to be included in the model was selected using a scree plot-like cut-off. Cut-offs were selected where there was a substantial decrease in the relative importance scores in the feature selection graph, with features below this 'shoulder' having a much lower importance score, indicating less association with the binary classification. However, it was noted that using this subjective approach may introduce bias into the model, so care was taken to use the same rule for selection across the project.

2.6.4. Model Generation

Seven commonly used supervised machine learning algorithms were compared for their performance in predicting the treatment responses of patients from the baseline omics features, using the resampling techniques, typically using repeated k-fold cross-validation. These included the following: extreme gradient boosting (XGB); support vector machine (SVM); random forest (RF); naïve Bayes (NB); k-nearest neighbour (KNN), logistic regression (GLM), and boosted logistic regression (GLMB), as described in Table 2.2. The selection of the optimal algorithm for a model was determined based on various performance metrics, primarily the area under the curve (AUC) for the receiver operating characteristic (ROC) curve and the Matthews Correlation Coefficient (MCC), both of which are described in Section 2.6.8.

Table 2.2. Commonly used supervised machine learning classification algorithms and their method (engine) and tuning hyperparameters.

Model	Engine	Hyperparameters
Random Forest	ranger	• Mtry • Trees • Minimum node size • Split rule • Minimum number
Naïve Bayes	naive_bayes	• Laplace • Use kernel • Smoothness
Extreme Gradient Boosting	xgbTree	• Number of rounds • Maximum depth • Eta • Gamma • Minimum child weight • Subsample
K-Nearest Neighbour	kknn	• Kmax • Distance • kernel
Support Vector Machine	svmRadial	• Kernel • C • Gamma
Logistic regression	glm	• None
Boosted Logistic Regression	glmboost	• Mstop • prune

2.6.5. Random Forest Overview

The RF algorithm is a flexible and non-linear tool in supervised machine learning. As an algorithm commonly used throughout this project, a brief description of its process follows.

As an ensemble algorithm, RFs are a supervised learning approach combining numerous decision trees and generating a single aggregated output from these (Breiman, 2001). To understand the RFs, decision trees, which are considered 'weak learners', should be explained briefly. Decision trees are useful in classification problems, where, starting at an initial or root node, a dataset is split into two or more subgroups based on the features within the dataset. This is illustrated in 'Tree 1' in Figure 2.5, where the rules a decision tree uses to categorise samples as negative or positive are shown based on three nodes.

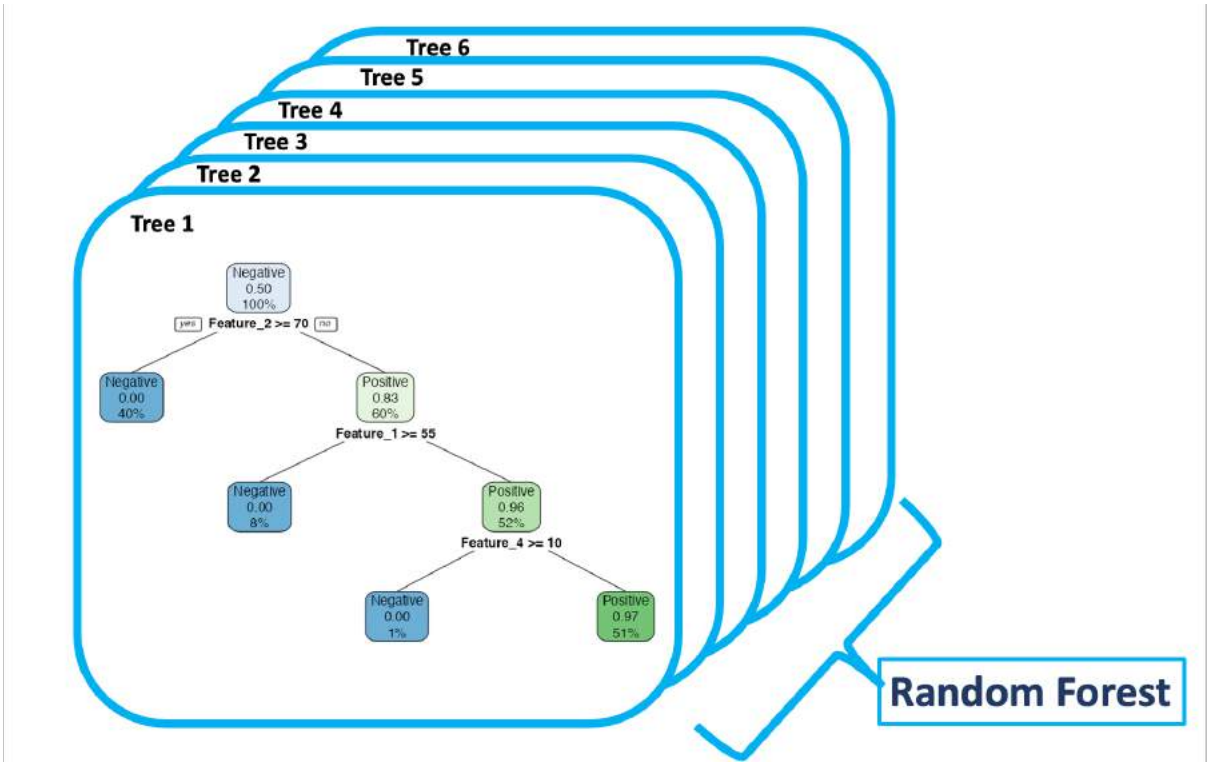

Figure 2.5. Illustration of random forest model. The random forest comprises numerous decision trees (the default is often 500). For binary classification, the decision tree splits the data's subgroups (bootstrap samples) based on the features that maximally discriminate the classes being investigated. The features most influential in this discrimination are at the top of the tree. The decision trees are aggregated, and the output prediction from the random forest is the majority vote of the entirety of the trees in the forest.

The algorithm splits the data into subgroups at decision nodes, classifying the data based on the features that are the strongest predictors of the subgroups until all the nodes are exhausted. This occurs when the subgroups of data cannot be split any further, resulting in terminal nodes with a given classification, as demonstrated using an example dataset in Figure 2.5. The splitting procedure used here was based on the Gini index, which describes the probability that a particular node at the end of each tree is incorrectly classified when randomly selected. For this reason, a low Gini index is preferable, which gives a measure of the uniformity of the data at the node.

By combining the outputs of many decision trees, RFs improve their robustness and are frequently used in machine learning for classification problems (Grissa *et al.*, 2016; L.-L. Zhao *et al.*, 2019; Takahashi *et al.*, 2020). Bootstrapping is used, where only a random fraction of samples is selected (with replacement) for each decision

tree in the random forest. This means that each decision tree is exposed to only a small handful of the samples in the training data, meaning that the choices used to categorise the samples may differ for each tree. By combining the trees, the most influential features in classifying the samples can be found, and a more robust model is produced. Indeed, by increasing the number of trees in the forest, the model becomes more robust and may offer greater accuracy in predicting the classes in new samples.

Correlating trees within a forest can be a problem. Despite each tree being generated independently, the strong relationships between features in each dataset can lead to trees ending up with very similar structures, which leads to the challenge of variance needing to be tackled. To decorrelate the trees and to deal with the variance, the RF randomly selects subsets of the features to be included in each tree, leading to different groups of features being used by each tree (Hastie, Tibshirani and Friedman, 2016). The number of features in each tree can be tuned in the *caret* package (Kuhn, 2019).

2.6.6. Naïve Bayes Overview

The naïve Bayes (NB) algorithm is a simple and efficient classification method that was used throughout this work as the basis of the models used to predict patient responses following treatment using baseline molecular features. As such, the NB algorithm will be described briefly to provide an understanding of its function, as well as its advantages and disadvantages.

The NB algorithm applies Bayes Theorem to a classification problem, where Equation 1 demonstrates its function:

$$P(A|B) = \frac{P(B|A).P(A)}{P(B)}$$

Equation 1. Bayes Theorem

Here, *P(A|B)* represents the probability of classifying a patient's response, *A*, by the feature, *B*. This is referred to as the posterior probability and is dependent on the likelihood probability, *P(B|A)*, multiplied by the prior probability, *P(A)*, divided by the marginal probability, *P(B)*. In the classification problem in this work, the likelihood probability refers to the probability of the omics feature being of a

certain value when the patient response is known. The prior probability describes the probability of the response before any of the feature levels are known. Similarly, the marginal probability is the probability of the features being at a given level without an influence by the patient response classification.

When multiple features are incorporated into the model, the algorithm accommodates these by multiplying them, as shown in Equation 2. This reflects the naïve component of the algorithm, which assumes that the features are independent (Lewis, 1998; Berry, 2006). In other words, the algorithm does not recognise any interactions or relationships between the features, which is noted in the literature as a common trait in real-world data. Nevertheless, the machine learning community have recognised that despite this assumption, the NB algorithm remains efficient even when this assumption is not met (Lewis, 1998; Rish, 2001).

$$P(A|B_1 \dots B_n) = \frac{P(B_1|A)P(B_2|A)\dots P(B_n|A).P(A)}{P(B)}$$

Equation 2. Naive Bayes algorithm with multiple features

The NB algorithm is comparatively fast and efficient as it does not require training numerous hyperparameters, such as with the RF or XGB algorithms. Instead, it takes a probabilistic approach to predict the sample classes based on the features incorporated into the algorithm, considering these as independent of each other (Narayanan, Arora and Bhatia, 2013). However, the assumption of independence may result in a loss of information relating to the biochemical proximity of the metabolites which are typically highly correlated. Nevertheless, the NB consistently performed well and comparatively to the RF algorithm throughout preliminary analyses for this project.

2.6.7. Feature Importance

From the final models, feature importance was carried out to investigate which features were considered most important in influencing the accuracy of predicting the correct sample class. This involved using the *varImp* function from the *caret* package in the R environment (Kuhn, 2019). The *varImp* function assigned thresholds to the data to predict the sample classes for a binary classification problem. The receiver operating characteristic (ROC) curve was generated using

the computed sensitivity and selectivity. The importance of the features was determined in terms of the ROC area under the curve (AUC) value and these values were then scaled to show the relative changes.

2.6.8. Final Model Generation and Evaluation

The generation of the final model involved a 10-fold cross-validation repeated 100 times. Different hyperparameters were tuned depending on the selected algorithm, as described in Table 2.2. These can be described as the inner mechanisms or settings that can be applied to the models during their training. The tuning procedure involved generating a vector of values for each hyperparameter for the given machine learning algorithm, which were then presented to the model as a grid with numerous combinations of each hyperparameter that the model can try out. The model selects the combination of hyperparameters from the grid based on its performance, measured in this work using the AUC-ROC.

After hyperparameter tuning, the model was then evaluated, with the performance being determined using two metrics, the AUC-ROC and the Matthews' Correlation Coefficient. The confusion matrix was first generated to assess the models, checking the predicted response of the samples against the actual response. This structure then provides a check for the types of errors being made by the model. The model performance can be determined by using a combination of these errors and the accuracy of the classification. From the confusion matrix, the accuracy of the model can be calculated, revealing the ability of the model to predict classes in terms of true positives (TP), true negatives (TN), false positives (FP) and false negatives (FN). However, the accuracy and other metrics, such as the F1 score, will often overestimate optimistic predictions, which are observed when there is an imbalance in the classes in a dataset. A dataset can be considered balanced when there is an equal number of samples in both classes described. An imbalance can occur, for example, if there is a much higher proportion of good responders in the sample after 3 months than poor responders. Accuracy should generally be avoided as an evaluation metric due to the over-prediction of the majority class in an imbalanced dataset.

The ROC curve involves the sensitivity (true positive rate, TPR) plotted against 1 minus specificity (false positive rate, FPR). Each point on the ROC curve represents the balance between the sensitivity and specificity of the model across the range of threshold values, from zero to one (Flach and Kull, 2015). The user can select the model parameters that provide the most acceptable balance between these measures of model performance.

A perfect model would have a curve going from the plot coordinates, 0,0 in the bottom left straight up to 0,1 in the top left, and then across to 1,1 in the top right, showing a high sensitivity which is maintained despite an increasing specificity. In other words, the model was intended to predict as many patient outcomes as possible (sensitivity) while avoiding incorrect predictions (specificity).

An important advantage of the ROC curve is its intuitive visualisation of the model's performance. It shows the curve alongside a diagonal line to demonstrate the successful prediction of the data classes compared to that occurring by chance. A ROC curve near the diagonal line, for example, with an AUC < 0.65, might reflect a poorly predictive model due to the prediction being only marginally better than a chance prediction.

The ROC metric is best used when the classes are balanced, with the precision-recall (PR) curve being better suited when there are extreme class imbalances, such as in the case of rare diseases, when 1 in 100,000 individuals may be in the positive class (Flach and Kull, 2015). This plots the precision (y-axis) against the recall (x-axis), where precision is the ratio of true positives to true and false positives. The recall is the ratio of true positives to the combined total of true positives and false negatives. The PR curve, therefore, ignores the potentially high number of true negatives and focuses only on the positives that are calculated. The ROC and PR curves were generated using the MLeval package in R (John, 2021).

The MCC provides an alternative metric, determining how similar the predicted sample classes are to the true sample classes by calculating a correlation between these sample class groups, shown in Equation 3. The MCC considers the TP, TN, FP and FN values, accommodating all components of the confusion matrix (Chicco and Jurman, 2020).

$$MCC = (TP \times TN - FP \times FN) / \sqrt{(TP + FP)(TP + FN)(TN + FP)(TN + FN)}$$

Equation 3. Matthews' Correlation Coefficient

2.6.9. Feature Interpretation

Various model-agnostic interpretation methods were employed to assess how each of the features included in the model influenced the probability of predicting a positive response to treatment. Such insights into the model's workings can be valuable in understanding how the molecules included in the model may have a mechanistic role in the progression or resolution of disease.

These included a variety of global and local model-agnostic tools. Global interpretation methods are used to understand how a model uses the features to make predictions across the entirety of the data being assessed, while local interpretation methods are used to understand why one sample might be given a particular classification based on the features included (Molnar, 2019; Viana *et al.*, 2021). Global interpretation methods used in this work contain the partial dependence plots (PDPs) and accumulated local effects (ALE) plots. In contrast, the Shapley Additive Explanation Plot (SHAPP) was used as a local interpretation method, all generated using the DALEX package (Biecek, 2018; Molnar, 2019).

Briefly, the PDPs can be used to understand the influence of a given feature on the probability of predicting a sample class in the provided data (Greenwell, Boehmke and McCarthy, 2018). In other words, the PDP provides a reflection of the rationale for how samples in an omic dataset might be classified using the model based on their molecular features. While the PDPs are most easily interpreted using a linear model, where there is a clear linear relationship between the feature and the probability of predicting a class, other models can also be used that do not necessarily show linear relationships, including RF and NB models (Molnar *et al.*, 2022).

Interestingly in PDPs, a causal relationship can be drawn in the context of the model since the rules for classifying the samples are defined as a function of the features themselves (Molnar, 2019). However, care needs to be taken where this does not necessarily mean a causal relationship between the feature and the class label, as this relationship may exist only within the confines of the model itself.

While the PDPs help visualise the influence of features on the average prediction of the model, they are limited when dealing with correlated features (Molnar *et al.*, 2022). In such a case, dependent features that are included to generate PDPs, for example, height and weight, the algorithm would generate unrealistic data points which can skew the plots (Apley and Zhu, 2020).

The ALE plots are generally preferential over these as they are unbiased when dealing with correlated features (Apley and Zhu, 2020). Like the PDPs, for a range of values for a given feature, the ALE plots describe the influence of the feature in terms of the average prediction or the probability of predicting a given class in the dataset. These methods differ in interpreting the features. The ALE plot's algorithm was designed to remove the influence of other features by calculating the differences in the average prediction for a feature's effect across small intervals of the feature's values. By doing so, the effect of correlation between features, which can lead to inappropriate feature values being incorporated into the PDP calculation, is ultimately cancelled out (Molnar, 2019; Apley and Zhu, 2020; Molnar *et al.*, 2022).

A useful local interpretation tool is the SHAP plot. For a given predictive model, a SHAP plot can be derived from Shapley values, which describe the marginal contribution that the individual features in a model made to the overall prediction when all of the other features are considered in combination with each other (Molnar, 2019; Merrick and Taly, 2020). A SHAP plot defines a baseline value, which is the average prediction, including all features. The boxplots shown in the plot for each feature illustrate each feature's positive or negative contribution when added relative to the average prediction. Multiple orderings of the features are assessed, with 25 being the default number, with the Shapley value showing the average contribution of the feature across these permutations (Molnar, 2019).

2.6.10. Comparing Models

Models generated to predict patient outcomes were compared within the datasets. For example, multiple models were developed from the TaSER cohort, including a metabolite-based model, a patient factor-based model, and a composite model to predict patient responses in the cohort. The ROC curves generated from each

model's evaluation were plotted simultaneously using the *MLeval* package, and the AUC-ROC and MCC values were compared. The ROC curves could be compared using DeLong's statistical test to determine whether the ROC curves are statistically different.

3. TaSER Metabolomics

3.1. Introduction

3.1.1. Overview

The first-line treatment of RA currently involves the use of conventional synthetic disease-modifying anti-rheumatic drugs (csDMARDs), the most common of which is MTX (Kerrigan and McInnes, 2020). Having been used in the clinic for over five decades, MTX is ineffective in up to 40% of MTX-naïve patients (Maciejewski *et al.*, 2021). In patients who do not respond optimally to MTX, an alternative strategy is required, often with the treatment being selected through a trial-and-error approach that ultimately delays the administration of an effective treatment (Ling, Bluett and Barton, 2018; Teitsma, Jacobs, *et al.*, 2018). The choice of agent is driven currently by application of guidelines and recommendations, for example, from EULAR, British Society of Rheumatology (BSR), National Institute for Health and Care Excellence (NICE) and the ACR.

Providing early and aggressive treatment to patients offers the best opportunity to prevent long-term damage to the joints and improve the quality of life (Sweeney *et al.*, 2016). To do so, a precision medicine-based approach involving the development of a molecular profile associated with treatment response would support the optimal administration of treatment to patients based on their molecular requirements.

3.1.2. Aims

Using the metabolomic data generated from baseline plasma samples from patients with RA in the TaSER cohort, this chapter investigated the metabolites that were associated with the clinical response to MTX. It was anticipated that response-associated metabolites from this work would inform biomarker discovery to predict responses to treatment and therefore guide optimal therapy for patients with RA.

This chapter sought to generate a metabolic model associated with MTX responses that could be used to predict the responses of future cohorts of patients with RA. This was intended to contribute towards a precision medicine approach to guide optimal therapy based on a patient's metabolic profile. The chapter describes the

exploratory analysis, the generation of this metabolic profile and its evaluation, followed by an investigation of the influence of metabolites within the profile and their association with the changing disease activity.

3.2. Methods

The Methodology in Chapter 2 comprehensively describes the methods used throughout this project. Additional study-specific components of the analysis are reported in this section.

3.2.1. Targeting Synovitis in Early Rheumatoid Arthritis (TaSER) Trial

The metabolomic data generated from patient plasma samples involving individuals enrolled on TaSER trial were analysed in this work (Liu et al., 2018; Zakharia et al., 2021). The TaSER trial was initially carried out to investigate whether adding musculoskeletal ultrasound (MSUS) to diagnose and evaluate disease activity and thereby guide the escalation of therapeutics would improve the clinical outcomes for patients (Dale *et al.*, 2016). The primary outcome for the trial was the patient response in terms of their disease activity score across 44 joints (DAS44), which was measured prior to treatment, after 3 months of treatment and after 18 months.

The TaSER trial recruited RA patients with active disease (n=79) using csDMARDs, including MTX (n=75) and sulfasalazine (n=4). Plasma samples were obtained at baseline, 3 months, and 18 months after treatment initiation. Only the baseline metabolomic data from the samples were used in this work. This allowed a baseline molecular profile predictive of the 3-month outcomes to be developed.

Alongside these baseline samples, the 3-month disease activity measures were used (Dale et al., 2016). Of the 75 patients who received MTX in the trial, 3 were removed from the analysis due to missing disease activity measures over the 3 months included in this work. Only the baseline metabolomic data of the remaining 72 patient samples were considered here, along with the baseline and 3-month disease measures. The disease activity and quality of life measures included the following:

- disease activity score across 44 joints (DAS44)
- disease activity score across 28 joints with ESR (DAS28-ESR)
- erythrocyte sedimentation rate (ESR)
- C-reactive protein (CRP)
- health assessment questionnaire (HAQ)
- swollen joint count (SJC)
- rheumatology attitudes index (RAI)
- patient general health assessment (GHVAS)
- pain visual analogue scale (PVAS).

The DAS28-ESR score was used as the primary measure of disease activity and treatment response in this work owing to its more popular use in clinical practice than the DAS44 score. In addition to these measures, patient data were of interest for the subgroup-based analysis and predictive model development, including those described in the literature as risk factors for RA (McInnes and Schett, 2007). These include age, sex, smoking status, autoantibody status and symptom duration.

Patients followed a treatment protocol which began with an initial administration period of MTX at 20 mg per week. During monthly reviews with a clinician, the treatment was escalated based on the progression of the disease, measured in terms of the DAS28-ESR score alone or with an additional MSUS as part of the study group. Using a TTT approach, targets for the disease activity were set and doses/treatments were adjusted if these were not met 3 months since the previous treatment change (Dale et al., 2016).

All patients had active RA at recruitment, where a DAS28 score < 3.2 was the threshold set for low disease activity at baseline, also described as the cut-off for a good response in Table 3.1 alongside other responses as recommended by EULAR (van Gestel *et al.*, 1996; Jerram *et al.*, 2008; Smolen *et al.*, 2016). The DAS28 can

be calculated using a combination of several clinician-measured outcomes (for example, SJC and ESR) and patient-reported outcomes (for example, TJC, HAQ and GHVAS) (Balsa et al., 2004). The DAS28 can be used to define response, with a DAS28 < 3.2 and a reduction in DAS28 > 1.2 describing a good response (Fransen and van Riel, 2005; Jerram *et al.*, 2008). Remission can be defined with a DAS28 < 2.6, although there is ongoing controversy regarding what measures should be used to define remission (van Gestel *et al.*, 1996; Wells *et al.*, 2009; Smolen *et al.*, 2016).

Indeed, the DAS28 is not a perfect measure of disease state, as shown when 25% of patients with RA in a cohort with low disease activity defined using DAS28 < 3.2 had symptoms reflecting active disease (Dale *et al.*, 2014). The DAS28 scoring, whether utilising CRP or ESR measures, was reported as not providing a stringent enough measure of improving disease activity where patients may experience residual symptoms without passing the threshold of active disease (Hirabayashi and Ishii, 2013; Sheehy *et al.*, 2014). There is, therefore, considerable debate surrounding how best to define a response to treatment (Jerram *et al.*, 2008; Pisaniello *et al.*, 2022). Therefore, the potential overestimation of remission based on DAS28-ESR scores was an important consideration in this work.

Table 3.1. EULAR clinical responses and disease activity changes in patients based on the DAS28-ESR/CRP and DAS44 cut-offs. DAS cut-offs in brackets reflect alternative criteria for responses.

Disease Activity Measure	Clinical Response	Improvement in DAS	Present DAS
DAS28	None	< 0.6 (or > 0.6 to ≤ 1.2)	(> 5.1)
	Moderate	> 0.6 to ≤ 1.2 (or > 1.2)	≤ 5.1 (or > 3.2)
	Good	> 1.2	≤ 3.2
	Remission	-	< 2.6
DAS44	None	< 0.6 reduction	> 3.7
	Good	> 1.2 reduction	< 2.4
	Remission	-	< 1.6

Nevertheless, the DAS28 will be used as the primary measure to determine response to treatment in patients since this is the most common clinical measure of disease activity.

3.2.2. Additional Details on Machine Learning Method

While the TaSER metabolome was not considered a particularly large dataset, a holdout cross-validation approach was used, which would typically be saved for larger datasets. This involved the data being split into training and testing subsets. The supervised model was generated and tuned in the training subset, followed by its evaluation in the testing subset.

This provided the opportunity to develop a supervised machine learning workflow using the training subset, which was used as the basis for analysing the data in later chapters. The workflow was optimised, involving testing different algorithms, feature selection methods, packages, and environments within the training subset of data without introducing bias into the final model's performance. For example, by assessing multiple commonly used supervised machine learning algorithms within the training subset, it was apparent that the RF, NB and XGB algorithms performed well in predicting the 3-month response groups using the features provided.

It is important to note that only the tentatively identified and putative metabolites were included in the modelling. This allowed greater ease with which the final model could be tested in other related datasets, where the same features could be largely detected. While there was an expected loss of information due to including only identified features, by removing the non-identified peaks there was an improvement in the performance of the final model, as well as its computational efficiency due to fewer features being included in the modelling. However, a parallel model was developed which included all features, regardless of their identification status, allowing the incorporation of non-identified peaks in a predictive model. This additional model was described in Supplementary Figure 3 with the final all-peaks model consisting of seven features and performing poorly (AUC-ROC= 0.54, 95% CI = 0.28-0.80) compared with the annotated model described in the remainder of this chapter.

3.2.3. Comparing Models

The metabolite model generated to predict the DAS28-ESR-based patient response to treatment was compared with additional models generated from baseline

disease and clinical data, along with the baseline metabolomic data. Comparing the metabolite model with the disease measures model would first indicate whether the model could predict patient responses better than using only data describing clinical data and disease measurements at baseline. These measurements included risk factors for RA, including smoking status, age, autoantibody status, and baseline disease measurements. These typically predict which patients will likely respond to treatment or progress to greater disease severity. As such, comparing the different models would determine whether the metabolite model provides greater predictive ability than the existing markers.

In addition, a composite model was generated by combining the metabolomic data and the disease measures, and this was compared with the metabolites and disease measures models. These models were generated using the same approach as the metabolite model, involving feature selection, hyperparameter tuning and algorithm selection. The performance of these disease measures models was compared with that of the metabolite models. A statistical test was performed to determine whether their respective performance in the test subsets was significantly different.

Since the DAS28 was calculated using the ESR, SJC and TJC, these measures were removed from the model generation process. Additionally, dummy variables were used in place of the discrete factors to allow for these factors, such as sex, smoking status and autoantibody status, to be incorporated into the model. For example, patients could be classed as current, former or non-smokers regarding the smoker status factor. The same was true of the RhF status, where the dummy variable representing RhF-positive patients was incorporated into the model.

3.3. Results

3.3.1. Patient Data

The baseline and 3-month disease activity and other patients were reported and are summarised in Table 3.2. The baseline disease activity was determined using the DAS28-ESR, with a baseline score of 5.0 (SD: ±1.2), which reduced to 3.0 (SD: ±1.2) after 3 months.

Table 3.2. Demographics and disease activity measures of patients in TaSER cohort at baseline and after 3 months. The mean and standard deviation of disease activity measures were reported.

Demographics	**n=72**	
Female Sex, n(%)	50 (69%)	
Age (y)	56 ± 12	
Disease Duration (months)	5.2 ± 3.1	
Current Smoker, n(%)	21 (29%)	
Baseline Bone Erosion Detection, n(%)	24 (33%)	
Rheumatic Factor Positive, n(%)	49 (68%)	
Anti-Citrullinated Protein Antibody (ACPA) Positive, n(%)	40 (55%)	
Disease Acitivity Measures	**Baseline**	**3 Months**
Disease activity score across 28 joints with ESR (DAS28-ESR)	5.0 ± 1.2	3.0 ± 1.2
Disease activity score across 44 joints (DAS44)	4.4 ± 1.2	2.4 ± 1.3
C-reactive protein (CRP)	45.2 ± 56.3	14.6 ± 26.2
Erythrocyte sedimentation rate (ESR)	37.1 ± 25.6	21.9 ± 22.0
Health Assessment Questionnaire (HAQ)	1.5 ± 0.7	0.7 ± 0.8
Patient global health assessment rated on visual analogue scale (GHVAS)	56.2 ± 25.2	23.5 ± 27.6
Pain visual analogue scale (PVAS)	47.9 ± 22.5	24.0 ± 27.8
Rheumatology attitudes index (RAI)	20.1 ± 12.5	7.7 ± 11.6
Swollen joint count (SJC)	9.6 ± 6.5	2.3 ± 3.2

3.3.2. Responses to Treatment

The response to treatment was determined using the DAS28 score, with the final DAS28 at 3 months being the principal measure of response as part of a treat-to-target strategy. The distribution of the DAS28 scores is shown in Figure 3.1, with the change in DAS28 (ΔDAS28) between baseline and 3 months in Figure 3.1A and the final score in Figure 3.1B.

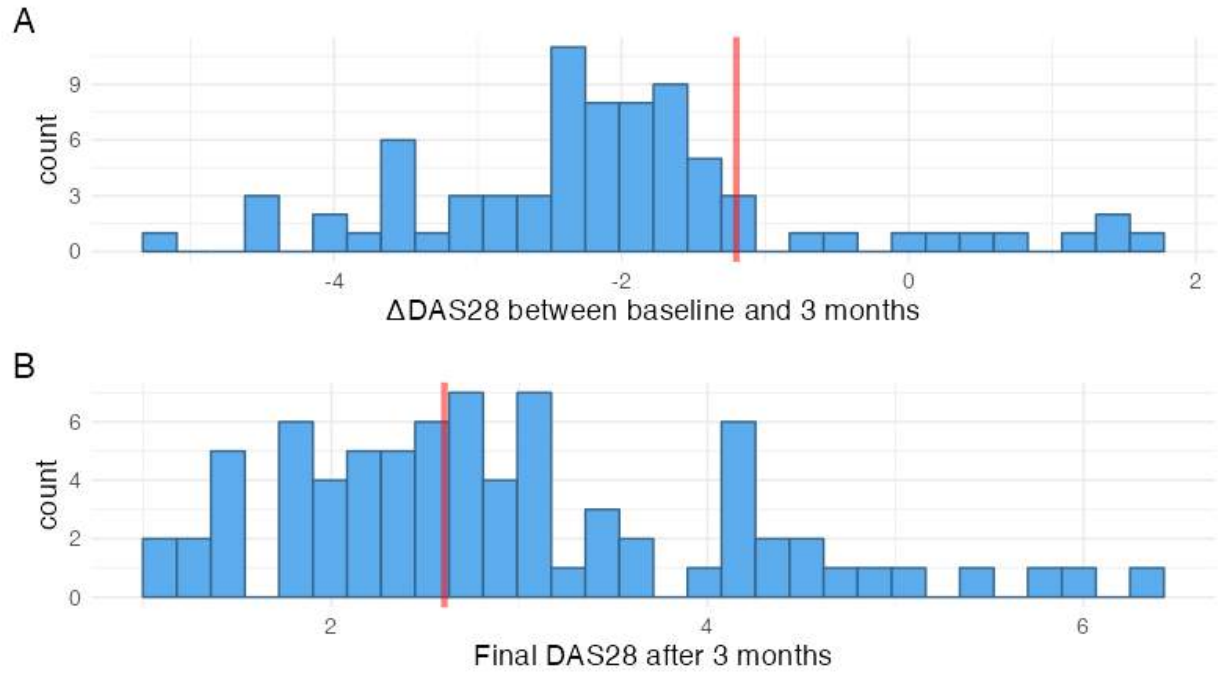

Figure 3.1.Histograms of DAS28-based responses to treatment after 3 months. A. ∆DAS28 over 3 months with red line marking change required to achieve low disease activity or a good response B) Final DAS28 after 3 months with the red line marking the remission threshold of the DAS28-ESR. The cut-offs were based on the EULAR recommendations for a good response (ΔDAS28) and remission (final DAS28).

3.3.3. Multivariate Analysis of TaSER Metabolome at Baseline

The results from the PCA of the baseline metabolome with the samples labelled based on their 3-month DAS28-ESR-based responses are shown in Figure 3.2. From the scree plot in Figure 3.2A, a shoulder was observed around PC3-4, indicating that PCs 1-3 were sufficient to explain the variance across the dataset. However, the low amount of variance described by each component meant that this approach was unlikely to be useful in understanding the influence of the metabolome across the samples and their response groups. The first PC (PC1) explained 8.4% of the variance across the samples, with PC2 describing 7% and PC3 describing 5.4%, as shown in Figure 3.2B-C.

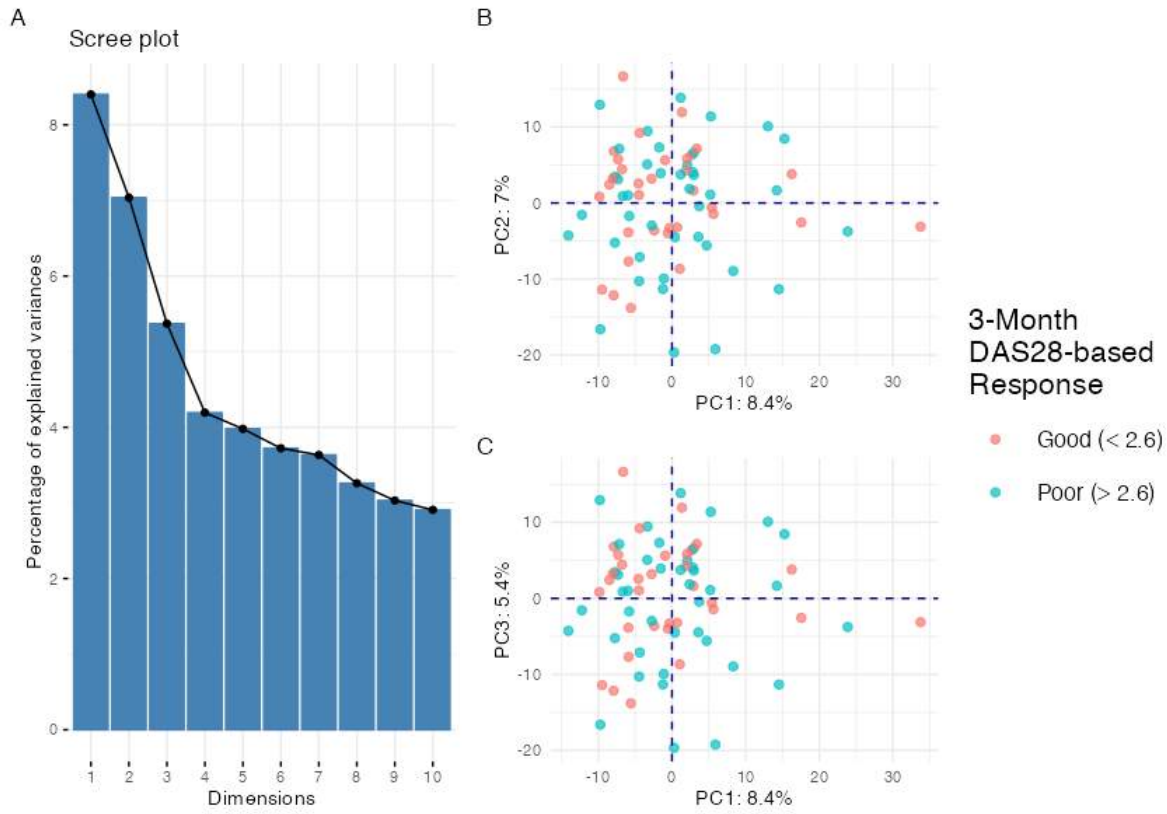

Figure 3.2. Principal components analysis results. A) Scree plot showing variance explained by each component. B. Scatter plots showing samples projected in space defined by PCs 1 and 2 with DAS28 responses labelled. C. Scatter plots showing samples projected in space defined by PCs 1 and 3 with the 3-month DAS28-based responses labelled.

The PCA plots did not reveal a discernible global separation of the samples at baseline based on the metabolome when the samples were labelled based on patient responses at 3 months. There was, therefore, no evidence from this analysis of a whole-metabolome profile of these response groups.

3.3.4. Explaining the Variance of the Metabolome

The factors influencing the variance of the metabolome were investigated with the results shown in Figure 3.3, with age being the most influential factor in explaining the variance across the entirety of the metabolome. The very high percentage for the residuals factor highlights that most of the variance of the metabolome is explained by factors not reported within this dataset.

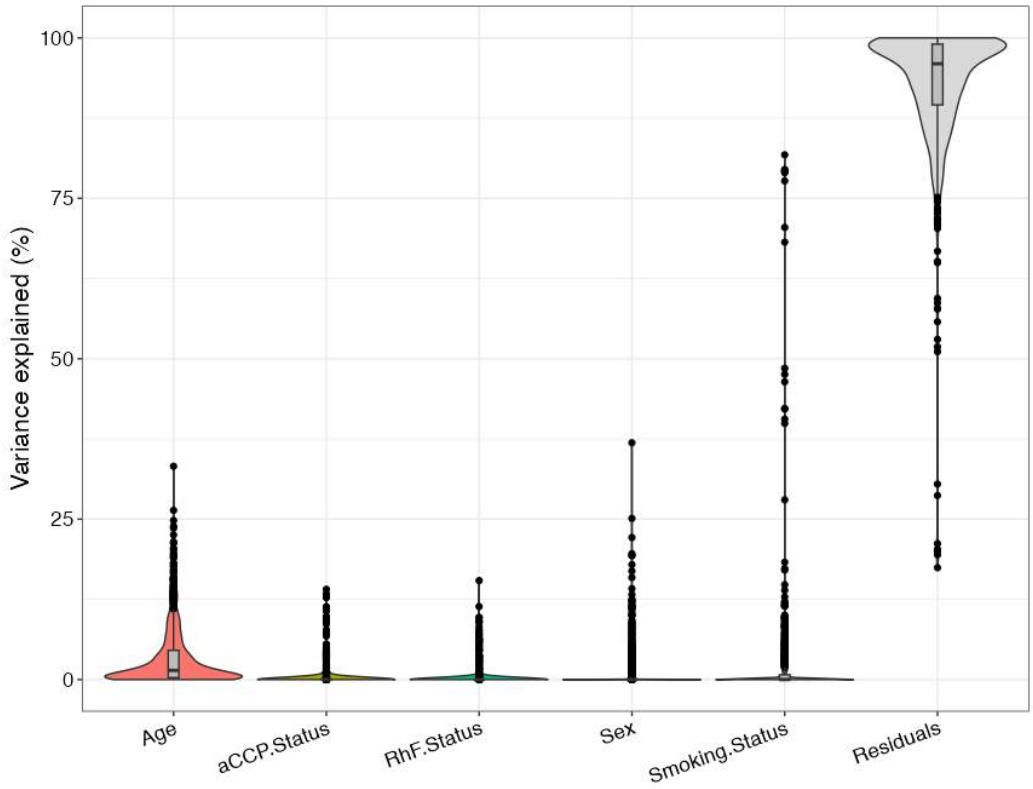

Figure 3.3. Violin plots show the influence of patient factors on the variance across the whole metabolome. Boxplots were superimposed to aid the visualisation of the distribution of the data.

Each factor considered in this analysis explained a relatively low variance, with age explaining the highest median variance of ~5%. The influence of age on the metabolome is becoming clearer, with the recent development of the metabolomic data repository, MetaboAge DB, demonstrating the increasing volume of data that describes the relationship between ageing and a changing metabolome in healthy individuals (Bucaciuc Mracica *et al.*, 2020). Indeed, the changes observed in the metabolome as individuals age may influence the emergence of diseases such as RA, where age is an established risk factor.

Interestingly, as indicated in the violin plot in Figure 3.3, smoking status explained a large proportion of the variance of the metabolome of a handful of patients with a variance up to ~80% for some individuals. This was anticipated due to the detection of nicotine-derived or other smoking-associated metabolites in these samples. Therefore, a search was performed for such features, including tentatively identifying nicotine, 2-hydroxynicotine and cotinine. These are shown

in Figure 3.4, and as expected, smoking status considerably influenced the variance of these metabolites. The caveat to this, and the remainder of the analysis here, is that no associated fragmentation data were generated as part of the TaSER study. Such data would allow a more comprehensive investigation into the nicotine-derived metabolites while providing greater confidence in identifying these features.

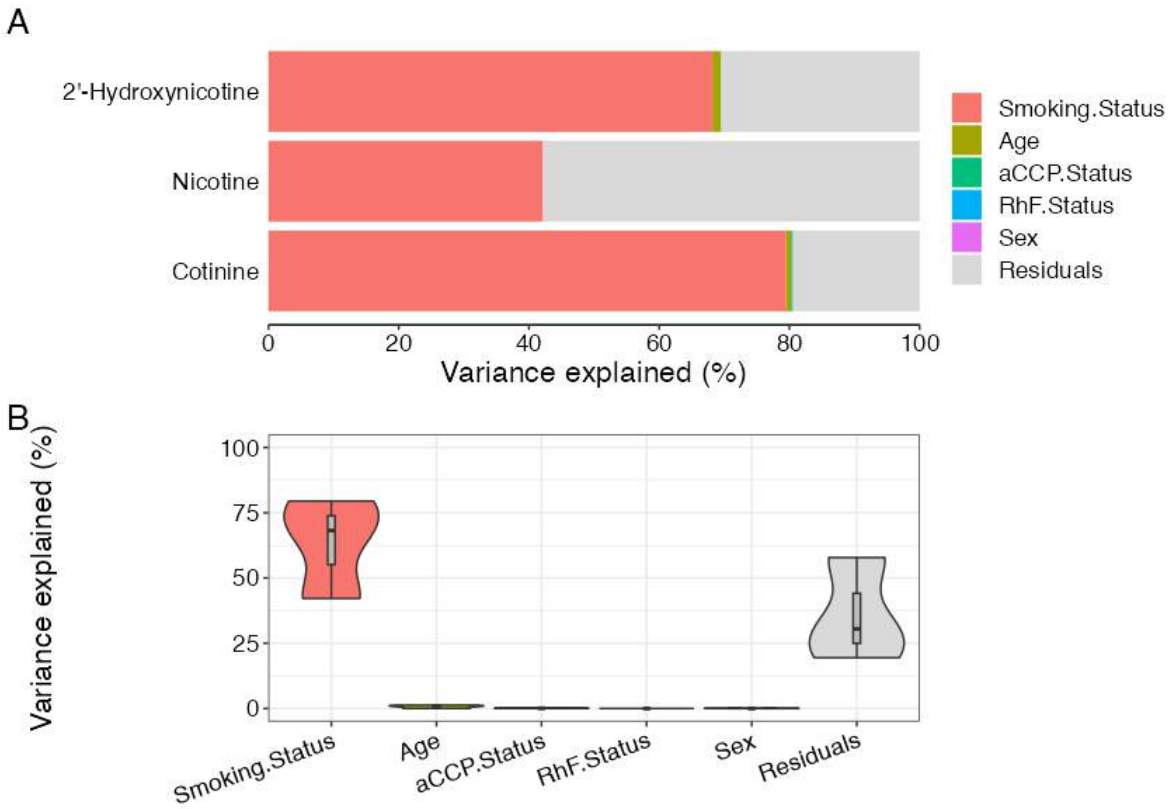

Figure 3.4. Explaining the variance across smoking-associated metabolites. A. Bar plot showing the influence of patient factors on metabolites in terms of the variance explained. B. Violin plots showing the average (median) variance explained across the metabolites of interest based on the patient factors.

3.3.5. Differential Analysis of Metabolites Across Response Groups

The results from the differential analysis of the metabolome features across the binary response groups are shown in the volcano plot in Figure 3.5. The response groups were defined based on the DAS28-ESR remission cut-off (3-month DAS28-ESR < 2.6), termed in this work as a good response with a poor response defined as

DAS28-ESR ≥ 2.6. Importantly, no significantly associated metabolites were found after the BH correction for multiple testing (Benjamini and Hochberg, 1995). This may reflect the subtlety of the metabolic changes across the groups, or the relatively large number of features compared with samples, which may hide biologically meaningful events after the p-value correction.

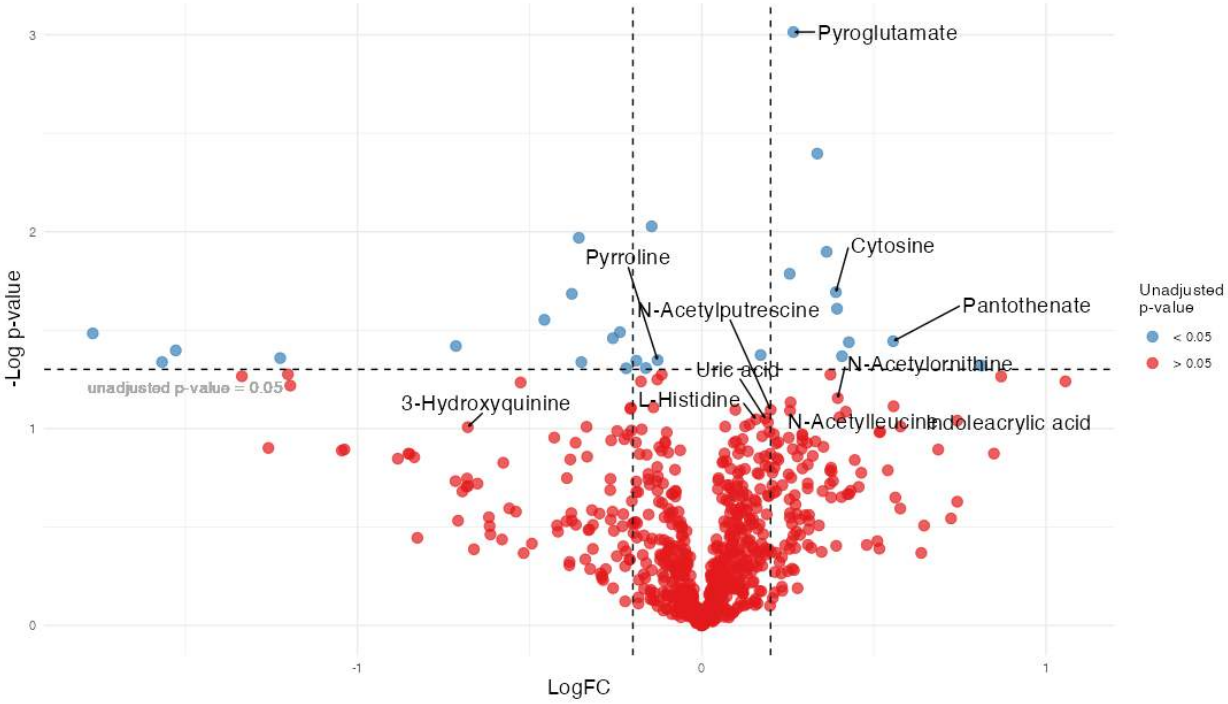

Figure 3.5. Volcano plot showing differential analysis of baseline peaks from both ion modes across response groups. Analytes were coloured based on their unadjusted p-values with a cut-off of 0.05 being used. Only metabolites with at least a tentative identification based on mass were labelled where these had an unadjusted p-value < 0.05.

The metabolites that were increased at baseline in the good responders included pyroglutamate, cytosine, pantothenate, indoleacrylic acid, N-acetylornithine, N-acetylleucine, L-histidine, N-acetylputrescine, and uric acid. This group of metabolites had unadjusted p-values less than 0.05 and were showed only small difference in the metabolite abundances between the response groups. Nevertheless, the fact that the acetylated derivatives of ornithine and putrescine had slight increases in their abundance in the good responders may be biologically meaningful. For instance, these may be linked to increased arginase activity, which may be elevated in patients with RA compared with healthy individuals (Chandrasekharan *et al.*, 2018).

Considering the lack of statistical significance and noting the small fold change of the metabolites, the features with a log fold change > 0.1 or < -0.1 were selected from the differential analysis. The features from this list that had at least tentative identifications underwent pathway analysis with the results in Figure 3.6.

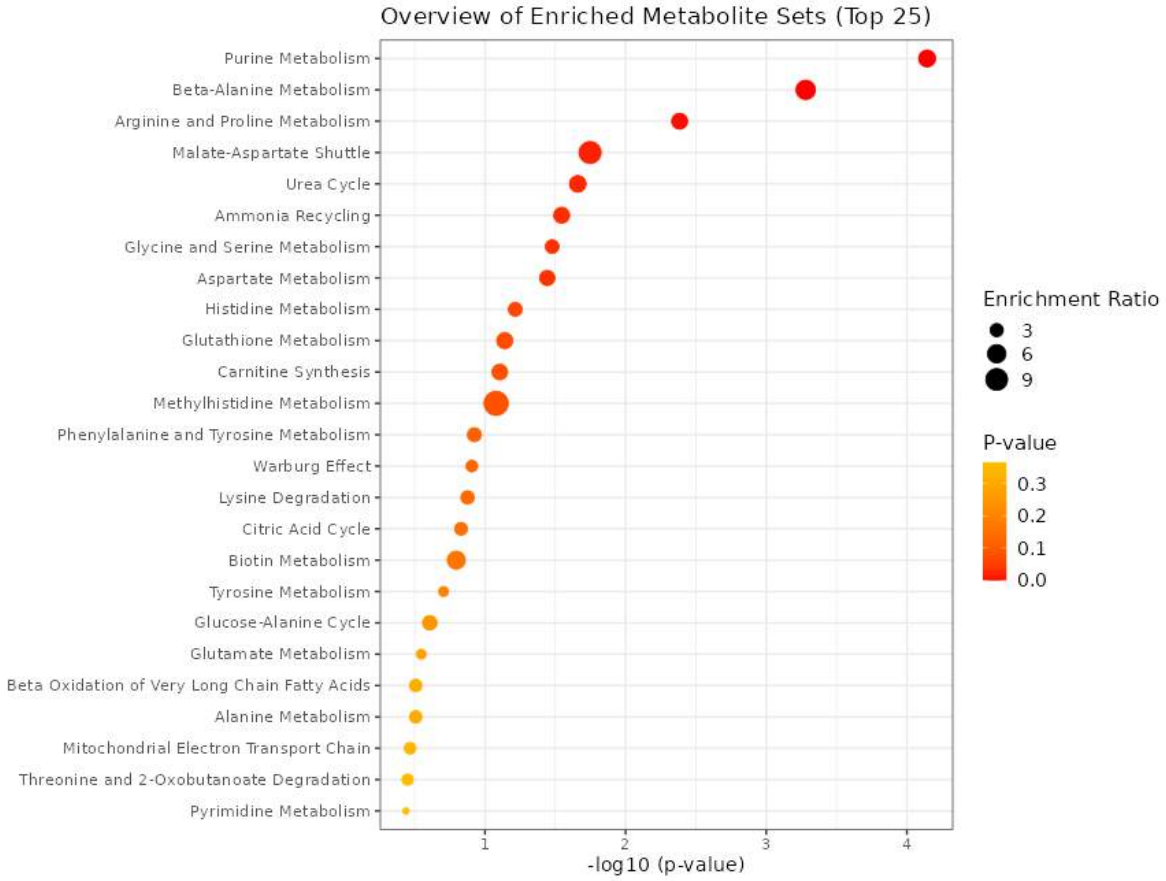

Figure 3.6. Pathway analysis from most differentially abundant metabolites from TaSER cohort shown as dots representing the extent of the enrichment, in terms of enrichment ratio and significance. Plot was generated using the MetaboAnalyst MSEA tool for overrepresentation analysis.

The most enriched pathways included purine metabolism, arginine and proline metabolism and the urea cycle, which included fumarate, glutamate, 2-oxoglutarate, ornithine, guanidinoacetate and citrulline from the differentially abundant metabolites. However, care needs to be taken when interpreting these findings since the metabolite identification is often biased towards those that can be identified most easily where reference standards can be found, for example, amino acids. Nevertheless, the perturbations of the amino-acid pathways may be biologically meaningful and will be assessed alongside the additional findings

throughout this work. Additional pathways are still likely to be present and are expected to be uncovered with the use of larger reference libraries and the use of fragmentation methods to aid metabolite identification.

3.3.6. Correlation Analysis of Baseline Metabolites

All peaks were included in the correlation analysis, involving the baseline peak intensities being correlated against the 3-month DAS28 scores, with the results shown in Figure 3.7. Spearman correlation coefficients ranged from 0.23 to 0.33 in both positive and negative directions, with the strongest correlation shown for the peak with a m/z ratio = 85.064 and RT of 8.208.

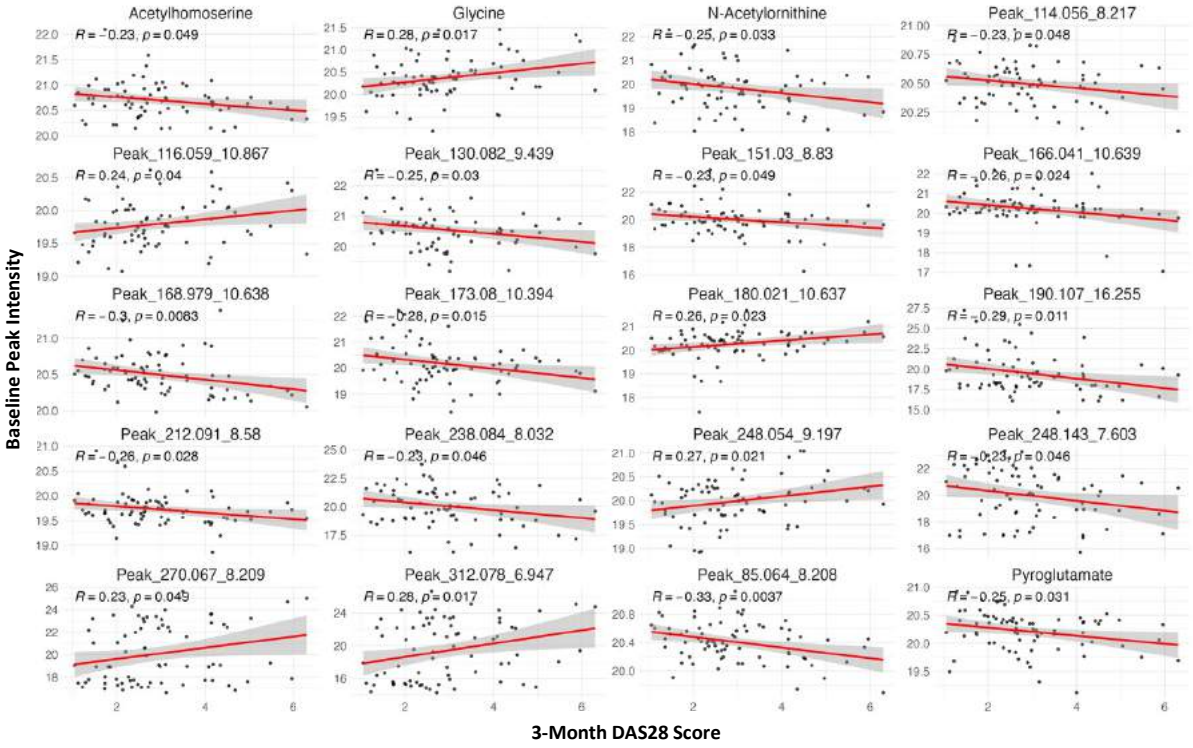

Figure 3.7. Correlations of baseline metabolomic signals and 3-month DAS28. For each signal, the relationship between the peak abundance at baseline and the disease activity at 3-months was determined by calculating the Spearman correlation coefficient and p-values.

However, upon investigating the quality of this peak using the *PeakML viewer* tool, it was apparent that this was not a quality signal, and its m/z ratio did not match that of any known metabolite within the mass accuracy of 3 ppm used for the study. Since a similar pattern was seen across the other non-annotated peaks in this analysis, only those that could be tentatively annotated and had quality signals

were reported in detail. These included acetyl homoserine (R=-0.23, p =0.049), glycine (R=0.28, p=0.017), N-acetyl ornithine (R=-0.25, p=0.033) and pyroglutamate (R=-0.25, p=0.031), shown in Figure 3.7.

3.3.7. Subgroup Analysis

Further analysis was performed on subgroups defined using the established risk factors for RA. These included age, smoking status, sex, rheumatoid factor (RhF) status and ACPA status (Deane *et al.*, 2017).

The differential abundance of the metabolites at baseline was assessed within each of the subgroups, as were the correlations between the metabolites and the DAS28 measures (DAS28 after 3 months and final DAS28 after 3 months). The subgroups were defined as follows:

- age: <= 50 years, > 50 years
- sex: male; female
- smoking status: current smoker, former smoker, non-smoker
- RF status: positive, negative
- ACPA status: positive, negative

None of the metabolites were significantly associated with the disease activity in any subgroups (adjusted p-value < 0.05). Additionally, the subgroups were combined to produce a ‘high-risk’ individual, such as a post-menopausal (> 50 years old) smoker with an autoantibody-positive status. However, a subgroup-specific metabolomic profile of responses remained elusive since no metabolites were significantly associated with response, potentially due to the decreasing number of patients found within each individual/composite subgroup. A larger sample size was required to generate such a metabolomic profile with any confidence.

3.3.8. Developing a Baseline Metabolic Profile Associated with Treatment Response

The previous sections revealed no robust associations between the individual metabolites and the 3-month treatment response. As such, a supervised machine learning approach was taken to investigate whether a combination of metabolites could be uncovered that were associated with the 3-month outcomes. This was expected to reveal a panel of metabolites that could be used to predict the outcome of future patients with a similar profile.

3.3.9. Feature Selection

The feature selection results, using the RFE algorithm, are shown in Figure 3.8, including pyroglutamate, L-kynurenine, indoleacrylic acid, pyrroline, cytosine, N-succinyl L-citrulline, L-ornithine and 5-methylcytidine.

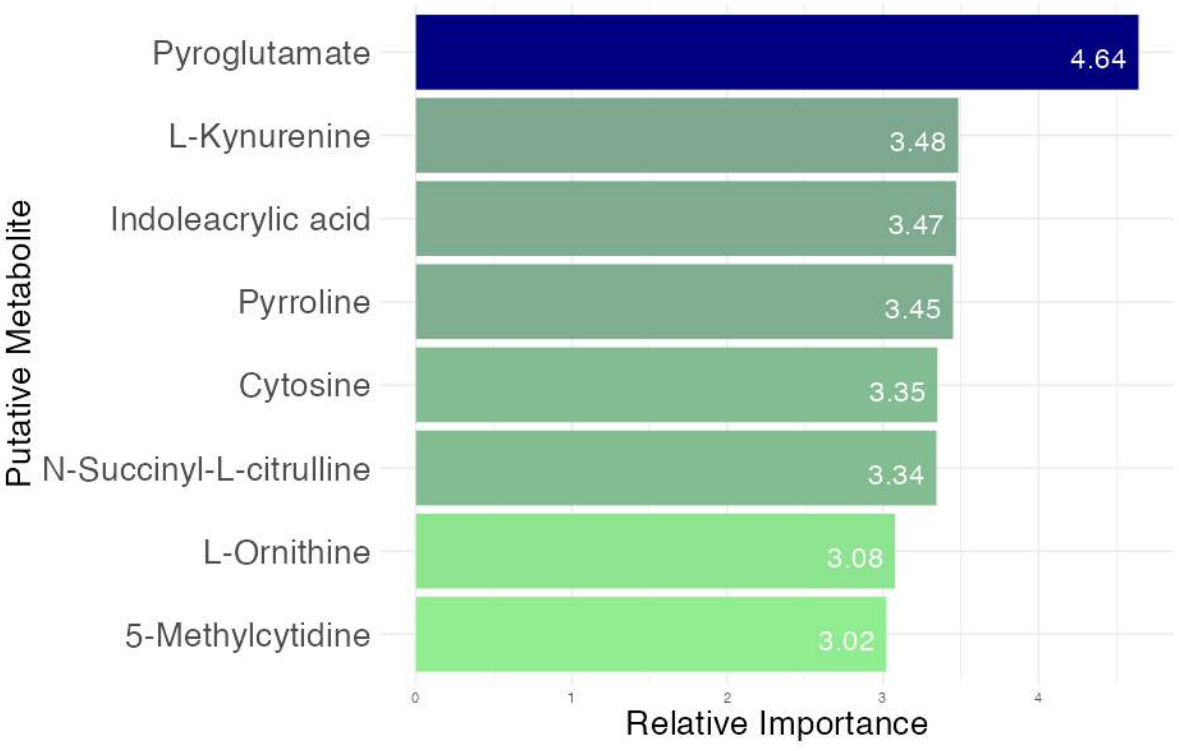

Figure 3.8. Bar plot showing the results from the feature selection for the metabolites model. The metabolites were selected using the recursive feature elimination algorithm and were ranked using their relative importance for the classification of samples to response groups.

It is notable that L-ornithine was selected for the model, where the acetylated derivative was one of the few correlating metabolites with the 3-month DAS28.

Both metabolites were identified through their shared m/z ratio and RT to the authentic standards. However, these metabolites did not correlate significantly with each other, indicating that the acetylated derivative was not directly reflective of levels of ornithine in the circulation.

3.3.10. Algorithm Selection

Seven commonly used machine learning algorithms were evaluated for use in the model, with the results shown in Figure 3.9 with the ROC curves being plotted. The extreme gradient boosting (XGB) algorithm was selected for the final model, with the best performance in terms of the AUC-ROC and the MCC, shown in Figure 3.9 and Table 3.3. Within the training set, the XGB algorithm achieved an AUC-ROC of 0.76 (95% CI: 0.63-0.89) and an MCC of 0.528 after a 10-fold cross-validation was repeated 10 times.

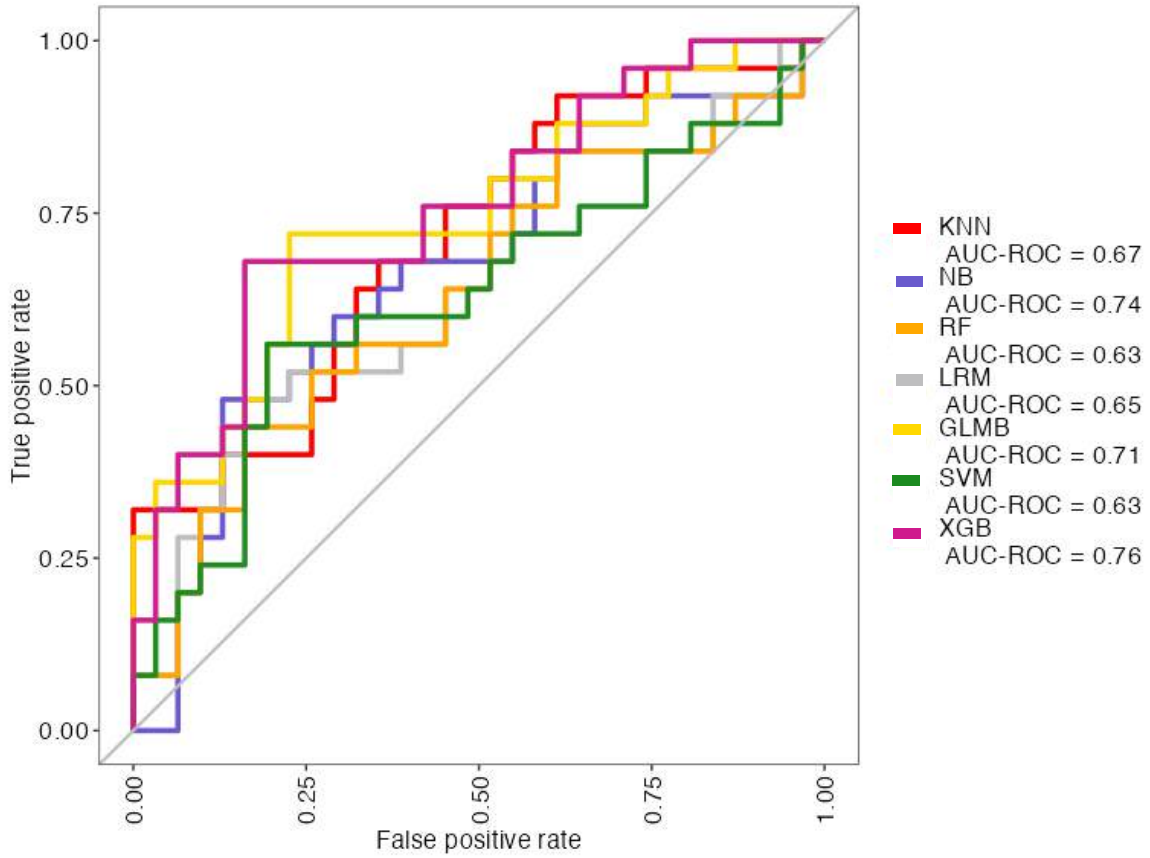

Figure 3.9. ROC curves shown for the algorithm optimisation process, involving seven commonly used classification algorithms in supervised machine learning. The algorithms' ROC curves were plotted together to allow a comparison of their performances and the AUC-ROC values were used as primary metric for the selection.

Table 3.3. Performance metrics for the algorithm testing for the generation of the TaSER metabolites model. Highlighted in green is the XGB algorithm which was used in the final model after comparing its performance metrics to the other algorithms tested.

Measure	KNN.Score	KNN.CI	NB.Score	NB.CI	RF.Score	RF.CI	LRM.Score	LRM.CI	GLMB.Score	GLMB.CI	SVM.Score	SVM.CI	XGB.Score	XGB.CI
SENS	0.560	0.37-0.73	0.440	0.27-0.63	0.560	0.37-0.73	0.520	0.33-0.7	0.520	0.33-0.7	0.520	0.33-0.7	0.68	0.48-0.83
SPEC	0.710	0.53-0.84	0.871	0.71-0.95	0.613	0.44-0.76	0.710	0.53-0.84	0.710	0.53-0.84	0.806	0.64-0.91	0.839	0.67-0.93
MCC	0.273		0.349		0.172		0.234		0.234		0.343		0.528	
TP	14.000		11.000		14.000		13.000		13.000		13.000		17.000	
FP	9.000		4.000		12.000		9.000		9.000		6.000		5.000	
TN	22.000		27.000		19.000		22.000		22.000		25.000		26.000	
FN	11.000		14.000		11.000		12.000		12.000		12.000		8.000	
AUC-ROC	0.670	0.53-0.81	0.740	0.61-0.87	0.630	0.48-0.78	0.650	0.5-0.8	0.710	0.57-0.85	0.630	0.48-0.78	0.760	0.63-0.89
AUC-PR	0.570		0.710		0.560		0.580		0.670		0.570		0.700	

3.3.11. ROC Curves and Performance Metrics

The final model's performance in the testing subset of data is reflected by the ROC curve in Figure 3.10A. Further performance metrics are shown in Figure 3.10B. With an AUC-ROC value of 0.77 (95% CI: 0.54-1.00) and an MCC of 0.575, the XGB model performed relatively well in its prediction of patient responses after 3 months within the testing set. However, the wide CI shown for the AUC-ROC may reflect the high variance of the metabolite abundances across the response groups used in the classification. A larger sample size would provide greater confidence in this panel of metabolites in its prediction of patient responses. Nevertheless, these findings point towards the selected metabolites having a predictive ability and association with the clinical response.

A

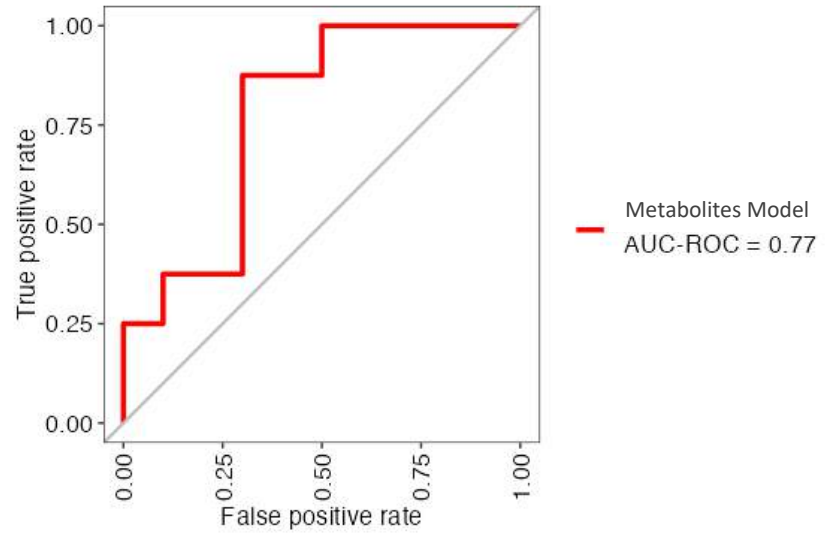

B

Metric	Score	CI
SENS	0.875	0.53-0.98
SPEC	0.700	0.4-0.89
MCC	0.575	NA
Informedness	0.575	NA
PREC	0.700	0.4-0.89
NPV	0.875	0.53-0.98
FPR	0.300	NA
F1	0.778	NA
TP	7.000	NA
FP	3.000	NA
TN	7.000	NA
FN	1.000	NA
AUC-ROC	0.770	0.54-1
AUC-PR	0.600	NA
AUC-PRG	0.200	NA

Figure 3.10. Model's performance from TaSER metabolome in the testing subset of the data. A. ROC curve of model's performance in testing subset B. Performance metrics of the final model.

3.3.12. Feature Interpretation: Shared Pathways

Model-agnostic interpretation methods are increasingly being used to understand the involvement of individual features within the model (Ribeiro, Singh and Guestrin, 2016). The correlations between the baseline metabolites included in the model are shown in Figure 3.11, where only weak correlations were observed between each pair of metabolites.

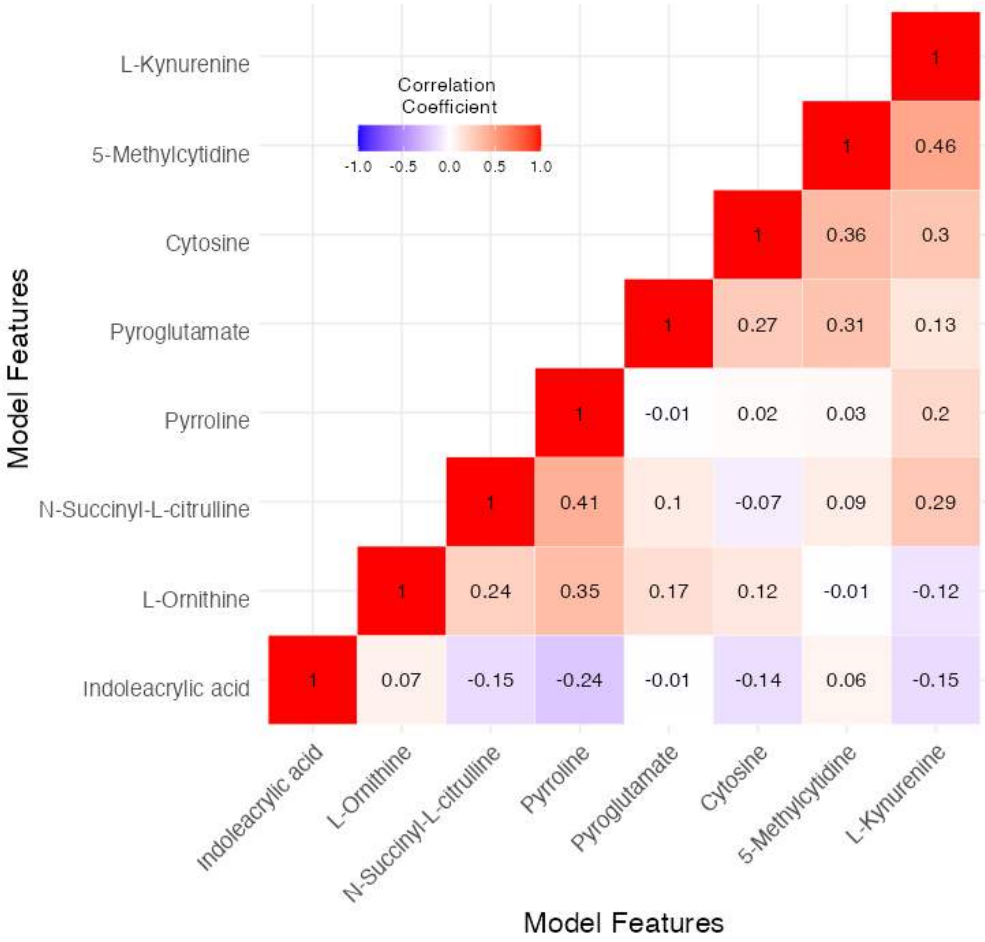

Figure 3.11. Correlation heatmap of metabolites from the model. Spearman correlation coefficients calculated for each metabolite pair.

Several of the metabolites from the model can be mapped to a shared network of pathways involving arginine metabolism and the urea cycle, with the caveat that their identity was not confirmed. Among these metabolites included L-ornithine, N-succinyl L-citrulline and pyrroline, which were all positively correlated with each other. Since these metabolites collectively contributed to the metabolic profile associated with the response to MTX, the question arose whether changes to the activity of arginine metabolism and the urea cycle contribute towards a favourable molecular environment for the action of MTX in resolving inflammation.

3.3.13. Model Agnostic Feature Interpretation Methods

There were non-linear relationships for each metabolite included in the model at their baseline abundance with the probability of predicting a positive response, as

shown in the ALE plots in Figure 3.12A. The SHAPP in Figure 3.12B shows the additive contribution of the metabolites on the model, although this provides only an insight into influence at a given metabolite abundance so does not provide the same level of insight as the ALE plots.

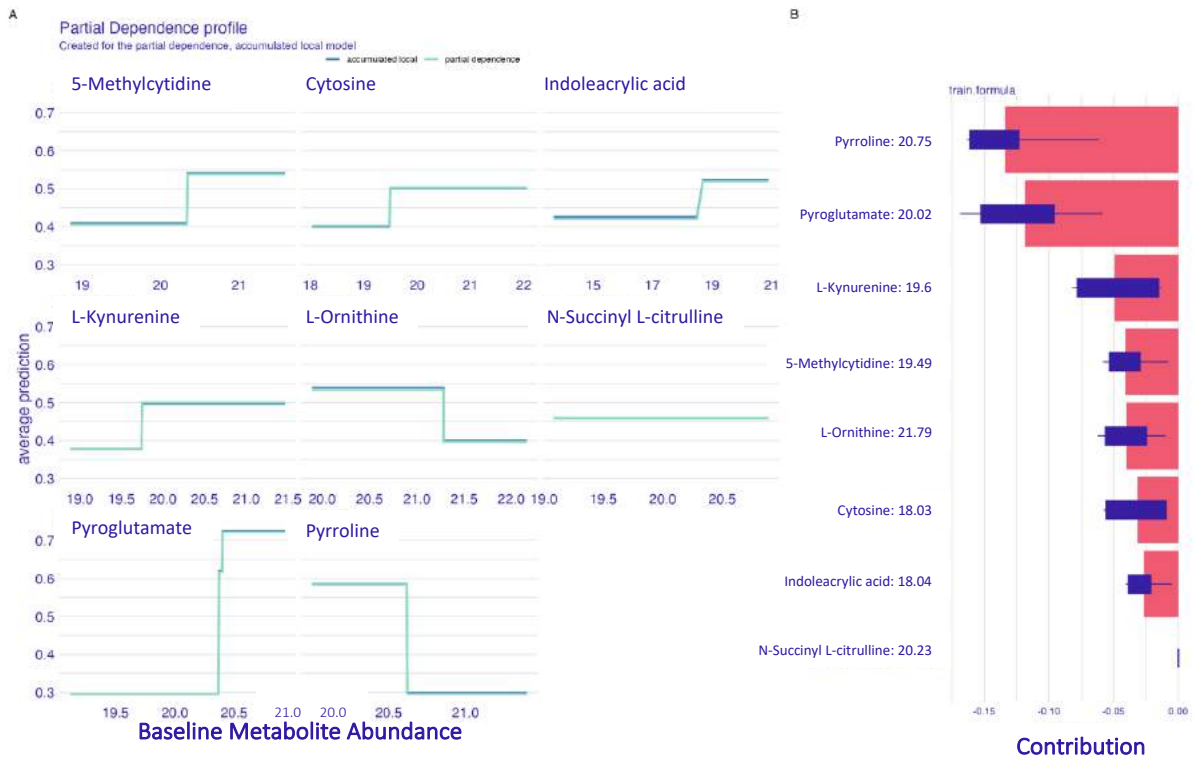

Figure 3.12.Model agnostic interpretation methods for the features included in the TaSER metabolite model. A) Partial dependence and accumulated local effects plots. B) Shapley Additive Explanation Plot (SHAPP).

Across their ranges of abundances across the cohort, higher levels of cytosine, indoleacrylic acid, L-kynurenine, and pyroglutamate were associated with a greater probability of predicting a good response. Meanwhile, lower levels of L-ornithine, N-succinyl L-citrulline and pyrroline were associated with a lower probability of predicting a good response. The influence of N-succinyl L-citrulline

on the model was not clear from these plots, potentially indicating only a marginal association with response.

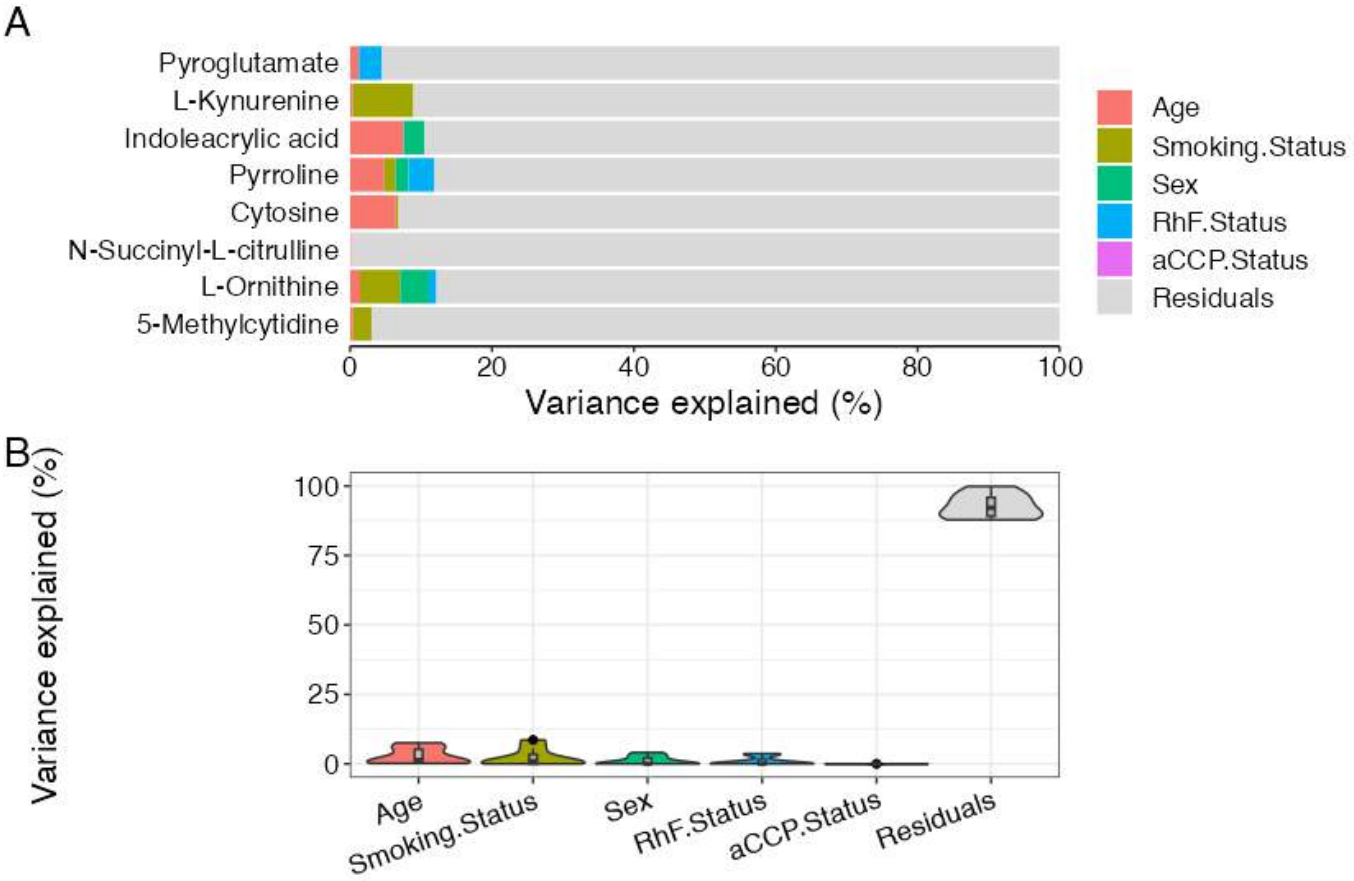

Figure 3.13. Influence of patient factors on the variance of the model's metabolites in the TaSER cohort. A. Bar plot of variance explained of each feature by patient factors B. Violin plot of variance explained of features by patient factors.

The influence of established risk factors on the variance of the metabolites in the model was assessed using the *variancePartition* tool, with the results shown in Figure 3.13. Smoking status appeared to have a pronounced influence on the variance of L-kynurenine abundance in the cohort. This was explored further where the differential abundance of L-kynurenine across the current, non-smokers and former smokers showed a significant increase in non-/former-smokers compared to current smokers, as shown in Figure 3.14.

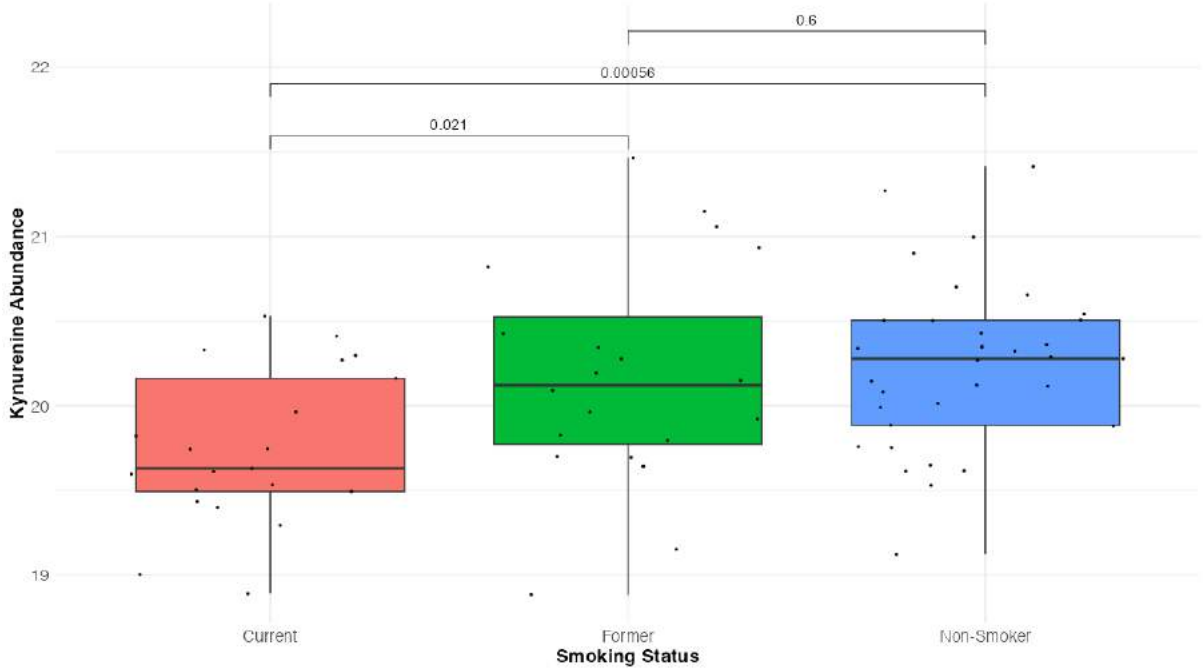

Figure 3.14. Boxplot showing kynurenine abundance across the smoking status groups. Plotted across smoking status groups are the p-values, calculated using Wilcoxon tests.

The reduction in L-kynurenine in current smokers may be due to the suppression of IDO activity in smokers (Pertovaara *et al.*, 2006). This smoking-induced reduction of L-kynurenine may be clinically important owing to the immunomodulatory effects described for this metabolite, possibly leading towards a greater inflammatory profile in patients (Mathai *et al.*, 2016).

Interestingly, a combination of the factors included in Figure 3.13 could explain only up to ~10% of the variance of most of the metabolites in the model, except for N-succinyl L-citrulline, which had virtually none of its variance explained by these factors. Compared to the other metabolites, tentatively identified N-succinyl L-citrulline had virtually none of its variance explained by patient factors which cast concern over its biological identification. It was uncertain whether the signal for this metabolite was actually an artefact detected from the instrumentation. The lack of influence that N-succinyl L-citrulline showed in the feature interpretation plots in Figure 3.12A also led to concern over its identification.

Age appeared to be an important factor in explaining the variance of cytosine and indoleacrylic acid, pyrroline, and cytosine, as well as pyroglutamate and L-ornithine, although to a much lower degree. Indeed, age-related changes to

tryptophan-derivatives, such as indoleacrylic acid, have been reported and may be attributed to changes in the microbiome over the lifespan (Ruiz-Ruiz *et al.*, 2020; Wu *et al.*, 2021). Smoking status influenced the variance of L-kynurenine and L-ornithine. In contrast, the RhF status and ACPA status contributed to the variance of pyroglutamate. As was seen with the similar analysis of the entirety of features included in Figure 3.3, there was a large contribution of the residuals on the variance of the metabolites in the model. The fact that these metabolites were detected in patients' circulation meant that numerous factors, including homeostatic processes and environmental factors, were likely to explain their variances across the samples.

3.3.14. Actual Differences in Metabolite Abundance

The actual changes of the metabolites from the model are shown in Figure 3.15, with their baseline abundances plotted in relation to the patients' 3-month DAS28-based response. As indicated in the univariate analysis performed earlier, only small differences were found in the abundances of these metabolites between the EULAR-defined response groups.

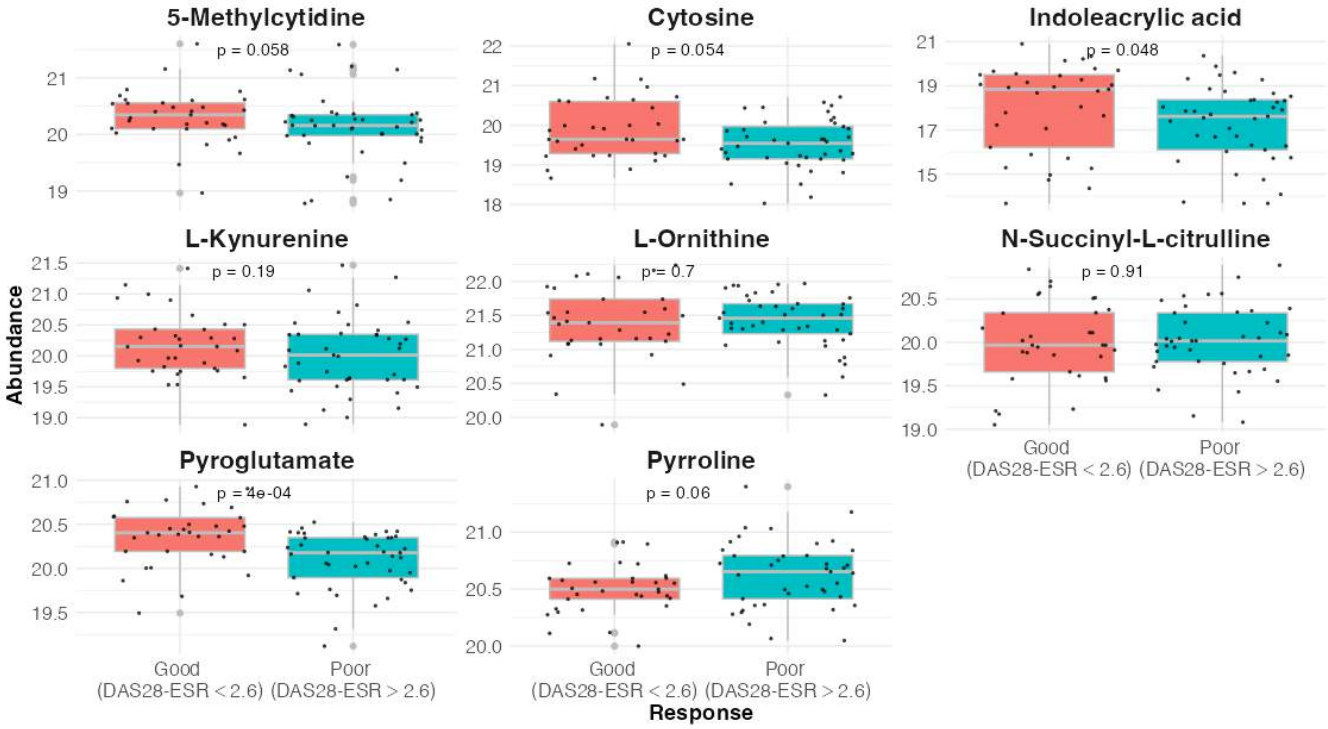

Figure 3.15. Differential abundance showing actual changes in metabolites from the TaSER model across the 3-month DAS28-ESR response groups.

While the earlier univariate analysis did not highlight any significant changes across the features in the metabolome, there were some potentially meaningful differences in the metabolites in the model across the response groups. Herein lies the power of the model — the individual metabolites that were weakly associated with treatment response were combined to provide a predictive tool that was more robust than its parts. Nevertheless, care needs to be taken in interpreting these findings, where it was apparent from the plots in Figure 3.15 that there was substantial variance in the abundances of most of the metabolites in both response groups. Where the variances overlapped across the response groups for the metabolites, it may be questioned whether these would provide robust biomarkers of response even if included alongside others in a model. However, since only relative quantification was achieved for these metabolites, an important subsequent step would involve performing a targeted analysis of the samples to provide absolute measurements of these metabolites. However, this was not achieved as part of this project.

Notably, only indoleacrylic acid and pyroglutamate had abundances significantly different across response groups, both being increased in good responders. Meanwhile, pyrroline was borderline significant, being increased in poor responders. Since pyrroline was correlated with and biologically linked to L-ornithine and N-succinyl L-citrulline, the increased activity of the urea cycle — giving rise to increased ornithine, which can be converted to pyrroline — may act as a valuable biomarker of response. However, further doubt over the biology of what was tentatively identified as N-succinyl L-citrulline was raised where there was no apparent difference in its abundance across response groups. From the previous results involving this feature, it was increasingly apparent that it was likely included in the model because of background noise within the data which influenced the modelling process.

3.3.15. Disease Measures and Composite Models

This section aimed to determine whether the metabolite model offered a better predictive tool than the baseline disease measures that may be used in the clinic to predict patient responses. The comparison of the models is shown in Figure 3.16 and Figure 3.17.

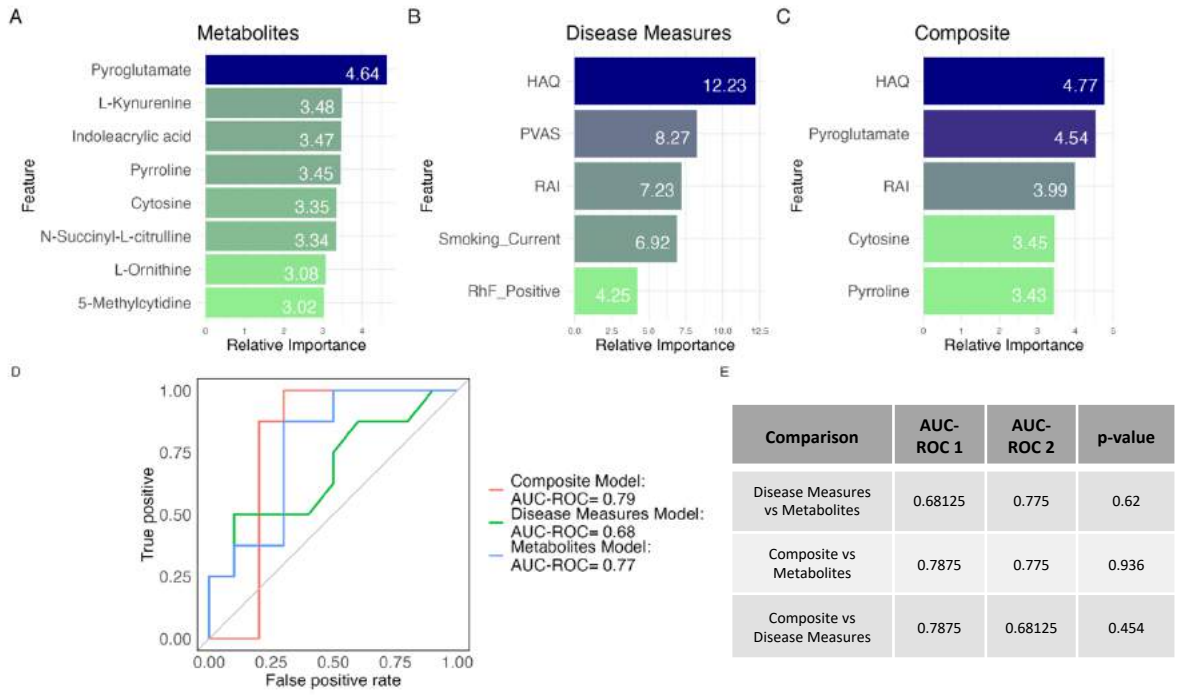

Comparison	AUC-ROC 1	AUC-ROC 2	p-value
Disease Measures vs Metabolites	0.68125	0.775	0.62
Composite vs Metabolites	0.7875	0.775	0.936
Composite vs Disease Measures	0.7875	0.68125	0.454

Figure 3.16. Generation and comparison of metabolites, disease measures and composite model. A-C. Feature selection for respective models. D. ROC curves of each model compared. E. DeLong's statistical tests for two ROC curves.

A

Metabolite Model

Metric	Score	CI
SENS	0.875	0.53-0.98
SPEC	0.700	0.4-0.89
MCC	0.575	NA
Informedness	0.575	NA
PREC	0.700	0.4-0.89
NPV	0.875	0.53-0.98
FPR	0.300	NA
F1	0.778	NA
TP	7.000	NA
FP	3.000	NA
TN	7.000	NA
FN	1.000	NA
AUC-ROC	0.770	0.54-1
AUC-PR	0.600	NA
AUC-PRG	0.200	NA

B

Disease Measures Model

Metric	Score	CI
SENS	0.500	0.22-0.78
SPEC	0.900	0.6-0.98
MCC	0.444	NA
Informedness	0.400	NA
PREC	0.800	0.38-0.96
NPV	0.692	0.42-0.87
FPR	0.100	NA
F1	0.615	NA
TP	4.000	NA
FP	1.000	NA
TN	9.000	NA
FN	4.000	NA
AUC-ROC	0.680	0.42-0.94
AUC-PR	0.560	NA
AUC-PRG	0.090	NA

C

Composite Model

Metric	Score	CI
SENS	1.000	0.68-1
SPEC	0.700	0.4-0.89
MCC	0.714	NA
Informedness	0.700	NA
PREC	0.727	0.43-0.9
NPV	1.000	0.65-1
FPR	0.300	NA
F1	0.842	NA
TP	8.000	NA
FP	3.000	NA
TN	7.000	NA
FN	0.000	NA
AUC-ROC	0.790	0.57-1.01
AUC-PR	0.570	NA
AUC-PRG	0.300	NA

Figure 3.17. Performance metrics of TaSER models in test subset. A. Metabolites model. B. Disease measures model. C. Composite model.

Disease Measures Model

Firstly, the features were selected using the same RFE algorithm as the metabolites model, with features included in the disease measures model shown in Figure 3.16B, including HAQ, PVAS, smoking status (current smoker), RAI and RF status (positive). The selected features were then used in multiple models that

were tuned for their hyperparameters, and the best-performing algorithm was selected. After choosing the KNN algorithm as the best-performing algorithm, the model was adjusted and evaluated in the test subset, achieving an AUC-ROC of 0.68 (95% CI: 0.42-0.94) and MCC of 0.444, with these results shown in Figure 3.16B.

Composite Model

By combining the metabolomic data and patient/disease measures data into a single model, shown in Figure 3.16C. It was anticipated that a more robust model could be developed, using features from different data types to predict patient responses. As with the metabolites and disease measures models, the composite model was generated using the same train/test data split and with a similar workflow. The selected features included those observed in the two prior models, including HAQ, pyroglutamate, RAI, cytosine and pyrroline. The final model performed marginally better than the previous, with an AUC-ROC of 0.79 (95% CI: 0.57-1.01) and an MCC of 0.714, as shown in Figure 3.16D.

3.3.16. Comparison of Models

Compared with the performance of the metabolites model (AUC-ROC: 0.77), the composite model (AUC-ROC: 0.79) appeared slightly superior when comparing the ROC curves, as shown in Figure 3.16D. However, Delong's test for two ROC curves revealed no significant difference (p=0.936), with a table describing the statistics in Figure 3.16E. This statistical test showed no evidence that the composite model predicted the 3-month DAS28-based response better than the metabolites model. The disease measures model did not perform as well as the other two models (AUC-ROC: 0.68) although, again, the Delong's test did not reveal any significant difference across the models' ROC curves, shown in Figure 3.16E.

Additional metrics were provided to compare these models, including MCC shown in Figure 3.17. This indicated that the metabolite model (MCC: 0.575) performed relatively well in predicting the responses compared to the other models, although the composite model appeared to perform better (MCC: 0.714). Nevertheless, based on the ROC curves, the metabolite model was just as accurate in predicting

the patient outcomes as the other models consisting of patient factors in the testing subset of the TaSER cohort.

3.4. Discussion

3.4.1. Summary of Key Findings

The TaSER trial and the metabolomic analysis on its plasma samples provided an opportunity to develop a baseline molecular profile of RA patient responses to MTX. Since RA is an autoimmune disease with a critical immune component, the changing immune activity in response to treatment may be reflected by changes to the metabolism. For example, succinate, lactate and itaconate have been linked to altered immune cell activity and may be detected in the circulation of patients (Rubic *et al.*, 2008; Lampropoulou *et al.*, 2016; Hooftman and O'Neill, 2019; Pucino *et al.*, 2019; Daly *et al.*, 2020).

It was hypothesised that differences in metabolite levels in the circulation at baseline would be observed in patients who experienced differing responses to treatment. These differences may reflect a molecular profile in patients with a greater propensity to respond to treatment, potentially due to establishing a metabolic environment favouring MTX's successful action. As a result, developing a predictive tool that measures multiple metabolites associated with response would provide a more precise medical approach to guide optimal treatment for patients based on their individual molecular needs. However, it may also provide insights into novel treatment strategies, such as supplementing MTX with exogenous immunomodulatory metabolites.

From the analyses performed in this section, it was concluded that tryptophan and arginine related metabolic pathways were notably associated with the response to MTX treatment in the TaSER cohort. While the individual metabolites in the predictive model were weakly associated with the treatment response, it was their collective association within the model that proved to be most revealing of the metabolic pathways potentially associated with the response. However, given the tentative identifications for several of these metabolites, including N-succinyl L-citrulline and indoleacrylic acid, re-running the samples using a tandem MS approach to generate fragmentation data would assist in identification of the

metabolites. Moreover, while promising in predicting patient outcomes in the TaSER cohort, these findings ought to be validated in an independent cohort and determine whether the metabolites are robust biomarkers for use across demographics and geographical regions. Nevertheless, the results described in this section mark an important first step in this project, not only in generating preliminary findings which describe metabolic associations with treatment response but also in developing an analytical workflow that was expected to be similarly useful in guiding biomarker discovery in other datasets.

3.4.2. Considering Future Clinical Applications

While a clinically helpful tool might involve a sample-to-lab-based approach, where patient samples would be analysed using a validated quantitative mass spectrometer-based approach, an alternative would involve a lab-to-sample approach (Steigmann *et al.*, 2020). This would involve the tool being available at the point-of-care (POC) — in other words when a patient visits the clinic for initial diagnosis or monitoring.

The development of such a tool is increasingly feasible where POC chip-based technologies have demonstrated accuracy and clinical value in diagnosing patients (Wu *et al.*, 2018). For example, the Abbot i-STAT analyser uses chip technology to measure a variety of blood markers, including pH, lactate, blood gases, glucose, and creatinine, providing a measurement within two minutes with a handheld device that can be used at a patient's bedside (NICE, UK). Opportunities for similar technologies can be found where patients with chronic diseases require regular biomarker monitoring. In this case, treatment decisions may be made based on a patient's molecular profile. A recent technological development using a complementary metal oxide silicon chip platform measured four metabolites, including glutamate, choline, sarcosine and the total L-amino acids from the plasma of patients with prostate cancer (Annese *et al.*, 2021). In its initial study, this technology could measure multiple metabolites from a patient's plasma sample and performed well in detecting prostate cancer, with an AUC-ROC of 0.78, while also ticking off a number of the REASSURED criteria for a POC diagnostic tool (real-time, ease of sample collection, affordable, sensitive, specific, user friendly,

rapid and robust, equipment free and deliverable to the intended end users) (Annese *et al.*, 2021; Otoo and Schlappi, 2022).

Developing a similar tool to concurrently measure circulating metabolites in patients with inflammatory rheumatic diseases to guide their treatment would be the ideal culmination of this work, recommending treatment options for patients based on their metabolic profile. However, the metabolic model requires further development at this early point in the process.

3.4.3. Development of a Response-Associated Metabolomic Profile

Single metabolites with clear differential abundances across study variables, such as patient responses, may be rare and provide a narrow view of the potential metabolic mechanisms that may lead to such responses. In a heterogeneous disease like RA, incorporating multiple markers into a model rather than using a single molecule may be more helpful, providing a more robust predictive tool and a more comprehensive picture of the molecular mechanisms potentially at play. This may be especially true if molecules found within the same biological pathways are included in the model.

A predictive molecular profile to guide treatment strategies for patients with RA is urgently needed to improve outcomes and avoid the administration of treatments that not only produce unpleasant side effects but are often ineffective in controlling the disease. Previous work has indicated metabolic markers of responses to treatment in RA, and this work aims to expand on these previously reported findings (Cuppen *et al.*, 2016; Gosselt *et al.*, 2020; Hur *et al.*, 2021; Maciejewski *et al.*, 2021). For example, Gosselt et al. (2020) describe baseline levels of homocystine, uric acid, taurine, glycerol-3-phosphate and 1,3/2,3-diphosphoglyceric acid being significantly different between sufficient (DAS28-ESR <= 3.2) and insufficient responders (DAS28-ESR > 3.2), which were used together in a RF model, being able to predict patient outcomes with an AUC-ROC of 0.81.

Another study reported 33 baseline metabolites as being differentially abundant between patient response groups, defined using DAS28, therefore indicating an association with responses to treatment, including tryptophan, hypoxanthine,

methionine, N-acetyltryptophan, N-acetylcitrulline, N-acetylglutamine, carnitine, serine, lysine, palmitoylcarnitine, bilirubin and biliverdin (Hur *et al.*, 2021). This paper revealed eight metabolites (bilirubin, biliverdin, 6-bromotryptophan, serine, trigonelline, N-acetyltryptophan, glucuronate and N-acetyltyrosine) as being both differentially abundant between the response groups and having an association with the DAS28-CRP, determined using a generalised linear model (Hur et al., 2021). Where Hur et al. (2021) uncovered eight differentially abundant metabolites across response groups and linearly associated with the DAS28, no such results were found in this work. No baseline metabolites were found to be statistically differential or correlated with DAS28 after the first 3 months of treatment after correcting the p-values for multiple testing. However, Hur et al. (2021) do not explicitly mention adjusting the p-values from their analyses for multiple testing, so the associations of the metabolites with disease activity may include some false positives. Nevertheless, there were few shared features between this dataset and the TaSER metabolome in association with treatment response, although tryptophan-related metabolites were noted across both cohorts.

Cuppen et al. (2014) developed a metabolomic model to discriminate between good and non-responders, using the DAS28 to define these responses to TNF-α inhibitors using baseline metabolites, including ethanolamine, lysine and several fatty acids, such as sn1-LPC(18:3-ω3/ω6) and sn1-LPC(15:0). By incorporating these metabolites alongside clinical measures in a predictive model, the model significantly improved the discrimination of patient responses compared with a patient factors-only model (p-value = 0.01) (Cuppen *et al.*, 2016). This current work took a similar approach and combined the metabolic features alongside the patient factors, which initially seemed to improve the prediction of response classes but did not cause a significant improvement.

3.4.4. Metabolite-Only Model

A machine learning approach was taken to compile multiple metabolites that by themselves were not found to be individually associated with the patient responses. Using a feature selection process, eight metabolites were combined in an XGB model, successfully predicting the 3-month DAS28 binary response groups

within a testing subset from the TaSER patient cohort. These metabolites included pyroglutamate, L-kynurenine, indoleacrylic acid, pyrroline, cytosine, N-succinyl L-citrulline, L-ornithine and 5-methylcytidine. However, throughout the analysis, concern over the inclusion of N-succinyl L-citrulline in the model was raised.

3.4.5. Composite Model

In addition to the development of the metabolomic model and the disease measures model, a composite model was generated via a distinct, parallel process consisting of disease measures and other clinical features alongside metabolomic data. These data had distinct formats, variances and ranges, presenting a clear challenge during their integration, including one of the datatypes dominating the other (Buescher and Driggers, 2016). Rather than concatenating the different datatypes and performing a single analysis, an alternative approach may be required, which will be explored in the following chapter using the example of integrating the TaSER metabolomic and transcriptomic datasets.

In considering the metabolomic model, it was important to consider that high variances were observed for each metabolite, and the abundances of several of the metabolites were similar across response groups. For these reasons, the models generated with the disease measures may provide a more robust method of predicting patient responses in other cohorts, especially where the identity of several of the metabolites was not certain, such as N-succinyl L-citrulline. However, the fact that pyroglutamate, cytosine, and pyrroline were included in the composite model may mean this was a more appropriate model since these features were found to be significant/borderline-significant in their differential abundance across the response groups.

Additionally, the inclusion of the baseline disease measures in the composite model may be advantageous in that disease measures would typically be measured in the clinic to evaluate the emergence and progression of the disease. The composite model offers a closer representation of what is seen in the clinic. The disease measures directly measure the disease activity, while the metabolic component reflects the molecular events that may contribute to successful treatment.

3.4.6. Model Comparison

There is a trade-off between pragmatism and performance when considering the value of a clinical tool. For example, using only patient factors and disease activity measures at baseline to predict how a patient may respond to treatment may be practical since these are typically measured during a patient's routine examination. However, the disease measures often introduce variance when, for example, multiple clinicians examine joint symptoms. In this case, when measuring joint tenderness and pain, clinicians may inadvertently apply various degrees of pressure for the same joint, leading to inconsistent measuring. There is, therefore, value in introducing molecular technologies, such as an easy-to-use chip detection platform, where the technology has been developed and validated to accurately measure multiple molecules from a biofluid with minimal variance between replicates. Such technology, however, remains elusive and would likely require expensive and time-consuming processes of selecting the analytes to include for assay development and validation across demographics. This, therefore, reflects the balance between a clinically pragmatic tool and one that provides a robust response prediction.

Other studies have sought to include patient factors in their molecular models to develop predictive models for RA patient responses to treatment (Gosselt *et al.*, 2021; Maciejewski *et al.*, 2021). Indeed, the prediction of responses to MTX in patients with RA after 6 months of treatment was attempted with a machine learning approach, utilising the baseline lipidome (Maciejewski et al., 2021).

In addition, a recent paper described the use of a machine learning approach to predict 3-month DAS28-ESR- based responses to MTX using six clinical features, including baseline tender joint count across 28 joints (TJC28), HAQ, BMI, smoking status, ESR and the prior use of DMARDs or corticosteroids (Gosselt et al., 2021). This model was comparable to that developed in this work involving the disease measures. The RF model generated by Gosselt et al. achieved an AUC-ROC value of 0.76 (95% CI: 0.66-0.85).

3.4.7. Feature Interpretation and Roles in Disease

The incorporation of model-agnostic interpretation methods revealed the influence of the metabolite features in the models in predicting patient outcomes. However, it is important to note that the additional analysis of the metabolites following the model development and evaluation revealed only subtle associations between the metabolites and disease activity changes. For example, only indoleacrylic acid ($p=0.048$) and pyroglutamate ($p=0.0004$) had significant differences in their baseline abundances across the response groups, with cytosine ($p=0.054$), 5-methylcytidine ($p=0.058$) and pyrroline ($p=0.06$) being borderline-significant. Increasing the sample size to investigate whether these changes would be significant with a larger cohort would be helpful. Since an effect size can be obtained from these findings, performing power calculations could allow an appropriate number of samples to be determined. However, increasing patient numbers may also increase variance and reveal the lack of robustness of these findings.

The following chapters will investigate whether the same metabolites were detected and associated with patient responses in other related datasets. These subsequent analyses will incorporate datasets generated during trials described in this section, including Hur et al. (2021) and Gosselt et al. (2020).

3.4.8. Pyroglutamate

Having been included in the metabolic model of response in this work, putatively identified pyroglutamate, also called 5-oxoproline, was increased at baseline in patients who experienced a good response to MTX in the TaSER cohort. However, the initial differential analysis noted that no metabolites had adjusted p-values < 0.05, so this finding needs to be considered with caution. Additionally, it remains to be seen whether this is a real metabolite or a by-product from the ionisation process. Since no internal standard was available for pyroglutamate, this was only tentatively identified. The generation of fragmentation data would support the annotation of this feature with greater confidence.

As a downstream metabolite of the antioxidant glutathione (GSH), pyroglutamate has been associated with oxidative stress, which results in a worse outcome for

patients with heart failure, where 5-oxoprolinase, the enzyme that converts pyroglutamate to glutamate and back to GSH may become dysfunctional and pyroglutamate accumulates (Sourdon *et al.*, 2018; van der Pol *et al.*, 2018). While there has been no apparent link between pyroglutamate and RA, increased pyroglutamate in the circulation may influence MTX activity, possibly contributing towards oxidative stress.

3.4.9. Indoleacrylic acid

Indoleacrylic acid was also found in the model and was similarly increased in its abundance in good responders, albeit with a great variance across each response group. Interestingly, indoleacrylic acid and L-kynurenine are derived from tryptophan, but they are generated via different pathways, shown in Figure 3.18. L-Kynurenine is produced when IDO is activated, often in response to inflammatory stimuli, for example, IFN-γ (Sorgdrager *et al.*, 2019). The anti-inflammatory actions of kynurenine are believed to be due to its action upon the aryl hydrocarbon receptor (AhR), which plays an important role in modulating inflammatory processes. For example, the NRF2 transcription factor, associated with anti-inflammatory products, can be stimulated through the AhR activation (Kaiser, Parker and Hamrick, 2020). By blocking IDO — which is believed to modulate an immunosuppressive mechanism — new therapies are emerging for the treatment of cancers and autoimmune diseases, including RA, for example, by specifically inhibiting IDO2 (Prendergast *et al.*, 2017; Liu *et al.*, 2018; Zakharia *et al.*, 2021; G. He *et al.*, 2022).

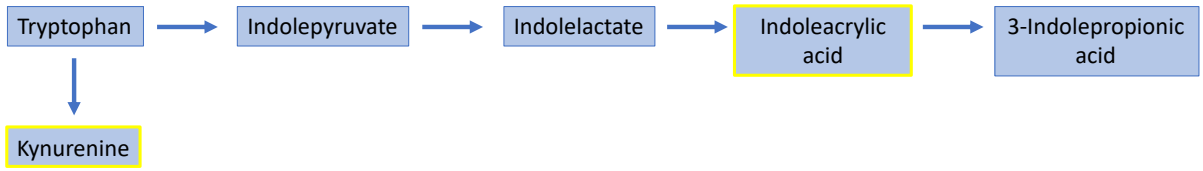

Figure 3.18. Tryptophan metabolism to indoleacrylic acid.

Indoleacrylic acid is produced via the gut microbiome, with several species capable of metabolising tryptophan within the intestine (Roager and Licht, 2018). Like kynurenine, indoleacrylic acid was also found to exert anti-inflammatory effects

via the increased activity of NRF2 by AhR stimulation, while also reducing the release of pro-inflammatory cytokines, notably IL-1β and IL-6, from stimulated PBMCs (Wlodarska *et al.*, 2017a; Ye *et al.*, 2022).

3.4.10. Hypothesis Related to the Gut Microbiome

Since indoleacrylic acid and other tryptophan metabolites are generated primarily via the gut microbiome, this raises a question regarding the use of biotics to supplement treatment with traditional pharmacological agents. These may include probiotics, including specific strains of bacteria known to produce these metabolites being administered to patients to encourage this favourable anti-inflammatory milieu (Wlodarska *et al.*, 2017a; Han *et al.*, 2021; Li *et al.*, 2021)

Along with many other species, gut bacteria can produce numerous compounds that can modulate the host immune system (Scher and Abramson, 2011). These include polysaccharides, such as polysaccharide A (PSA); short chain fatty acids (SCFAs), such as butyrate; pathogen/microbial-associated molecular patterns (P/MAMPs) and other metabolites, including indole-derived compounds (Negi *et al.*, 2019; Li *et al.*, 2021; J. He *et al.*, 2022).

Unfortunately, aside from the indole-based metabolite, none of these other gut microbiome-derived features were associated with the response to MTX in the TaSER study. The association of these features with disease activity changes in response to treatment will be explored in later chapters.

3.4.11. Urea Cycle and Arginine Metabolism

The pathway analysis following the differential analysis of the baseline metabolome across the 3-month DAS28-defined response groups indicated an altered urea cycle activity across these groups. Further investigation into this pathway and the involvement of the associated metabolites and genes encoding related enzymes was performed in the following chapter, involving an integration of the transcriptomic data from the TaSER study.

4. TaSER Transcriptomics and Metabolomics Integration

4.1. Introduction

4.1.1. Harnessing the Transcriptome and Metabolome

The work described in this chapter involved a secondary analysis of the transcriptomic data generated from the TaSER trial and an integration of the metabolomic data from the same trial (Dale et al., 2016). This chapter intended to expand on the analysis from the previous chapter, involving an investigation into the transcriptomic features associated with treatment response and considering how the findings from each omic dataset may overlap in terms of their connected biology. This may shed light on the pathways associated with the response to treatment in patients with RA.

It was anticipated that a more accurate and robust predictive model could be generated by integrating these datasets. Incorporating another omics platform would provide an alternative molecular perspective that would enhance the understanding of the mechanisms involved in the resolution of inflammation in response to treatment. For example, since the metabolic model in the previous chapter included tryptophan and arginine-derived metabolites, the genes that encode enzymes involved in these metabolic pathways were assessed in this chapter for their associations with disease activity changes in response to treatment. These included the genes encoding IDO and arginase (ARG), which have been associated with immune activity and inflammation in previous studies (Rath *et al.*, 2014; Ogbechi *et al.*, 2020).

4.1.2. Integrating Omics Datasets

The detection and measurement of the highly heterogeneous molecules on the journey from the DNA to the phenotype can be performed using a multitude of technologies and omics platforms. Since the data from the omics platforms are intrinsically linked – for example, the expression of genes that encode enzymes involved in metabolism – their integration can help to develop the understanding of the molecular mechanisms behind a phenotype (Yan *et al.*, 2017; Subramanian

et al., 2020). Indeed, the phenotype of a complex disease like RA is likely driven by multiple features spanning the different omics platforms (Cavill *et al.*, 2011).

Mechanistic insights and predictive biomarkers may be uncovered by taking this approach, as demonstrated with the COMBINE study where genomic, transcriptomic, proteomic and clinical data were integrated to develop a tool predictive of response to anti-TNF drugs in patients with RA (Folkersen *et al.*, 2016). This study had a larger sample size than that of the TaSER cohort, consisting of 185 patients with RA and a healthy cohort of 61. However, a cohort consisting of thousands of patients would provide greater confidence that a molecular profile of response would translate to the population of patients with RA and not just a single cohort.

In their analysis, Folkersen et al. (2016) only included analytes that were described in the literature as having an association with an anti-TNF response. This led to eleven molecules being chosen for the integrated model which limited the selection process, where molecules not previously associated with response were ignored, thus leading to some potentially valuable insights being missed. As such, this approach demonstrated a limitation of a biology-driven integration approach, where the prior knowledge of the biological mechanisms informs the process. Nevertheless, the authors reported that the final model consisting of the eleven molecules predicted the anti-TNF response after 3 months, with an AUC-ROC of 0.815, demonstrating its ability to accurately predict responses (Folkersen *et al.*, 2016).

A different approach was taken to integrate transcriptomic and metabolomic data to characterise the molecular differences between murine macrophages across activation states (Jha *et al.*, 2015). The authors described the development of an untargeted integration method: concordant metabolomics integration with transcription, which utilised data from a Quadrupole Time of Flight mass spectrometer and HiSeq 2500 sequencer. Together with an *in vitro* method to validate their findings, the authors uncovered molecular profiles characteristic of the pro-inflammatory (M1-like) and anti-inflammatory (M2-like) phenotypes. One of the prime examples of the pathway-wide changes uncovered in the murine M1-like macrophages involved the disruption to the TCA cycle, whereby the isocitrate

to α-ketoglutarate ratio was increased in M1-like macrophages (Jha *et al.*, 2015). The elevated abundance of isocitrate, reduction of α-ketoglutarate and accompanying reduced expression of the IDH1 gene, which encodes the enzyme that links these two metabolites, revealed that this pathway was impacted upon M1 activation. Moreover, the authors describe the increased expression of the gene encoding IRG1 in M1-like macrophages, which produces itaconate from the TCA cycle, providing further evidence of the perturbed TCA cycle during pro-inflammatory stimuli (Jha *et al.*, 2015).

This chapter deals with the expression of genes that may be linked with treatment response. For example, the IRG1 gene will be investigated for its association with disease activity, where the production of itaconate was reported to have immunomodulatory effects *in vitro*. By effectively harnessing an integrative approach, the association of the TCA cycle break and the resulting increase in itaconate with a pro-inflammatory phenotype contributed towards a great deal of research into the immunomodulatory effects of this pathway (Lampropoulou *et al.*, 2016; Domínguez-Andrés *et al.*, 2019; Hooftman and O'Neill, 2019; O'Neill and Artyomov, 2019; Yu *et al.*, 2019).

4.1.3. Aims

Following the development of a metabolic profile of MTX treatment response from the TaSER cohort, this chapter intended to develop a transcriptomic profile of treatment response from the same patients. Since the expression of genes may contribute towards changes in metabolic pathway activity, the genes associated with the metabolites mentioned in Chapter 3 were investigated.

The primary aim of this chapter was to develop a predictive model of the 3-month DAS28-ESR-based response to treatment using the baseline transcriptome. An additional aim was to determine whether findings from the transcriptomic and metabolomic analyses — and their integration — enhance the understanding of a molecular environment in the circulation that favours or improves the response to treatment.

4.2. Methodology

In this chapter, the transcriptomic dataset was analysed using various computational methods, including those introduced and applied in the previous chapter. Additionally, pathway analysis was performed using the ShinyGo v0.77 online tool, described in more detail in Section 2.5 (Ge, Jung and Yao, 2020).

In addition, an integration of the transcriptomic and metabolomic datasets was performed. This involved concatenating the datasets and investigating the correlated features across these blocks by calculating the Spearman correlation coefficients for each pair of features. The immediate limitation of this approach was the sheer amount of data that could be analysed, so the correlational analysis focused on addressing only the transcripts of interest from the pathway analysis and investigating which metabolites correlated with these. Doing so provided insight into the potentially biologically related molecules from the different datasets. For example, the association of metabolites with genes involved in immune-related pathways may point towards the immunomodulatory roles of the metabolites, therefore informing mechanisms that may be meaningful in the context of the response to MTX in the TaSER trial cohort.

4.3. Results

4.3.1. Patient Data

The baseline and 3-month demographics and clinical features of patients were reported, which were previously shown in Section 3.3.1.

4.3.2. Multivariate Analysis

A similar analytical approach was taken for the transcriptomic dataset as that used for the metabolomic data in the previous chapter. Like the metabolome analysis, there was no global separation of the samples based on the transcriptome across the response groups, as shown in Figure 4.1.

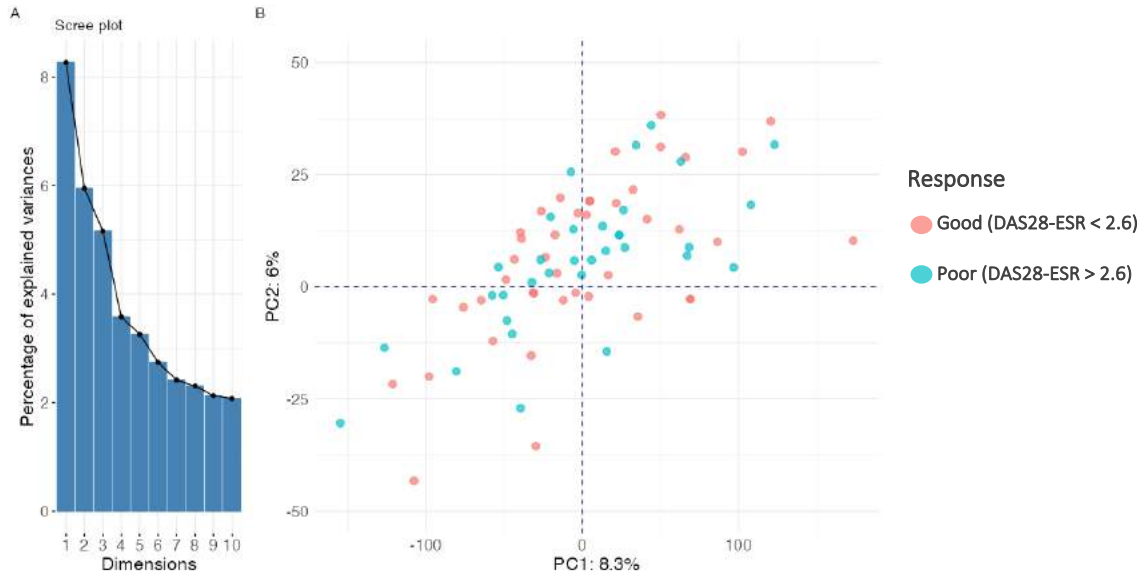

Figure 4.1. Multivariate analysis of the transcriptomic data from the TaSER cohort. A. Scree plot. B. Scatter plot showing patient samples were projected in space defined by PC1 and PC2, with labelling based on their 3-month DAS28-ESR-based responses.

4.3.3. Differential Expression Across Response Groups

The differential expression of genes across the treatment response groups was investigated, with the results shown in the volcano plot in Figure 4.2.

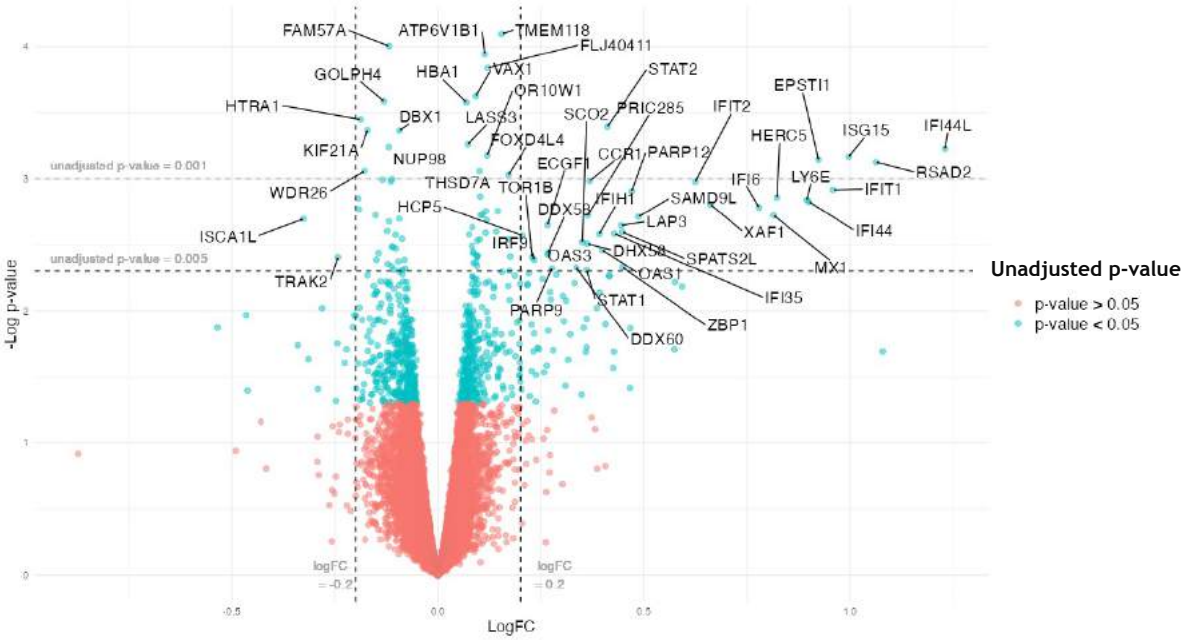

Figure 4.2. Volcano plot showing differential analysis of transcriptomic data across 3-month DAS28-based binary response groups. Genes in blue had unadjusted p-values < 0.05 and genes in red had unadjusted p-values > 0.05. Annotated genes were those with unadjusted p-values < 0.001 or had absolute log fold change > 0.2 and unadjusted p-values < 0.005.

Based on the adjusted p-values, none of the genes at baseline were differentially expressed across the 3-month DAS28-based response groups. Like the metabolomic analysis, the high number of features compared with the relatively small sample size meant that the BH correction that was used was potentially too conservative and may have removed genes with meaningful differences across the response groups. As such, the features from the differential analysis with unadjusted p-values < 0.05 were included in the subsequent pathway analysis with the caveat that these may include genes that were not truly differentially expressed across the response groups.

As shown in Figure 4.3, several pathways implicated in the host response to viral infection were enriched, including RIG-I-like receptor signalling pathway, influenza A, measles, hepatitis C and coronavirus infection responses. Many of the genes were involved in multiple pathways.

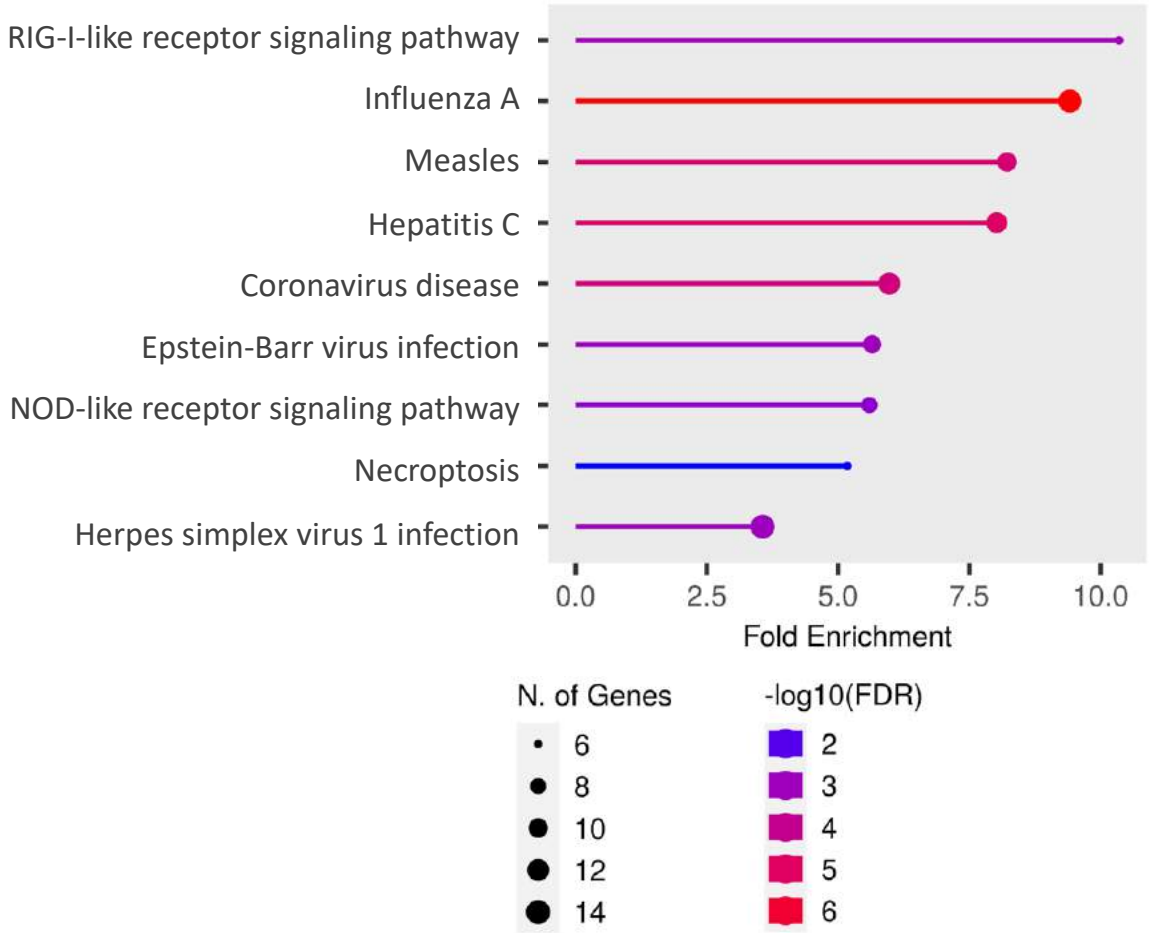

Figure 4.3. Results of the pathway analysis of differentially expressed genes from the TaSER transcriptomic dataset across response groups defined by the 3-month DAS28 score.

It is important to consider how concurrent infection during treatment may explain the enrichment of these immune pathways. However, infection was not included in the patient data so this could not be investigated further. Nevertheless, the involvement of the immune response in RA and its association with disease activity meant that it remained feasible that these pathways were related to the treatment response in patients.

The genes contributing to the pathway analysis were then further analysed. Their differential expression across the response groups shown in Figure 4.4, as were their correlations with the DAS28 at 3 months, shown in Figure 4.5. Of these transcripts, only tumour necrosis receptor-associated factor 6 (TRAF6) gene was increased in poor responders (Figure 4.4) and positively correlated with the DAS28-ESR score at 3 months (Figure 4.5). The other genes were increased in expression in the good responders and were negatively correlated with the DAS28-ESR at 3 months.

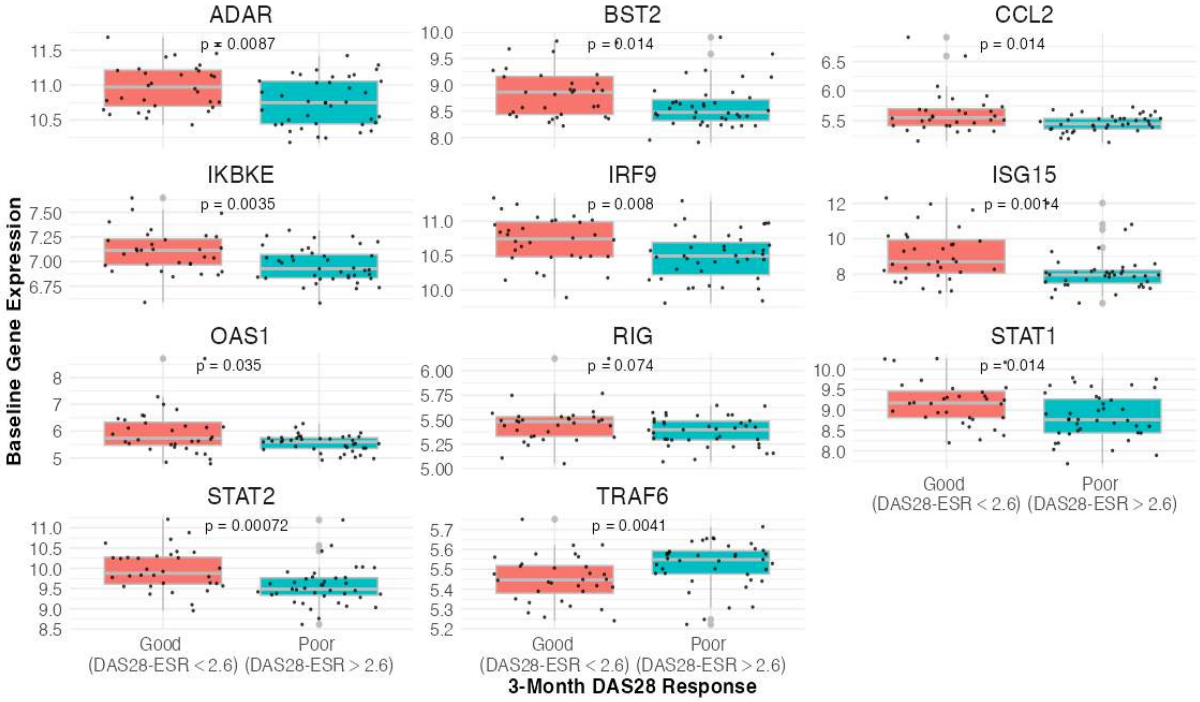

Figure 4.4. Boxplots showing differential expression of genes across 3-month DAS28-based response groups. Genes were those that contributed to pathway analysis

Generally, patients with high expression of these features, except TRAF6, experienced good responses at 3 months. Interestingly, many of these features have inflammation-modulatory effects, including, for example, ADAR, IKBKE, IRF9,

CCL2, OAS1, STAT1 and STAT2 (Kasperkovitz *et al.*, 2004; Patel *et al.*, 2015; Jiang *et al.*, 2020; Moadab, Khorramdelazad and Abbasifard, 2021).

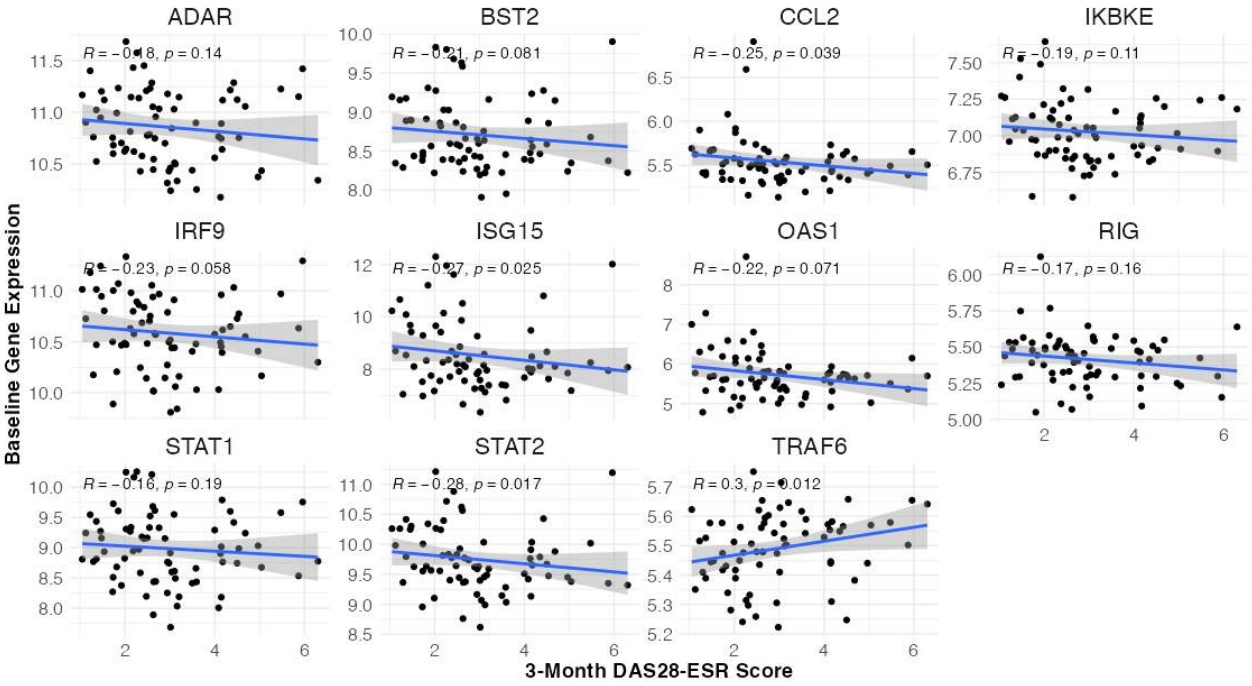

Figure 4.5. Correlation analysis of baseline transcripts against the 3-month DAS28 scores. Spearman correlation coefficients were calculated and plotted alongside the associated p-values. Regression lines were included to depict the relationship.

4.3.4. Metabolites Associated with Differentially Expressed Genes

An investigation into the metabolites associated with the genes that were differentially expressed across the patient response groups was then performed, including several of the potentially immune-related genes. Due to itaconate and its production being linked with a pro-inflammatory phenotype in macrophages, described by Jha et al. (2015), IRG1 was assessed for its correlation with the DAS28-ESR score at 3 months. However, no meaningful association with treatment response was found for this gene.

Taking the top 100 differentially expressed genes across response groups, a further correlation analysis was performed to examine the correlations between each of these genes

of interest and the metabolites. The results are shown in the heatmap in

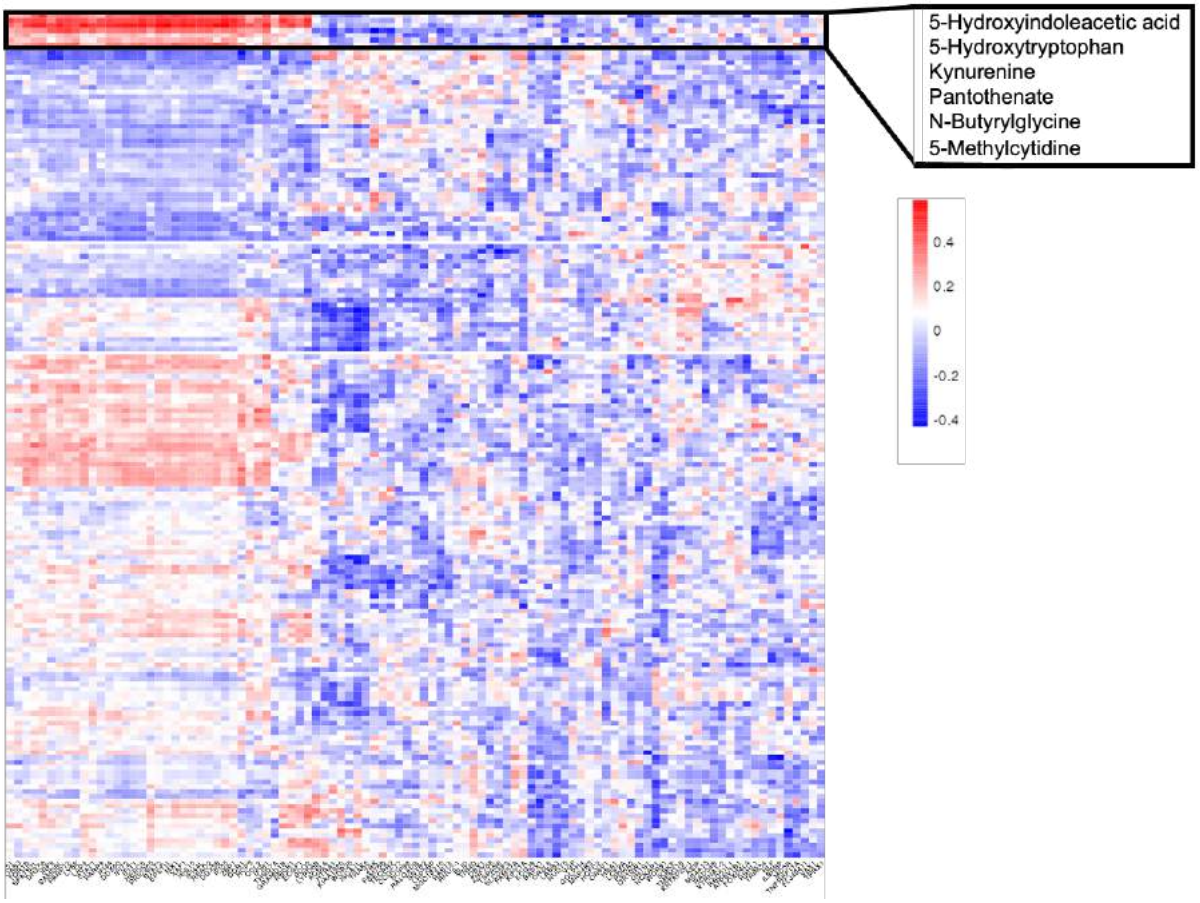

Figure 4.6.

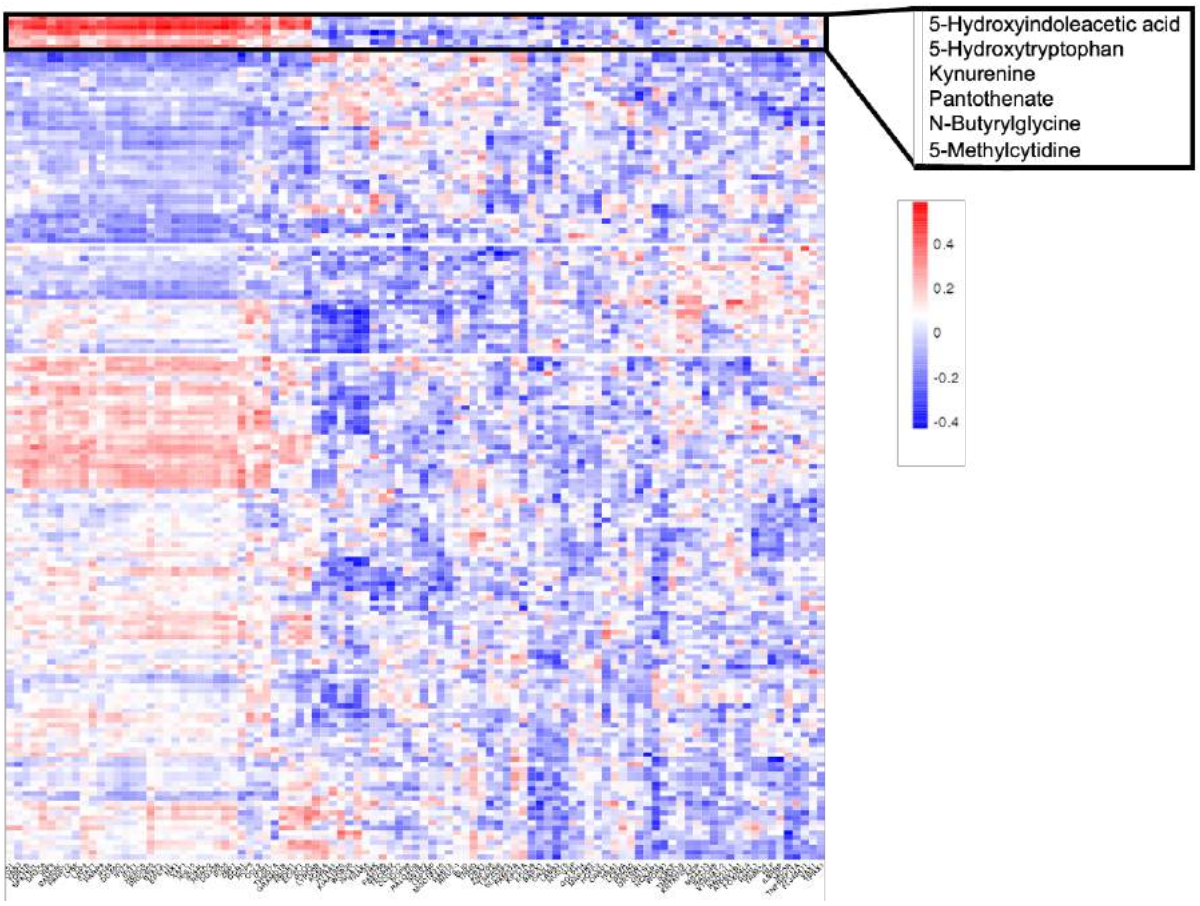

Figure 4.6. Heatmap showing correlation coefficients of associated metabolites with the top 100 genes from the differential expression performed using the limma package.

Several of the metabolites found in the metabolic profile of treatment response from the previous chapter were correlated with the immune-related genes. Tryptophan-related metabolites, including 5-hydroxtryptophan, 5-hydroxyindoleacetic acid and kynurenine and correlated with a group of genes, many of which may have a role in immunity, such as MX1, RSAD2, OAS1 and CCL2. These associations of tryptophan-related metabolites with genes involved in inflammatory processes may provide evidence of the involvement of these metabolites in regulating immune activity.

For example, kynurenine correlated strongly with several of these genes, depicted in Figure 4.7 with IFI35 (R=0.48, p-value = 1.9×10^{-5}), STAT1 (R=0.46, p-value = 4.9×10^{-5}) and STAT2 (R=0.51, p-value = 5×10^{-6}). The involvement of STAT1 and STAT2 with IFN signalling pathways may point towards an immunomodulatory role of kynurenine, whereby it may be elevated in its production because of the increased activity of IDO, the enzyme involved in its production, in response to IFN

stimulation. The expression of genes encoding IDO1, IDO2 and TDO were assessed later with the results described in the targeted analysis in Section 4.2.10.

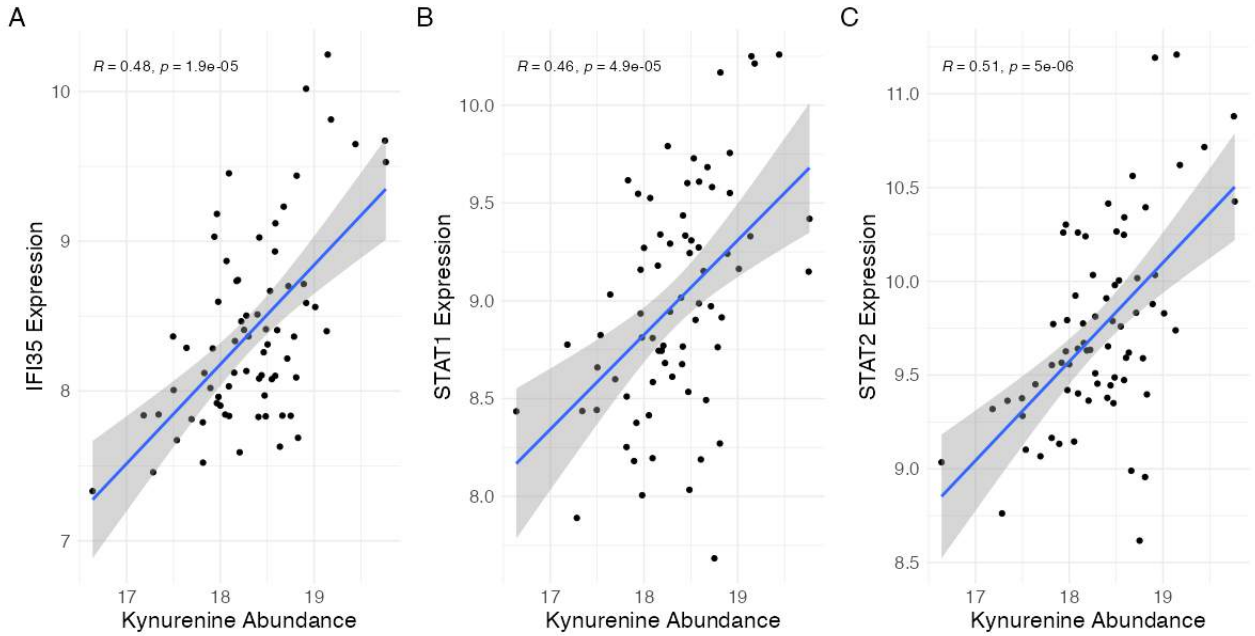

Figure 4.7. Correlation plots of kynurenine abundance against genes of interest selected from heatmap in Figure 31.

The association of these immune-related genes with several metabolites may allow these circulating metabolites to be used as surrogates of the IFN pathway activity and predict the MTX response with the changing immune activity.

It was worth mentioning that, aside from PDHA2, which encodes a subunit of pyruvate dehydrogenase — involved in converting pyruvate to acetyl coenzyme A, which then enters the TCA cycle — no other known metabolism-related genes were differentially expressed. However, there remained to be clear correlations between metabolites and genes, largely relating to immune activity.

It was expected that the increased immune activity would lead to an upregulation of immunomodulatory metabolites, such as itaconate, as a result of the metabolic reprogramming of immune cells (Mills and O'Neill, 2016; O'Neill and Artyomov, 2019). Whether the metabolism-related genes are differentially expressed in localised tissue, such as the synovium, or are modulated in their expression within the gut microbiome, remains to be seen — but may help explain this disconnect

between the perturbed metabolite levels and the seemingly unchanged metabolism-related genes.

4.3.5. Supervised Machine Learning

A supervised machine learning approach was undertaken to determine whether a collection of transcripts could be used to predict the 3-month DAS28-based response.

4.3.6. Initial Transcriptomic Model

An initial model was generated within the training subset of the transcriptomic data. The transcripts were selected for the model via a purely statistical route using the RFE algorithm used for the model developed in the previous chapter. These genes included VAX1, PDHA2, BAPX1, NCKAP1 and FAM57A, as shown in Figure 4.8A. As per the workflow, algorithm selection was then performed, involving the selection of the NB algorithm as the best-performing and most computationally efficient, shown in Figure 4.8B. The final tuned model was evaluated within the testing subset, with the results shown in Figure 4.8C and Figure 4.8D, whereby the AUC-ROC of 0.82 (95% CI: 0.63 -1.01) and MCC = 0.611 revealed a good performance.

These genes appear to have isolated functions, showing no known shared pathways or biological role. It should be noted, however, that there remains the possibility of hitherto unidentified connections between these genes.

The main aim of this work was to develop a molecular tool that could be used to predict treatment response in patients with RA. A secondary aim was to identify possible molecular mechanisms at baseline that contribute to the resolution of inflammation which may explain how patients might respond differently to treatment. It was evident from the results of this initial model that taking a purely statistical approach while achieving the first aim of creating a predictive molecular tool misses the second aim of identifying the molecular pathways likely involved in the resolution of treatment.

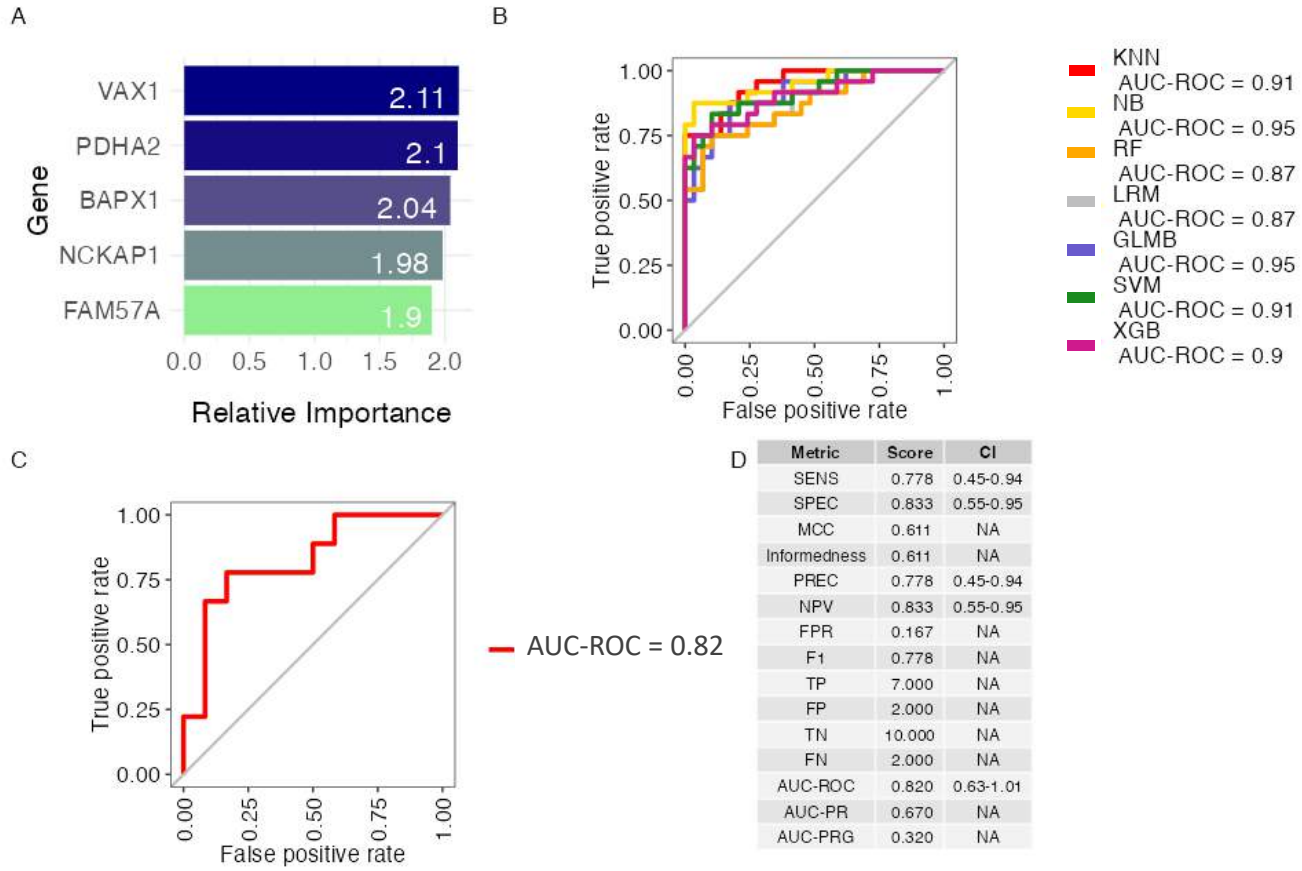

Figure 4.8. Transcriptomic profile of 3-month DAS28-based binary response A. Feature selection using RFE algorithm within training subset. B. Algorithm selection with the selection of the NB algorithm. C. Receiver-operating characteristic (ROC) curve showing the performance of the model within the testing subset. D. Performance metrics.

4.3.7. Incorporating Pathway Analysis into the Feature Selection

Since the features from the model described in Figure 4.8 were seemingly unrelated in their biological roles, the feature selection process was expanded with pathway analysis being incorporated to guide the selection of transcripts included in the model. This involved taking the training data and selecting the genes that were differentially expressed (unadjusted p-value < 0.05) across the response groups.

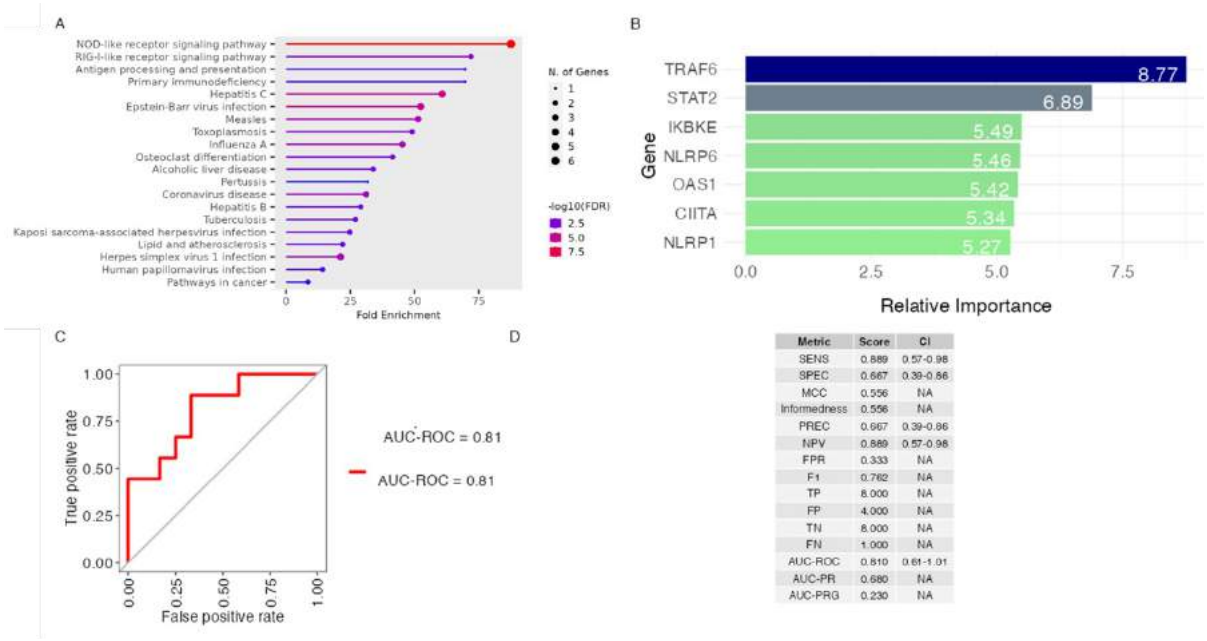

Figure 4.9. Pathway analysis informing the development of the transcriptomic predictive model of 3-month DAS28-based response. A. Top 100 differentially expressed genes across response groups in training data selected for pathway analysis. Bar chart shows the results from the pathway analysis in terms of fold enrichment. B. Results from the feature selection using the differentially expressed genes, those found in pathways from Figure A and with the RFE algorithm applied within the training subset. C. Receiver-operating characteristic (ROC) curve showing model performance within the testing subset. D. Performance metrics including confusion matrix with TP, TN, FP and FN shown.

Using this list of differentially expressed genes, pathway analysis was then performed, and the genes that had common pathways were kept, resulting in 20 genes. The pathways in which these were found are shown in Figure 4.9A, including several immune-related pathways, such as NOD-like receptor signalling and host immune responses to various viral infections. Feature selection was then performed using the RFE algorithm on the condensed training subset consisting of 20 genes, with the results shown in Figure 4.9B. The selected features included TRAF6, STAT2, IKBKE, NLRP6, OAS1, CIITA and NLRP1. Comparing the features selected in Figure 4.9B with those in Figure 4.8A, the higher relative importance scores could be explained by the reduced number of features analysed using the RFE algorithm, therefore dividing the overall importance by fewer features. As with the model described in Figure 4.8, the NB algorithm was selected.

The final model performed similarly to that generated using a purely statistical approach, with an AUC-ROC = 0.81 (95% CI: 0.61-1.01) and MCC = 0.556. It should

be noted that there was a slight imbalance in the number of patients with a good or poor response, which may mean the model's performance was slightly exaggerated, considering the higher number of poor responders in the cohort. Importantly, using an integrated biological/statistical approach may be more helpful in uncovering an interrelated molecular profile of response that underlines the possible involvement of immune-associated pathways in modulating how patients with RA respond to treatment.

4.3.8. Feature Interpretation

Paying attention to the model generated using the integrated biological and statistical approaches, the features used in the model were assessed using model-agnostic feature interpretation methods. The partial dependence plots (PDPs) and accumulated local effects (ALE) plots, describing global interpretation methods, are shown in Figure 4.10.

For example, increased expression of CIITA, IKBKE, OAS1 and STAT2 in the cohort was associated with an increased probability of predicting a good response. In contrast, increased expression of NLRP1, NLRP6 and TRAF6 was associated with a higher probability of predicting a poor response.

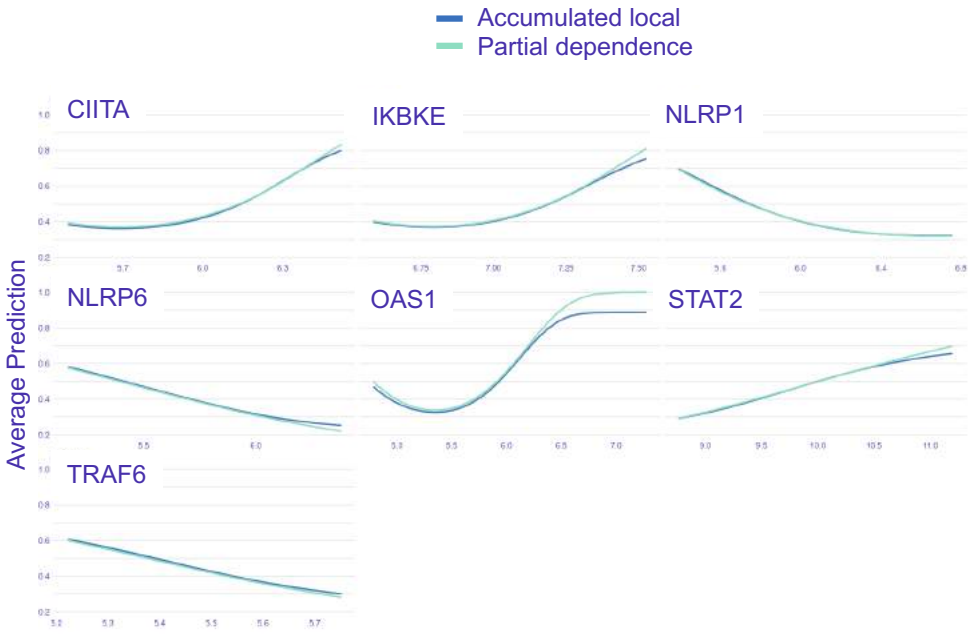

Figure 4.10. Global interpretation of the features in the transcriptomic model. Accumulated local effects (ALE) plot and partial dependence plots (PDPs) for each feature.

These results are most helpfully interpreted alongside the actual associations of the features with the continuous DAS28, shown in the correlation plots in Figure 4.11. For example, NLRP1 (R=0.28, p-value = 0.015), NLRP6 (R=0.24, p-value = 0.042), and TRAF6 (R=0.31, p-value = 0.0077) were positively correlated with the 3-month DAS28-ESR. Increased expression of these genes was associated with a worse outcome in patients which was notable owing to the involvement of these genes in recruiting the NRLP1 and NLRP6 inflammasomes, activating NF-κB and ultimately driving inflammation by inducing the release of pro-inflammatory cytokines, including IL-1β (Grenier *et al.*, 2002; Martinon, Burns and Tschopp, 2002; Wang *et al.*, 2020; Zheng, Liwinski and Elinav, 2020). Contrastingly, the increased expression of STAT2 (R=-0.29, p-value = 0.011) was associated with a lower DAS28-ESR after 3 months of treatment, whereas IKBKE (R=-0.19, p-value = 0.11) and OAS1 (R=-0.21, p-value = 0.074 did not have significant correlations with the DAS28-ESR score at 3 months.

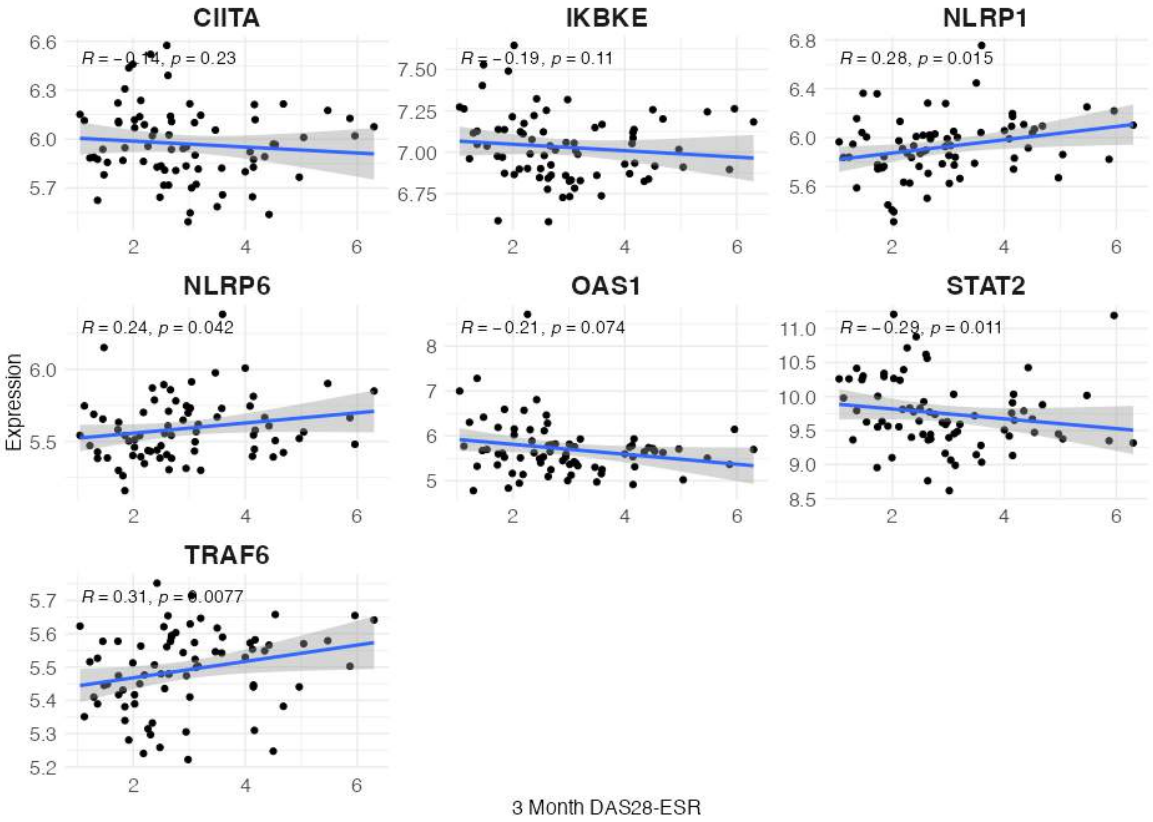

Figure 4.11. Correlation of features from the model with the 3-month DAS28 continuous score with linear regression plotted. Spearman correlation statistics were calculated for each gene and its relationship with the 3-month DAS28-ESR score.

Since the modelling involved a binary classification of the patient responses, the differential expression of the genes included in the model was also performed, with the results shown in Figure 4.12. These results underline that while these transcripts may be associated with either a good or poor response to treatment, the differences in their expression across the groups were small, with sizeable variation and overlap of the expression of each of the genes across the groups. Considering these actual correlations and differences across the response groups, several of these genes were unlikely to be robust biomarkers owing to their weak associations with the DAS28-ESR and response groups. For example, CIITA, OAS1 and IKBKE had relatively weak associations with the responses, indicating these would be unlikely to have value as individual biomarkers in future cohorts.

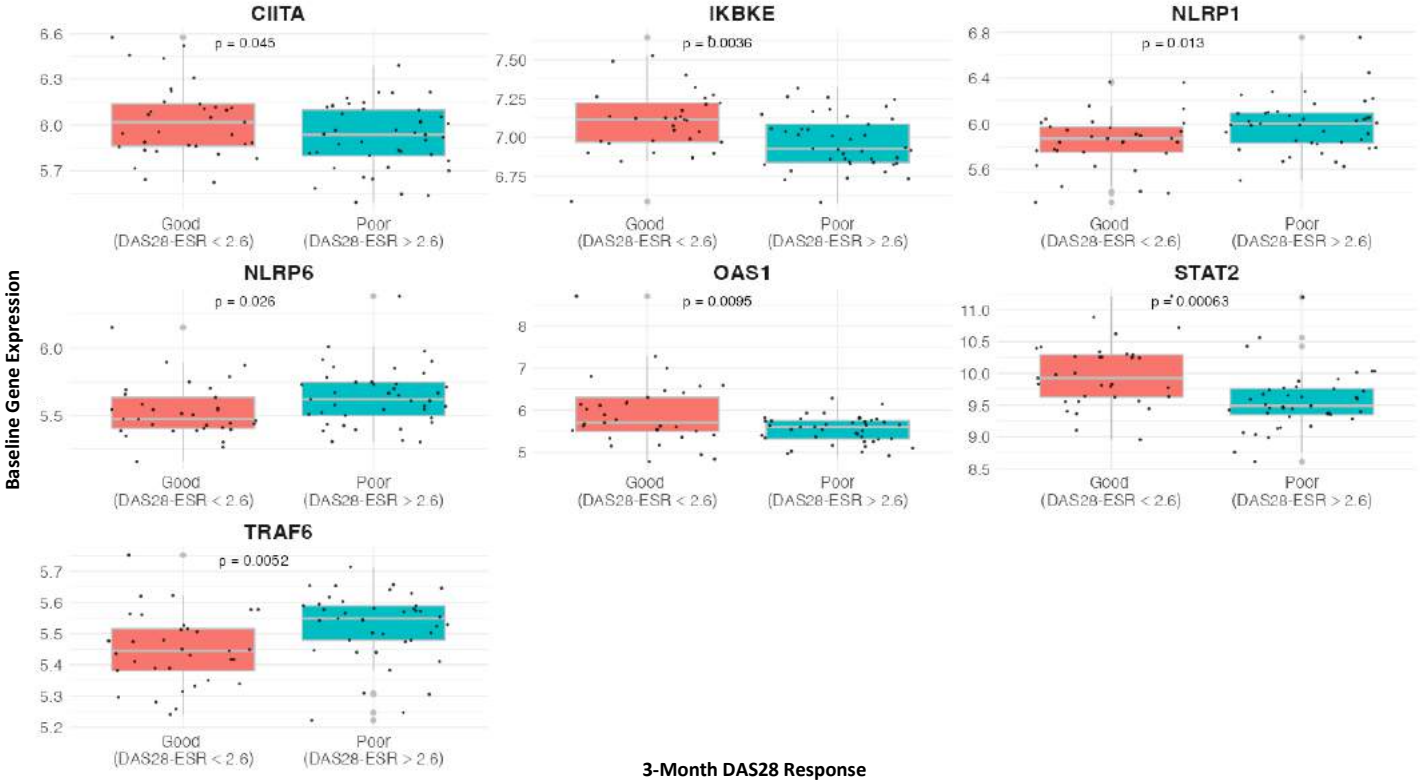

Figure 4.12. Differential expression of features from the model across the 3-month DAS28 response groups. Wilcoxon tests were performed to calculate a p-value statistic to compare the gene expression across the 3-month response groups.

However, the association of NLRP1, NLRP6, STAT2 and TRAF6 across response groups and with the continuous DAS28-ESR score was more substantial. These genes were more convincing biomarker candidates to predict DAS28-ESR-related

outcomes. Nevertheless, the value of these transcripts was believed to be greatest as a collection of molecularly related biomarkers whose collective predictive ability was likely to be greater than the model's constituent parts.

4.3.9. Correlations of Model's Features with Metabolites

The metabolites that correlated with these genes from the model were assessed using a similar method as performed in the earlier section, with the results shown in Figure 4.13.

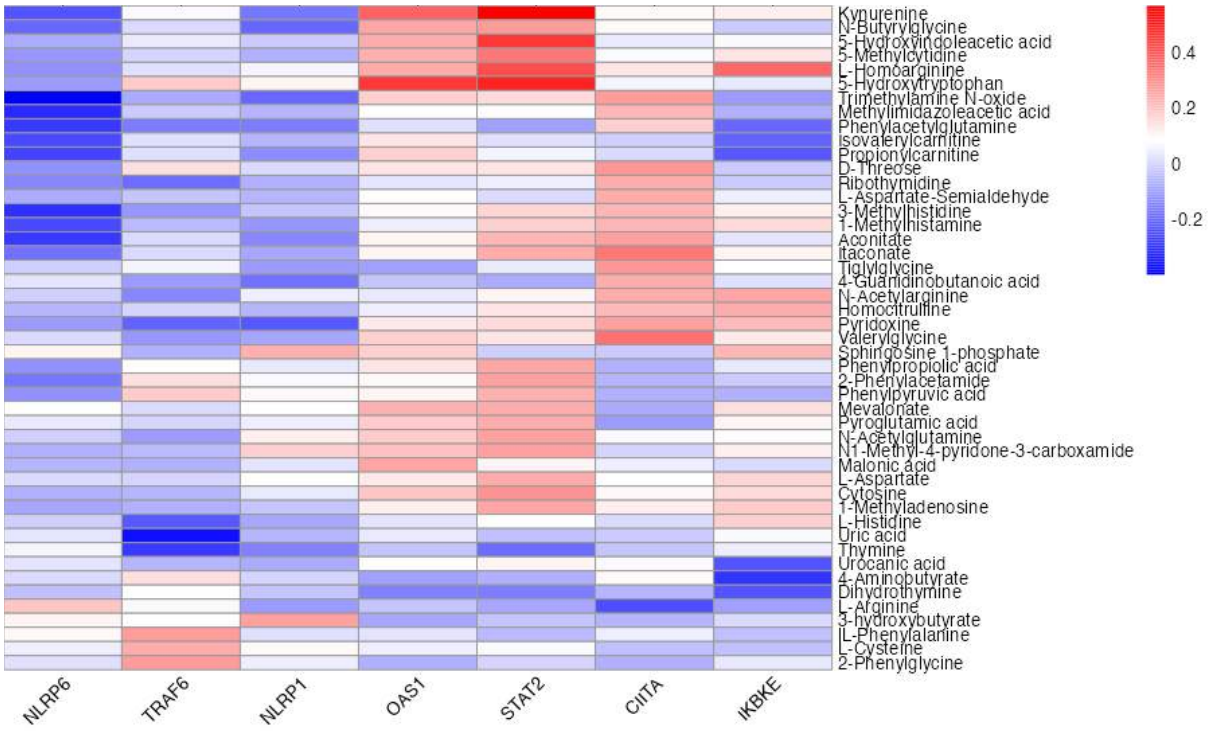

Figure 4.13. Correlation heatmap of genes from the refined model and correlating putative metabolites.

Interestingly, the metabolites were loosely clustered, largely driven by their correlations with NLRP1, TRAF6, CIITA, OAS1 and STAT2, albeit with fairly weak correlations, as indicated by the low coefficients in the legend of Figure 4.13. Itaconate and aconitate had a similar pattern across the genes, where they had positive correlations with CIITA (itaconate: R=0.34, p-value = 0.0036; aconitate: R=0.26, p-value 0.043), along with an inverse correlation with NLRP1 and NLRP6, although these were not significant correlations (p-value < 0.05). Other metabolites that clustered closely with itaconate included 1-methylhistamine and

3-methylhistidine, both being putatively identified. Since these tentatively identified metabolites had very similar RTs (1-methylhistamine: 9.39; 3-methylhistidine: 9.31), it was likely that they were closely related. For example, their difference in m/z ratio might suggest that 1-methylhistamine was a decarboxylated product of 3-methylhistidine. Trimethylamine N-oxide was negatively correlated with NLRP6 (R=-0.26, p-value = 0.031) while being positively correlated with CIITA (R=0.27, p-value= 0.023).

4.3.10. Targeted Analysis of the Integrated Datasets

Finally, a targeted analysis was performed to investigate the expression of genes relating to metabolites of interest, focusing on those included in the model from the previous chapter. The features were investigated based on their involvement in tryptophan and arginine metabolic pathways. Genes whose products were involved in these pathways were searched for using databases, including HMDB, KEGG and UniProt and were assessed for their correlations with disease activity (Wishart *et al.*, 2018; Kanehisa and Sato, 2020; UniProt Consortium, 2023). Of these, the INDO gene, which encodes the IDO enzyme, was correlated with kynurenine (R= 0.52, p-value = 3.9x10-6), shown in Figure 4.14A.

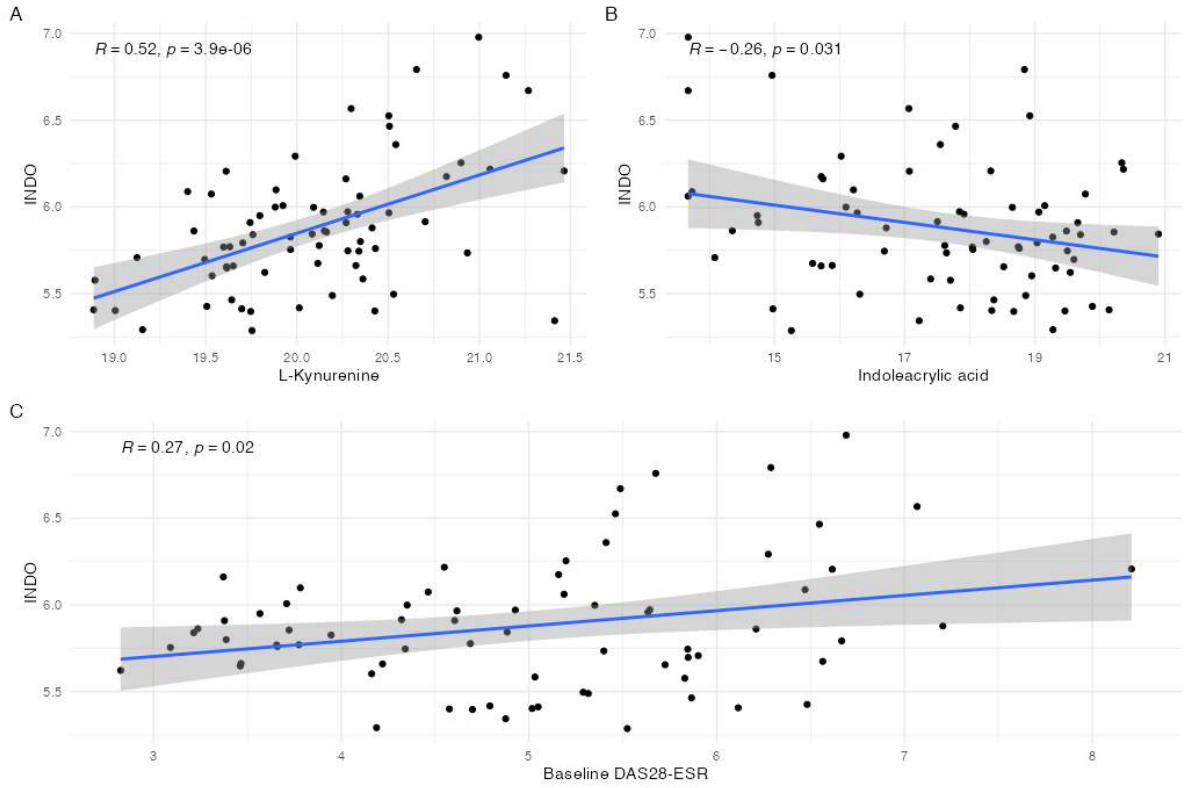

Figure 4.14. Correlation plots of INDO expression with related metabolites and disease activity. A. Correlation with L-kynurenine B. Correlation with indole acrylic acid. C. Correlation with DAS28-ESR score at baseline.

Additionally, INDO negatively correlated with indole acrylic acid (R=-0.26, p-value = 0.031), shown in Figure 4.14B. The positive correlation of INDO with kynurenine showed an increased expression of INDO associated with an increased abundance of kynurenine. The production of indoles, including indole acrylic acid, may reflect an alternative fate of tryptophan involving microbial metabolism (Wlodarska *et al.*, 2017a). The negative correlation between INDO and indole acrylic acid was logical since increased INDO expression may lead to tryptophan's metabolism towards kynurenine rather than the indole-based routes.

Interestingly, while INDO was not correlated with the DAS28-ESR after 3 months, it correlated with the DAS28-ESR at baseline (R=0.27, p-value = 0.02), shown in Figure 4.14C. The increased INDO expression in patients who had a higher disease activity at baseline may indicate a greater drive towards kynurenine metabolism, which has complicated immunomodulatory effects, rather than towards indole-based metabolism, several products of which were described as having anti-inflammatory effects (Munn and Mellor, 2013; Wlodarska *et al.*, 2017b; Z.-H. Zhao *et al.*, 2019). The findings reported in Figure 4.14 may underline the biological connections between the features found in the transcriptomic and metabolomic datasets, paying particular attention to tryptophan-related pathways.

This association of the kynurenine-related pathway with higher disease activity may be supported by the fact that kynurenine was positively correlated with many of the genes involved in immune processes found in the earlier pathway analysis, including ADAR, BST2, CCL2, and IRF9. It would be interesting to compare this with the expression of the genes involved in indole metabolism, but because these metabolites are produced largely in the gut microbiome, this was not possible using the whole blood transcriptome.

Similar results were shown in arginine metabolism-related features. Arginine metabolism was investigated due to the presence of ornithine, pyrroline, and N-succinyl L-citrulline in the metabolic model of response from Chapter 3 (albeit with the caveat of N-succinyl L-citrulline not likely to be truly associated with

response). However, it was noted that while pyrroline may be produced via ornithine, it is more often described in the literature as a component of Δ1-pyrroline-5-carboxylate which is involved in proline metabolism, indicating that the pyrroline detected in this work may be a fragment of a larger molecule derived from proline (Chalecka *et al.*, 2021).

Genes whose expression related to arginine metabolism and were detected in the dataset included ARG1, ARG2, NOS1, NOS2, ASS1, ASL, and GATM. Notably, there was an increased expression of ARG1 in negative responders based on the 3-month DAS28-ESR (Wilcoxon test, p-value = 0.015), although there was a high variance of its expression across the good and poor response groups, as described in Figure 4.15A.

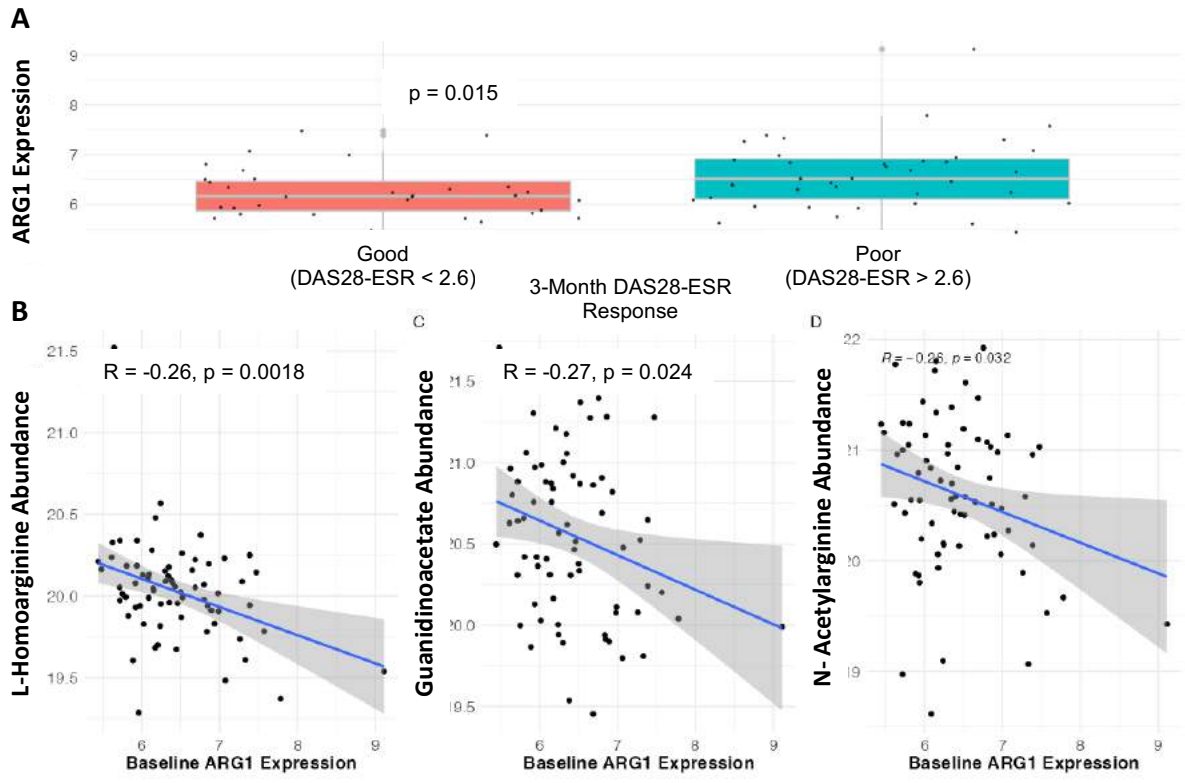

Figure 4.15. Exploring ARG1 expression and relationship to related metabolites. A. Boxplot showing differential expression of ARG1 gene across the 3-month DAS28-ESR based responders. B-D Correlation of ARG1 with related metabolites. B. L-Homoarginine C. Guanidinoacetate D. N-Acetylarginine.

The correlations of ARG1 with related metabolites were assessed, including those found in the urea cycle, such as arginine, ornithine, citrulline, and arginosuccinate, but none of these was significantly correlated. Interestingly,

ARG1 was negatively correlated with homoarginine (R=-0.36, p-value =0.0018) and guanidinoacetate (R=-0.27, p-value = 0.024). These correlations may help in understanding the fate of arginine, where the increased ARG1 activity may divert arginine away from homoarginine and guanidinoacetate production, which occurs via AGAT. Since ARG1 did not correlate significantly with L-arginine, it was surprising that it was negatively correlated with the tentatively identified acetylated form of the metabolite, N-acetylarginine, shown in Figure 4.15D (R=-0.26, p-value = 0.032). However, these correlations were not strong, so it was not clear whether they would be reproducible in other datasets.

In fact, the associations (or lack thereof) between the arginine-related genes and treatment response were surprising. Since arginase, encoded by ARG1, is typically associated with an anti-inflammatory state, as demonstrated *in vitro* using M2-like macrophages, it was expected that it would be increased in good responders and NOS would be associated with a poor response to treatment. However, the latter gene was not significantly associated with either response group, nor were those encoding the ASS or ASL genes also involved in the urea cycle.

4.4. Discussion

The transcriptomic data from the TaSER trial was analysed using a similar workflow used for the metabolomic dataset from the same trial. One of the key outputs from this chapter was the demonstration of how the analytical workflow could be used across omics datatypes. From the transcriptomic analysis, one of the key findings was the discovery of the association of several immune-related genes with the patient response to MTX. The machine learning revealed TRAF6, STAT2, IKBKE, NLRP6, OAS1, CIITA and NLRP1 as a panel of genes whose expression was collectively predictive of treatment response in the cohort. Since these could be linked to the IFN signaling pathway it was suggested that it could modulate how patients with RA responded to MTX treatment. However, an important limitation was that these genes were not validated using qRT-PCR. The predictive model also required validation in an independent and related cohort which was not performed in this project.

The aim of the integration here was to develop a molecular profile that could be used to predict MTX response in patients with RA. A secondary objective of this work was to explore the molecular mechanisms involving altered gene expression and metabolite abundance in patients with RA who have different responses to MTX treatment.

The analysis performed in this chapter largely focused on the transcriptomic data, with the later portion of the chapter involving a simple integration of these datasets. It was hoped that the analysis and integration of the transcriptomic data would complement the metabolites associated with MTX response from the previous section. However, only ARG1 and INDO were found as transcripts that were associated with treatment response and were related to the metabolites, being implicated in arginine and tryptophan metabolism.

4.4.1. Uncovering Transcriptomic Features of Response

The transcriptomic data from the TaSER trial, generated via whole blood samples of patients with RA, provided a rich source of information from various cell types found in the blood. Such cells included immune cells whose activity is perturbed in autoimmune diseases like RA, whereby inflammatory mechanisms may be influenced by circulating autoreactive immune cells (Chaussabel, Pascual and Banchereau, 2010). The differential gene expression that was described in this work may alternatively describe a differential cell type abundance across the response groups. As a result, incorporating pathway analysis into the workflow was expected to provide insights into the possible immune-related pathways implicated in the resolution of inflammation via the response to MTX treatment in RA, including IFN signalling. These may point towards a different immune cell panel associated with the response groups.

4.4.2. Developing a Transcriptomic Profile of Response

An initial supervised machine learning model predictive of treatment responses in the TaSER cohort consisted of a collection of transcripts, including VAX1, PHDA2, BAPX1, NCKAP1 and FAM57A. These are largely isolated genes in that they do not directly share known biological functions with each other, although hitherto unidentified connections are possible. As demonstrated by these results, the

machine learning approach used here, involving a purely statistical method, prioritised the selection of the most statistically powerful features rather than those that may have the greatest biological value. However, these findings may be limited due to possible overfitting of the model to the data, thus making it unlikely to be of use in the population of patients with RA.

The statistical method did not appear to contribute to the secondary aim of the project of uncovering mechanisms that may be involved in response to treatment. To this end, the incorporation of pathway analysis, reflecting current biological knowledge, was expected to provide insights into mechanisms involved in the resolution of the disease. These may offer new therapeutic targets that may be used to supplement existing treatment. Another model was generated using an integrated biological and statistical approach involving differential expression analysis, pathway analysis and the RFE algorithm for feature selection.

The new model included a completely different set of transcripts from the original model. However, these transcripts were closer to the set of genes included in the first section of analysis in this chapter. The model included TRAF6, STAT2, IKBKE, NLRP1, NLRP6, OAS1 and CIITA, which predicted the responses of patients in the test subset of the cohort with a similar performance to the model generated using purely statistical means.

4.4.3. Integrating Transcripts with the Metabolome

The differential analysis and the supervised machine learning approach indicated that patients with RA who experienced different responses to MTX may have altered transcriptomic profiles involving immune responses focusing on IFN signalling. This was especially notable when a recent study showed that an increased IFN gene signature, including OAS1, ISG15, MX1 and other related genes, was associated with a worse outcome for patients with early RA (Cooles *et al.*, 2022). From these findings, the authors underlined the value of targeting IFNα signalling as a therapeutic strategy.

Genes relating to IFN signalling that were associated with treatment response in this work included ADAR, BST2, CCL2, CIITA, IKBKE, IRF9, ISG15, NLRP1, NLRP6, OAS1, RIG, STAT1, STAT2, TRAF6. This included those in the predictive model and

those that had an association via differential expression across response groups or correlated with the DAS28-ESR score.

As shown throughout this chapter, whole blood samples are a rich source of transcripts which may be derived from a diverse population of cell types. These may include immune cells, platelets and even bacteria, typically detected at low levels during infection or in diseases involving a dysfunctional intestinal barrier (McLaughlin *et al.*, 2002; Amar *et al.*, 2011; Sato *et al.*, 2014; Païssé *et al.*, 2016; Olde Loohuis *et al.*, 2018).

4.4.4. ADAR

The expression of several of the genes from the model was previously reported as being associated with inflammatory processes, including CCL2 and STAT1, while others, such as ADAR, ISG15 and STAT2, were not inherently inflammatory but may play a role in modulating these processes (Kasperkovitz *et al.*, 2004; Durfee *et al.*, 2010; Wright *et al.*, 2015; Vlachogiannis *et al.*, 2020; Moadab, Khorramdelazad and Abbasifard, 2021). For instance, the adenosine deaminase RNA specific (ADAR) gene was reported to be increased in the synovial fluid of patients with RA (Vlachogiannis *et al.*, 2020). In the same study, the authors described the association of adenosine-to-inosine (A-to-I) RNA editing with the expression of inflammatory genes, including cathepsin S, encoding a protease which can cause increased activity of immune cells, and TNF receptor-associated factors (TRAFs). This was noteworthy where TRAF6 was similarly associated with the response to treatment in the TaSER cohort, albeit correlating with the DAS28 in the opposite direction.

4.4.5. IRF9 and IKBKE

Transcripts described as having inflammation-regulatory effects included IRF9 and IKBKE, both of which were elevated in good responders (Patel *et al.*, 2015; Jiang *et al.*, 2020). Only IKBKE, however, was included in the predictive model. The inhibitor of κ B kinase epsilon (IKBKE) gene was reported as being a key regulator of NLRP3 inflammasome in macrophages, an important inflammatory mechanism that leads to the production of inflammatory cytokines, including IL-1ß (Patel *et al.*, 2015). The authors described how the expression of IKBKE was increased

following pro-inflammatory stimulation, leading to a regulatory effect via impairing NLRP3 inflammasome activation, which was curtailed in macrophages whose gene encoding IKBKE was knocked out. The inclusion of other inflammasome-related genes, including NLRP1 and NLRP6, was, therefore, of note, especially where the expression of these genes was increased in poor responders. At the same time, IKBKE was reduced in poor responders. The inverse relationship between these closely related transcripts may therefore point towards a dysregulated inflammasome in patients who do not respond well to treatment.

4.4.6. TRAF6

Additionally, the protein encoded by TRAF6 is also involved in immune activity, produced by several immune cells, notably including fibroblast-like synoviocytes (FLS) which are critical in driving the pathology of RA (Wang *et al.*, 2020). The TRAF6 protein may play an important role in RA whereby it largely acts via activation of the NF-κB pathway, leading to an increased release of pro-inflammatory cytokines, activation and differentiation of osteoclasts and causing immune cell infiltration of the synovium (Wang *et al.*, 2020). Indeed, the TRAF6 gene was highly expressed in cells found in the synovium, including FLS, macrophages and various T cell populations, while the authors also reported that TRAF6 also correlated with the severity of joint inflammation in patients with RA ($R = 0.41$, p-value = 0.006) (Zhu *et al.*, 2012). TRAF6 was also shown to be important in driving arthritis in the collagen-induced arthritis (CIA) model, whereby the use of small interfering RNA against TRAF6 blocked its expression in the mice, which reduced the joint inflammation observed (Wang *et al.*, 2015). Such is the potential importance of TRAF6 in RA that efforts have already been undertaken to block its activity (Brenke *et al.*, 2018). Elevated expression of TRAF6 at baseline in patients with a poor response to treatment after 3 months may therefore be clinically meaningful, whereby such individuals would likely have an exacerbated inflammatory profile with increased osteoclast activity.

4.4.7. CIITA

Another important gene in mediating osteoclast activity is the CIITA gene, which encodes major histocompatibility complex (MHC) class II transactivator (MHC2TA)

(Swanberg *et al.*, 2012). In particular, the CIITA was investigated for its involvement in driving osteoclast activity resulting in reduced bone density in osteoporosis. Here, the increased expression of CIITA was associated with lower bone mineral density in patients aged 75, while patients aged 25 did not show this association, therefore pointing towards age as an important factor in the loss of bone density (Swanberg *et al.*, 2012). Indeed, the knockdown of the CIITA gene in mice resulted in reduced osteoclast differentiation, while mice over-expressing the gene had increased osteoclast differentiation and activity, linked to the onset of osteoporosis (Benasciutti *et al.*, 2014). The fact that CIITA expression was increased at baseline in the good responders after 3 months of treatment was surprising due to its reported involvement in driving osteoclast activity and bone resorption. However, since the response to treatment in the TaSER study was defined using the DAS28-ESR, which focuses on joint inflammation and pain, and not the radiography of patients, patients who have a good response may also have a reduced bone density as a result of increased CIITA expression.

4.4.8. STAT1 and STAT2

Further genes of note include STAT1 and STAT2, which were mentioned in the differential analysis, with STAT2 being included in the modelling. These genes encode important proteins involved in modulating the immune response, often to viral infection, as depicted in the pathway analysis results (Tiwari *et al.*, 2019). The products of these genes are co-localised with IRF9 in the same pathway, involving the response to the immune-activating cytokine, IFN, whereby the stimulation of the IFN receptor, IFNAR, leads to the formation of a complex consisting of STAT1, STAT2 and IRF9 (Honda and Taniguchi, 2006; Tiwari *et al.*, 2019). This complex can then migrate to the nucleus, thereby stimulating transcription factors that lead to increased expression of genes such as BST2, which may have a regulatory effect on the IFN response by triggering ubiquitination via E3 ubiquitin ligases, causing the degradation of proteins, notably including a product of RIG-I activity, also mentioned in this analysis (Jin *et al.*, 2017). While being a major molecular driver of the response to viral infection, an overactive or dysregulated IFN pathway may lead to the induction of autoimmunity, thereby linking the expression of the genes from the pathway

analyses with RA (Gota and Calabrese, 2003). Since these genes were associated with the response to treatment, it was hypothesised that the IFN pathway was a critical target for achieving a successful response to MTX.

4.4.9. Transcriptomic Therapeutic Targets

Since the expression of the genes discussed in this chapter may be associated with treatment response in the wider population, thus requiring further investigation, targeting their gene products may therefore be of therapeutic value. Such an approach could supplement the treatment of patients with conventional drugs like MTX. Indeed, small molecule inhibitors have been tested for several of the gene products, including bindarit, which blocks CCL2 (MCP-1), the experimental drug DMXD-011 (Domainex, UK), pralnacasan which targets caspase-1, the downstream effector of the NLRP1 and NLRP6 inflammasomes, and C25-140, which was shown to block the downstream signalling of TRAF6 (Mora *et al.*, 2012; Miklossy, Hilliard and Turkson, 2013; Brenke *et al.*, 2018; Xu *et al.*, 2019). Many of these treatments were in development as anti-cancer therapeutics. A list of the genes, their known biological roles, and associated pharmacological agents are listed in Supplementary Figure 4.

4.4.10. Correlating Metabolites

The genes associated with patient responses to MTX from the differential analysis and the supervised machine learning modelling were then assessed for their relationships with features from the metabolomic data obtained from the same samples. The correlation heatmap provided a helpful overview of the metabolites that correlated with the immune-related genes. For example, kynurenine was negatively correlated with NLRP6, with a borderline-significant negative correlation with NLRP1. Additionally, there was an association of kynurenine with STAT2, STAT1, ADAR, BAST2, and ISG15. This was similar for itaconate and aconitate, along with several tryptophan-related metabolites, including 5-hydroxyindole acetic acid and 5-hydroxytryptophan.

Another study successfully used linear regression to investigate the connections between the serum metabolome and the synovial fluid transcriptome (Narasimhan *et al.*, 2018). The authors reported that several metabolites —including alanine,

aspartate, glutamate-related metabolites, and ketone bodies — were associated with the expression of genes involved in driving inflammatory arthritis, including those encoding TNF and MMPs. Their findings highlighted the value of statistical methods and the incorporation of pathway analysis to integrate omics datasets to understand the molecular changes within the joint that could be targeted.

In the same way, this work involving the transcriptomic and metabolomic datasets from the TaSER trial indicated where metabolites such as itaconate and kynurenine have potential as biomarkers of immune activity. These metabolites were correlated with genes involved in modulating immune-related pathways. Their altered levels in future patients may reveal important immune differences that may make an individual more or less susceptible to MTX. This integration of the two datasets from the TaSER trial showed potential in the development of a multi-omic profile of treatment response, which may reflect altered immune activity which may be modulated by a variety of metabolites whose levels may be perturbed in the circulation.

5. TaSER Multivariate Integration

5.1. Introduction

The previous chapter integrated the transcriptomic and metabolomic datasets obtained from the TaSER trial using biological and statistical methods. Valuable insights were obtained from this analysis, where there were differences in the expression of genes associated with immune activity across response groups. This chapter describes an additional integration approach, thus exploring an alternative method of combining and analysing complex multi-omic datasets. By using a multivariate approach for the integration, it was anticipated that a multi-omic profile consisting of correlated and biologically related features would be uncovered that was associated with treatment response.

5.1.1. Integration Methods

The substantial variety of technologies used to generate omics data means that increasingly sophisticated integration methods are required to deal with the inherent challenges of dealing with highly heterogenous data (Gomez-Cabrero *et al.*, 2014). Such challenges include handling the different sizes and formats of the data, along with the variances and the background noises specific to each data type. For instance, in terms of the number of features, the transcriptome can include more than ten times that detected during a typical metabolomics study. As a result, when using a simple statistical integration method, the transcripts would likely overwhelm the metabolites and so may hide meaningful results. There is an expectation that incorporating additional omics datatypes into an analysis will provide a more complete perspective of the mechanisms of disease. Another integration method was used with the intention of demonstrating how complex datasets can be robustly analysed and valuable insights could be revealed that were previously hidden.

Data integration methods can be broadly classified as biology or data-driven, as described in a landmark paper for the field (Thomas and Ganji, 2006). The biology-driven methods include pathway analysis, which involves tracking the molecular

events from the results of each dataset using pre-existing biological knowledge through databases like KEGG (Cavill *et al.*, 2016).

Pathway analysis and a conceptual data integration method are most typically favoured by biologists, where the tools and interpretation are most user-friendly. Many tools are available, including open-source and online tools, such as GraphOmics, MiBiOmics and MetaboAnalyst (Chong, Wishart and Xia, 2019; Wandy and Daly, 2021; Zoppi *et al.*, 2021). While useful in mapping the features to known pathways, such tools may miss meaningful features, where they usually depend on prior knowledge and established databases, and so may struggle where a pathway is not fully characterised. Additionally, these tools rely on the features being identified and annotated using a standard approach, which may be limited during metabolomics analysis. This is partly due to the different metabolite aliases and the fact that multiple isomers can be detected, thus confusing the identification.

Using purely statistical methods may therefore be more favourable, especially during an exploratory analysis where complete knowledge of the pathways may not exist. These include correlation-based, concatenation-based and multivariate methods (Cavill *et al.*, 2016). Cavill et al. note that the multivariate method provided the most robust approach, despite requiring a more complicated interpretation than the other two. Correlation-based methods involve investigating how features across the datatypes may correlate. In contrast, the concatenation method combines the datasets into a single structure which can then be investigated as the researcher desires. A major flaw of these two simpler methods is especially apparent when integrating datasets with different structures and variances, such as the transcriptome and metabolome, where the features of one dataset vastly outnumber the other.

5.1.2. Overview of the Multivariate Method

Using the multivariate integration method allows the datasets to be treated as individual ‘blocks’ rather than being merged as with the alternative methods. This is beneficial because the differences in each dataset's variances, structures, ranges, and background noise do not affect how the other dataset is handled. In other words, each dataset remains independent. Multivariate methods involve

dimension reduction techniques, which can be either unsupervised, such as PCA, or supervised, for example, PLS-DA, both commonly used methods when analysing single omics data. When integrating the datasets, these tools can be used to generate artificial variables, or components, composed of a collection of related features from each dataset that may maximise the difference between sample classes. These components from each dataset can then be assessed for their correlations and a model generated using these components from each block, selected based on their ability to discriminate the samples as well as correlating across the datasets. This is the essence of the data integration analysis for biomarker discovery using latent variable approaches for omics studies (DIABLO) tool used in this work. The DIABLO tool extends the sparse generalised canonical correlation analysis (sGCCA) to balance out the correlations between the artificial components across the blocks and the model's discriminative ability. By using this tool, the intention was to generate a model that could be used to uncover a multi-omics molecular profile associated with the patient responses in the TaSER cohort while also revealing potentially connected multi-omic features (Cavill *et al.*, 2016; Rohart *et al.*, 2017; Singh *et al.*, 2018).

5.1.3. DIABLO in Action: Biomarker Discovery

Given the ability of the DIABLO tool to not only discriminate sample groups but also to identify correlating features across the datasets that influence the classification of samples, this tool has been harnessed in several studies (Singh *et al.*, 2018). For example, it was used to extract multi-omic molecular profiles of cerebrospinal fluid (CSF) samples from patients suffering from medulloblastoma (Lee *et al.*, 2022). The study by Lee et al. (2022) used transcriptomics, metabolomics and lipidomics, which were generated using RNAseq and high-resolution LC-MS/MS. From these data, a multi-omic profile of 19 transcripts, 28 metabolites and 16 molecules from the lipidome was generated that could differentiate patients with medulloblastoma from healthy individuals. Importantly, the authors reported biological connections between the different datatypes. For example, S-adenosyl L-methionine was correlated with UFM1 and with LPC 17:0. It was reported that S-adenosyl L-methionine had cell-cycle modulatory effects, with the expression of UFM1 being associated with the regulation of the cell cycle. They

also reported how several metabolites and lipids were related via tumour hypoxia metabolic pathways.

Like the work performed in this chapter, Lee et al. (2022) performed a differential analysis of each dataset used in the integration, which then informed the molecules to be taken forward, involving the selection of the top 100 features being incorporated into the integration. Refining the features prior to the integration would reduce the computational cost since the modelling can be especially time-consuming.

In another example, the DIABLO tool complemented the analysis that led to the discovery of many potential osteoporosis biomarkers, a small number of which were found to have an influence on bone mineral density (BMD) (Qiu *et al.*, 2020). The metabolomic dataset was generated from serum samples analysed using an LC-MS platform. In contrast, the transcriptomic and methylomic datasets were generated via RNAseq and reduced representation bisulfite sequencing, respectively. Again, initial differential analysis was performed to refine the datasets to the features most associated with the sample class: high BMD and low BMD. By integrating these datasets using the DIABLO tool, the authors revealed a multi-omic molecular profile consisting of 74 genes, 75 methylated CpG sites and 23 metabolites as prominent osteoporosis biomarkers. By performing further analyses involving pathway/network analysis using the STRING interaction tool, Qiu et al. (2020) then described the involvement of these biomarkers in various bone metabolism-related pathways (Szklarczyk *et al.*, 2019). The authors demonstrated the value of applying multiple integration and analytical methods to uncover and further investigate biomarkers associated with the study conditions. For example, taking the results from the multivariate analysis and performing STRING interaction analysis allowed the numerous prominent osteoporosis biomarkers to be traced to shared biological pathways that may inform the disease's pathogenesis mechanisms.

5.1.4. Aims

The incorporation of a multivariate approach for the integration of the transcriptomic and metabolomic datasets from the TaSER cohort was expected to

expand on the findings reported from the previous chapters. The multivariate method was designed to uncover a correlated multi-omic profile capable of discriminating patient classes, such as response to treatment. The main aim of this chapter was to investigate the value of using the multivariate integration for developing a predictive multi-omic profile of treatment response. The secondary aim was to explore whether the multivariate approach uncover treatment response-related mechanisms.

5.2. Methodology

5.2.1. Integrating the Datasets: Multivariate Integration

The multivariate-based method involved generating virtual variables from each omic block by combining linearly related variables to maximise their association with the sample classes. Applying a sparse assumption then allows the classification to be explained using only a handful of features from the components generated. An example of this is the sPLS-DA, of which a derivative was used in this analysis, involving the DIABLO tool from the *mixOmics* package (Rohart et al., 2017; Singh et al., 2018). DIABLO was used to produce a multi-omic molecular profile consisting of correlated features that could be used to predict good and poor responders to MTX from the TaSER cohort. Investigating the correlated features between the datasets was expected to help inform biomarker discovery and understand the biology contributing to response.

Briefly, like other dimension reduction methods, DIABLO reduces the features from each dataset to a smaller number of components consisting of statistically related features with assigned weights based on the covariance between the components and the category being predicted (Singh et al., 2018). Extracting the contents of the components from each dataset can then reveal the molecules that may be biologically related to the changing disease activity in patients.

The DIABLO tool is, in essence, an extension of the multi-block sPLS-DA and the sGCCA to provide an integrative model with a predictive ability (Singh et al., 2018). A regularised GCCA (RGCCA) is another dimension reduction technique, also known as a component-based technique, that extracts correlated components from multiple datasets with shared samples, therefore allowing the relationship

between datasets to be examined (Tenenhaus and Tenenhaus, 2011). The RGCCA can be extended with sparsity introduced through the application of a lasso-based weight which ultimately removes redundant features from the model and allows for feature importance to be performed (Lykou and Whittaker, 2010; Tenenhaus et al., 2014).

5.2.2. Development of the Multi-Omic Integrative Model

Before the model was generated using the DIABLO tool, a sPLS-DA was performed to investigate how the components from each dataset correlated with each other. This was done using the *spls* function from the *mixOmics* package. The top features from each dataset were selected in a pairwise fashion based on their ability to differentiate the response groups of their shared samples. Only the features that had a pairwise correlation coefficient > 0.5 were included (Singh *et al.*, 2018). The features from the pairwise sPLS-DA model were then plotted in relation to the first two components of the model, showing their contribution to these artificial variables that could discriminate the response groups.

The transcriptomic and metabolomics datasets from the initial analysis was used in the following integration analysis, and only peaks that could be at least tentatively identified based on their m/z ratio were included in the analysis. In addition, in keeping with the methods described in other studies that used the DIABLO tool, only the most differentially expressed/abundant features from each dataset were included in the analysis, leading to 219 transcripts and 50 metabolites included for the 72 samples. There was an inevitable loss of information from the metabolomic dataset due to the inclusion of only the putatively identified metabolites, but this was considered acceptable due to the reduced computational cost involved in the modelling and showing only biologically known features in the results, which could be further investigated.

The model was tuned for several parameters, with the *tune* function in mixOmics being used for this. The number of components was tuned based on the classification error rate. The balanced error rate (BER) and the overall error rate (OER) were assessed, along with the distance metrics to estimate the error rate.

5.2.3. DIABLO: Model Development

The first of the hyperparameters to be tuned was the design matrix, which was used to define how closely the transcriptomic and metabolomic datasets related. For example, it would be expected that datasets from the same source material, such as synovial fluid, and covering a short molecular distance between data types, such as between genomic and transcriptomic data, would have a high design matrix value of 0.8-1.0. However, since the transcriptomic and metabolomic data used here covered a greater distance in molecular terms, which was more complicated because they are derived from whole blood and plasma, respectively, there may be little connection between these blocks. To maximise the ability of the model to discriminate samples based on their response groups, therefore not prioritising the correlation between features, a design matrix value of 0.1 was selected (Tenenhaus and Tenenhaus, 2011; Tenenhaus et al., 2014).

5.2.4. Tuning the number of components

The number of components in the model refers to the number of orthogonal groups of features used in the classification. Ten components were initially assessed in the tuning stage, with the optimal number of components in the model selected based on the initial sPLS-DA model generated using a 10-fold cross-validation repeated 10 times. The optimal number of components was selected based on the classification error rate, shown as the overall error rate (ER) or the balanced error rate (BER), which report the classification accuracy of the model. As shown in Figure 5.1, the BER decreased to ~0.05 with two components when the maximum distance variable was used in the classification of the samples.

The distance variable is the measure of the degree of separation across the sample groups using the components in the model. The maximum distance is a measure of the greatest distance between the two groups based on the Euclidean distance, whereas the centroid distance is the separation between the centroids (average point) of the two groups and the Mahalanobis distance is a measure of the difference between groups with the distribution of the data being considered rather than simply being the distance between two points (centroids).

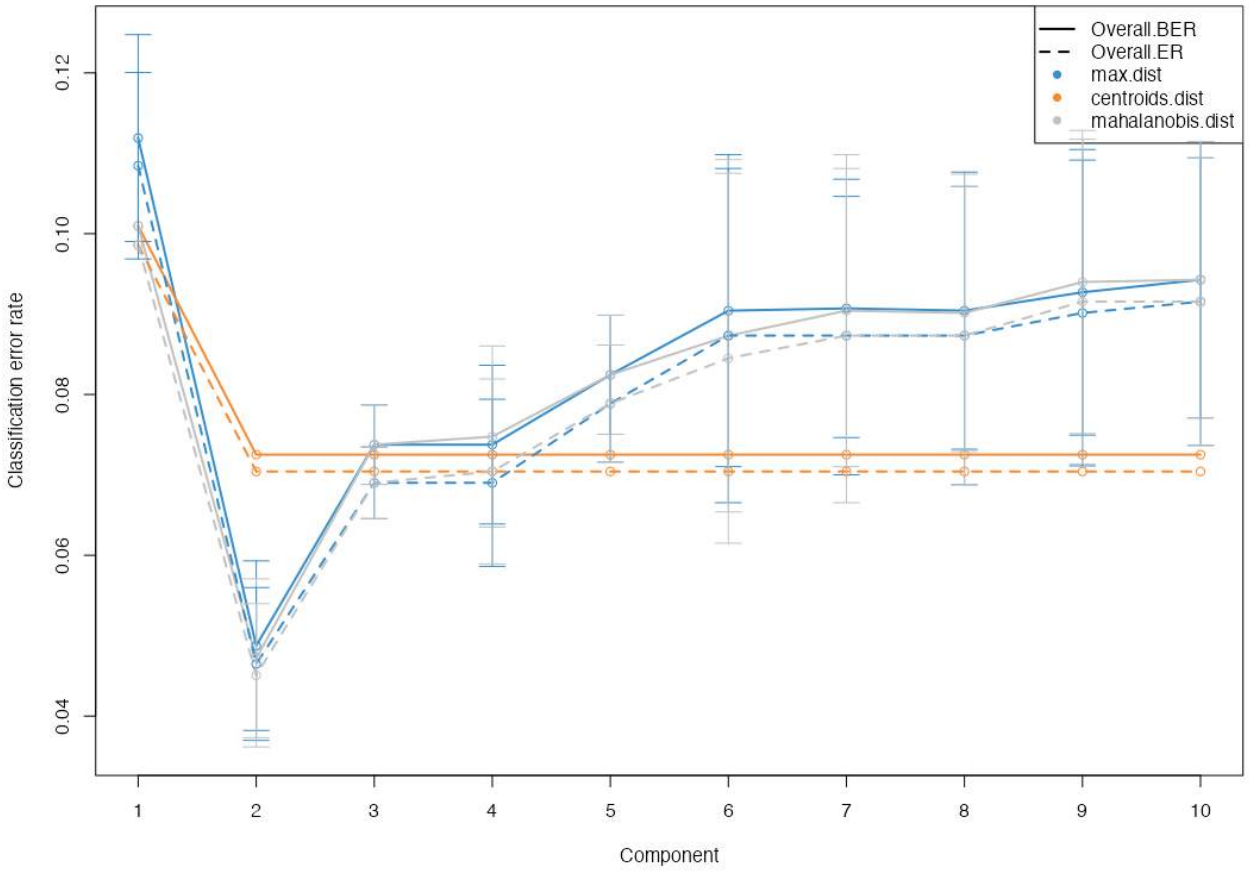

Figure 5.1. Optimising number of components for the DIABLO model , with the error rate against the number of components used in the mixOmics model for tuning. Error rate was calculated across components with three methods of calculating the distance between sample groups: maximum distance (blue), centroids distance (orange) and Mahalanobis distance (grey).

With two components, the features included in the model were then determined using a grid search that generated combinations of features from each block which were then tested using the BER as a performance metric to determine the panel of features to proceed with.

5.3. Results

5.3.1. Investigating Data Format, Ranges and Variances

To compare the differences in the ranges, variances, and overall format of the two datasets from the TaSER trial, the data were concatenated using the shared sample identities in each. These differences are highlighted in Figure 5.2, where

Figure 5.2A includes boxplots for each patient sample, showing the range of abundances of the metabolites included in the dataset and the range of expression of each individual's transcriptome. It was clear from Figure 5.2A that the measured metabolome and transcriptome had different dynamic ranges and variances.

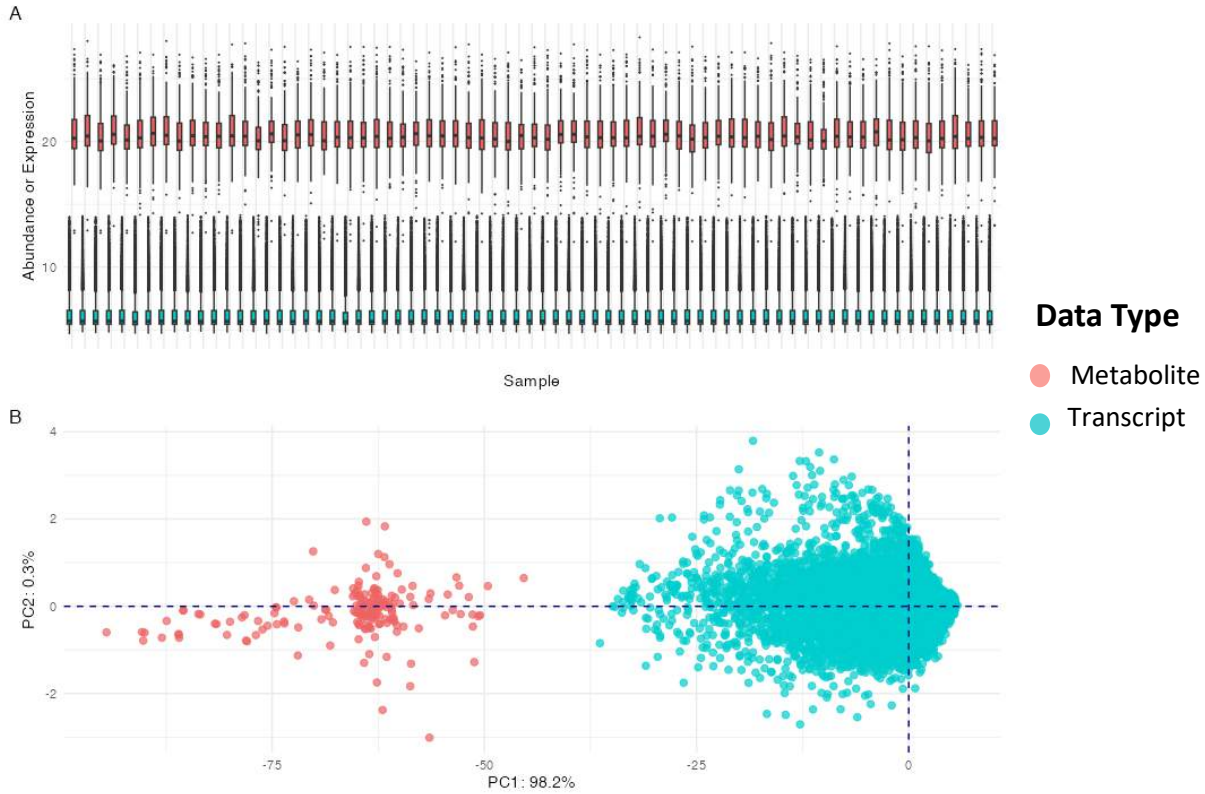

Figure 5.2. Differences in the transcriptomic and metabolomic datasets. A. Boxplots showing a range of abundances/expressions of features for each sample. B. PCA analysis of the features labelled based on the data type.

A PCA was then performed, with the results in Figure 5.2B, which shows the spread and differences of the features from the metabolome and transcriptome. As can be seen in Figure 5.2B, the sheer number of genes in the transcriptome would be expected to overwhelm the metabolites, making the use of methods used in the previous chapters redundant. As such, it was logical to apply a statistical method that would handle each datatype, or block, independently of the other, thereby preventing the inherent differences in the datatypes from influencing the analysis.

5.3.2. Multivariate Approach: Non-Integrative Context of Distinct Datasets

The results from the non-integrative approach involving the sPLS-DA generated for each block of data are shown in Figure 5.3, with the results from each block superimposed. The results indicated that the features from the transcriptome more strongly correlated with components 1 and 2 than the metabolome features. Loosely clustered groups of features from the transcriptomic data were positively correlated with components 1 and 2, with a smaller group that was negatively correlated to each component, primarily component 2.

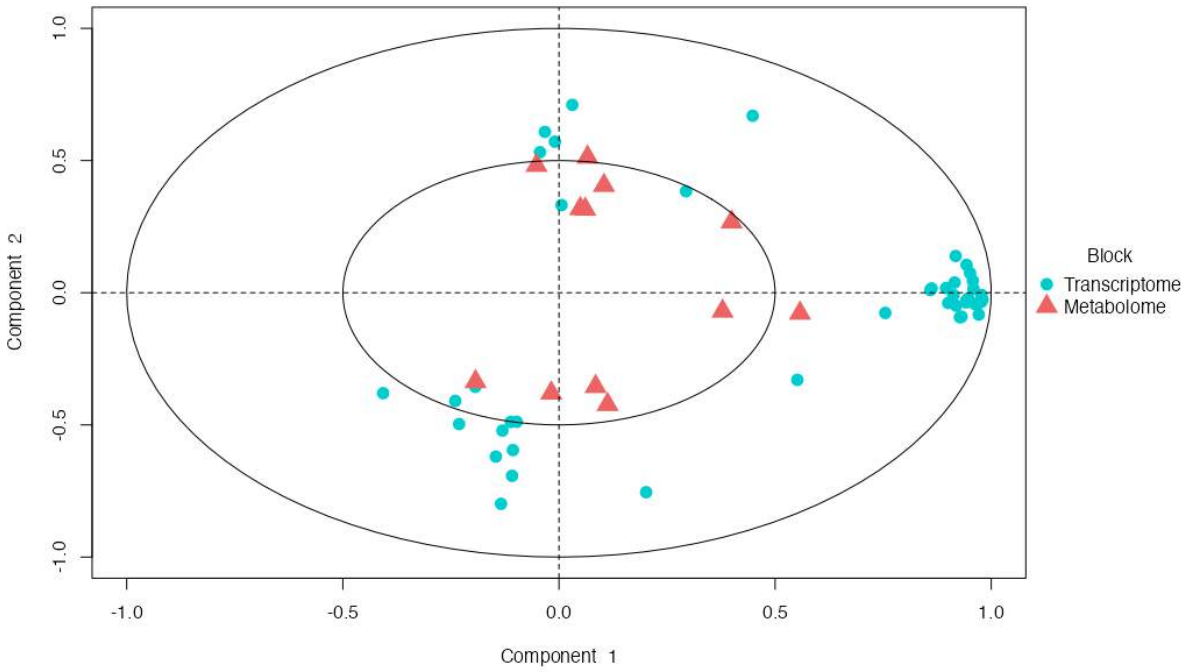

Figure 5.3. Correlational plot showing the results from the pairwise PLS models generated from the transcriptomic and metabolomic datasets from the TaSER trial. The inner ring shows a coefficient of 0.5 with the components, and the outer ring shows a coefficient of 1. Coefficients were calculated, showing features that correlated with the components.

The metabolomic features were weakly correlated with the model's components, with fewer features passing the coefficient of 0.3 for a correlation with these components, hence why few metabolites were included in the plot relative to the transcriptomic features. A coefficient of 0.3 was selected based on the approximate values observed for the correlation coefficients in the previous chapter between the metabolites and transcripts.

Correlations were likely to exist between the transcriptomic and metabolomic features, indicating there may be some relationship between features across the datasets, mainly those that contributed towards component 1. The correlation coefficients of the components defined by the top features from each dataset were then calculated, with the first components from the two blocks having a coefficient of 0.66 and the second component having a coefficient of 0.72 across the blocks.

5.3.3. Applying the DIABLO Model

Using the DIABLO model, the samples were projected into the space defined by the first and second components generated from the transcriptomic and metabolomic datasets, as shown in Figure 5.4. The samples were separated based on the 3-month DAS28-based response groups with the 95% confidence interval ellipses around the coloured points reflecting the good and poor responders.

As shown in Figure 5.4, the correlations between the transcriptomic and metabolomic data for the first (A) and second (B) components were weak (first component correlation coefficient = 0.60; second component correlation coefficient = 0.55), with greater discrimination between good and poor responders being shown for the first component. There was a smaller separation for the second component of the transcriptomic and metabolomic data, indicating that this could not distinguish the response groups using the second component from the transcriptomic and metabolomic datasets.

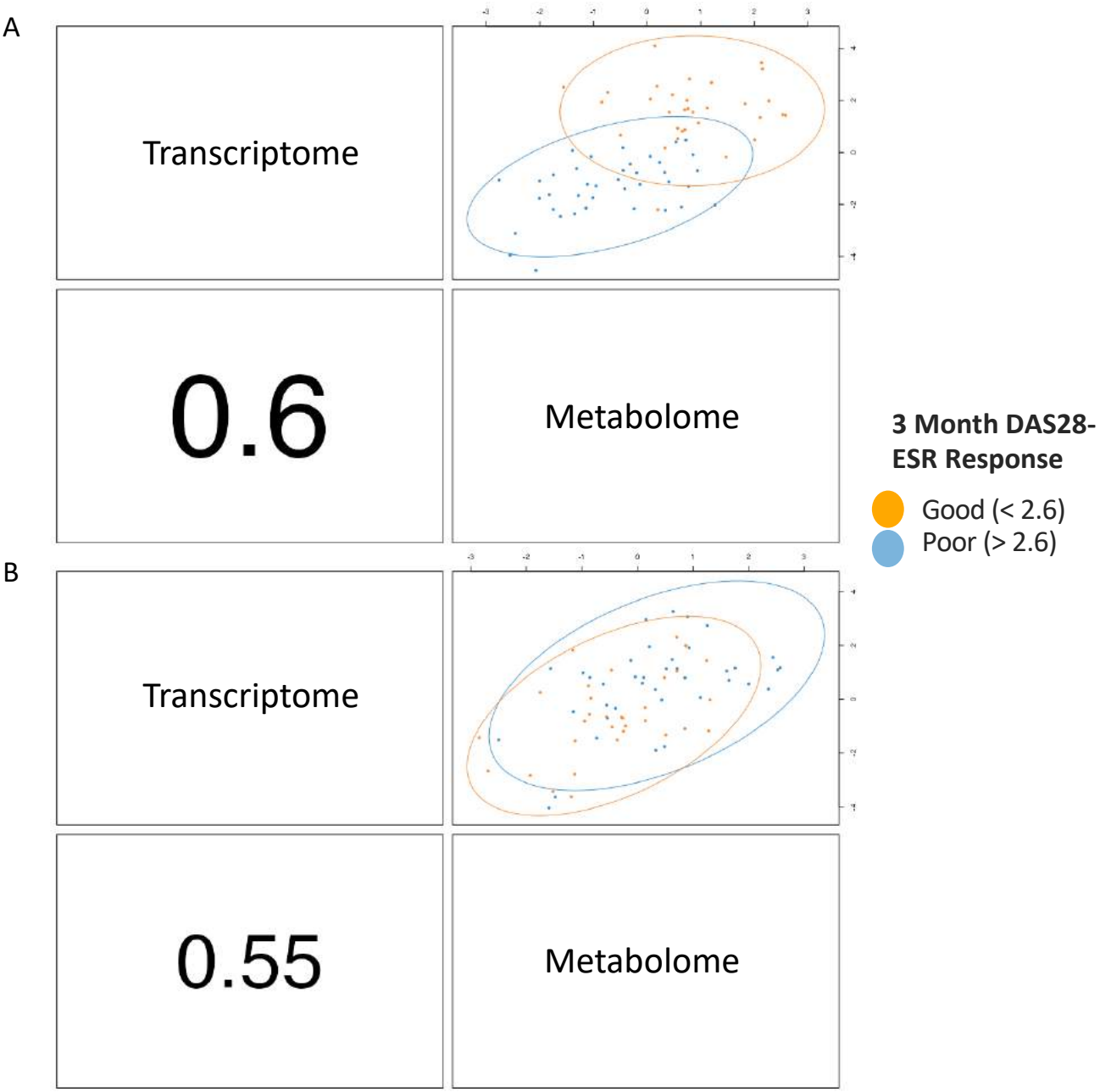

Figure 5.4. Diagnostic plots from mixOmics model. Correlation coefficients were calculated from the components in each plot. A. Component 1 from two blocks. B. Component 2 from two blocks.

The samples were then plotted within the space defined by the components generated from the model from the metabolomic and transcriptomic datasets, shown in Figure 5.5.

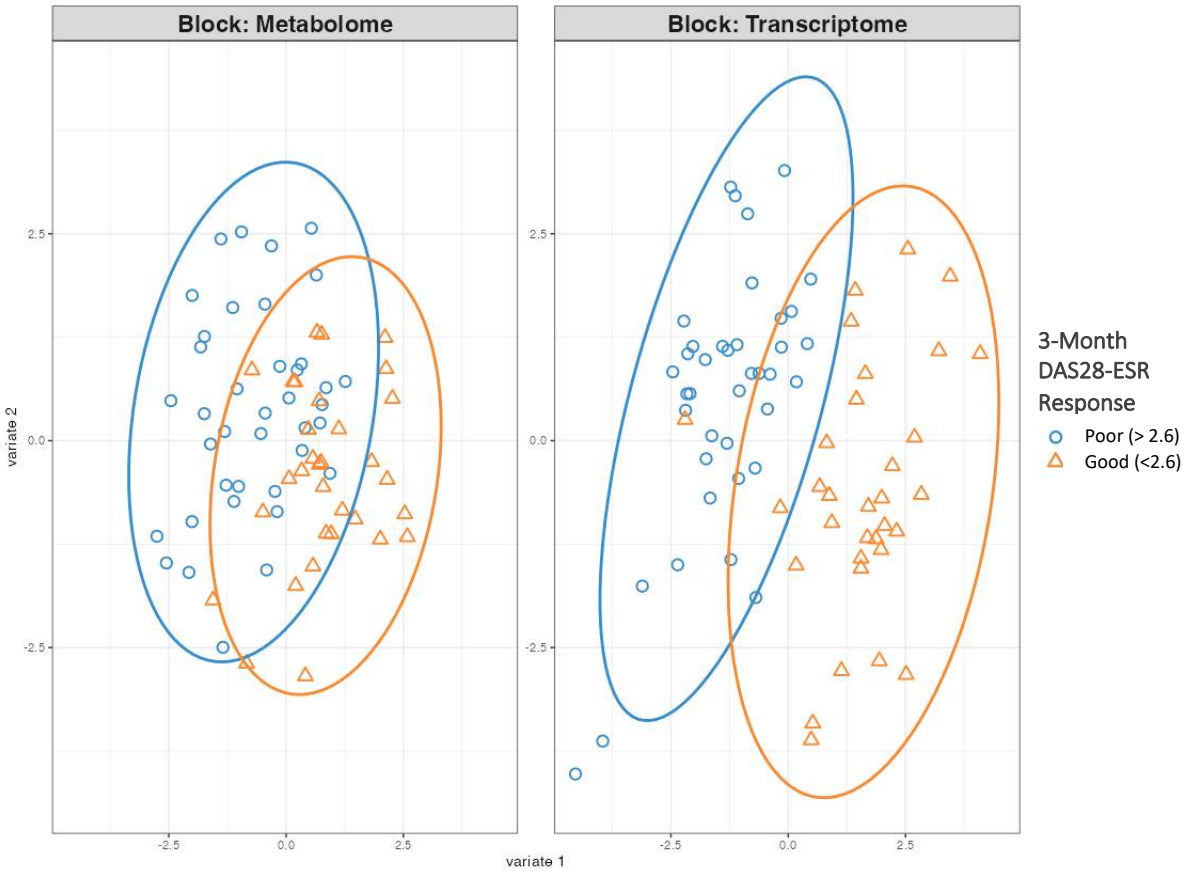

Figure 5.5. Projection of samples in space defined by the components in each block. Samples were labelled based on the 3-month DAS28-based response. Each sample was plotted based on the coordinates for each dataset's two components included in the model. The 95% confidence interval ellipses encapsulated the response groups, with greater clustering observed using the transcriptome components than the metabolome, indicating a greater ability to discriminate the response groups from the transcriptomic block.

The arrow plot in Figure 5.6 was then generated, showing a high variance between the blocks for the sample coordinates reflected by the long arrows. Even though the samples could be clustered relatively well based on the response label, the overlap of the samples from each response group indicated that the model might not provide a robust prediction of patient responses in future cohorts. Nevertheless, an impression of the multi-omic profile associated with response in the TaSER cohort could still be obtained, providing insights into the molecular events contributing to response to treatment.

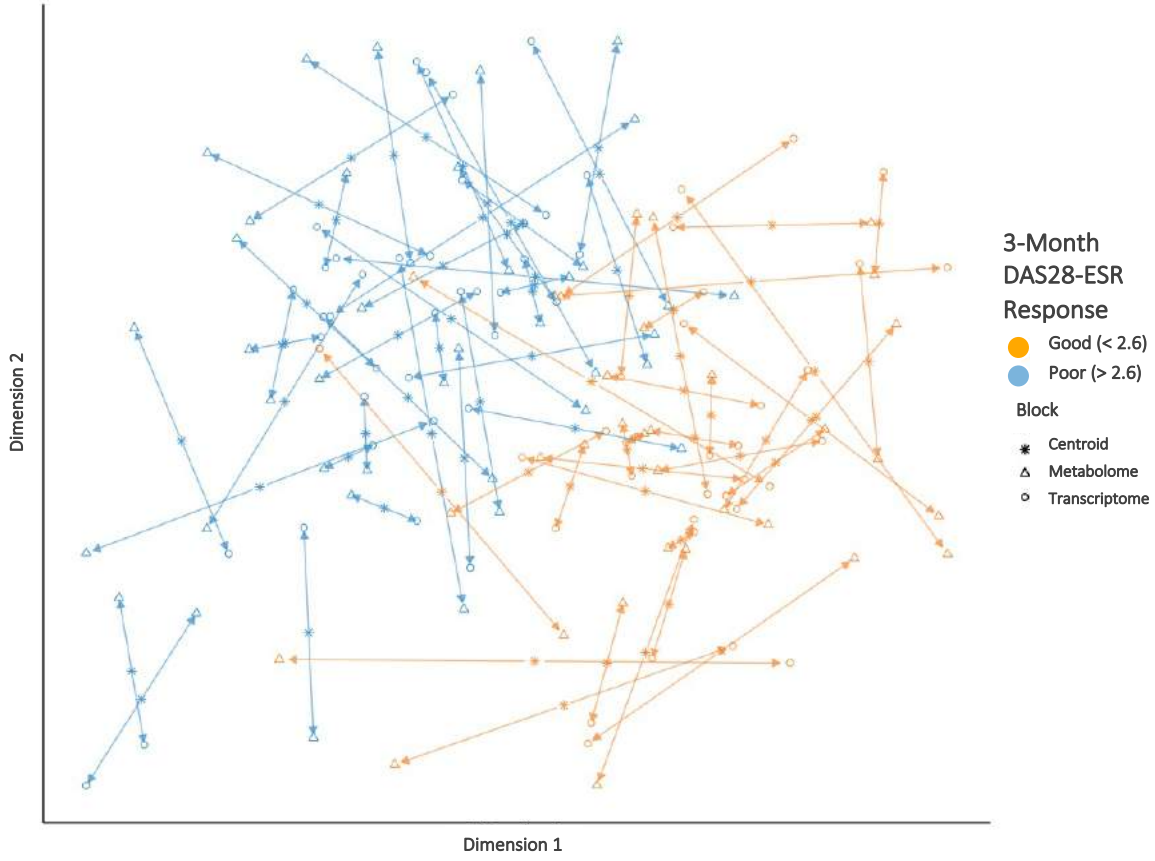

Figure 5.6. Arrow plot showing the projection of the samples in space defined by each block's components. Each arrow comprises three points: the centroid marks the median position between the datasets, and the tips of the arrow mark the position of the sample based on the distinctive blocks.

5.3.4. Feature Plots

The collection of features used in the model across both components is shown in the Circos plot in Figure 5.7, which highlights the correlations between the transcriptomic and metabolomic features.

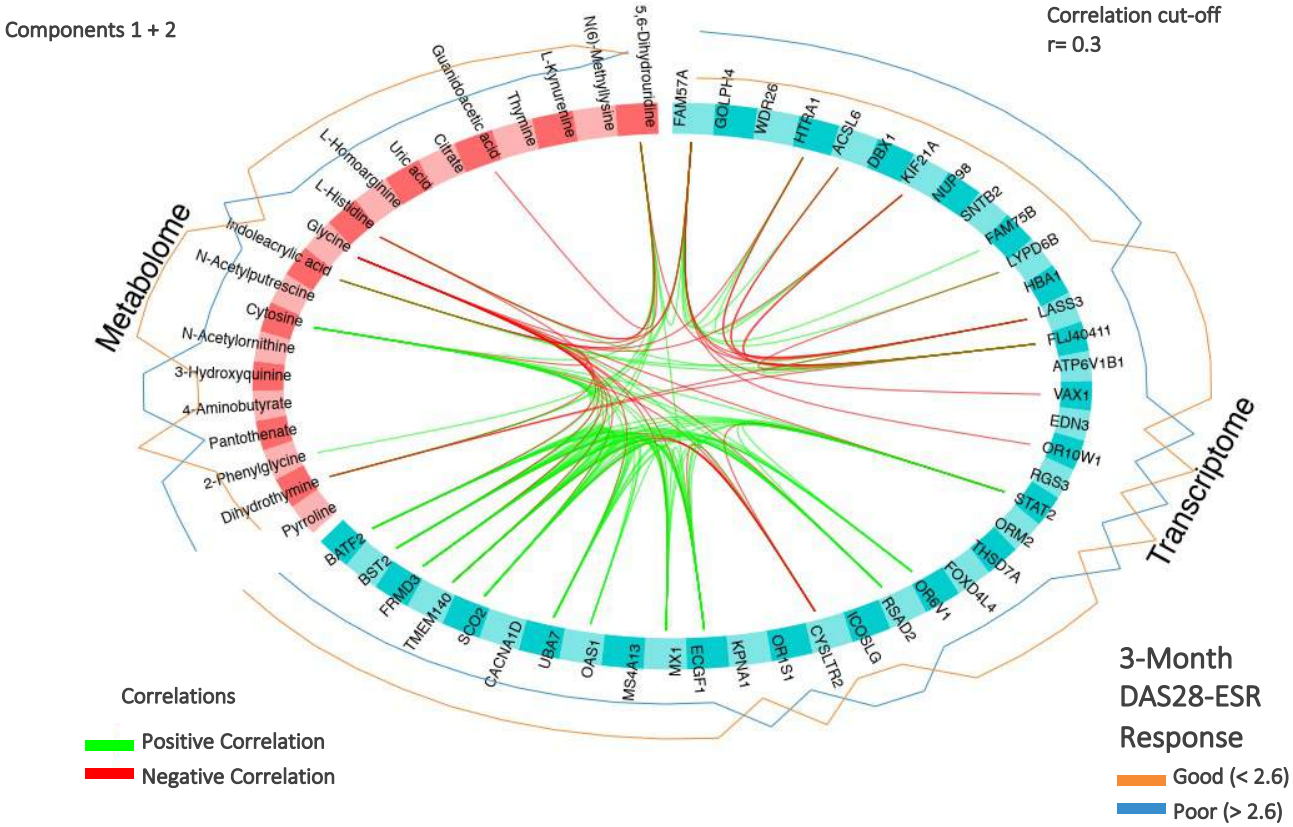

Figure 5.7. Circos plot of the features across the blocks. Correlations between the features from each block were shown, with a coefficient cut-off of 0.3 applied. Positive (green) and negative (red) correlations are shown across blocks. The outer line plots around the Circos plot show in which response group the mean expression/abundance of the features were highest.

Finally, a clustered heatmap was then plotted, which showed the relative levels of each feature across the samples in the cohort, shown in Figure 5.8. The samples were clustered relatively well, with good and poor responders being mostly clustered together. However, the relative levels of the features did not appear to be drastically different across these clustered sample groups.

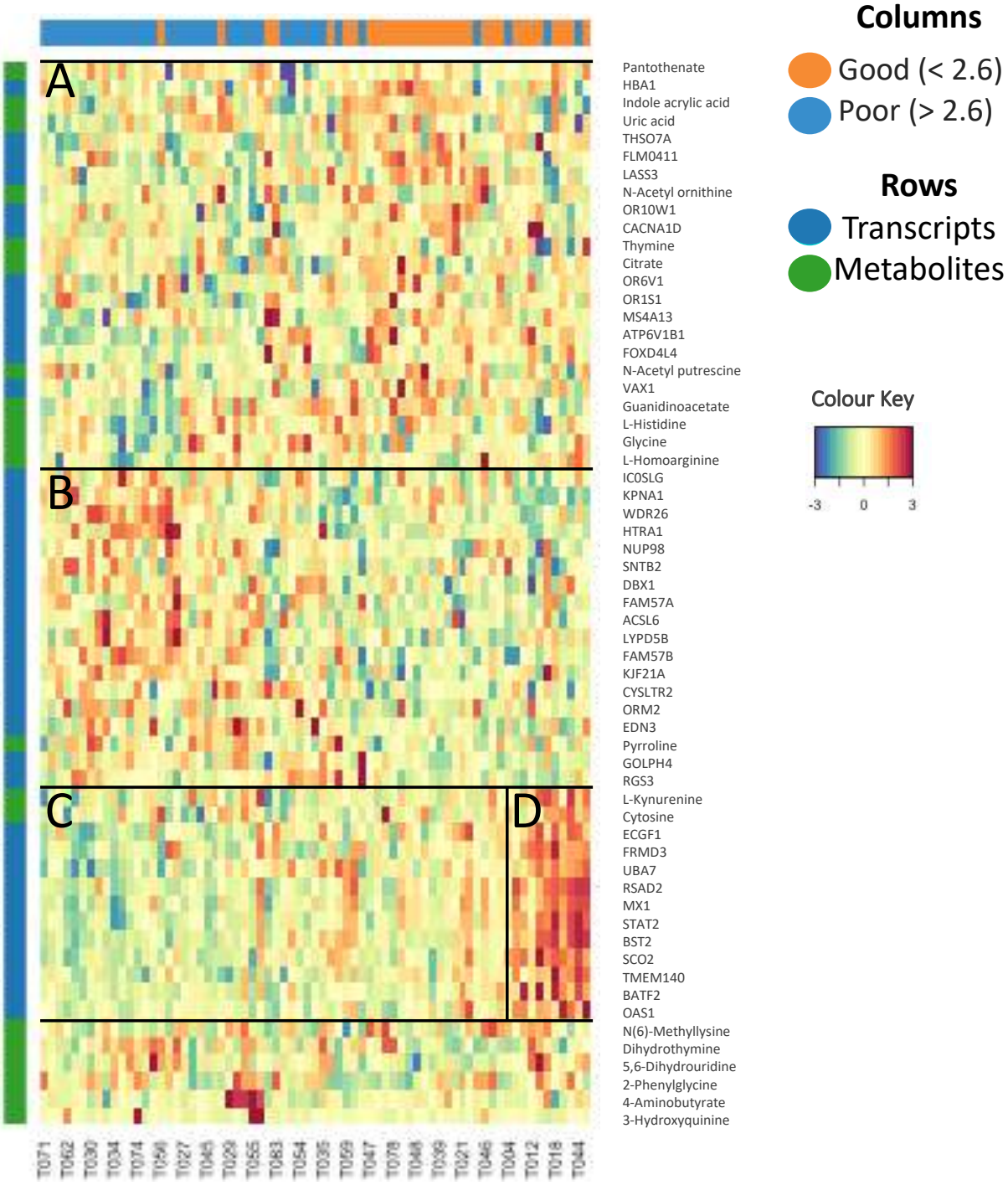

Figure 5.8. Heatmap of the features from each block included in the model. Samples were clustered based on Euclidean distances. The features were labelled in the rows, with their datatype noted on the y-axis, while the samples were labelled in the columns, with their respective responses shown on the x-axis. The clustering of the samples was based on their similar feature abundance/expression, determined using the Euclidean distance.

For example, box A in Figure 5.8 highlights a group of features of which a reasonable proportion was increased in the good responders, albeit subtly. These included pantothenate, indole acrylic acid, uric acid, N-acetylornithine, N-acetyl

putrescine, guanidinoacetate, and HBA1, LASS3, FOXD4L4 and VAX1, among others. Again, including mostly subtle changes in their abundance/expression across the responders, the features in box B appeared to be elevated in the poor responders, including pyrroline, FAM57A, FAM75B, HTRA1 and ACSL6. Several of the metabolites were related, including N-acetylornithine, N-acetyl putrescine, guanidinoacetate, pyrroline and L-homoarginine, along with L-kynurenine and indole acrylic acid. These metabolites were mentioned throughout this thesis. However, none of the associated genes from the related pathways were included in these analyses. These findings were not surprising having considered the results from the previous chapter and how the statistical approach was not expected to necessarily reveal biologically related analytes.

Interestingly within box C was a smaller cluster in box D showing features that were found to largely characterise a subgroup of good responders. The DAS28-ESR of the two patients in this group (T031 and T044) were checked as it was expected these would be near the cut-off of 2.6 for a positive response, which was confirmed where T031 had a score of 2.62, and TO44 had a score of 2.78. The features that characterised this box included kynurenine, cytosine, STAT2, BST2, ECGF1, FRMD3, UBA7, RSAD2, MX1, SCO2, TMEM140, BATF2 and OAS1. Several of these features were found in the metabolic and transcriptomic models described in the previous chapters. These results suggested that the inclusion of these features in the model may be driven by the influence of a small subgroup of patients who had high relative levels of these features. These features may only be helpful as biomarkers in a small proportion of patients with RA.

5.4. Discussion

Integrating multiple omics datasets generated from the same patients can provide valuable perspectives on the molecular mechanisms involved in disease that may be missed if the datasets were analysed individually. The application of integration methods in the analysis of the TaSER metabolomic and transcriptomic datasets was expected to reveal a molecular profile associated with treatment response. The previous chapter explored a simple integration approach, using concatenation and correlations of the features from each dataset. This chapter utilised a more

complicated multivariate method involving the mixOmics package (Singh *et al.*, 2018).

5.4.1. Unpacking the Final Model

The final model consisted of 61 features, of which 16 (26%) were from the metabolomic dataset. Many of these features were associated with the MTX response from the previous chapters, including STAT2, BST2, OAS1, cytosine, L-kynurenine, and indole acrylic acid. Additional features related to these were also included, including other transcripts that provided further evidence of the involvement of IFN signalling, such as MX1 and RSAD2, which are both IFN-induced genes. Other metabolites related to those already explored and included in the multivariate model were homoarginine, guanidinoacetate, N-acetylornithine, N-acetylputrescine, pyrroline, pantothenate and dihydrothymine. In particular, the inclusion of homoarginine and guanidinoacetate in the model was notable since these were explored in detail in the later chapter reporting on the metabolomic data generated from patients with psoriatic arthritis (PsA), another RMD.

However, the value of the multi-omic multivariate method in identifying new biomarkers of response may be limited. This was demonstrated in the heatmap in Figure 5.8 by the lack of a strong discriminatory profile of molecules that characterised the response of patients to MTX. However, the value of these findings may lie in the more subtle differences observed, such as in the collection of features that appeared to characterise the subgroup of positive responders in box D of Figure 5.8. The inclusion of kynurenine and cytosine, as well as several genes that may implicate IFN signalling in association with the positive response in these patients, may be biologically meaningful. For example, kynurenine production can be induced via IFN signalling through the increased activity of the IDO enzymes that metabolise tryptophan (Gustafsson *et al.*, 2020). In another study, the production of kynurenine-related metabolites, notably xanthurenic acid and 3-hydroxyanthranilic acid, was associated with the increased IFN pathway activity in patients with osteoporosis, therefore linking kynurenine metabolism with the inflammation that may lead to bone-related disease (Apalset *et al.*, 2014).

5.4.2. Evaluating the Multivariate Integration Approach

The aim of this chapter's analysis was to search for molecules from different omics platforms that inform predictive biomarker discovery, done so using a multivariate integration. One of the benefits of the multivariate method was that it allowed the datasets to be treated as individual entities, not being combined in such a way that may lead to favouring the results from either of the datasets (Cavill *et al.*, 2016). Furthermore, by first generating artificial components of features that maximised the discrimination of the sample classes in each dataset, followed by investigating the correlations between these components, the molecules that were statistically related could be extracted and explored. The value of this was that new biological pathways could be uncovered that explain the differences between the sample classes, including the processes that lead to a good or poor treatment response.

However, while effective at revealing the features most strongly associated with the differences between the sample classes, the effect of noise and overfitting to the data can mean that entirely unrelated molecules can be incorporated into the final model. This may lead to a model that is not reproducible across other datasets and may lack value despite the initial promising results. The same concern was raised in the previous chapter, where the generation of a supervised machine learning model from the transcriptomic dataset led to a high-performing model that consisted of biologically sparse molecules. Integrating a biological approach into this method was beneficial and gave greater confidence in the model's robustness. A similar approach in this work may benefit, where a multivariate approach not only discriminated sample classes and revealed correlating features across datasets but also used prior biological knowledge to guide the selection of features. Embedding a pathway analysis tool, such as the ShinyGo or Metaboanalyst tools, into existing multivariate techniques may therefore be feasible for the development of an upgraded tool.

An alternative approach to the integration of the datasets may be to apply multiple tools within a pipeline. For example, the value of the multivariate method was that it revealed correlating features in a model that successfully discriminated sample classes. By starting the pipeline with this method, followed

by subsequent pathway analysis on these features, using an existing tool, like GraphOmics, it is anticipated that a biologically connected and correlated panel of molecules could be determined that could be used to guide predictive biomarker discovery (Wandy and Daly, 2021).

The development of more sophisticated and biologically informed statistical methods is expected to cause the field to flourish, where the creators of the Multi-Omics Graph Convolutional Networks reported their novel approach as progressing the field in comparison to related tools such as DIABLO (Wang *et al.*, 2021). Their use of graph convolutional networks (GCNs), a type of deep learning approach, may surpass the use of the multivariate methods used in DIABLO, where GCNs work especially well with complex graph-based data, which includes biological multi-omic datasets.

6. Multi-Centre Metabolomics of Treatment Response in RA

6.1. Introduction

6.1.1. Overview

The prevalence of RA varies around the world, with a recent meta-analysis noting the highest prevalence being reported in Australia (2% of the population), whilst rural parts of South Africa were reported to have close to zero reported cases (0.0026%) (Brighton *et al.*, 1988; Almutairi *et al.*, 2021). Such a range in prevalence may reflect the reported differences in the diagnosis of individuals with RA in developed and developing countries, as well as between urban and rural areas, where those in rural areas are more likely to have a late diagnosis and greater disease burden (Hodkinson, Tikly and Adebajo, 2014; Almoallim *et al.*, 2021). Across Europe and North America, the prevalence also varies, with 0.54% (95% CI: 0.50- 0.59) and 0.7% (95% CI: 0.57- 0.86), respectively (Almutairi *et al.*, 2021). Since RA is a disease with genetic and environmental factors, the differences in geography and culture may drive this variance. However, care in interpreting the rates is needed, with the age and sex being other important risk factors in the disease (Finckh *et al.*, 2022). For example, exposure to industrial waste, smoking and lifestyle habits, including diet, are all risk factors for the emergence of RA, which may explain a higher prevalence of the disease in industrialised countries (Smolen *et al.*, 2018; Finckh *et al.*, 2022).

6.1.2. Treatment response metabolic profiles in other research centres

Two metabolomic datasets were obtained to evaluate the TaSER metabolic profile of treatment response and to continue investigating the metabolites associated with response. Doing so was expected to develop the understanding of the role of the metabolome in contributing towards a successful response to treatment, including MTX and other commonly used treatments. These datasets were obtained via an advanced search using PubMed, described in the Section 6.2.1, and represented independent populations from that investigated in the TaSER trial (Gosselt *et al.*, 2020; Hur *et al.*, 2021). The analysis by Gosselt et al. was performed on the Treatment in the Rotterdam Early Arthritis Cohort (tREACH),

involving plasma samples from patients being analysed using an LC-MS platform. A semi-targeted approach was taken, providing a dataset of semi-quantified metabolites since they were measured relative to exogenous metabolite reference standards (Gosselt *et al.*, 2020). The tREACH metabolomic dataset was kindly shared by Professor Robert de Jonge and Dr Helen Gosselt from Amsterdam UMC. The work by Hur et al. (2021) involved plasma samples from patients with RA being analysed using a UPLC-MS/MS platform described in their recent publication. This metabolomic dataset was publicly available as part of their publication and its analysis in this thesis was supported by Professor Jaeyun Sung.

Both studies revealed unique panels of metabolites that were associated with the change in disease activity with the response to treatment in their cohorts. These studies, therefore, provided insights into the metabolites that may contribute towards the resolution of inflammation in RA in response to treatment. In the original publications, the authors of these studies did not report the similar response-associated metabolites as that obtained from the TaSER trial. These findings were mentioned in Section 3.4.3 as part of the discussion of the metabolic profile of MTX-response in the TaSER trial.

6.1.3. Aims

This chapter intended to firstly investigate the reproducibility of the TaSER metabolic profile of treatment response in cohorts of patients with RA from other regions and countries, namely the Netherlands and the USA. Additionally, using the workflow developed throughout this project, a secondary analysis of the datasets included in this chapter was performed to determine whether there were similar trends across these datasets generated in the Netherlands and the USA. It was anticipated that differences would exist between the cohorts owing to lifestyle factors and the differences in the instrumentation used to generate the data, but common metabolic features would be identified relating to the resolution of inflammation with treatment.

6.2. Methods

6.2.1. Identifying the Datasets

A secondary analysis was performed on the datasets generated from the studies described by Gosselt et al. (2020) and Hur et al. (2021). An advanced search identified these studies using PubMed, with the following search terms: *(rheumatoid arthritis) AND (metabolomics) AND (predictive biomarkers) AND (blood)*. Having read through the first dozen studies, the datasets included in these were pursued for further analysis.

The metabolomic data generated from samples from the tREACH trial provided the initial section of this chapter (Gosselt *et al.*, 2020). Important to note, the metabolomic data was semi-quantitative, whereby single concentrations of each reference standard were run alongside samples, making comparisons with datasets from other institutes and studies difficult. This was mentioned in the original publication. Only metabolites with matching standards based on their m/z ratio and RT were included in the analysis, drastically reducing the dataset's number of features.

Following the tREACH metabolomic analysis, the metabolomic data generated at the Mayo Clinic as part of the work by Hur et al. (2021) was then analysed. This study involved an untargeted approach to measuring the metabolome, using a UPLC-MS/MS platform. Compared with the tREACH dataset, this provided a greater coverage of metabolites including those that could be found in the TaSER dataset. This provided another group of patients with RA whose response to treatment was measured along with a baseline metabolome.

Since these data were previously analysed and reported in work by Gosselt et al. (2020) and Hur et al. (2021), this chapter involved independent analyses involving the application of the workflow developed in the chapter describing the TaSER metabolomics. Additionally, the treatment response-associated features from the previous chapters were assessed in this chapter in other patient cohorts to determine the robustness of these findings.

The results from these metabolomic analyses were expected to reiterate those found in the prior publications and so only novel findings were reported in detail.

These were only discussed where similar results were generated and where they underline the reproducibility of the analytical workflow used in this project.

6.2.2. Defining Treatment Response

The DAS28-ESR was used to track changes to disease activity in response to treatment, with the tREACH and Mayo Clinic studies reporting good responses when patients had DAS28-ESR at 3 months < 3.2. However, since the analysis of the TaSER dataset applied the more stringent cut-off for remission to define the binary classes of responses (DAS28-ESR < 2.6), the same threshold was used in this chapter. It was expected that there would be differences in the metabolites associated with these response groups compared with the results described in the original publications.

6.2.3. Notes on the Mayo Clinic Dataset and Treatments Used

The study performed at the Mayo Clinic (Rochester, MA) involved patients with active RA, satisfying the criteria described by EULAR and ACR (Aletaha *et al.*, 2010; Hur *et al.*, 2021). Patients (n=64) had plasma samples taken at baseline and again after a period of 6 to 12 months, which were then analysed via UPLC-MS/MS by Metabolon Inc. (Durham, NC, USA). The original dataset included a further 12 samples as a validation set. However, these samples were taken at a single time point, and no information was provided on the treatments used, so these samples were not included in this analysis.

Patients received a variety of treatments, including csDMARDs, like MTX, sulfasalazine and hydroxychloroquine, or biologics, including TNF-inhibitors, such as etanercept, infliximab, adalimumab and certolizumab. As a result, incorporating this dataset provided an opportunity to investigate whether there was a common metabolic profile in the circulation that was associated with general treatment-agnostic response in RA. It was anticipated that similar metabolites would be associated with successful treatment, regardless of the drug used, whereby the presence of particular metabolites may be beneficial in resolving inflammation associated with RA, along with other RMDs. However, given the different molecular targets of each drug, such as nucleotide syntheses, adenosine release, TNF activity

or B/T cell signalling molecules, like CD20 or CD80/86, it was also expected that different levels of metabolites would provide more favourable environments.

6.3. Results

6.3.1. tREACH Cohort: Demographics

Patients (n=82) enrolled on the tREACH study had various clinical factors and disease activity measures recorded, including the DAS28-ESR score at baseline and after 3-months of treatment, as shown in Table 6.1. At baseline, patients had a mean DAS28-ESR of 4.91 (SD: ± 1.20), which reduced to 3.05 (± 1.35) after 3 months. After 3 months of treatment, 39 (51.2%) patients achieved remission, as per EULAR definitions.

Table 6.1. Patient demographics in the tREACH cohort at baseline and after 3 months. Included are patient factors and disease activity measures.

Demographics	**n = 82**	
Female Sex, n(%)	59 (71.95%)	
Age (y)	51.28 ± 14.55	
BMI	26.23 ± 5.11	
Current Smoker, n(%)	27 (32.92%)	
Anti-Citrullinated Protein Antibody Positive, n(%)	48 (58.52%)	
Rheumatoid Factor Positive, n(%)	44 (53.65%)	
Disease Activity Measures	**Baseline**	**3 Months**
Disease activity score across 28 joints with ESR (DAS28-ESR)	4.91 ± 1.20	3.05 ± 1.35
EULAR Remission Response (DAS28-ESR < 2.6)	-	39 (51.21%)
Erythrocyte sedimentation rate (ESR)	26.47 ± 20.74	
C-reactive protein (CRP)	16.35 ± 25.36	
Health Assessment Questionnaire (HAQ)	37.96 ± 189.65	
Tender joint count across 28 joints (TJC28)	7.88 ± 5.68	
Swollen joint count across 28 joints (SJC28)	7.20 ± 5.54	
Rheumatology attitudes index (RAI)	8.54 ± 6.27	

6.3.2. Correlations of Baseline Metabolites and 3-Month DAS28 Response

The metabolites at baseline that correlated with the DAS28-ESR score at 3 months were investigated, although the correction for multiple testing led to no significantly correlated metabolites being identified. The metabolites that

correlated with DAS28-ESR with unadjusted p-values < 0.05 are shown in Figure 6.1. These metabolites had weak correlations with the disease measure, making it uncertain whether these were meaningful associations. Indeed, it was unlikely that these metabolites would hold much value as individual biomarkers of response.

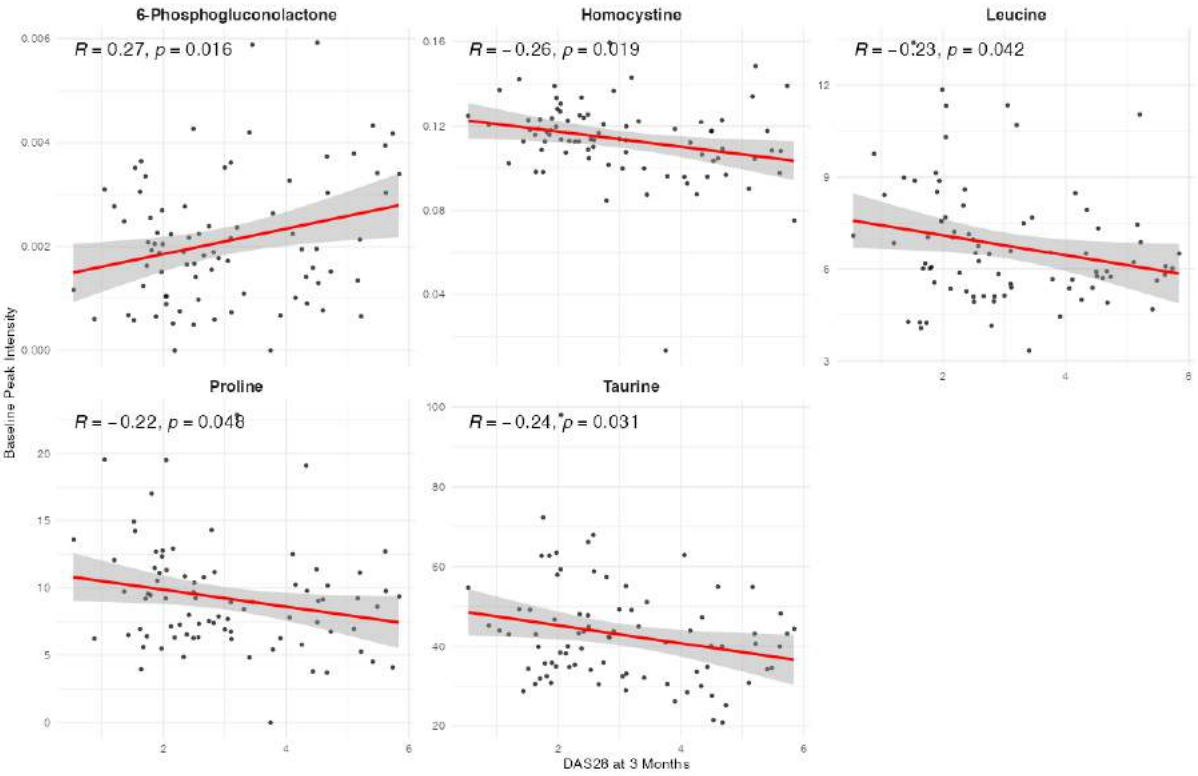

Figure 6.1. Correlational analysis of the baseline metabolites with the DAS28-ESR at 3 months. Spearman correlation coefficients and p-values plotted for each metabolite.

Homocystine and taurine were both included in the original metabolic model from Gosselt et al. (2021), while the other metabolites, including 6-phosphogluconolactone, leucine and proline were not discussed in detail in the study. Aside from 6-phosphogluconolactone, these were negatively correlated with the DAS28-ESR at 3 months, where patients with higher levels of these metabolites at baseline generally had lower DAS28-ESR scores at 3 months.

6.3.3. Differential Analysis of Metabolites Across Response Groups

The binary classification based on the 3-month DAS28-ESR was used to investigate the differential abundance of the baseline metabolites, with the results shown in

Figure 6.2. Like the correlational analysis, none of the metabolites were significant across the two groups after adjusting for multiple testing using the BH correction. However, using a less stringent approach with a threshold based on an unadjusted p-value < 0.05 revealed several metabolites that were potentially differentially abundant across response groups, including fumarate, phosphoenolpyruvate, and ribose 5-phosphate, threonine, and valine.

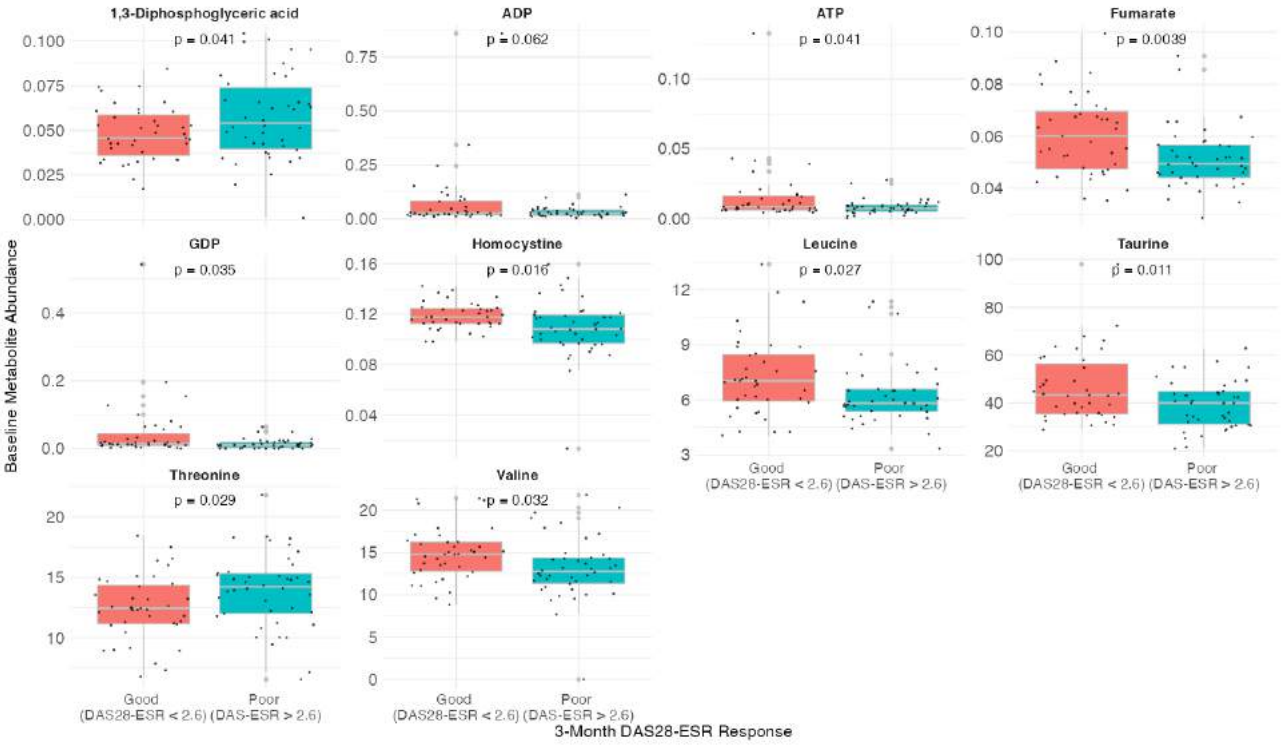

Figure 6.2. Boxplots showing the differential abundance of the metabolites at baseline across the 3-month DAS28-ESR-based response groups.

6.3.4. Attempting to Validate the TaSER Metabolic Model

The metabolic model from the TaSER trial that was generated to predict 3-month DAS28-ESR-defined responses was then assessed for its reproducibility in another related but different cohort. The TaSER model consisted of pyroglutamate, kynurenine, indoleacrylic acid, pyrroline, cytosine, N-succinyl L-citrulline, ornithine and 5-methylcytidine. The tREACH cohort was selected to evaluate the performance of the TaSER metabolic model owing to the fact it was generated similarly to the TaSER dataset, using LC-MS, and the patients had early RA and were primarily treated with MTX. However, the initial correlational and

differential analyses did not reveal any of the same metabolites as those shown in the TaSER metabolic model. As a result, it was not expected that the TaSER metabolic model would accurately predict the treatment responses of the patients in the tREACH cohort.

Additionally, despite both using LC-MS, the differences in the instrumentation involved meant that differences in the ranges and variances were observed across the datasets from TaSER and tREACH. This meant that the model from TaSER could not be directly applied to the tREACH dataset. Moreover, the tREACH dataset did not contain many of the metabolites included in the TaSER model because only metabolites with matching reference standards were included in the tREACH dataset. As a result, the TaSER model was not directly evaluated using the tREACH dataset. It should be noted that a similar approach was also applied to the dataset generated by Hur et al. (2021), but this proved to be similarly poor in terms of its reproducibility, and so was not described at length in this work.

6.3.5. Developing a Metabolic Profile of 3-Month DAS28-ESR Response

Moving forward, the tREACH metabolomic data was then used to generate a new model using the same approach in the TaSER model's generation. As shown in Figure 6.3, the tREACH metabolome was used to generate a model, predicting the good (DAS28-ESR < 2.6) and poor responders (DAS28-ESR > 2.6), with the number of patients in each group shown in Figure 6.3A. Using the RFE, a panel of metabolites was selected for the model, including homocystine, R5P, fumarate, IMP, leucine, UTP, valine, taurine, 1,3-diphosphoglyceric acid and GDP, shown in Figure 6.3B.

The model included several metabolites mentioned in the original work's modelling, including homocysteine, taurine, and 1,3-diphosphoglyceric acid, therefore providing evidence that the workflow performed as expected (Gosselt *et al.*, 2020).

The final tuned model predicted the patients' responses well, with an AUC-ROC of 0.81 (95% CI: 0.72-0.90) and an MCC of 0.585. It should be noted that the repeated

k-fold cross-validation was used as the primary resampling method rather than the holdout method used in the TaSER analysis.

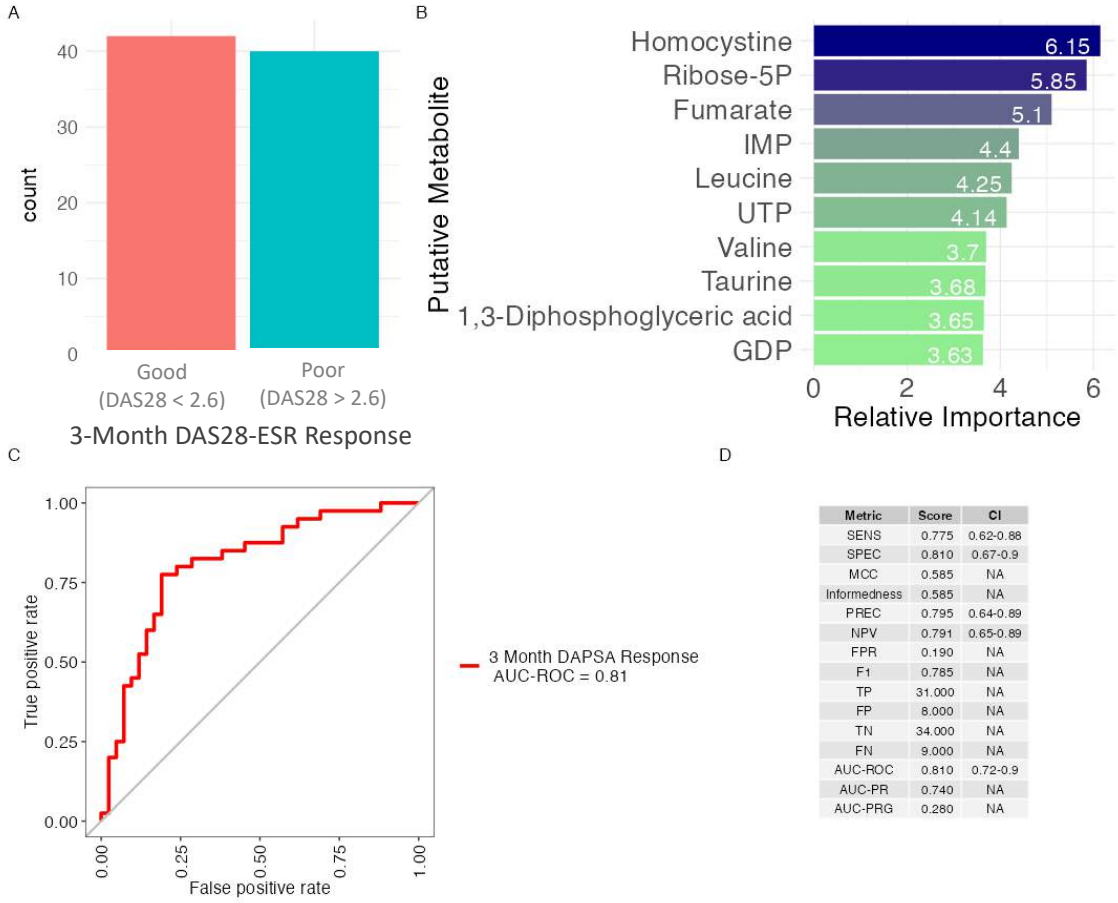

Figure 6.3. Supervised machine learning workflow and results for generation of model from tREACH metabolomic data. A. Number of samples whose patients achieved good or poor responses at 3 months. B. Results from the RFE-feature selection C. ROC curve showing performance of final model having undergone 10-fold cross-validation repeated 100 times. D. Additional performance metrics from the model evaluation.

No shared metabolites were included in the TaSER and tREACH response-associated metabolite models. This suggested that a metabolic profile associated with MTX response in patients with RA may be very loosely associated in the first place, indicating weak associations between the metabolites and the patient outcomes. Alternatively, or indeed in addition to this, the models may have been overfitted to their data, making them unable to be reproduced across different cohorts of patients. A larger sample size would help to determine this, reducing the impact of noise that may be influencing the selection of features within the models.

6.3.6. Mayo Clinic Sung Metabolomics: Demographics

The patients whose samples were included had active RA at baseline, with a mean DAS28-CRP of 3.08 ± 1.31, and after 6-12 months, the mean DAS28-CRP was 3.04 ± 1.39, as described in Table 6.2. There was, therefore, very little change in the mean disease activity of patients over the study period, although 31 (48.44%) of patients achieved remission, based on the DAS28-CRP < 2.6, as per EULAR guidelines.

Despite having more features than the tREACH dataset, and therefore being more likely to include the metabolites mentioned in the TaSER metabolic model, the metabolomic dataset from Hur et al. (2021) could not be used to fully evaluate the TaSER model as had been initially hoped. This was due to the treatment responses of patients being measured after 6 or 12 months — not the 3-month period of treatment as in TaSER and tREACH. Additionally, since patients were treated with MTX in TaSER, the involvement of other DMARDs, notably the biological drugs, meant that a like-for-like comparison could not be performed.

Table 6.2. Patient demographics, disease activity and treatments received in the Mayo Clinic plasma metabolomics study by Hur et al. (2021).

Demographics	**n = 64**	
Female Sex, n(%)	44 (68.75%)	
Age (y)	62.73 ± 10.50	
BMI	30.56 ± 5.66	
Current Smoker, n(%)	7 (10.93%)	
Anti-Citrullinated Protein Antibody Positive, n(%)	44 (68.75%)	
Rheumatoid Factor Positive, n(%)	36 (56.25%)	
Disease Activity Measures	**Baseline**	**6-12 Months**
Disease activity score across 28 joints with CRP (DAS28-CRP)	3.08 ± 1.313	3.04 ± 1.39
EULAR Remission Response (DAS28-CRP < 2.6)	-	31 (48.44%)
Treatment		
Methotrexate (MTX)	48 (75%)	
Sulfasalazine	6 (9.38%)	
Hydroxychloroquine	14 (21.88%)	
Biologic	32 (50%)	
TNF-inhibitor	23 (35.94%)	

Nonetheless, the secondary analysis of the Mayo Clinic's metabolomic dataset was expected to provide valuable insights into the metabolites associated with treatment response.

6.3.7. Correlations of Baseline Metabolites and Treatment Response

The same approach as in previous chapters was taken to investigate the metabolites at baseline that correlated with the DAS28-CRP after a treatment period, with the results shown in Figure 6.4. Most metabolites had correlation coefficients in a similar range to those from TaSER and tREACH, which indicated relatively weak global metabolite correlations with the disease activity following treatment.

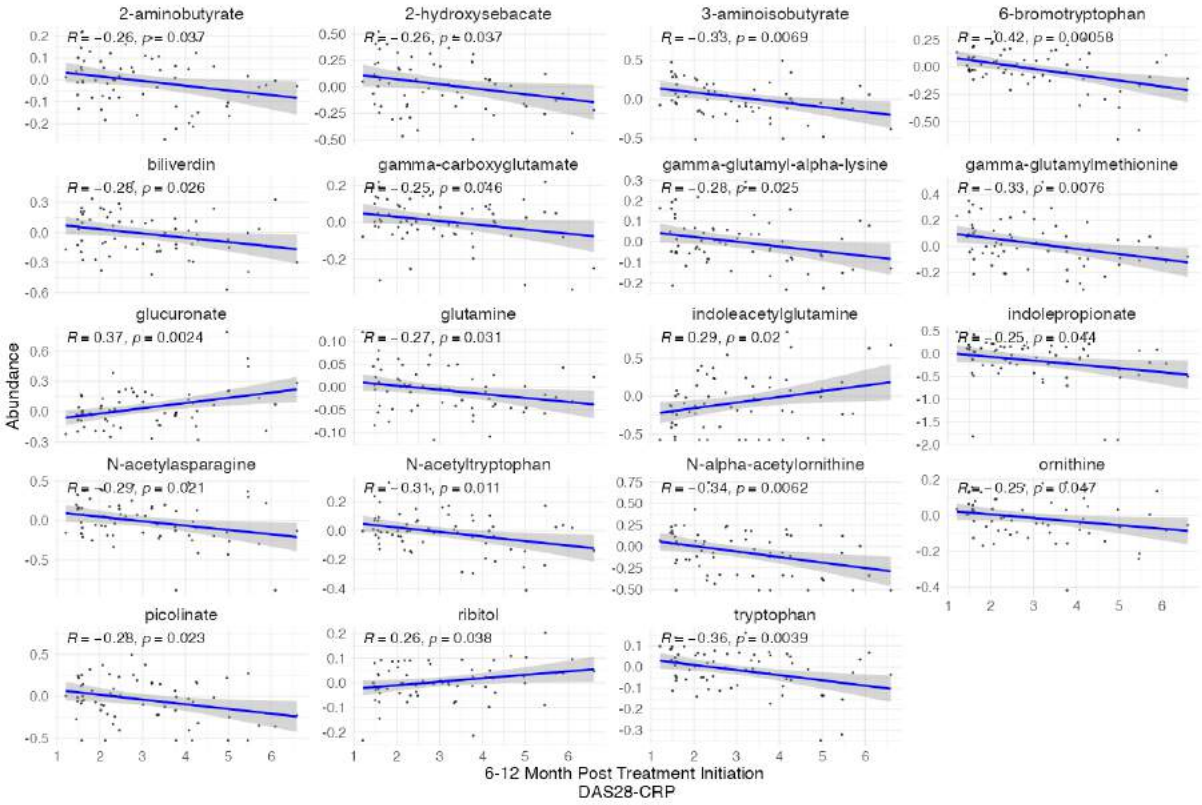

Figure 6.4. Correlations between Mayo Clinic study's baseline metabolites and the DAS28-CRP after treatment (all treatments). Spearman correlation coefficients and p-values calculated for each metabolite's correlation with the DAS28-CRP score after a period of treatment.

Interestingly, several metabolites (and their acetylated forms) appeared more than once across these datasets, including glucuronate, indole propionic acid (IPA), and

ornithine. The correlations of these metabolites with the DAS28-CRP score after a 6-12-month period of treatment are shown in Figure 6.4 alongside the other correlating metabolites.

For example, tryptophan (R= -0.36, p-value = 0.0039), N-acetyltryptophan (R= -0.31, p-value = 0.001), IPA (R= -0.25, p-value = 0.044) and 6-bromotryptophan (R= -0.42, p-value = 0.00058), were all detected and negatively correlated with the DAS28-CRP, indicating that they were elevated in patients at baseline in patients who went on to have a positive response to treatment or had a relatively low DAS28-CRP at the time of measurement. The fact that tryptophan strongly correlated with both 6-bromotryptophan (R=0.65, p-value < $2.2x10^{-16}$) and N-acetyltryptophan (R=0.43, p-value = $3.9x10^{-7}$) indicated that these latter metabolites were likely adducts of tryptophan. IPA was negatively correlated with DAS28-ESR, also appearing in the PsA dataset which potentially indicated changes to tryptophan metabolism along the indole-pathway. This is downstream from indole acrylic acid, which was tentatively identified and correlated with DAS28-ESR in the TaSER study, therefore indicating indole pathway differences associated with treatment response across RMDs.

In addition, the presence of SCFAs was noteworthy — for example, 2-amino butyrate was negatively correlated with the DAS28-CRP (R=-0.26, p-value = 0.037). SCFAs were briefly mentioned in Section 3.4.11, whereby the potential involvement of the gut microbiome in modulating immune activity was discussed following the discovery of tentatively identified indole acrylic acid in association with the TaSER cohort response to treatment. SFCAs are largely produced by the gut microbiome, along with the indole-derived metabolites. They may be involved in regulating the immune response by stimulating the differentiation of T_{reg} cells and impairing the activity of osteoclasts, which is important in driving bone pathology in RA (J. He *et al.*, 2022).

Since these metabolites are largely produced via the gut microbiome, these findings indicate that certain species of bacteria may be involved in producing an anti-inflammatory environment that supports successful responses to treatment in RA.

6.4. Discussion

6.4.1. Limitations of the Multi-Centre Analysis

The multi-centre analysis reported in this chapter provided the opportunity to investigate the robustness of the metabolic profiles of response to treatment in cohorts of patients from different geographical regions. These included the West of Scotland (TaSER trial), the Netherlands (tREACH trial) and the USA (Hur et al. study, Mayo Clinic).

The intention for the multi-centre approach was initially to evaluate whether a metabolic profile of response to treatment in patients with RA that was developed in the TaSER cohort was reproducible in other related cohorts of patients. However, it was apparent early in this process that applying the metabolic profile of response from one dataset to another would be challenging. This was due to sources of variation across the metabolomic datasets generated by each research centre. For example, while variations of the same LC-MS platform were used at each centre, these differed in terms of the chromatography column, the mass spectrometers, the pre-processing steps (including data normalisation), and the downstream analytical workflows used to generate the output data. A consistent panel of metabolites associated with treatment response was not ultimately found across the cohorts. The findings in this chapter indicated that a robust biomarker profile from the metabolome that can predict the patient responses to treatment was unlikely to be found with high accuracy across cohorts. A more reliable approach to this investigation would involve analysing all the samples across cohorts using the same analytical platform, hence removing the instrumentation and operator as sources of variation.

Since untargeted metabolomics provides a relative quantification of the metabolites from a given sample, the comparison of the same metabolite from the same sample across research centres can often show very different measurements. This can be attributed to the fact that the metabolite's measurement — without a standard curve to provide an absolute quantification — is determined based on its peak intensity relative to either the authentic standard provided for the metabolite or the total ion count. In addition, the measurement of a metabolite can be heavily influenced by various instrumentation factors, such as the ionisation

efficiency and the sensitivity of the mass spectrometer's detector, hence causing shifts in the total ion count. This means the instrumentation itself, along with the operator, can have a substantial and meaningful influence on the measurement of the metabolome.

As such, the initial application of the TaSER model to the tREACH dataset, for example, had to be approached differently, involving an attempt to develop another model using the same features as that from TaSER within the tREACH dataset. This was also attempted with the Hur et al. dataset. However, this was not possible owing to differences in the features included in the data, and where the same metabolites appeared across the datasets, these had different dynamic ranges and variances, meaning they were not consistently measured across the cohorts.

These issues with the multi-centre approach underline the inherent challenges with the metabolomics approach. Using targeted metabolomics may mitigate against these challenges of reproducibility across datasets where quantification of the identified molecules can be done using agreed-upon metabolite standards. However, the targeted approach would first require determining the metabolites to measure, therefore requiring an initial untargeted approach for the hypothesis generation stage (Schrimpe-Rutledge *et al.*, 2016).

6.4.2. Findings from the tREACH and Mayo Clinic Metabolomic Analyses

Following the failed attempt to validate the TaSER metabolic model in these additional datasets, the analytical workflow used for previous datasets was then applied to those included in this chapter. The publications that reported the findings from these datasets followed a similar approach, involving supervised machine learning to investigate the metabolites that contributed to the binary classification of the patient responses to the treatment (Gosselt *et al.*, 2020; Hur *et al.*, 2021). However, there was little in the way of overlapping metabolites that helped characterise responders from non-responders in the cohorts of patients with RA. For example, the metabolic profile of response generated from the tREACH metabolomic data included homocystine, ribose-5-phosphate, fumarate,

leucine, valine, and 1,3-diphosphoglyceric acid, along with IMP, UTP and GDP. Meanwhile, the TaSER metabolic profile of MTX response consisted of L-kynurenine, cytosine, 5-methylcytidine, pyroglutamate, pyrroline, L-ornithine, N-succinyl L-citrulline and indoleacrylic acid.

While the original study reported similar metabolites in their analysis, supporting the methodology's robustness, these metabolites did not appear in the results from the other datasets. Indeed, the potential for the influence of geographic/cultural factors and lifestyle differences may mean that no shared metabolic profile of response can be found across different regions. As such, the validation of the findings from each of these datasets may be limited in that it can only be done in metabolomic data generated from the same demographic as the original model was developed upon. However, this obviously limits the value of any clinical tool that emerges from this work since it would be useful for only a small proportion of geographically limited patients. While precision medicine would consider these potential geographic differences to deliver the optimal treatment for the individual based on their molecular, clinical and environmental circumstances, the high cost of generating metabolic profiles of response across a multitude of regions would likely make the campaign largely unattainable and have little value for understanding the metabolic mechanisms that contribute to the response of treatment.

However, the Mayo Clinic metabolomics revealed several metabolites of interest that were mentioned in other chapters in this thesis, including glucuronate, IPA tryptophan and ornithine. One of the advantages of using this dataset was that there was a reasonably high number of tentatively identified metabolites. Contrastingly, the semi-targeted approach used for the tREACH metabolome meant that only metabolites selected by the authors were included in the analysis.

Tryptophan and IPA are related via indole-based metabolism, involving metabolism by the gut microbiome. These metabolites were found to be negatively correlated with the DAS28-CRP after a 6–12 month period of treatment. Since these metabolites were therefore increased in patients with lower disease activity at these time points, they may point towards changes in the gut microbiome,

producing favourable metabolites that may have immunomodulatory and anti-rheumatoid arthritis effects (Negatu *et al.*, 2020; J. He *et al.*, 2022).

Additionally, ornithine was negatively correlated with the DAS28-CRP, which was also seen with N-acetylornithine in the TaSER metabolome, whereby it negatively correlated with DAS28-ESR at 3 months. Additional arginine-related metabolites were associated with the reduced disease activity in analysing the PsA metabolome in a later chapter, including homoarginine and guanidinoacetate, making arginine metabolism a pathway of interest in these RMDs. Moreover, the PsA metabolomic analysis also showed a positive correlation of glucuronate with disease activity after 3 months. Since glucuronate was similarly correlated with DAS28-ESR in the Mayo Clinic study, this may point towards a perturbed xenobiotic processing pathway, where glucuronate, while being involved in glucose metabolism, is better known for its involvement in the removal of drugs and other xenobiotics from the body, a process called glucuronidation (Silva *et al.*, 2003). This was discussed in more detail in the next chapter, in Section 7.4.4.

7. CENTAUR Metabolomics

7.1. Introduction

7.1.1. Background

Patients with PsA are often treated using similar drugs for RA, including MTX, sulfasalazine and TNF inhibitors, such as etanercept (Gossec *et al.*, 2020). As with RA, patients with PsA require early and successful treatment to manage their symptoms and improve their long-term outcomes. Perhaps related to the difficulty in diagnosing PsA, there is a noticeable lack of validated biomarkers for PsA, with clearly fewer studies being performed to obtain candidate biomarkers from the omics platforms that could be used to predict treatment responses in PsA.

This chapter intended to explore the metabolome of patients with PsA as a source of novel biomarkers associated with the response to treatment. The metabolomic data was generated from serum samples obtained via the CENTAUR trial involving patients with PsA treated using various DMARDs. Where the TaSER trial primarily involved patients treated using MTX, the analysis described in this chapter incorporated the treatment of patients using several different DMARDs, similar to the Mayo Clinic cohort from the previous chapter. As a result, a metabolic profile associated with a treatment-agnostic response was investigated here, providing insights into the metabolites that were associated with the resolution of inflammation in patients with PsA. Since this chapter introduces PsA as an additional RMD, a secondary aim of this chapter was to investigate the shared metabolites associated with treatment responses that were expected across these diseases.

As described earlier, there are marked differences between PsA and RA, involving different clinical presentation, genetic and molecular components and differences in the treatments used and how patients respond (Veale and Fearon, 2015). Given the distinction between these diseases, the metabolome from the patients with PsA from the CENTAUR cohort was investigated and compared with the metabolomes generated from cohorts of patients with RA described in previous chapters.

The DAPSA score was used as a primary measure of disease activity in the CENTAUR study and was therefore used to define the responses to treatment after the 3-month period of treatment in this work. Alongside DAPSA, the fibromyalgia (FM) score, SJC66, TJC68, CRP, PVAS, and GVAS were reported. In this chapter, the continuous DAPSA score at 3 months or binary classes based on the DAPSA score were used to explore the metabolites at baseline associated with the response to treatment.

7.1.2. Aims

The metabolomic analysis of the serum samples from patients with PsA enrolled in the CENTAUR study was performed in this chapter. The main aim was to investigate the metabolic features associated with the response to treatment in PsA. The metabolites associated with treatment response in the PsA cohort were compared to the other metabolite panels described in this project.

Since this chapter introduces PsA as an additional RMD, a secondary aim of this chapter was to examine whether shared metabolic features were associated with the response to treatment across these RMDs.

The use of similar DMARDs in RA and PsA for the effective control of disease led to the hypothesis that the common resolution of inflammation might be linked with shared metabolic pathways that may influence the efficacy of these treatments. However, differences were reported in terms of the clinical presentation and the molecular component across these diseases, described in Section 1.3.2.

Investigating differences and similarities in metabolites across diseases may reveal those that modulate the treatment-associated resolution of RMDs and provide new opportunities for targeting these pathways. For example, the targeting of tryptophan metabolism — mentioned in the analysis of the TaSER cohort — using, for example 1-methyltryptophan, may alter the environment that regulates the response to treatment and supplement MTX treatment.

7.2. Methodology

A comprehensive methodology describing the analytical workflow for this work was described in Chapter 2. Since this metabolomic analysis for the CENTAUR dataset

consisted of an additional unique component, specifically the analysis of cytokines in the serum samples of patients, a brief description of this method was provided below.

7.2.1. CENTAUR Study Overview

The CENTAUR study was performed to investigate and characterise the pain pathways involved in PsA, involving neuropathic and nociceptive pain. Since pain and joint inflammation were of interest as part of the CENTAUR study, the DAPSA composite score was used, providing a comprehensive measure of the articular disease and the resolution of joint-based disease in response to treatment. Patients enrolled on the CENTAUR study (n=50) were subject to several inclusion criteria, including the following:

- Patients had active disease having been defined using the CASPAR criteria.
- Clinical examination revealed evidence of ongoing inflammation (synovitis).
- Patients were due to be treated using a new immunosuppressant drug as part of their disease management.

Patients were initially referred by their direct care team in the rheumatology department, which they had been attending. Having not achieved successful management of their disease, patients were due to be switched to an alternative DMARD. As a result, patients were not DMARD-treatment naïve at baseline.

The study's primary aim was to investigate and characterise the phenomenon of centralised pain in patients with PsA. Clinical examinations and measurements of pain, including fibromyalgia (FM) score and the DAPSA, were taken at baseline, 3 months, and 6 months, along with blood samples at these time points. Due to the focus on pain pathways in the original study, the DAPSA score was used as the primary disease activity measure, concentrating on joint-based pain. Patients also underwent brain MRI scans and quantitative sensory testing performed by Dr Flavia Sunzini which was not reported in this work.

Serum samples from patients were prepared by Dr Flavia Sunzini using a standard protocol (Luque-Garcia and Neubert, 2007). These were then analysed via the LC-MS platform at Glasgow Polyomics, with further detail provided in Section 2.2.

Only the baseline samples were analysed to measure the metabolome prior to patients receiving the new treatment, therefore allowing for an investigation into metabolites associated with subsequent treatment response. The treatment response was defined using the 3-month DAPSA score, with a binary classification of patients being established, where patients were considered to have a good response with a 3-month DAPSA score ≤ 14 and a poor response with a DAPSA score ≥ 28. Patients with DAPSA scores between 14 and 28 were considered to have a partial/limited response to treatment.

7.2.2. Additional Component to Workflow: Cytokine Analysis

The serum samples were subject to further analysis to measure the levels of a panel of cytokines selected for their involvement in inflammatory processes and in processes relating to FM and related pathologies in PsA. For example, molecules that regulate and modulate hunger may be important factors in PsA, along with the association of fatigue and the neurological component of the disease (Cañete and Mease, 2012; Baker *et al.*, 2017; Conaghan *et al.*, 2020). Indeed, several cytokines were previously linked with the pathology of psoriasis and PsA, including the following: IL-1β, IL-2, IL-10, IL-12, IL-17, IL-22, IL-23, IFN-γ and TNF-α (Nestle *et al.*, 2005; Nograles *et al.*, 2008; Tonel *et al.*, 2010; Zaba *et al.*, 2010; Lynde *et al.*, 2014).

The cytokines were detected using the MSD platform, involving the MESO QuickPlex SQ 120MM analyser (Meso Scale Diagnostics, LLC, Rockville, Maryland, USA). The MSD S-plex immunoassay was used to measure IL-17A and IL-1β, while the U-plex immunoassay was used to measure the remaining cytokines, as performed by Dr Flavia Sunzini. The raw data were kindly shared by Dr Flavia Sunzini and analysed alongside the patient and metabolomic data within the R environment.

7.3. Results

7.3.1. Patient Demographics

The disease activity measurements of patients from the CENTAUR trial were taken at baseline and after 3 months, with the 3-month DAPSA being used to determine

the response to treatment. The patient demographics and disease activity measures obtained from the CENTAUR trial are shown in Table 7.1.

Table 7.1. Patient demographics from CENTAUR study with clinical factors and disease measurements at baseline and 3 months.

Patient	**n= 50**	
Female Sex, n(%)	23 (52.3%)	
Age (y)	49 ± 11.50	
BMI	29.77 ± 4.43	
Current Smoker, n(%)	4 (9.1%)	
Disease Activity Measures	**Baseline**	**3 Months**
Disease Activity in Psoriatic Arthritis (DAPSA)	41.64 ± 20.68	31.38 ± 20.32
Fibromyalgia (FM) score	12.59 ± 5.81	
C-reactive protein (CRP) (mg/dl)	0.59 ± 0.70	
Swollen joint count across 66 joints (SJC66)	4.54 ± 5.00	
Tender joint count across 68 joints (TJC68)	16.44 ± 14.91	
Pain visual analogue scale (PVAS)	5.44 ± 2.22	
Global visual analogue scale (GVAS)	4.58 ± 2.64	

7.3.2. Multivariate Analysis

The results from the PCA of metabolite profile with 3-month DAPSA scores are shown in Figure 7.1. The samples were plotted in the space defined by PCs 1 and 2, and the samples were labelled based on the DAPSA score at 3 months.

As was the case for the baseline metabolome from the TaSER cohort there was no global metabolomic profile associated with the 3-month response to treatment. To examine whether any specific features were associated with treatment response, the individual metabolites were then investigated for their associations with the 3-month DAPSA score.

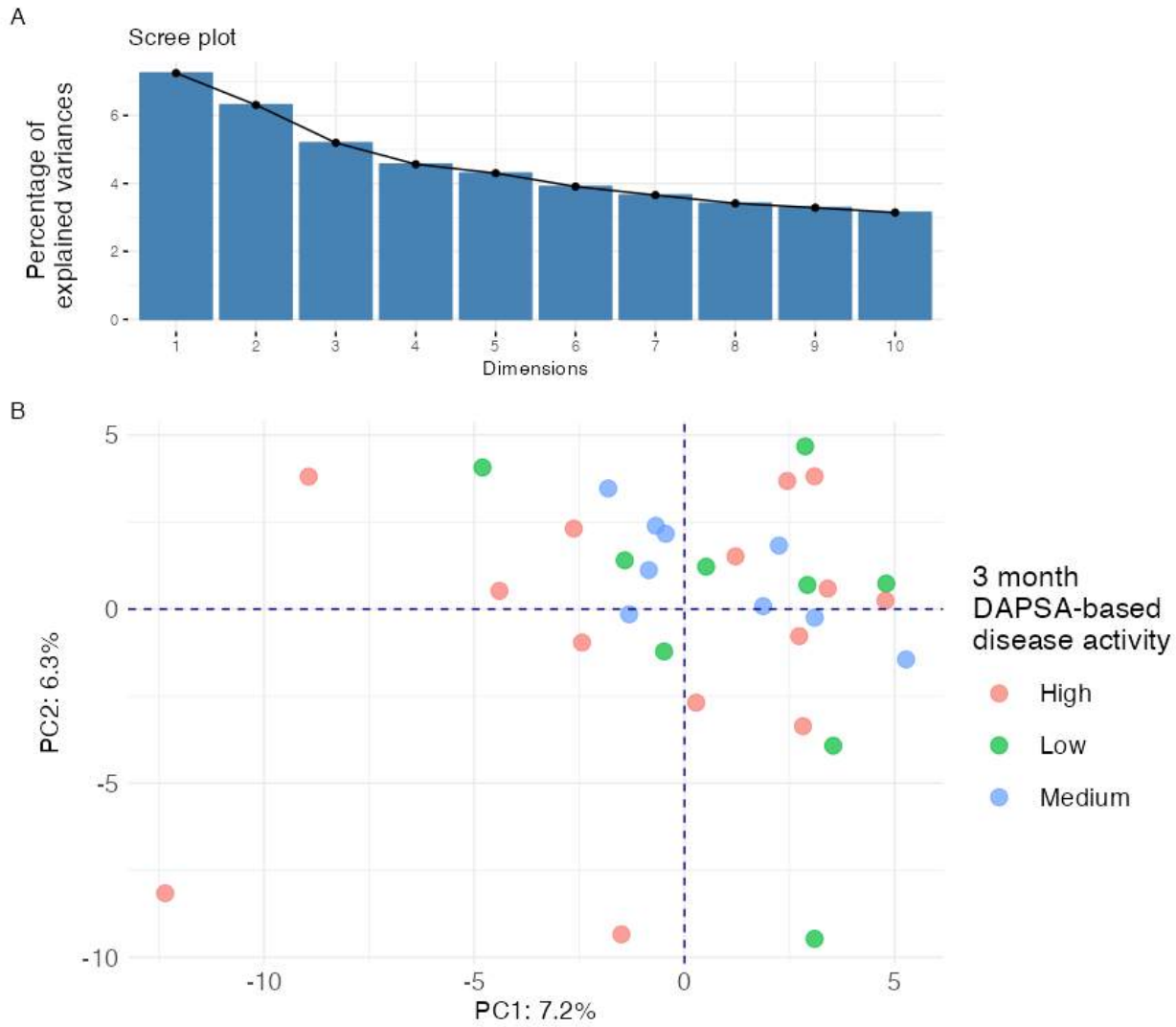

Figure 7.1. PCA shows the samples at baseline, and samples were labelled using disease measures. A. Scree plot. B. Samples projected in space defined by PC1 and PC2, with 3-month DAPSA-based response used to label samples.

7.3.3. Metabolites Associated with the 3-Month Response

The metabolites correlated with the 3-month DAPSA were explored, correlating the baseline metabolite abundances against the 3-month DAPSA. Initially, only the metabolites with an adjusted p-value < 0.05 were included, but no significantly correlated metabolites were found after the correction. As a result, a less stringent selection was performed, using an unadjusted p-value of 0.05, with the results shown in Figure 7.2, with the caveat that these metabolites may not be truly correlated with the 3-month DAPSA score. Nevertheless, the correlation

coefficients of the metabolites in Figure 7.2 indicate there may indeed be associations between these metabolites and the 3-month DAPSA score.

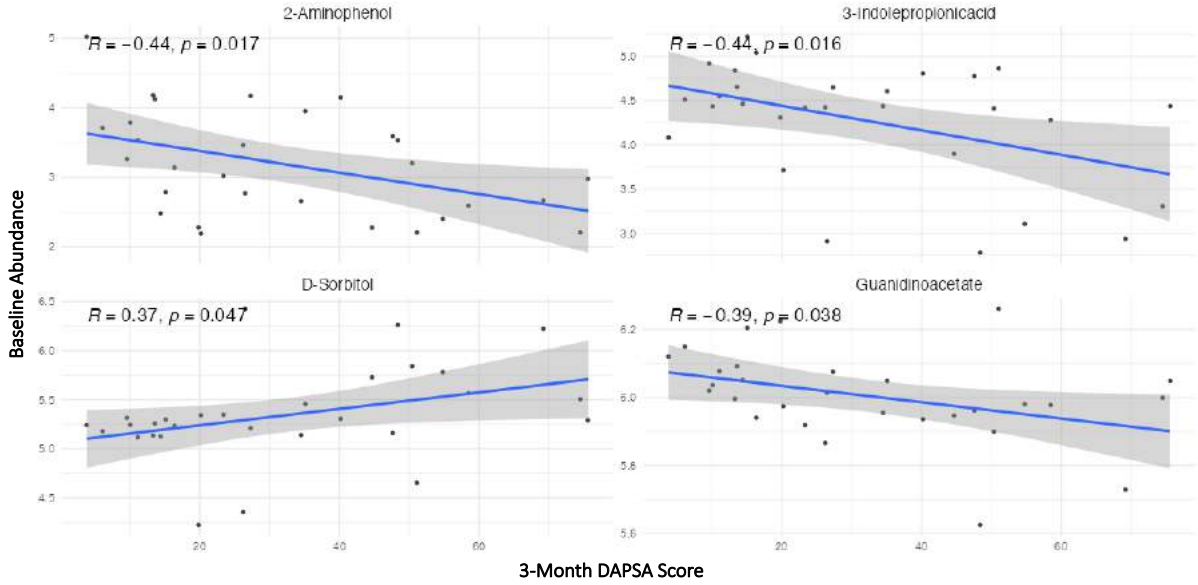

Figure 7.2. Correlating metabolites at baseline with 3-month DAPSA from CENTAUR cohort. Spearman correlation coefficients and associated p-values were calculated and plotted alongside the regression lines.

Care may need to be taken in interpreting these findings since these metabolites were only tentatively identified based on the mass alone matching known biological molecules from HMDB. In particular, the m/z ratio and potential molecular formulae generated for these metabolites also matched several other molecules. As a result, these may be identified as other metabolties. Their true identities were not determined, given the lack of authentic standards for these compounds and fragmentation data that would otherwise support the identification.

Tentatively identified guanidinoacetate and IPA were negatively correlated with the 3-month DAPSA and were elevated in patients with a lower DAPSA after 3 months of treatment. In particular, IPA was of interest due to its involvement in tryptophan metabolism, a pathway described in the literature as having immunomodulatory effects in vitro (Krishnan *et al.*, 2018; Cussotto *et al.*, 2020). Despite only tentative identification of these metabolites being possible with this work, their appearance (or that of related metabolites) in the analysis of

metabolomic data from other cohorts provided greater confidence that these analytes had an association with treatment response.

Next, the differential abundance of the metabolites across the 3-month DAPSA groups was investigated. The results from the differential analysis are shown in Figure 7.3.

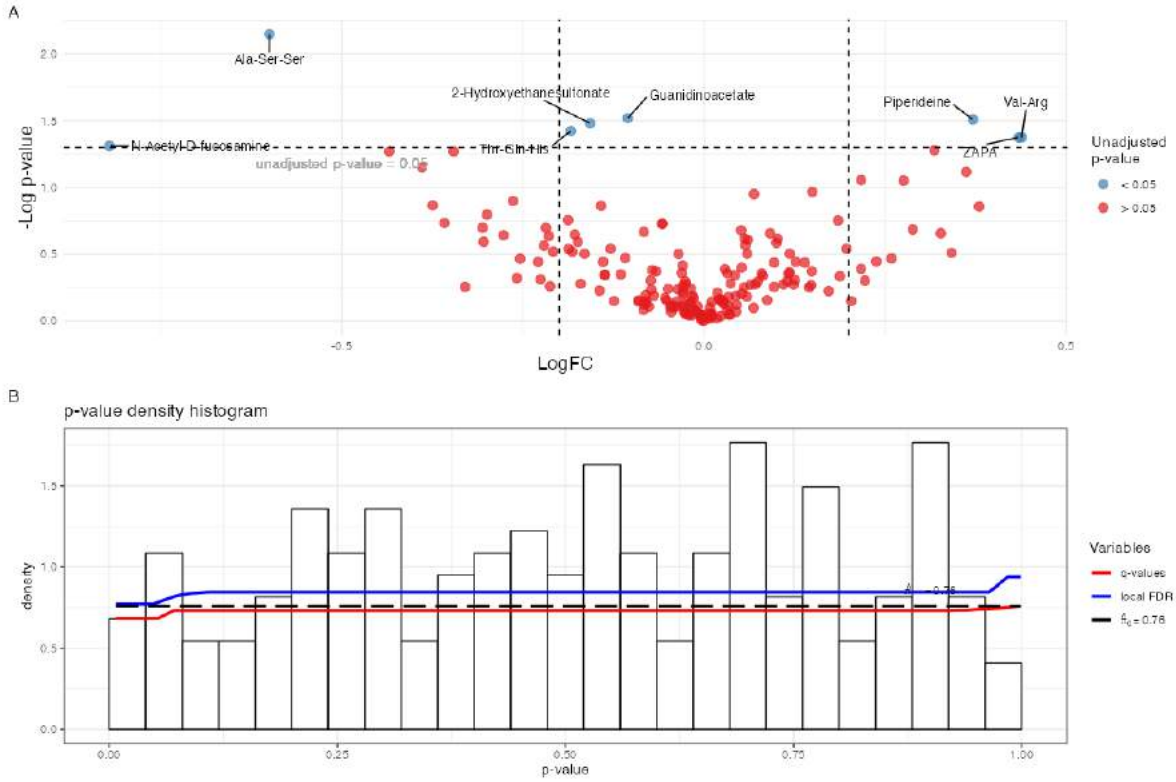

Figure 7.3. Differential analysis of the metabolites across the 3-month DAPSA groups. A. Volcano plot B. p-value histogram showing the distribution of p-values across the features. Significantly different features across the conditions would be reflected by a high number of low p-values, shown as a peak to the left of the plot.

Again, a p-value adjustment was applied to correct for false positives, but no metabolites remained significant after this, leading to a low unadjusted p-value being used. This cut-off is displayed in the volcano plot in Figure 7.3A. The p-value histogram in Figure 7.3B highlighted that there were few metabolites that were significantly different across the response groups, where there was a low occurrence of p-values < 0.05 in the dataset. From the volcano plot, guanidinoacetate was slightly increased in the good responders, supported by the correlation plot in Figure 7.2, where the same metabolite was negatively correlated with the 3-month DAPSA score. However, these results as a whole were

not convincing owing to the weak associations shown and high variance of the metabolite abundances observed across the sample groups.

7.3.4. Developing a Metabolomic Profile of 3-Month DAPSA Response

The supervised machine learning workflow developed using the TaSER cohort was applied to the metabolomic data from the CENTAUR study. Patients were designated into response groups based on their 3-month DAPSA score, with a good response as DAPSA ≤ 14 and a poor response defined as DAPSA ≥ 28. The number of patients in each group is shown in Figure 7.4A.

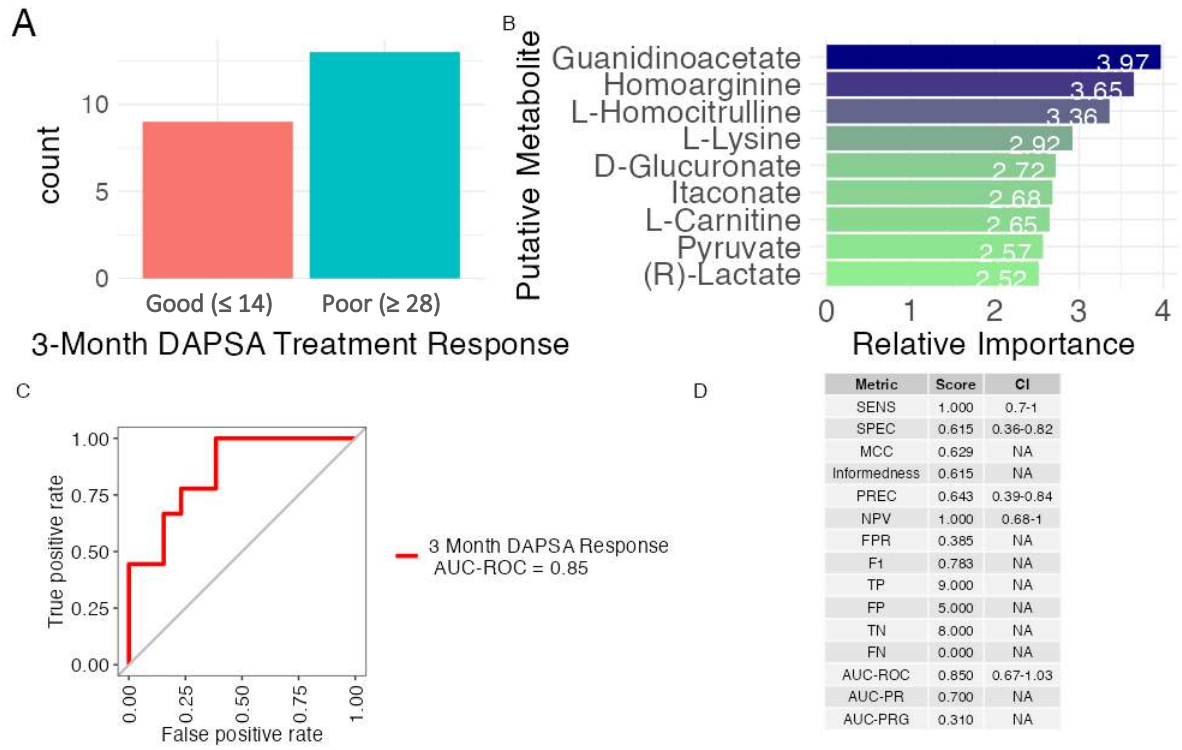

Figure 7.4. Supervised machine learning to generate a metabolomic profile of binary 3-month DAPSA response. A. Number of patients included in the good and poor response groups based on the 3-month DAPSA score. B. Results of the RFE-based feature selection process, with the top features and their respective relative importance scores shown. C. ROC curve showing the trained model's performance in predicting patients' responses in the testing subset with 10-fold cross-validation repeated 100 times. D. Table showing additional performance metrics and several true positive (TP), false positive (FP), true negative (TN) and false negative (FN) predictions.

The results from the feature selection are shown in Figure 7.4, involving the selection of metabolites that were together able to predict whether samples came

from patients with a good (3-month DAPSA ≤14) or poor (3-month DAPSA ≥ 28) response to treatment. These included guanidinoacetate, homoarginine, homocitrulline, lysine, glucuronate, itaconate, carnitine, pyruvate, and lactate, as shown in Figure 7.4B. Interestingly, several of these relate to arginine metabolism –also mentioned in the TaSER metabolic model in Chapter 3 – including guanidinoacetate, homoarginine, homocitrulline, and lysine.

As shown in Figure 7.4C and Figure 7.4D, the model performed well with an AUC-ROC value of 0.85 (95% CI: 0.67-1.03) and an MCC of 0.629. However, as can be seen in Figure 7.4D, a reasonably high number of false positives (FP) were predicted owing to the slight imbalance in the number of low DAPSA and high DAPSA scores, reflecting good and poor responders, respectively. Given the imbalance and the potentially over-optimistic evaluation of the model using the ROC curve and the AUC-ROC value, the AUC-precision recall (AUC-PR) was likely a better evaluation of the model, with an AUC-PR value of 0.70 being reported, as shown in Figure 7.5.

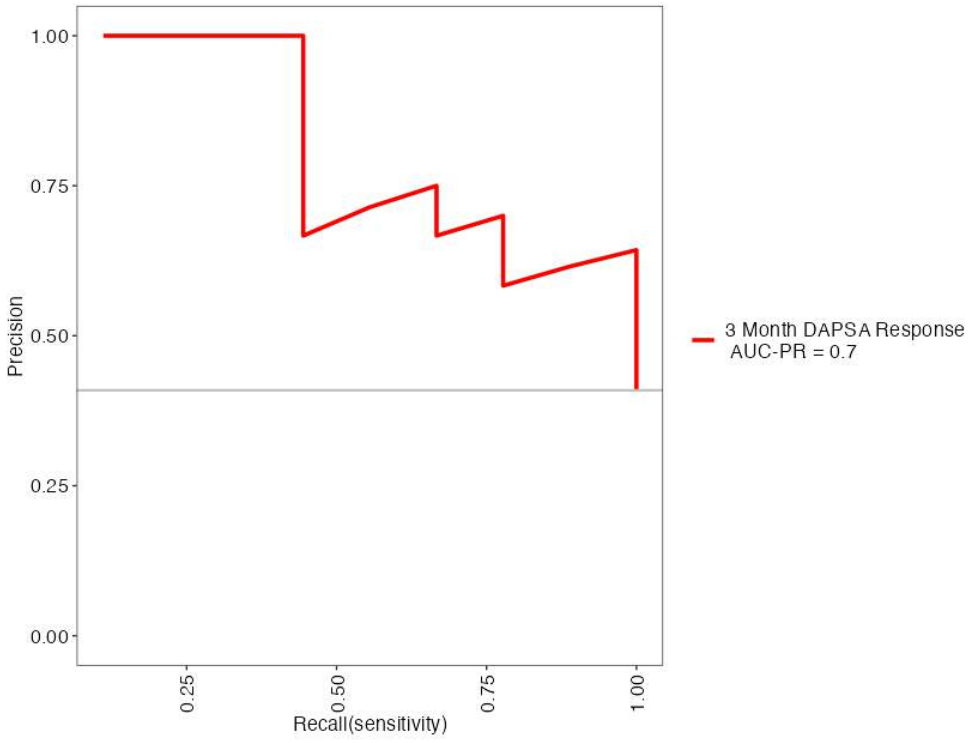

Figure 7.5. Precision recall curve for the metabolic model generated to predict the 3-month DAPSA-based response of patients with PsA to treatment. The grey horizontal line (no-skill line) represents the adjustment based on the imbalance across sample classes, and the performance of the model is calculated relative to its distance from this line.

The PR curve may be more helpful in understanding the model's performance, where the associated curve incorporates a ‘no-skill’ horizontal line. This was due to the imbalance of the classes, where there were more patients with a high DAPSA (poor response to treatment) in this sub-cohort.

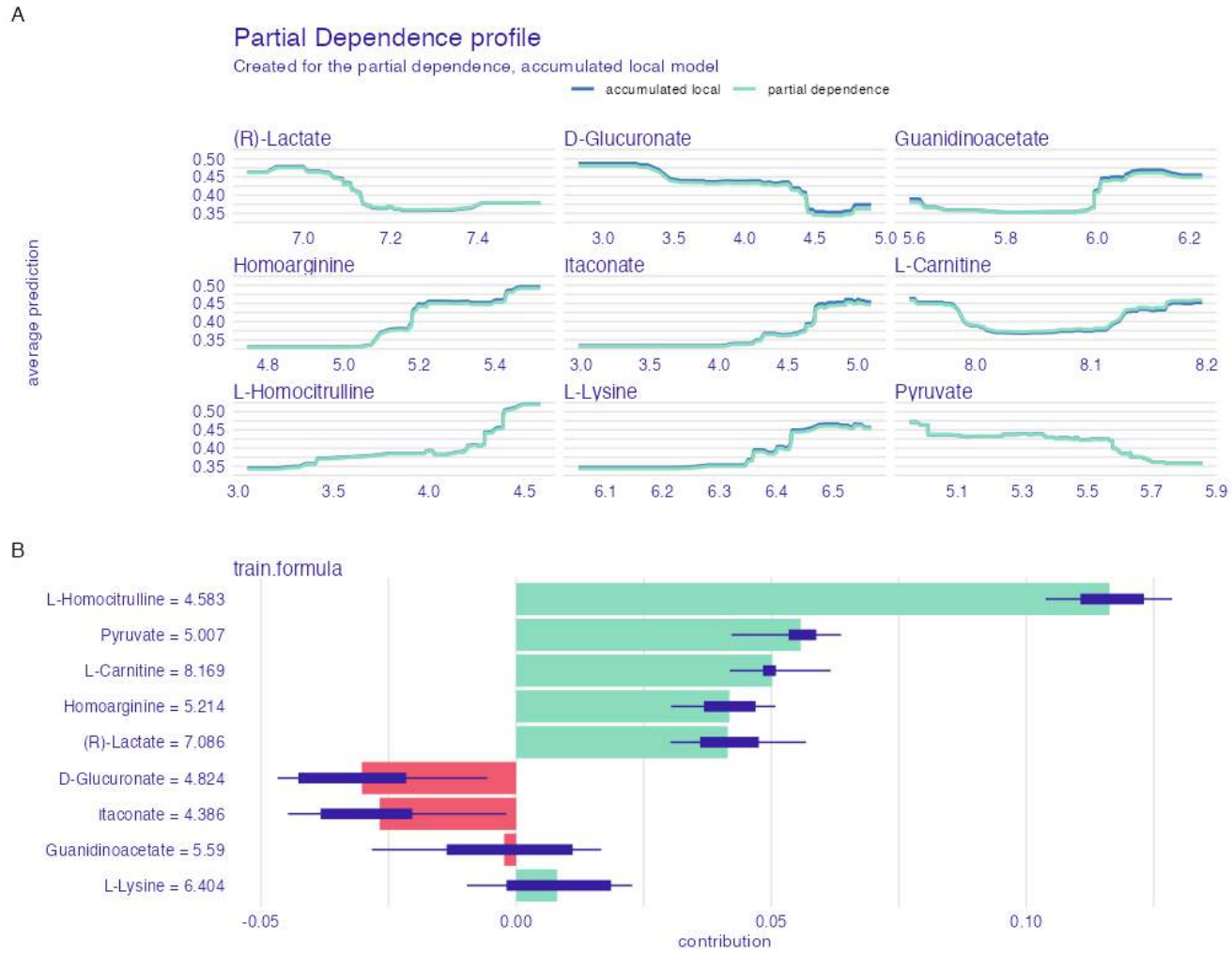

Figure 7.6. Model-agnostic feature interpretation plots A. Accumulated local effects and partial dependence plots B. SHAP plot.

Model-agnostic feature interpretation plots were generated to investigate the causative influence of each metabolite on the model’s predictive capacity, as shown in Figure 7.6. It was apparent that higher abundances of guanidinoacetate, homoarginine, itaconate, homocitrulline and lysine were more influential on the model's probability of predicting a good response to treatment. On the other hand, higher levels of lactate, glucuronate, and pyruvate were associated with a greater

probability of predicting a poor response to treatment. These effects are shown in the ALE plots and PDPs in Figure 7.6A. They are also indicated in the SHAP plot in Figure 7.6B, reflecting the additive influence of each feature on the prediction by the model.

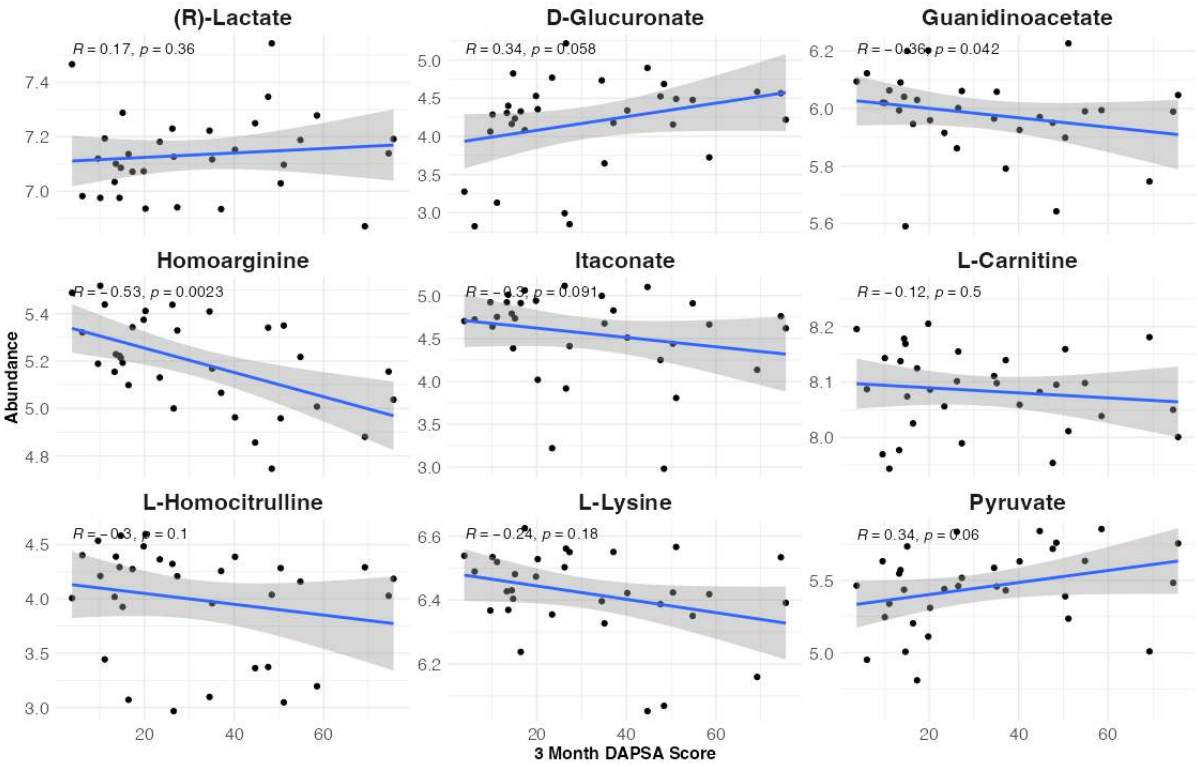

Figure 7.7. Correlations of the model's metabolites at baseline with the 3-month DAPSA. Regression lines plotted and Spearman correlation coefficients were calculated for each metabolite's relationship with the DAPSA score at 3 months.

The actual abundances of the metabolites selected for the model and their associations with the DAPSA score at 3 months and the response to treatment are shown in Figure 7.7 and Figure 7.8. From the analysis shown in Figure 7.7, guanidinoacetate and homoarginine were correlated with the DAPSA. Despite not being below the p-value threshold of < 0.05, glucuronate, itaconate, and pyruvate indicated some association with the 3-month DAPSA score, which was investigated further. It should be noted that all the patients were included in this analysis rather than just the patients with extreme DAPSA scores.

The correlational analysis was repeated in the subgroup of patients who had received MTX as part of their treatment. Only homoarginine was correlated with

the MTX-mediated response, with a similar trend as that shown in Figure 7.7 (R=-0.52, p-value = 0.0066). This was shown in Supplementary Figure 6.

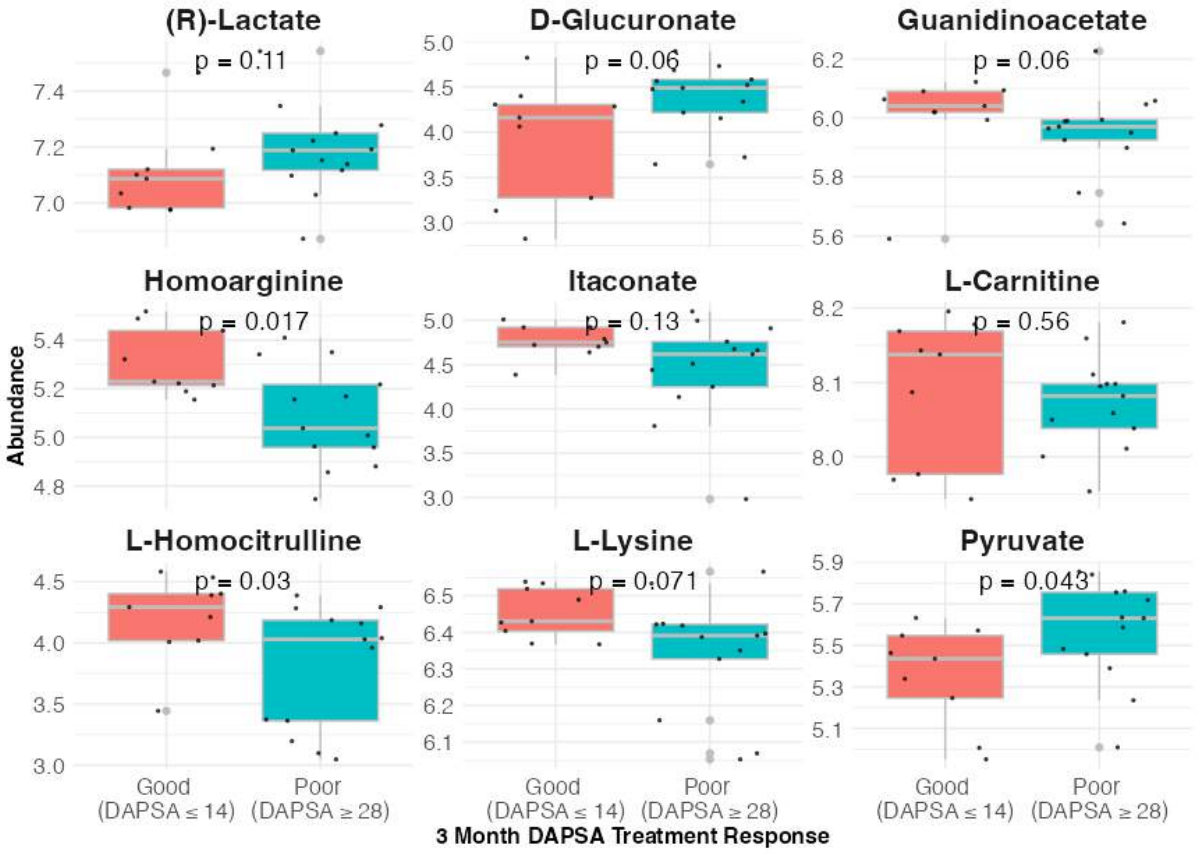

Figure 7.8. Boxplots showing differential analysis of the abundances of the metabolites from the CENTAUR model. Only the extreme response groups were included: good response (DAPSA ≤14) and poor response (DAPSA ≥28). Wilcoxon tests were used to generate the p-value statistic for each metabolite across the response groups.

Likewise, the differential analysis of these metabolites, shown in Figure 7.8, indicated that homoarginine, homocitrulline and pyruvate were differentially abundant across the 3-month DAPSA poor and good response groups. Glucuronate, guanidinoacetate and lysine were borderline significant. This analysis only included the sub-group of patients from the CENTAUR cohort who achieved LDA/remission (DAPSA ≤ 14) or had HDA (DAPSA ≥ 28) after 3 months, referred to throughout as having a good or poor response, respectively.

Several metabolites reported in Figure 7.8, including glucuronate, guanidinoacetate, homoarginine, homocitrulline, lysine and pyruvate, showed some potential as biomarkers of treatment response. However, the other

metabolites in the model without a clear association with treatment response may indicate a limitation of the machine learning process. This may occur owing to their selection due to high noise in the dataset which can occur with complex matrices like human serum. Additionally, since the cohort was relatively small, the effect of background noise was likely more pronounced than in a larger cohort.

The model's ability to separate the samples was further scrutinised using a PCA. Compared with the earlier PCA involving the entire metabolome, there was a greater separation of the response groups using the model's features only. However, while loose clustering of the response groups could be seen in Figure 7.9A, the overlapping samples from each group indicated that the model's ability to predict the responses of future cohorts may be limited. Since the response groups were mostly separated across PC1, the contribution of the metabolites in defining this component was assessed, with the results shown in Figure 7.9B. From this, lysine, homoarginine and guanidinoacetate were most influential in defining PC1.

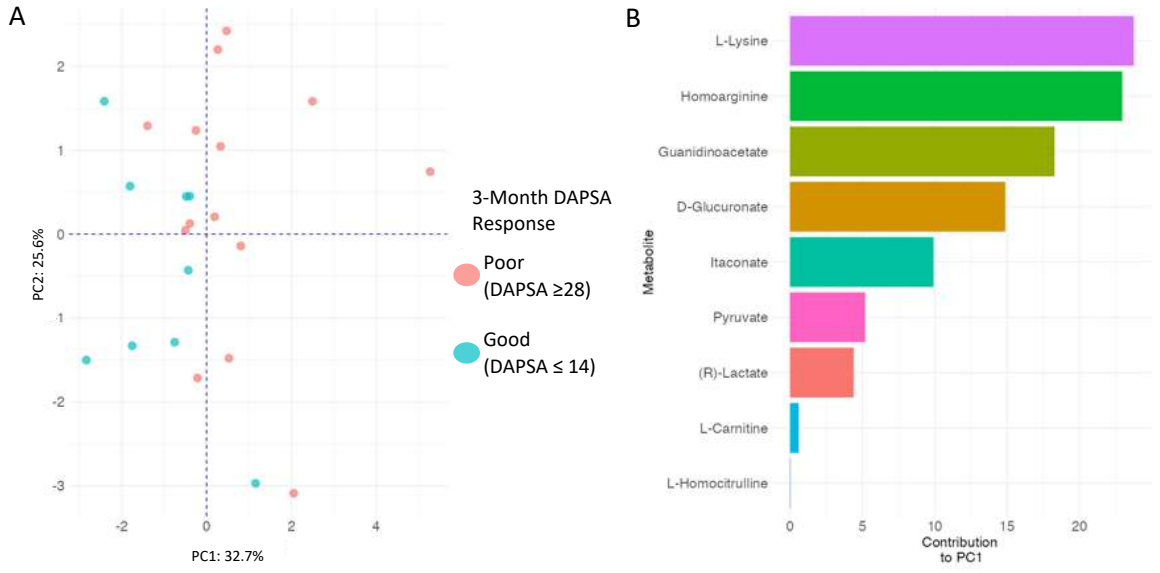

Figure 7.9. Investigating the separation of samples using PCA with labels based on the 3-month DAPSA-based response. A. PCA of samples with only the features from the metabolic model included. B. Features included in the model were ranked for their importance in defining PC1, the component that provided the greatest separation of the response groups.

In addition to investigating how the circulating metabolites are associated with the response to treatment, the influence of different clinical factors on the variance of each of the model's metabolites was investigated with the results shown in Figure 7.10. Notably, age influenced the variance across all metabolites except itaconate, although this was particularly low (< ~5%) for homocitrulline, shown in Figure 7.10A. This was considerably higher for homoarginine and carnitine, where age explained ~15% of their variance. BMI also explained ~20% of the variance of guanidinoacetate and ~5% of homoarginine, homocitrulline, lysine and pyruvate. Alcohol proved influential in explaining ~5% of the variance of itaconate, guanidinoacetate and ~10% of the variance of carnitine. As shown in Figure 7.10B, of the patient factors, age was the most influential factor on the variance of the features in the model.

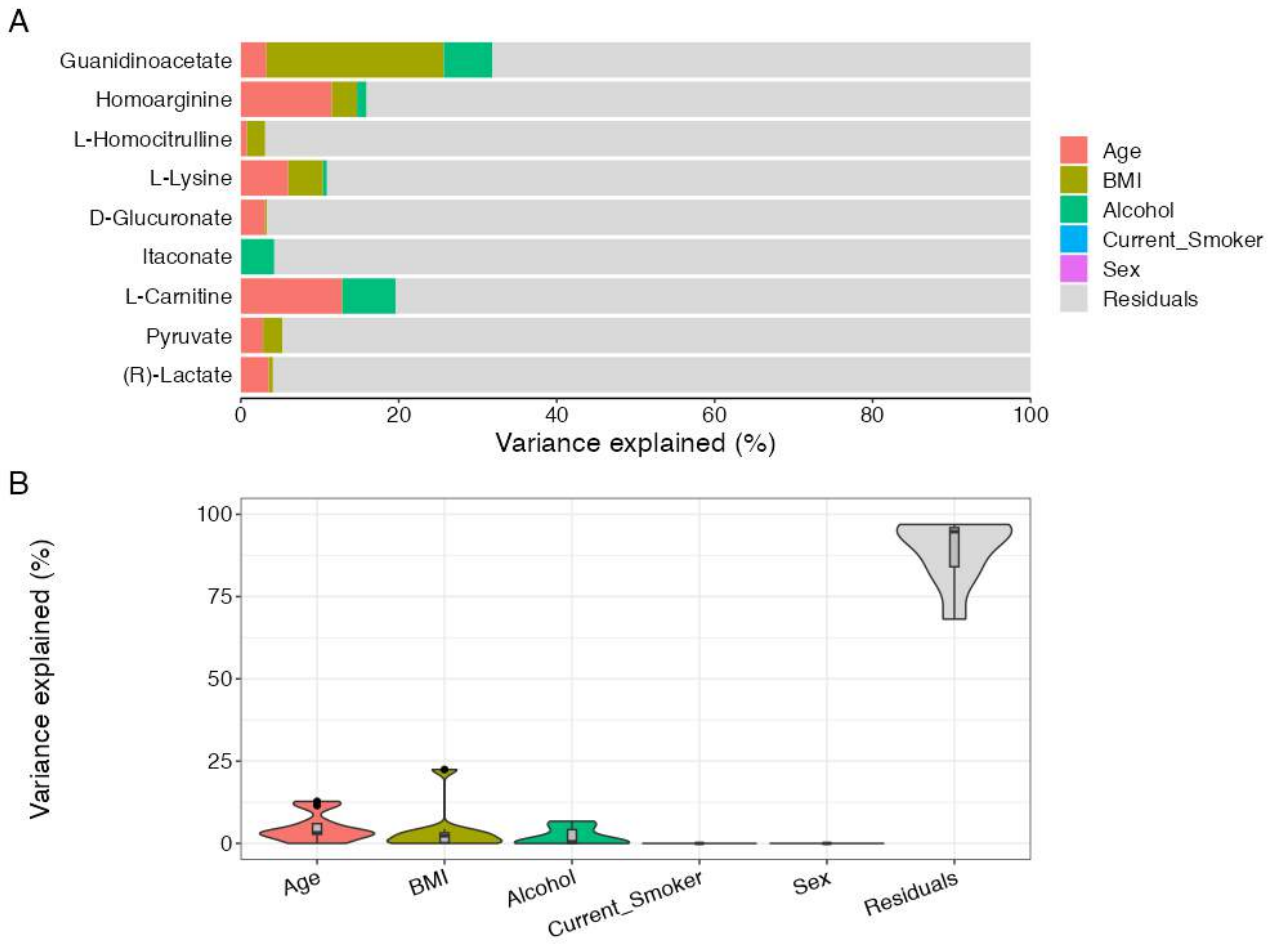

Figure 7.10. Explaining the variance of the CENTAUR model's features using patient factors. A. Bar plot showing the influence of the patient factors on the variance of the metabolites included in the metabolic model of treatment response. B. Violin plot showing the average variance explained by the patient factors across all the metabolites considered.

7.3.5. Pathway Analysis

From the tentative identifications, several metabolic pathways may be implicated in the metabolic profile for the 3-month DAPSA-defined response. Given the inclusion of homoarginine, guanidinoacetate, pyruvate, lactate and itaconate, such pathways may include arginine and central carbon metabolism. The top 50 tentatively identified metabolites from the differential abundance analysis were taken forward for pathway enrichment analysis using the online Metaboanalyst tool (Chong, Wishart and Xia, 2019).

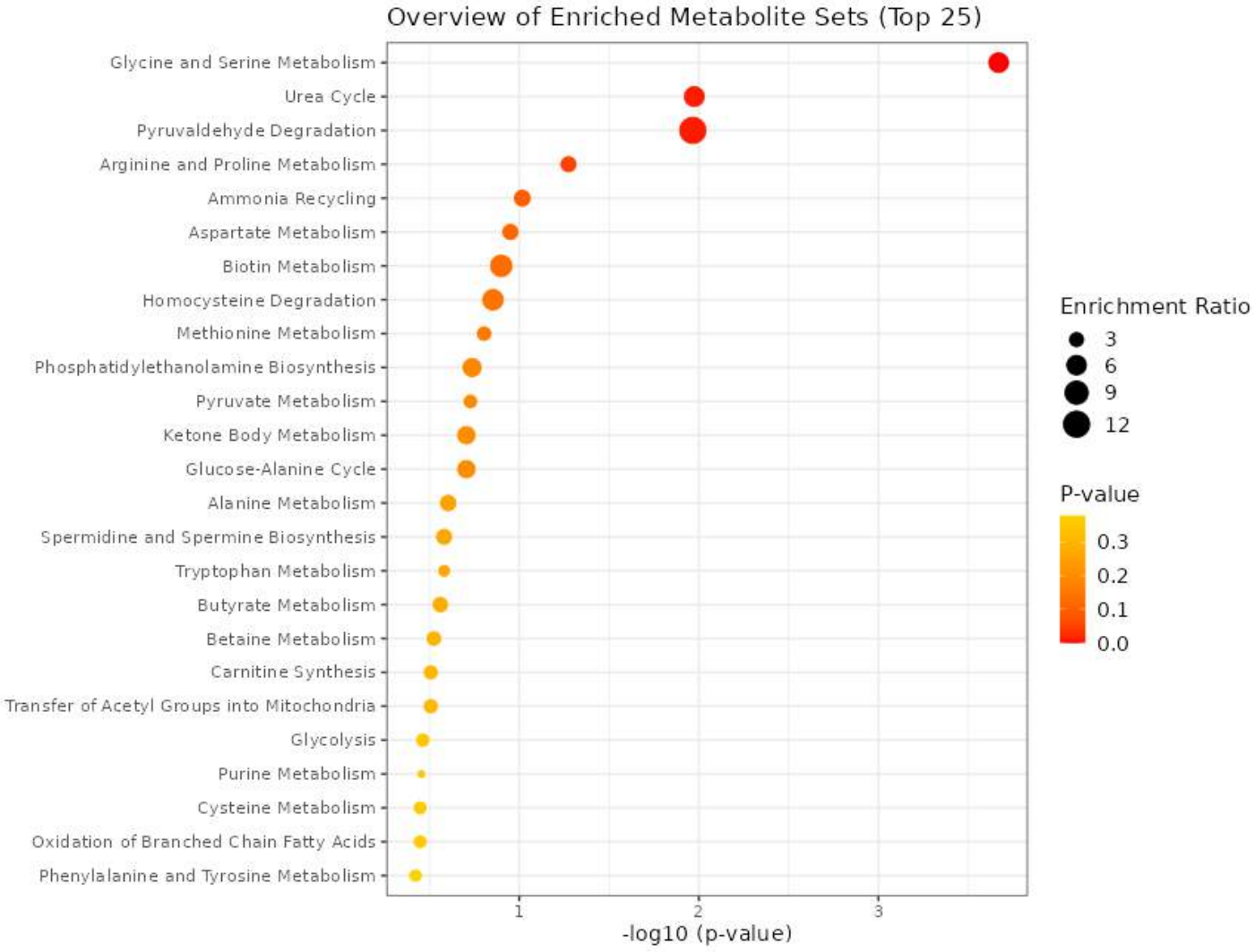

Figure 7.11. Metabolite set enrichment analysis results from Metaboanalyst. The enrichment ratio described the ratio between observed metabolites and expected hits in the pathway (Chong, Wishart and Xia, 2019).

From this analysis using the differentially abundant and tentatively identified metabolites, the most enriched pathway was glycine and serine metabolism, shown in Figure 7.11. This pathway includes pyruvate, ornithine, arginine, citrulline, and 2-oxoglutarate. Also noteworthy were the urea cycle and arginine and proline metabolism; the latter included guanidinoacetate, proline, 2-oxoglutarate, ornithine, arginine and citrulline. However, since metabolites intersect across the pathways, care needs to be taken in considering the importance of these results, since the same metabolites were likely to appear in multiple pathways.

7.3.6. Metabolic Ratios

As shown in Figure 7.12A, the abundance ratio of guanidinoacetate and homoarginine, both metabolites included in the final DAPSA-response associated mode, was assessed for its correlation with the 3-month DAPSA.

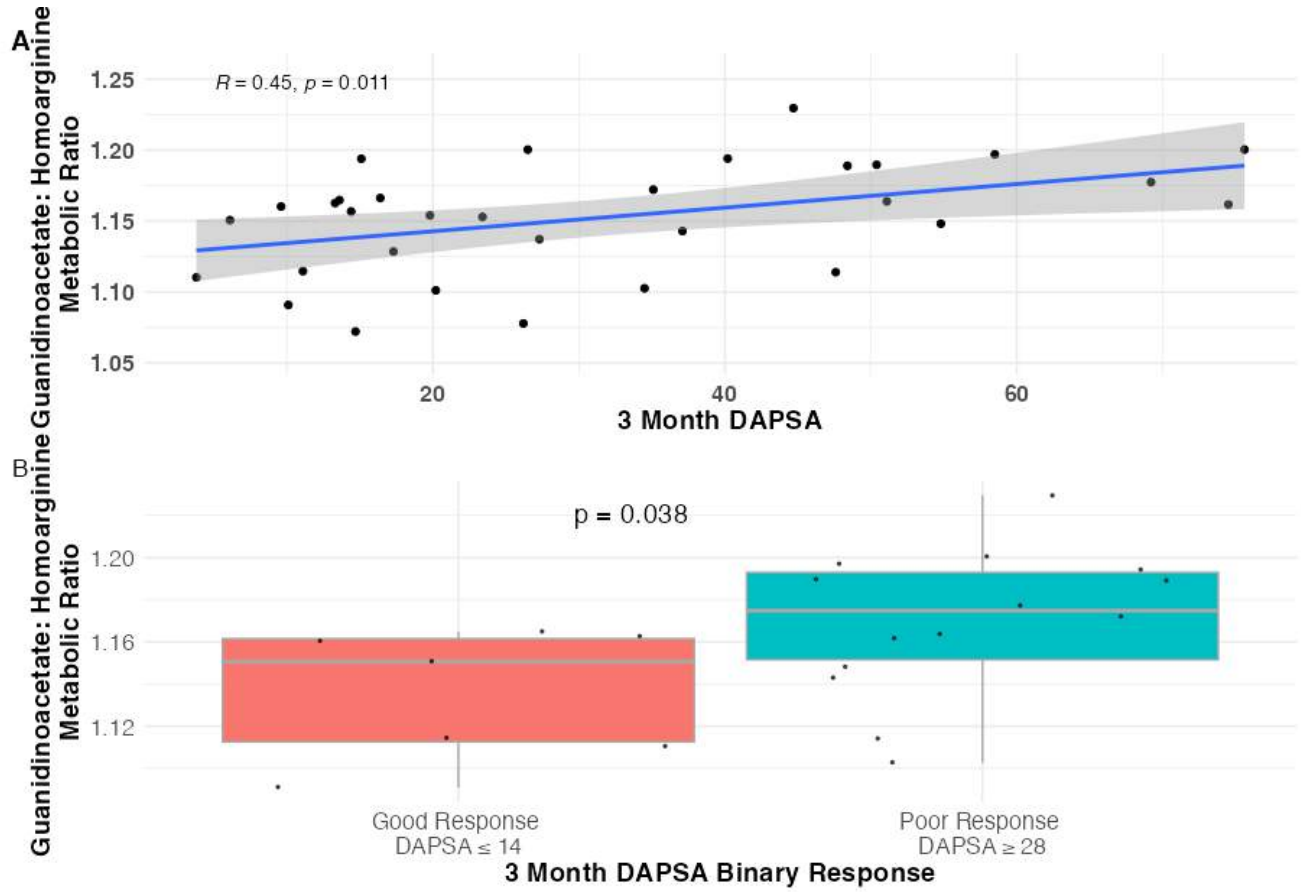

Figure 7.12. Metabolic ratio of guanidinoacetate: homoarginine and its association with the 3 month DAPSA response. A. Correlation of ratio with continuous DAPSA score at 3 months with regression lines B. Boxplots showing increased ratio in negative responders

The correlational analysis showed that patients with a higher guanidinoacetate: homoarginine (GA: HA) ratio tended to have a higher 3-month DAPSA score, indicating a worse response to treatment (R=0.44, p-value = 0.012). Interestingly, the same metabolic ratio was associated with the cardiovascular mortality rate in patients undergoing renal transplantation, again suggesting an immunomodulatory role (Hanff *et al.*, 2019). Using ratios of metabolites was helpful since they provide a pathway-wide measure and can be more informative than using a single biomarker. This was demonstrated in a recent study where increased kynurenine: tryptophan ratio was associated with SARS-CoV2 infection (Lionetto *et al.*, 2021). Interestingly, the ratio of this same pair of metabolites has also been associated with RA, which may be due to the immunomodulatory roles of each metabolite (de Vries *et al.*, 2017; Kor *et al.*, 2022).

The boxplot in Figure 7.12B further reveals this association of the GA: HA ratio where only patients with extreme DAPSA scores ($\leq$ 14 or $\geq$ 28) after 3 months were plotted. It was shown that a higher GA: HA ratio tended to be found in patients with higher disease activity, reflecting a poor response to treatment (p-value = 0.019). A lower GA: HA ratio at baseline may therefore indicate a good response to treatment after 3-months, regardless of the treatment used.

Since the metabolic model described in this chapter included pyruvate, lactate, itaconate, and glucuronate — linked via central carbon metabolism — the ratios of each pair of metabolites were calculated and assessed in relation to the DAPSA score at 3 months, as shown in Figure 7.13. Additionally, binary response groups were generated using the extreme ends of the DAPSA scores in the cohort and the association of these ratios with the good and poor responders, as shown in Figure 7.13B, Figure 7.13D, and Figure 7.13F. From these figures, it was apparent that, generally, patients with higher ratios between the selected metabolites had lower DAPSA scores. The differential analysis shown in the boxplots showed a similar trend, where a higher itaconate: pyruvate ratio was found in good responders (p-value = 0.0082), shown in Figure 7.13B, similar to the trend shown for the itaconate: glucuronate ratio (p-value = 0.033) and the homoarginine: lactate ratio (p-value = 0.0023). The strongest association was found between the homoarginine: lactate ratio and the 3-month DAPSA, shown in Figure 7.13E (R=-

0.56, p-value = 0.00094). However, because homoarginine was already found to have a strong correlation with the 3-month DAPSA as an individual metabolite, it was unclear how much more value using its ratio with lactate would provide.

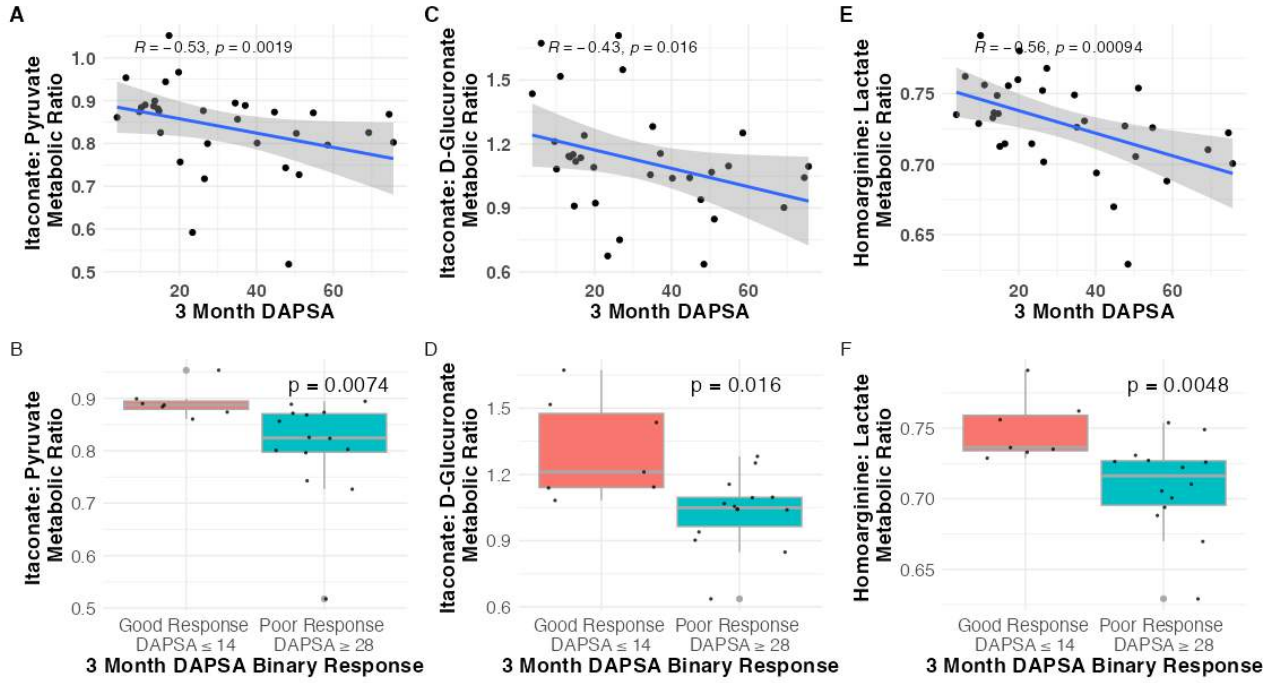

Figure 7.13. Metabolic ratios of selected metabolites from the model and their correlations and associations with the 3-month DAPSA-defined response to treatment. A, C, E. Correlations of each metabolite pair with the DAPSA at 3 months. B, D, F. Boxplots showing the differential analysis of the metabolite ratios across good and poor responders.

7.3.7. Cytokine Analysis and Association with Disease Activity

Results from the serum cytokine analysis are shown in Figure 7.14. The cytokines measured at baseline were evaluated to identify those correlated with the baseline DAPSA score, therefore reflecting higher levels of inflammation in the patients prior to receiving the novel DMARD.

Cytokines that correlated with the DAPSA score at baseline included eotaxin-3 (R=-0.33, p-value = 0.037), ghrelin (R=-0.62, p-value = 0.0046), GROα (R=0.0.43, p-value = 0.0049), IL-13 (R=-0.51, p-value = 0.0092), IL-17D (R=-0.35 p-value = 0.026), and leptin (R=0.36, p-value = 0.022). Additionally, IFN-γ was borderline-significant for its correlation (R=-0.29, p-value = 0.065) and may be biologically meaningful. Since IL-17D and IFN-γ represent cytokines described in the literature as having an association with the pathology and severity of PsA, the fact these

were correlated with the DAPSA at baseline was noteworthy. Additionally, eotaxin-3 and GROα (CXCL1) had particularly strong correlations with the baseline DAPSA score. CXCL1 is a pro-inflammatory chemokine whose expression is induced by numerous inflammatory cytokines, including IL-1β and TNF-α, via activating the inflammation-mediating transcription factor, NF-κB, and is implicated in recruiting neutrophils to sites of inflammation (Sawant *et al.*, 2016). As expected, the strong positive correlation between CXCL1 and DAPSA at baseline indicates higher inflammation in patients with high DAPSA at baseline. The negative correlation of eotaxin-3 with the baseline DAPSA was surprising since eotaxin-3 is also involved in inflammation and the recruitment of eosinophils, although it is primarily associated with the allergic immune response. Other eotaxin cytokines were not measured in this analysis.

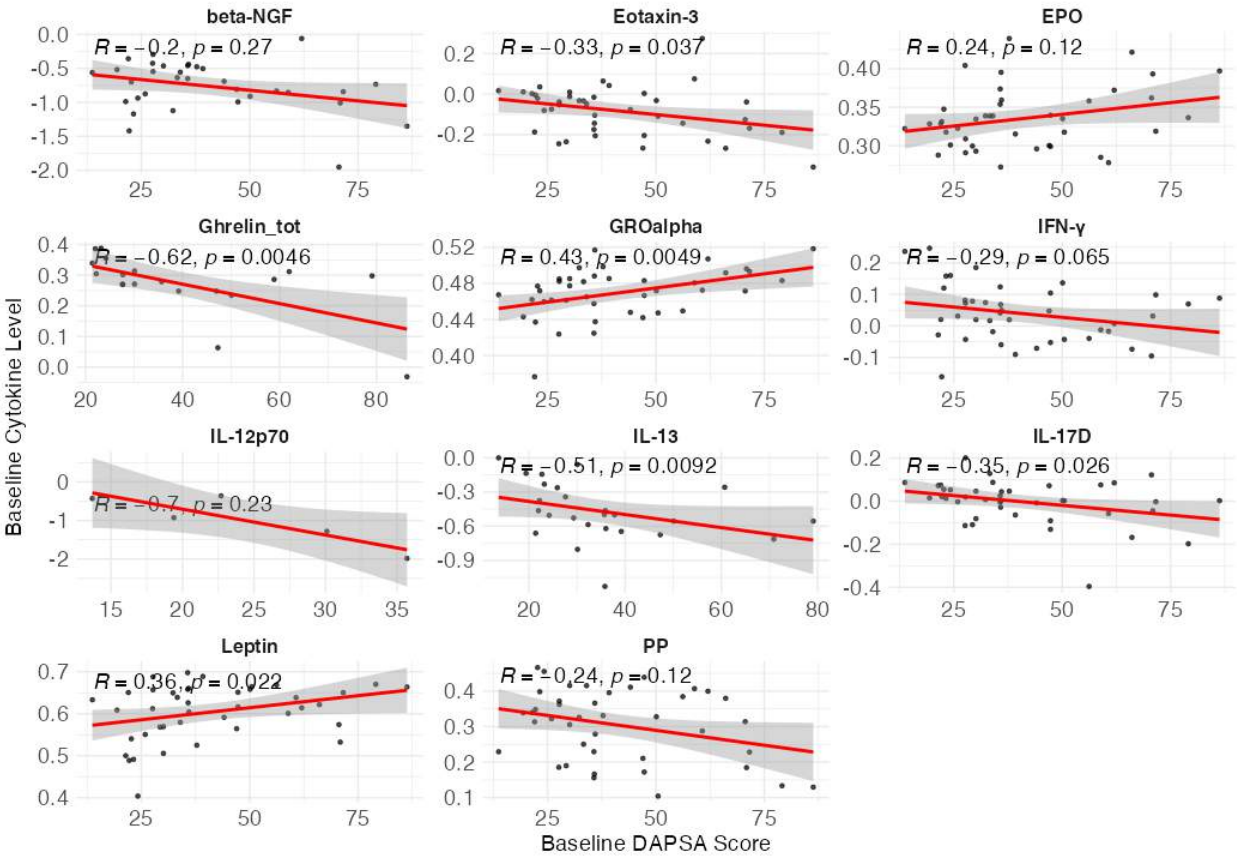

Figure 7.14. Correlation plots showing cytokine levels at baseline against the baseline DAPSA score in patients with PsA. Regression lines are plotted to aid the visualisation of the association. Spearman correlation coefficients and p-values plotted for each cytokine. Beta-NGF- beta nerve growth factor; EPO- erythropoietin; GROalpha- growth-regulated alpha protein; PP- pancreatic polypeptide.

Leptin was positively correlated with the 3-month DAPSA score (R=0.36, p-value = 0.022), generally elevated in its circulating levels in patients with a worse response to treatment, shown by the increased DAPSA. Leptin was reported in the literature as being an important driver of several immune cell populations, including macrophages, dendritic cells and T-cells, as well as mediating the production of pro-inflammatory cytokines, IL-1, TNF-α, IL-17, IL-23 (Gabay *et al.*, 2001; Mounessa *et al.*, 2016; Ziegler *et al.*, 2019). While beyond this project's scope, the increasingly understood link between obesity and psoriasis/PsA may underline the importance of leptin in mediating the inflammatory processes that drive the disease (Hwang *et al.*, 2021).

7.3.8. Associations Between Cytokines and Metabolites

Within the panel of cytokines generated in work performed by Dr Flavia Sunzini, the following were specially assessed for their associations with the metabolomic features: IL-1α, IL-1ß, IL-1RA, IL-6, IL-10, IL-12 subtypes, IL-17 subtypes, IL-23, TNF subtypes, IFN subtypes, ghrelin and leptin. Their correlations with the metabolites were assessed and visualised as a heatmap in Figure 7.15.

Several notable correlations shown within the heatmap were explored further to demonstrate a proof of concept, indicating the strong relationships between the cytokines and metabolites at baseline. Given the clustering patterns and their biological connection, IL-1RA and IL-1ß were included in the subsequent analysis, along with IL-17C, which showed strong correlations with several metabolites. Guanidinoacetate was selected due to its strong correlations with inflammatory cytokines and involvement in the metabolic model of treatment response in Section 7.3.4. At the same time, hypoxanthine and urate, being biologically related, shared a similar correlation with IL-1ß, making these especially interesting, with the results shown in Figure 7.16.

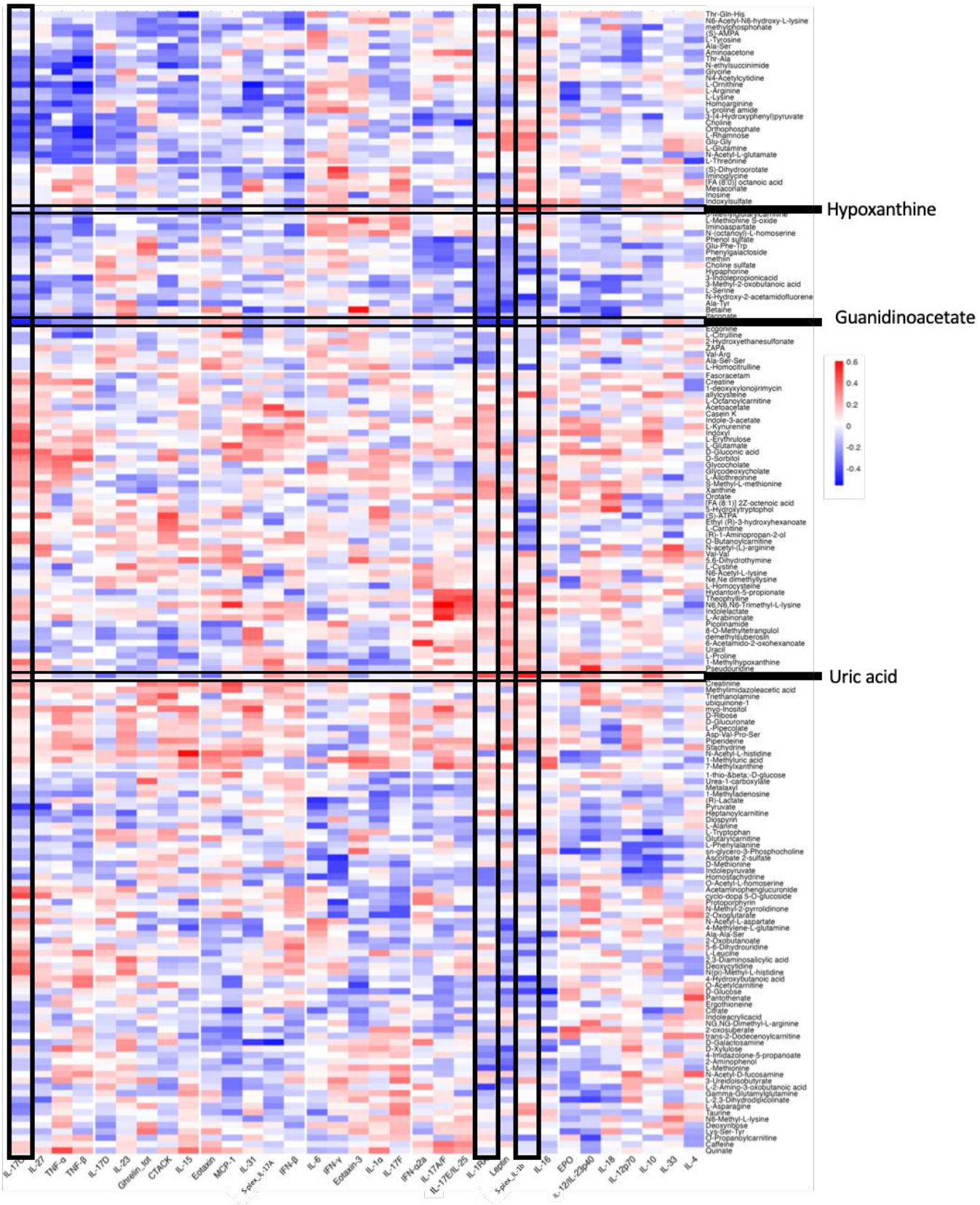

Figure 7.15. Correlation heatmap for cytokines and metabolites. Clustering was based on the Euclidean distances calculated between their Spearman correlation coefficients.

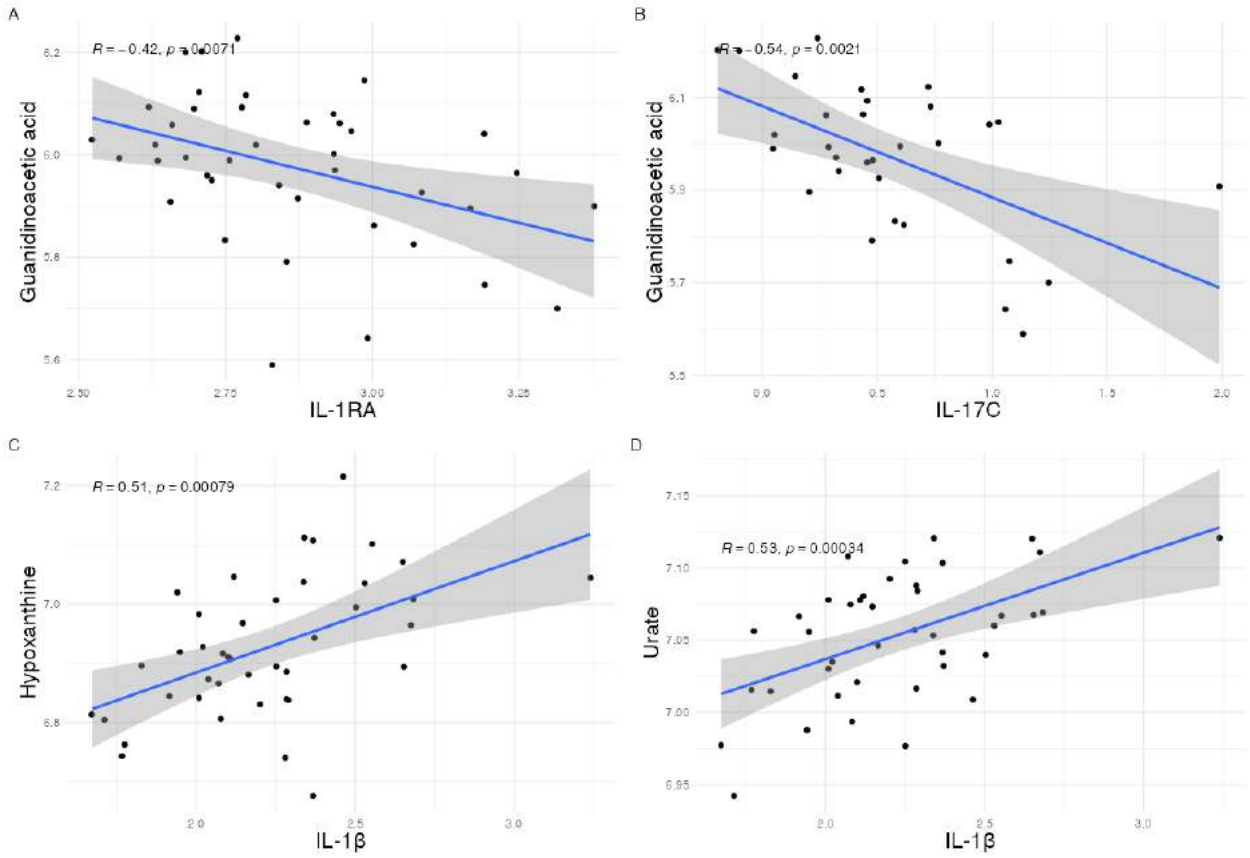

Figure 7.16. Correlations of cytokines of interest with associated metabolites. Regression lines plotted along with the Spearman correlation coefficient and p-values.

Strong correlations were observed between guanidinoacetate and IL-1RA (R=-042, p-value = 0.0071) and IL-17C (R=-0.54, p-value = 0.0021). Since guanidinoacetate was increased in good treatment responders, shown in Section 7.3.4, these inverse relationships with the pro-inflammatory and psoriasis-associated cytokines, IL-1RA and IL-17C, may indicate the increased use or consumption of guanidinoacetate by IL-17-mediated immune processes, therefore linking this metabolite to disease-related processes. These inverse correlations with pro-inflammatory cytokines, shown in Figure 7.16A and Figure 7.16B, suggest that guanidinoacetate may be potentially useful as a biomarker of disease activity in PsA and the prediction of treatment response.

In addition, hypoxanthine correlated strongly with IL-1ß (R=0.51, p-value = 0.00079), as did uric acid (R=0.53, p-value = 0.00034), shown in Figure 7.16C and Figure 7.16D, respectively. As hypoxanthine is converted to uric acid via xanthine

oxidase, their similar correlations with the pro-inflammatory cytokine IL-1β may indicate increased activity of this enzyme and overall purine metabolism associated with increased inflammation.

Since patients with PsA and psoriasis may also experience gout owing to hyperuricaemia, the fact that IL-1β was positively correlated with uric acid in this work may serve as a proof of concept that these are biologically and clinically relevant pathways (Tripolino *et al.*, 2021; Widawski *et al.*, 2022). This was discussed further in the next section.

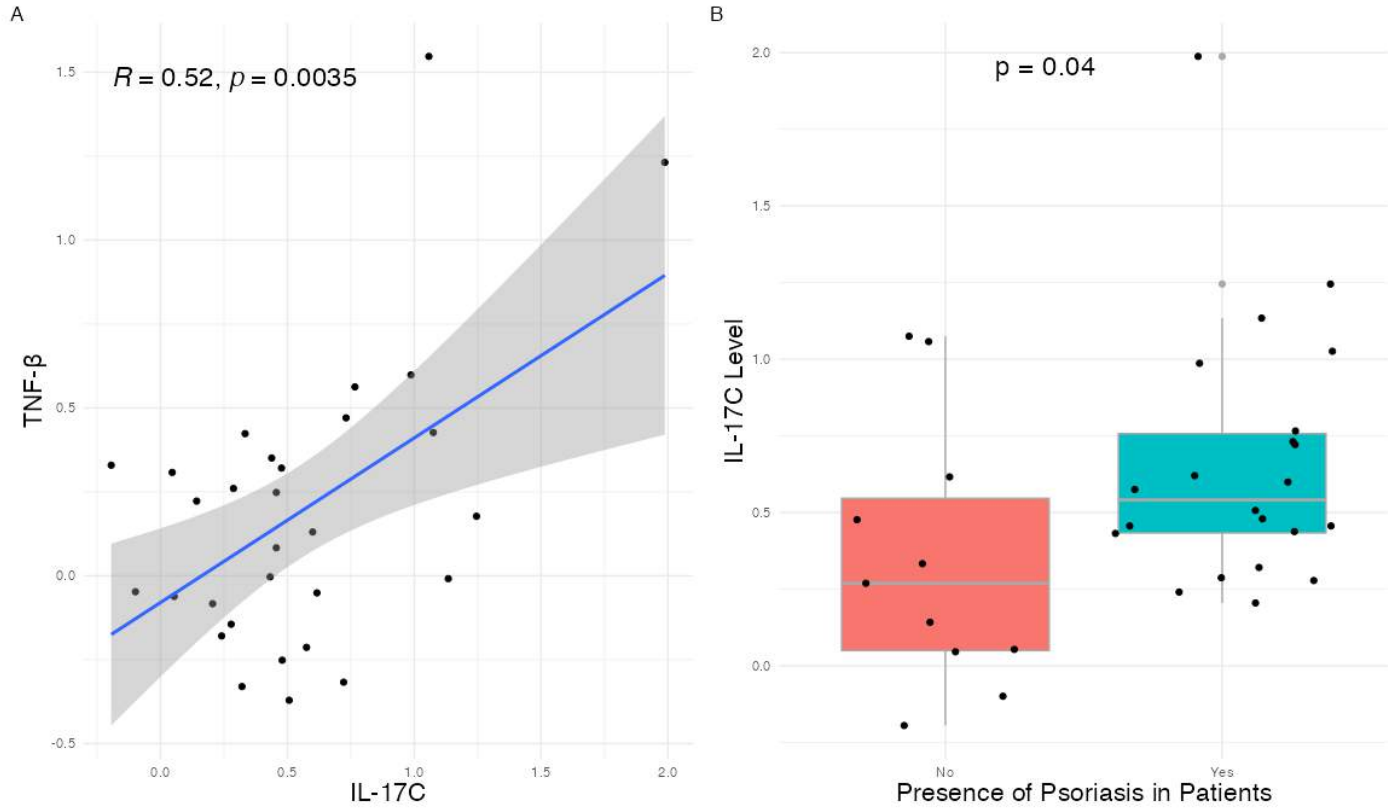

Figure 7.17. Involvement of IL-17C in PsA and psoriasis. A. Correlation of IL-17C with TNFβ. B. Differential levels of IL-17C between patients with and without diagnosed psoriasis as a comorbidity.

Although the involvement of IL-17C in PsA is relatively less understood than other members of the IL-17 cytokine superfamily, it has been described to behave similarly to other known subtypes (Brembilla, Senra and Boehncke, 2018). However, the production of IL-17C was found to be especially increased in patients with psoriasis, involving increased gene expression giving rise to IL-17C (Johansen *et al.*, 2010). This increased production of IL-17C in the skin of psoriasis patients is

reduced by anti-TNF treatment, indicating the involvement of TNF signalling in mediating IL-17C production. However, these inhibitors targeted only TNF-α (Johnston *et al.*, 2013). In our data, a strong correlation was shown between IL-17C and TNF-β (R=0.52, p-value = 0.0035), shown in Figure 7.17A. Additionally, when patients in the CENTAUR study were split into subgroups based on the previous/current diagnosis of psoriasis, the IL-17C level was significantly increased in patients who reportedly had psoriasis (Wilcoxon test, p-value = 0.04) (Figure 7.17B).

Finally, the metabolites correlated with at least two PsA-associated cytokines from the list of 88 cytokines measured were taken forward for metabolite set enrichment analysis (MSEA) using the Metaboanalyst tool (Chong, Wishart and Xia, 2019). As shown in Figure 7.18, the MSEA indicated several significantly enriched pathways, including glycine and serine metabolism, the urea cycle, arginine metabolism and polyamine metabolism. Since arginine metabolism was mentioned in the previous section, involving homoarginine and guanidinoacetate being linked with the response to treatment in RA, the results from the cytokine-associated MSEA were especially noteworthy, where these arginine-related pathways were correlated with changing inflammation-modulating cytokines.

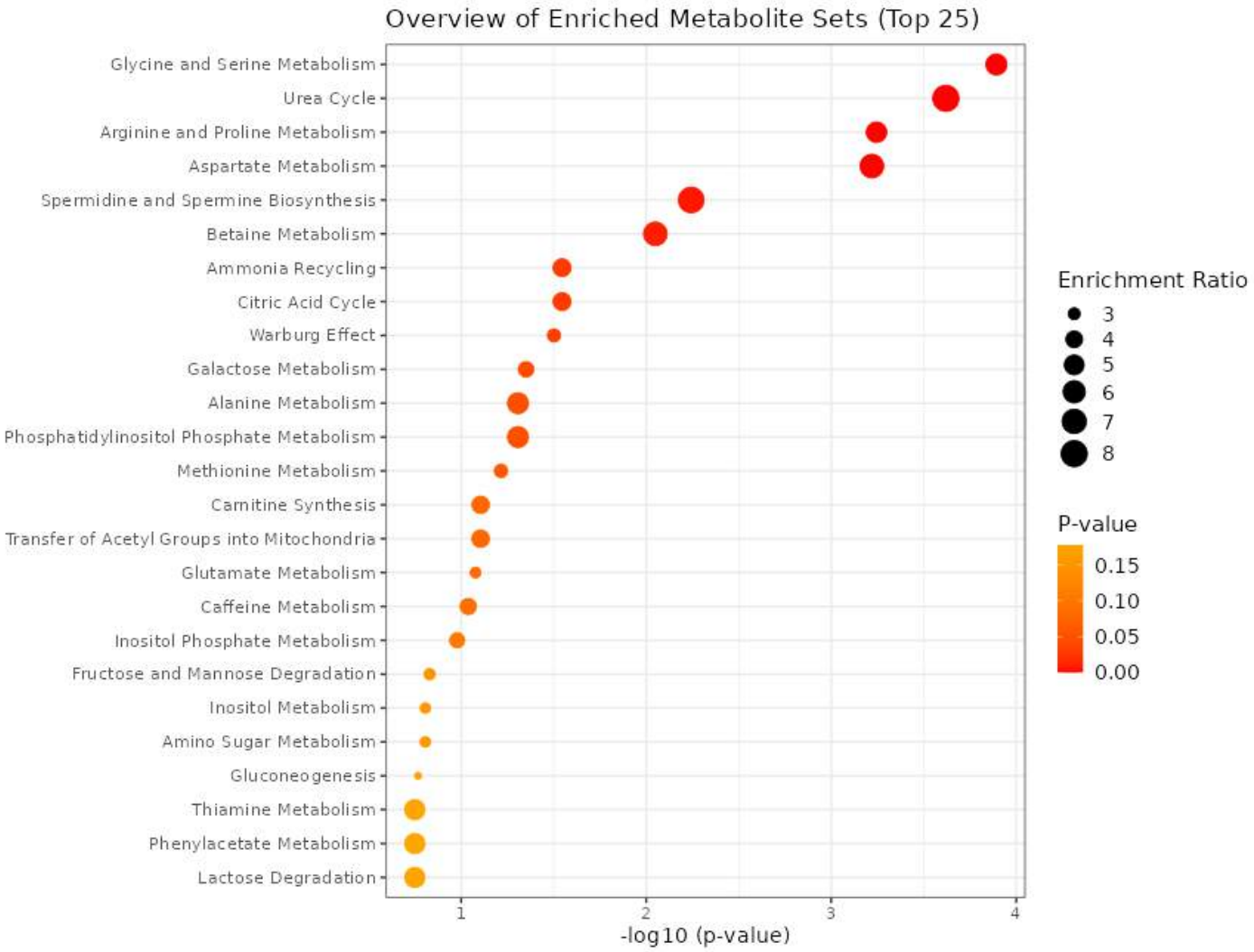

Figure 7.18. Enriched pathways from the list of metabolites that correlated with the PsA-associated cytokines. Metabolite set enrichment analysis using the MetaboAnalyst tool.

7.4. Discussion

7.4.1. Value and Limitations of the Response-Associated Metabolic Profile

The metabolomic data from the CENTAUR study — where patients with PsA had serum samples taken prior to their treatment with a new DMARD — provided an opportunity to investigate the metabolic features associated with treatment response in another RMD. Patients enrolled in the CENTAUR study were referred by their local rheumatology department and received prior treatment that had not successfully managed their disease. The subsequent analysis in this work was

performed to investigate the metabolites associated with the successful response to treatment based on the 3-month DAPSA score, regardless of the new DMARD used to achieve this.

A panel of metabolites combined using a supervised machine learning approach was associated with treatment response in the patients with PsA from the CENTAUR cohort. Included in the model were homoarginine, guanidinoacetate, pyruvate, lactate, glucuronate, homocitrulline, itaconate, carnitine and lysine. While homoarginine, guanidinoacetate, glucuronate, and pyruvate were correlated with the 3-month DAPSA score or were differentially abundant across the DAPSA-defined response groups, the other metabolites were found to have limited associations with the general treatment response. The fact that these were included in the model may reflect a limitation of the study and the use of the machine learning approach for this relatively small sample size. Additionally, the inclusion of various treatments in the cohort meant there was an inevitable loss of drug-specific metabolic associations observed.

The model generated from the PsA cohort was developed to predict the 3-month DAPSA-based responses of patients using a collection of metabolites measured from baseline serum samples. Cut-offs for LDA (good) and HDA (poor) were used to create a binary classification model of more extremes of response, which performed reasonably well with an AUC-PR value of 0.70 and MCC of 0.629. The metabolites from the model were then assessed for their collective ability to separate the samples using the PCA. The loose clustering of the samples based on their respective responses within these plots indicated that the model would likely have low accuracy in other cohorts. However, this was largely expected given the attempt to evaluate the TaSER model in independent cohorts and its lack of robustness across cohorts. Increasing the sample size in a subsequent study was expected to be of benefit in increasing the confidence in the associations between the metabolites and treatment response across patient cohorts.

While the DAPSA score at 3 months was the primary measure of the treatment response in patients in the CENTAUR study, other measures may generate better-performing models in that they may be more reproducible and applicable across patient cohorts. For example, a model could be generated that was associated

with a measure describing a single disease domain, such as the swollen joint count, or a more comprehensive measure, such as PASDAS, that incorporates more domains of PsA. The panel of metabolites from these models may provide additional valuable insights into the possible mechanisms involved in supporting treatment response in terms of the different features of the disease.

A logical next step in this work includes performing targeted analysis on the metabolites in the model to identify them relative to authentic reference standards along with the generation of fragmentation data using an LC-MS/MS. The absolute quantification of the metabolites would support the translation of the model across cohorts and allow its validation in external datasets.

Despite providing only an early stage in the biomarker discovery process, this chapter provided insight into tentatively identified metabolites that were associated with the 3-month DAPSA response. It was expected that an exploration of the immunomodulatory roles of the metabolites would follow this work, thus supporting the pursuit and development of biomarker strategies for clinical management of RMDs.

7.4.2. Hypothesis Related to the Gut Microbiome

IPA was negatively correlated with the DAPSA score at 3 months in the CENTAUR cohort with its upstream derivative indole acrylic acid being similarly associated with the DAS28-ESR at 3 months from the TaSER cohort. Indole-based metabolites are products of tryptophan's microbial metabolism, produced by species of bacteria found in the gut microbiome (Ye *et al.*, 2022). These bacteria include *Bacteroides*, *Clostridium* and *Peptostreptococcus* strains (Negatu *et al.*, 2020; Han *et al.*, 2021). In fact, *Clostridium sporogenes* was reported as the only bacteria strain that produces IPA (Dodd *et al.*, 2017). Since other studies have shown intestinal dysbiosis in psoriasis, it was feasible that the reduction of bacterial species that produce beneficial immunomodulatory metabolites, such as tryptophan-derived metabolites, may result in a change in systemic inflammation in patients with PsA (Chen *et al.*, 2020). For example, the *Bacteroidetes* phylum was decreased in patients with psoriasis compared with healthy controls in multiple studies, along with *Prevotella*, while species belonging to the Firmicutes

phylum were increased in psoriatic patients (Huang *et al.*, 2019; Shapiro *et al.*, 2019; Chen *et al.*, 2020).

It should be mentioned that IPA was only tentatively identified in this dataset, not having been matched to an internal reference standard, and so these findings need to be carefully interpreted. Nevertheless, variations in the abundance of IPA in the cohort of patients, as depicted in Figure 7.2 with the correlation of IPA with the 3-month DAPSA, may indicate patients had meaningful differences in their gut microbiomes, which led to perturbations in immunomodulatory metabolites being released into their circulation.

While there are known differences in the clinical presentation, molecular characterisation and therapeutic approaches between RMDs, an altered gut microbiome that influences a common inflammatory component may exist across autoimmune conditions (Miyauchi *et al.*, 2023). The gut microbiome may be an important source of common metabolites associated with response across RMDs. By modulating the levels of bacteria that produce immunomodulatory metabolites, biotics could be used to supplement existing treatments of IRDs and other autoimmune diseases.

Following the findings relating to the indole-based metabolites across the TaSER and CENTAUR datasets, investigating the sources of metabolites detected in the circulation would be a logical next step. To assess the gut microbiome as a root of the metabolites, an investigation into the strains of bacteria found in the guts of patients who experience variable responses to treatment may be performed as a next step (V. K. Gupta *et al.*, 2021; Wang *et al.*, 2022). Such datasets already exist and could be obtained for subsequent analysis, although this was beyond this project's scope. For example, Gupta et al. (2021) performed shotgun metagenome sequencing on 32 patients with RA, with baseline and 6–12-month follow-up samples being analysed.

The patients were treated with various drugs, including csDMARDs (MTX, sulfasalazine) and bDMARDs (infliximab, and adalimumab). The authors reported that patients who experienced an improvement in their disease activity, based on the minimum clinically important improvement (MCII) measure, had meaningful

differences in their gut microbiomes, including overall microbiome diversity, where patients with a better outcome after 6-12 months typically had a greater diversity of species in their gut (V. K. Gupta *et al.*, 2021). For example, the *Bacteroides vulgatus* species was increased in patients who met the MCII criteria, while the *Ruminococcus* genus was increased in those who did not meet the MCII. By harnessing the data generated by Gupta et al. (2021), it would be helpful to investigate whether patients who had a good outcome following treatment had differential levels of bacteria species known to produce the metabolites of interest in this work, including IPA and other indole-based compounds.

7.4.3. Disruption to Arginine Metabolism

The metabolic model for treatment response in patients with PsA revealed putatively identified metabolites related to arginine metabolism. These included homoarginine and guanidinoacetate, which are both produced via the conversion of arginine, as well as lysine, which is used in the production of homoarginine via arginine: glycine amidinotransferase (AGAT), depicted in Figure 7.19. Guanidinoacetate is produced via AGAT, which also creates L-ornithine (Edison *et al.*, 2007). Using the same enzyme, homoarginine can be produced, involving the incorporation of lysine and arginine to produce homoarginine and ornithine (Davids *et al.*, 2012). From guanidinoacetate, creatine can be produced using a methyltransferase enzyme, giving rise to urea and sarcosine.

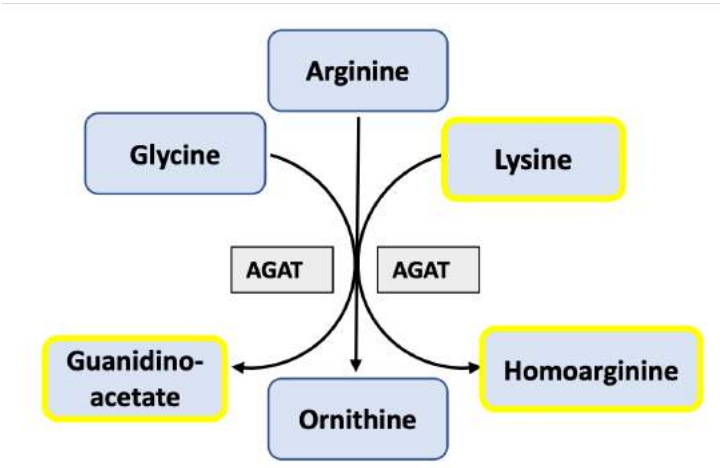

Figure 7.19. Production of guanidinoacetate and homoarginine from arginine. Adapted from Kanehisa and Sata (2020). Highlighted metabolites were included in the PsA metabolic model that was developed to report the 3-month DAPSA-based responses of patients.

Guanidinoacetate and homoarginine were negatively correlated with the 3-month DAPSA score (homoarginine: R = -0.53, p = 0.0023; guanidinoacetate: R=-0.36, p = 0.042), while lysine was not significantly correlated with the DAPSA score. Higher levels of guanidinoacetate and homoarginine at baseline were indicative of a better response to treatment in the cohort. Since the GA: HA ratio was reported in the literature as associated with an increased risk of death in individuals with a kidney transplant, the same ratio was assessed here for an association with the DAPSA-based response (Hanff *et al.*, 2019). This was especially important to note, as patients with PsA are at greater risk of early death due to CV disease. Indeed, there was a correlation between the GA: HA ratio at baseline and the 3-month DAPSA (R = 0.44, p = 0.017) and a significant difference was found for the distinction between low DAPSA (≤ 14) and high DAPSA (≥ 28), showing that a high GA: HA ratio was associated with a poor response to treatment based on the 3-month DAPSA score.

In the CENTAUR cohort, homoarginine and guanidinoacetate were generally reduced in their abundance in patients with higher 3-month DAPSA scores, which may point towards reduced AGAT activity in poor responders. This underlines the value of multi-omics analysis, whereby transcriptomics would provide insight into gene expression changes that control AGAT activity. Patients suffering from RMDs, primarily RA but also PsA, are at greater risk of developing CV disease (van Halm *et al.*, 2009; Zhu, Li and Tam, 2012). In fact, *in vivo* work performed elsewhere showed that mice that lacked AGAT through genetic knockout showed impaired heart function compared to WT mice, which was linked to reduced homoarginine production (Faller *et al.*, 2018). In addition, low homoarginine levels in the plasma of patients suffering from ischaemic stroke were associated with a worse outcome, indicating a potentially protective mechanism of homoarginine (Choe *et al.*, 2013).

Importantly, other arginine-related metabolites were included in the metabolic profile of MTX response in patients suffering from RA in the TaSER trial. These included ornithine and N-succinyl L-citrulline, which were associated with a response within the model, although concerns were noted surrounding the identity and true involvement of N-succinyl L-citrulline. The arginine metabolic pathways were located using the KEGG tool and are summarised in Figure 7.20 (Kanehisa and

Sato, 2020). The analysis of the transcriptomic data from the TaSER trial showed how the gene encoding arginase (ARG1) was increased in its expression at baseline in patients who had a poor response to MTX after 3 months. This may have indicated an increased metabolism of arginine and homoarginine towards ornithine, although it was noted that ornithine was not significantly associated with response by itself. The same was true of homocitrulline since it did not correlate significantly with the 3-month DAPSA score. Despite a p-value < 0.05 for its differential abundance across the response groups, the high variance observed meant it was not likely to be a meaningful association with response.

Since arginine metabolism was noted in both RA and PsA for its association with the response to treatment, the increased ARG1 expression shown in patients with a poor response to MTX in RA was considered alongside the decrease in homoarginine and guanidinoacetate in the poor responders with PsA. However, it was described in the TaSER transcriptomic analysis that the increased ARG1 in poor responders was contrary to what was expected, owing to its association with the anti-inflammatory M2-like macrophage phenotype that was reported during *in vitro* studies (Rath *et al.*, 2014).

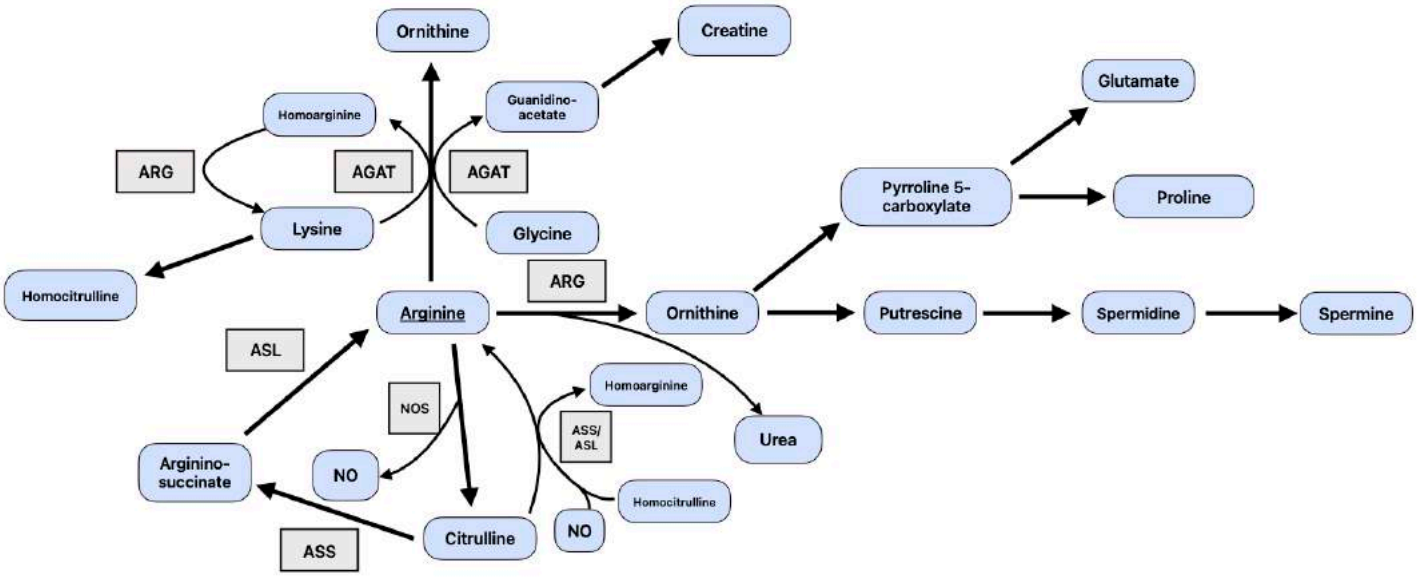

Figure 7.20. Network of arginine metabolic pathways. Adapted from Kanehisa and Sata (2020).

The cytokine analysis and MSEA provided further evidence of the involvement of arginine metabolism in association with inflammatory processes. The key cytokines known to be involved in PsA, including IL-17 subtypes, IL-1ß, IL-22, IFN-γ, and TNF-α, were assessed for their correlations with the patient metabolomic features. From this, it was found that guanidinoacetate was negatively correlated with IL-17C and IL-1RA, as shown in the earlier section, as well as IL-17A and leptin. In addition, homoarginine was also correlated, albeit weakly, with several other pro-inflammatory cytokines.

The correlation between guanidinoacetate and IL-17A, and IL-17C may be meaningful as these have been linked to PsA and psoriasis pathogenesis (Nograles *et al.*, 2008; Lynde *et al.*, 2014; Brembilla, Senra and Boehncke, 2018). While the understanding of IL-17C's role in disease is not fully understood, it was strongly correlated with TNF, increased in the circulation of patients in this work who also suffered from psoriasis and was reported to be increased in the skin of patients with psoriasis, supporting its likely involvement in influencing the pathology of PsA (Johnston *et al.*, 2013).

The literature describes IL-17A in PsA more substantially than other IL-17 family members, including IL-17C, where it describes an important involvement of IL-17A in PsA pathology. The production of IL-17A by various cells, including T_H17 cells, leads to inflammation and bone damage (McGonagle *et al.*, 2019). The use of the IL-17A inhibitor, ixekizumab, tested in the SPIRIT-P1 trial, reduced the disease activity of patients with PsA (Mease *et al.*, 2017). Additionally, the phase 3 trials for secukinumab, another IL-17A inhibitor, initially approved for clinical practice for managing psoriasis, showed significant improvement in the disease activity in patients with PsA (Langley *et al.*, 2014; Mease *et al.*, 2018). As such, there was a clear and established role of IL-17A in PsA, leading to the use of anti-IL-17A drugs being developed for its management.

In this current work, IL-17A did not correlate with the baseline CRP, DAPSA or FM scores, which was expected to indicate its association with disease activity in patients. However, given the increasingly understood tissue-specific immunological profiles in PsA, the lack of association of IL-17A with the joint disease reflected by DAPSA may be due to its prominent involvement in the skin-related disease and not

the joint (Siebert, Millar and McInnes, 2019). This is, therefore, an important example of how tissue-specific differences in the immunological profile may not necessarily be represented in the blood. Using other composite measures that cover more PsA disease domains would be a helpful addition to this work.

The association of arginine metabolism with the differing disease activity and pro-inflammatory cytokine profile was logical, where, in macrophage models, the fate of arginine was closely linked to the inflammatory phenotype of the cells (Rath *et al.*, 2014). For example, the pro-inflammatory M1-like phenotype can be characterised by increased nitric oxide synthase (NOS) activity, giving rise to ROS. In contrast, the anti-inflammatory M2-like phenotype was conversely characterised by arginase activity (Rath *et al.*, 2014). The differential activity of the urea cycle, potentially involving the altered behaviour of NOS or arginase, may lead to an altered immune profile, reflected by changes to these PsA-cytokines.

7.4.4. Disruption to Central Carbon Metabolism

In addition to the changes to arginine metabolism, central-carbon metabolites were differentially abundant, picked out as part of the pathway analysis or included in the treatment-response metabolic model. This included lactate, glucuronate, itaconate and pyruvate. However, aside from pyruvate, which had a stronger association with the treatment response, these metabolites showed weak associations with the 3-month DAPSA. These metabolites can be linked by central carbon metabolism, whereby glucose is metabolised along different pathways, including glycolysis, to give rise to pyruvate, or the uronic pathway, which produces glucuronate, as shown in Figure 7.21.

The uronic pathway acts as an alternative metabolic pathway of glucose, producing glucuronate, a metabolite that contributes to the formation of proteoglycans, intermediates for the pentose phosphate pathway, and supports the excretion of compounds via the urine or bile (Ho *et al.*, 2019). Their conversion to a glucuronide conjugate can support the excretion of drugs in the blood. Here, glucuronate is attached to the exogenous compound, which usually reduces the drug's pharmacological activity while also enhancing the body’s ability to excrete the drug by increasing its solubility in water (Silva *et al.*, 2003). Tentatively

identified glucuronate had a borderline-significant correlation with the 3-month DAPSA correlation (R=0.34, p-value = 0.058), which indicated it might be increased in patients with a worse response to treatment. It may be possible that increased glucuronate leads to increased excretion of certain drugs used in PsA treatment, thereby leading to reduced efficacy and increased disease activity. This requires further study, however, focusing on drugs where glucuronate is involved in their excretion.

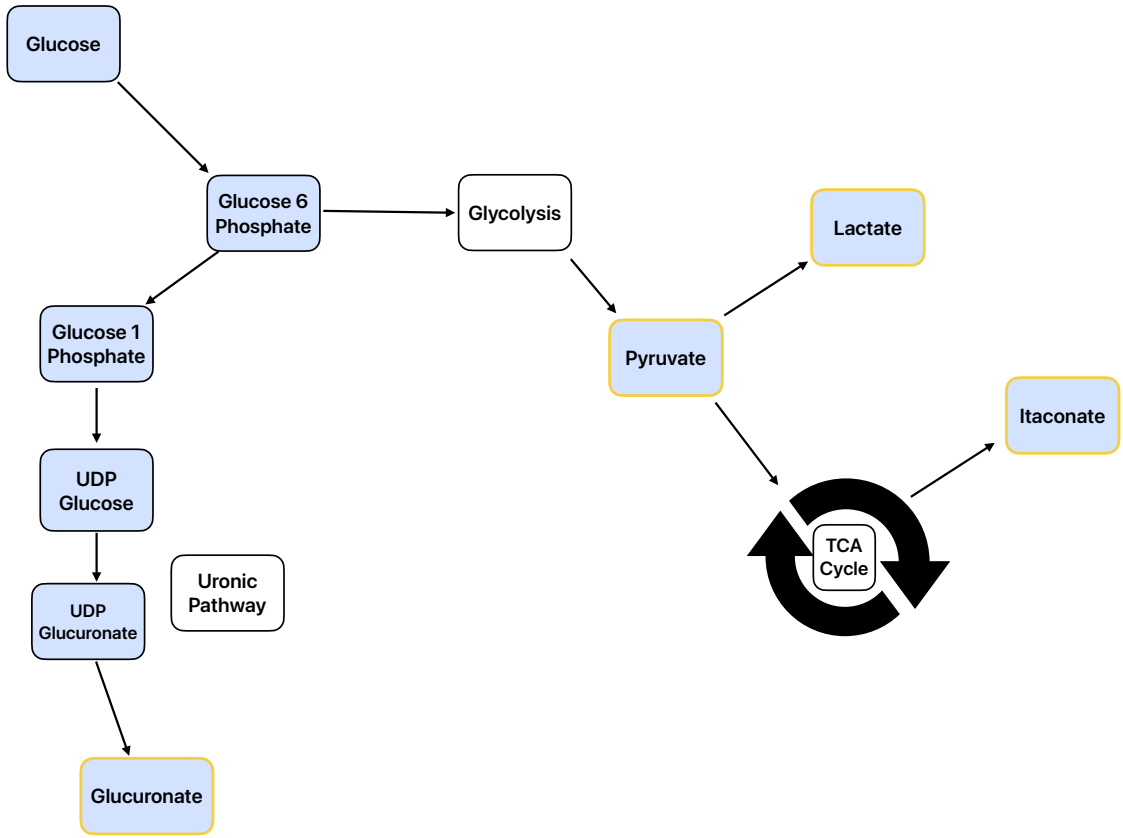

Figure 7.21. Central carbon metabolism summary with metabolites from PsA treatment response model highlighted. Adapted from Kanehisa and Sata (2020).

Moreover, the correlation of glucuronate with DAPSA was notable since glucuronate was described in the literature as a marker for predicting a worse overall state of health as an individual ages. As such, glucuronate may be a marker of ageing itself, where it was described in the literature as being significantly correlated with age across multiple populations (Ho *et al.*, 2019). In this work, age was an important factor in driving the variance of glucuronate. However, no

significant correlation was shown between age and glucuronate when these were assessed (not shown). The similar correlation of glucuronate with the DAS28-ESR score at 3 months in the cohort from the Mayo Clinic, described by Hur et al. (2021) was notable, suggesting that glucuronate may indeed be a shared metabolite associated with the resolution of RMDs.

Since the GA: HA ratio was associated with the 3-month DAPSA, the same approach was taken with the other metabolites in the model. Each possible pair of metabolites was assessed as a ratio for their relationship with the DAPSA-based outcomes. These included itaconate: pyruvate, itaconate: glucuronate and homoarginine: lactate. Along with the GA: HA ratio, these three additional metabolite ratios were also associated with the DAPSA at 3 months, indicating potential as predictive tools for the response to treatment in PsA.

Having been included in the model and discussed in the TaSER metabolomics chapter, itaconate was of interest as a metabolite contributing to this cohort's predictive model for treatment response. However, it was clear from the correlation and differential analyses that itaconate was not a robust marker of DAPSA in this cohort. Nevertheless, the itaconate: pyruvate/glucuronate ratios were associated with the DAPSA at 3 months, and so there may still be potential for its use in a predictive tool for the response.

The fact that itaconate, pyruvate, lactate and glucuronate share a similar pathway, relating to the products of glucose metabolism and the TCA cycle, may indicate a pathway-wide perturbation that provides a favourable metabolic environment for PsA treatments to exert their effects. The itaconate: pyruvate/glucuronate ratios may be key in understanding this environment, where the metabolism of glucose towards itaconate via the TCA cycle rather than towards lactate or glucuronate may result in a more favourable environment due to the apparent anti-inflammatory effects that were observed during *in vitro*/*vivo* studies (Lampropoulou *et al.*, 2016; Mills *et al.*, 2018). Indeed, the change in itaconate between baseline and 3 months negatively correlated with the change in disease activity (DAS44) in patients with RA in the TaSER trial over the same period (Daly *et al.*, 2020).

7.4.5. Gout and PsA

Finally, it was worth briefly discussing the cytokine and metabolome analysis findings, whereby strong correlations were shown, especially for hypoxanthine and uric acid with IL-1ß. These findings may be important in considering the relationship between PsA and gout, whereby patients with PsA and psoriasis may concurrently suffer from gout (Widawski *et al.*, 2022). Elevated levels of monosodium urate cause gout (MSU) crystals forming in the joints and inducing inflammation, with IL-1 implicated in mediating the disease (So, Dumusc and Nasi, 2017; Tripolino *et al.*, 2021). In the CENTAUR cohort, IL-1ß was positively correlated with uric acid which may suggest concurrent gout in patients with PsA.

Treating patients with PsA and gout with allopurinol, an inhibitor of xanthine oxidase, which converts hypoxanthine to xanthine and uric acid, may therefore be an option in improving patient outcomes, where residual disease following DMARD treatment may feasibly be due to symptoms caused by hyperuricaemia. Indeed, studies have investigated the efficacy of allopurinol treatment in patients with PsA and psoriasis (Feuerman and Nir, 1973; Goldman, 1981; Luis-Rodríguez *et al.*, 2021). Of these studies, the most recent reported a reduction in the expression of pro-inflammatory cytokines, namely TNF-α and IL-6, following the treatment of patients with asymptomatic hyperuricaemia with allopurinol, indicating a possible anti-inflammatory effect that arises by blocking uric acid production (Luis-Rodríguez *et al.*, 2021).

However, elevated uric acid in the circulation may also be a biomarker for metabolic syndrome (encompassing PsA), thus raising a question over the link with gout (Raya-Cano *et al.*, 2022). Nevertheless, targeting elevated uric acid with drugs like allopurinol may still be helpful in treating metabolic syndrome, although Raya-Cano et al. (2022) highlighted the need for further studies to explore the involvement of uric acid in metabolic syndrome with greater confidence.

7.4.6. Considering the Shared Metabolites Across RMDs

This chapter investigated the metabolomics of PsA and the response to various treatments in patients suffering from the disease. The primary aim was to identify metabolites that could be used to inform biomarker discovery to predict patient

responses to treatment. Since various treatments were used in the CENTAUR study, the panel of metabolites included in the response profile were not associated with any specific treatment. A secondary aim of the PsA metabolomic analysis was to investigate whether common metabolites were associated with a general treatment response in patients with RMDs, focusing on PsA and RA in this work.

The metabolic profile generated using a supervised machine learning approach, of patient responses to treatment in PsA included homoarginine, guanidinoacetate, pyruvate, lactate, glucuronate, homocitrulline, itaconate, carnitine and lysine. Unlike the similar molecular profiles generated in previous chapters, this one was developed to report either good (LDA/remission) or poor (HDA) response to treatment, leaving a subgroup of moderate/partial patients between these extreme responses. While this reduced the sample size, the resulting metabolic profile was potentially informative of the metabolites that may regulate the response to treatment in these groups. Indeed, two clear groups of biologically related metabolites were uncovered in the modelling, including arginine metabolism related and central-carbon metabolism-related features.

Since arginine-related metabolites were tentatively reported to be associated with the MTX response in patients with RA in the TaSER study, these findings may support the notion of common metabolites being associated with the resolution of inflammation across RMDs. However, an investigation into the metabolites correlated with the MTX response showed no additional metabolites relating to arginine metabolism. Only homoarginine was correlated with the MTX response with a similarly strong response, indicating that the patients treated with MTX likely drove the inclusion of homoarginine in the final metabolic model predictive of treatment response.

It was clear throughout the project that larger sample sizes would increase the confidence in these findings, and further validations in related datasets were required. As a result, this and the analysis reported in the previous chapters may indeed point towards a shared component of metabolites associated with treatment response in RA and PsA. Still, it was clear that additional analyses involving metabolomic datasets covering other RMDs, such as gout and axial spondyloarthrits, are required to improve upon these results.

To shed more light on these similarities and differences across the RMDs, further analyses should be done using the multiple omics platforms available. While not included in this thesis, later studies led by clinicians at the University of Glasgow, such as the Hippocrates trial, will provide further data to be analysed, including metabolomics. However, as hinted at throughout this work, the metabolomic analysis would most likely benefit from the parallel analysis of other omics datasets, such as transcriptomics and proteomics from the same samples. Additional data, such as the cytokine data described in this chapter, would also be beneficial in building up the multi-omic molecular profile associated with patient responses to treatment. Therefore, the analysis in this work should be taken as a steppingstone to uncovering further the molecular understanding of the features associated with treatment response. For example, given the multiple domains involved in PsA, it would be valuable to investigate the levels of the metabolites of interest and their immunomodulatory effects across different tissue types implicated in PsA. Such a molecular profile is believed to exist, but only a fragment of the puzzle may be found in the metabolome. Since a tissue-distinct immunological profile is reported in PsA, it is feasible that the different immune cells influencing disease across the tissue compartments would vary in their metabolic appetites.

8. Conclusions

8.1. Overview

This thesis has sought to investigate the metabolomics of treatment response in patients with RMDs, focusing on RA and PsA as archetypal diseases. Since patients with RMDs often require a stepwise escalation of treatment as part of a treat-to-target approach, predicting how patients will respond to the first-line and subsequent treatments is invaluable for improving their long-term outcomes. Where the project began by searching for metabolic biomarkers that could predict the 3-month response to MTX in patients with RA from the TaSER trial, this expanded to include patients treated with other drugs, as well as patients with PsA who received similar DMARDs.

The overarching aim throughout this work was to identify metabolites associated with treatment responses in these diseases — these were intended to inform the discovery of biomarkers that could be used to predict the probability of a patient's successful response to treatment. As a secondary aim, the project sought to explore whether the metabolites associated with the general treatment response indicated any involvement of the metabolites in providing a favourable molecular environment in which the various treatments can best take effect. This was especially true in the PsA chapter, where the various drugs used meant a treatment-agnostic metabolic profile of response was generated. The metabolic profiles generated throughout the project may contribute to the understanding of the potentially shared metabolic features associated with the resolution of inflammation across these RMDs.

However, due to the complexity of the metabolomic data analysis and the difficulty translating the findings across cohorts of patients, there remained an underlying uncertainty about the true clinical impact of the results throughout this thesis. As such, there remains a demand to validate these findings: doing so in the laboratory, investigating the immunomodulatory effects of the metabolites of interest using immune cell models, also validating the results in related clinical datasets, as attempted across the TaSER and tREACH cohorts.

Overall, the results from this thesis contributed to the research on a metabolomics approach for discovering predictive biomarkers in RA and PsA. These contributions are summarised in the following sections. Aside from the results from these analyses, one of the most valuable outputs from the project was the analysis workflow, which was developed and refined throughout. This provided a standard method for analysing each dataset obtained throughout the project. A representative script including the major processing and analytical steps was included in the Appendix.

8.2. TaSER Metabolomics

The TaSER metabolome provided a foundation for this work, being the initial dataset from which the analytical workflow was developed. Given the weak signals and associations observed with treatment response when using univariate analyses, a supervised machine learning approach was incorporated to reveal a panel of metabolites collectively associated with the MTX response. The model included pyroglutamate, kynurenine, indoleacrylic acid, pyrroline, cytosine, N-succinyl L-citrulline, ornithine and 5-methylcytidine. While several of these were only tentatively identified, including indoleacrylic acid and N-succinyl L-citrulline, this collection of metabolites may have pointed towards the involvement of tryptophan and arginine metabolic pathways being linked to a successful response in patients with RA to MTX.

The metabolic model was compared with models generated from the patient factors, including risk factors for RA and baseline disease measurements. This comparison showed the metabolic model performed just as well as the other models. However, this comparison raises an important consideration of the value of these findings in a clinical setting where the ease of incorporating a metabolic biomarker tool in the clinic is likely a limiting factor. Since disease activity measures and patient factors such as smoking are routinely recorded during routine clinical care, using these in a model to guide treatment would not place additional strain on an already stretched clinical team. Developing a clinically useful tool needs to be simple, quick to use for the clinician and able to provide clear and accurate results. Given the similar performance of the metabolic model to the disease measures model, it may not be practical for its inclusion in the

clinical setting until it demonstrates higher predictive performance across various cohorts with different demographics, something that was not achieved in this work.

The true benefit of the metabolic model generated in this chapter — and those that followed — was in uncovering the circulating metabolites that may modulate how patients respond to treatment. As such, measuring these metabolites in patients when they first present with symptoms may be useful in providing optimal treatment and potentially supplementing this with exogenous metabolites or pharmacological agents that target the metabolic pathways of interest.

8.3. TaSER Transcriptomics and Integration

The transcriptomic data generated from the whole blood microarray sequencing provided an alternative dimension to interrogate the TaSER cohort for potential biomarkers of treatment response. It was eagerly anticipated that an expression profile associated with responses to MTX would reveal changes to the genes involved in metabolic pathways. However, immune-related genes were those predominately found to be differentially expressed across the response groups, therefore pointing towards an exacerbated immune response in the poor responders, as might be expected. An important consideration from this chapter was whether prior biological knowledge ought to be included in the analysis. It was found that doing so provided a predictive model that performed just as well as the model generated using a purely statistical approach.

Including transcriptomic and metabolomic datasets from the same samples led to an initial integration using a simple correlational approach. Given the inclusion of several immune-related genes in the model, an investigation into the correlated metabolites was launched, potentially indicating those that might be involved in regulating the immune response. There were several strongly correlated genes and metabolites, although the biological relationship between these remained uncertain.

8.4. TaSER Multivariate Integration

Following the simple integration of the transcriptomic and metabolomic datasets, a more complex approach involving a statistical method, specifically a multivariate approach, was undertaken. The analysis used the *mixOmics* package in R, using the *DIABLO* tool within this environment. The multi-omic molecular profile developed to discriminate between good and poor responders to MTX from the TaSER cohort included many of the features in the previous chapters. Despite generating a multi-omic response profile, this was limited in its discriminatory capacity, failing to reveal highly distinct response groups characterised by the model's features. It did point out, however, where the correlating features across the blocks of data were found, although the simpler approach taken in the previous chapter meant this approach did not extensively progress the response-associated molecular profile.

Given the technological advancements in the generation of omics data and the analytical methods, often including complicated machine learning methods, the integration of omics datasets is becoming more important in understanding the influence of different molecular dimensions on the sample classes. However, the field of data integration is rapidly developing, leading to numerous methods with advantages and disadvantages. The DIABLO method was used as a multivariate method reported in other studies as effective in pulling out a panel of correlating features (therefore potentially biologically connected) and capable of discriminating sample classes. Had the multivariate approach been used as an initial tool in the analysis before that described in the previous chapters, it would likely have been of greater value than following these since it did not reveal many novel features that were not considered elsewhere. This section of the analysis was inconclusive about the value of the multivariate approach, especially when used in a relatively small sample size.

8.5. Multicentre Metabolomics

There are multitudes of data generated across research centres worldwide, and the workflow developed in this project was applied to the analysis of two datasets generated from cohorts of patients with RA from the Netherlands and the USA.

From this and other chapters, there was increasing evidence that metabolites that may be derived from the gut microbiome were perturbed in patients who had different responses to treatment. Whether this implicates the gut microbiome in modulating treatment efficacy is uncertain. However, it was feasible that changes to key populations of bacteria may lead to differences in immunomodulatory metabolites or may also lead to changes in the metabolism of the drugs themselves, particularly those that were orally administered. It was important to note that the Mayo Clinic study involved patients treated with a variety of drugs, therefore extending the focus of this thesis from an MTX-specific response to a general treatment response.

An important limitation of the metabolomic analysis across research centres was evident from this chapter. One of the intentions of using datasets generated from other research centres was to determine the reproducibility of the metabolic model of MTX response from the TaSER cohort. However, as described in this chapter, the model was not translatable owing to differences in the generation of the metabolomic data and the metabolites included. Where a similarly untargeted approach was used by the Mayo Clinic study, from whom the second metabolomic dataset was obtained, similar differences in the data structures made it difficult to compare findings. This chapter underlined the limitation of using data generated using untargeted metabolomics and only a relative quantification.

For a reliable comparison to be made, a targeted approach with authentic reference standards for all of the metabolites to be analysed should be performed. However, targeted analysis for the conceivable number of metabolites to investigate is considerably more expensive. As a result, there are far fewer publicly available metabolomic datasets whose analytes were measured with absolute quantification. This chapter attempted to use some of the available data to examine shared metabolites across cohorts without this targeted approach and so demonstrates the obvious limitations of doing so.

8.6. CENTAUR Metabolomics

This chapter involved the analysis of the metabolome from serum samples from patients with PsA who were enrolled on the CENTAUR study led by Dr Flavia

Sunzini. This analysis provided the opportunity to investigate the metabolomics of another RMD, to explore whether there were common metabolites across diseases associated with treatment response. Indeed, the similar inflammatory component between RA and PsA meant that it was expected that similar metabolites might be associated with the resolution of inflammation between these diseases. Interestingly, following the workflow developed from the TaSER metabolomic analysis, a panel of metabolites at baseline were associated with the treatment response involving guanidinoacetate, homoarginine, pyruvate, lactate, glucuronate, homocitrulline, itaconate, carnitine and lysine. The collection of these metabolites indicated that arginine-related and central carbon metabolic pathways might be perturbed in patients with variable responses to treatment. Since arginine-related metabolites were mentioned in previous chapters, this chapter might support the notion that perturbed arginine metabolism is associated with treatment response.

The primary aim of this thesis was to identify metabolic biomarkers that could ultimately be used to guide treatment options for patients. The involvement of patient cohorts who received multiple treatment types meant a general treatment-response-associated metabolic profile could be generated. While early in the search for metabolic biomarkers for treatment response, taking this profile forward for further development may prove valuable for patients, where the metabolic mechanisms that drive a treatment-agnostic resolution of inflammation may help to understand how best to treat patients.

Additional trials investigating the metabolomics of PsA are underway, but unfortunately, the samples were not analysed in time to be included in this thesis. Running these samples at Glasgow Polyomics may provide the additional datasets required to validate the findings from this PsA cohort.

8.7. Summary

The secondary analyses of the metabolomic and transcriptomic data from clinical trials involving patients with RA and PsA were performed throughout this project. While challenges included the identification of the metabolites and reproducibility of the results across datasets, these findings contributed to the field by pointing

towards a panel of diverse metabolites associated with treatment responses in patients with RA and PsA. Metabolites associated with treatment response throughout the project are shown in a summary metabolic network in Figure 8.1. The metabolites from the analysis were also plotted on the entire metabolomic network, as shown in Supplementary Figure 7.

The fact that several metabolites described in the literature as being derived primarily from the gut microbiome were included in this panel across the datasets may indicate the involvement of the gut microbiome in mediating successful treatment. This, therefore, highlights a potential therapeutic target that could supplement existing treatments using safe and established pharmacological agents, such as antibiotics and probiotics, to alter the balance of the microbiome towards that of a positive responder. One future direction for this work may involve closely examining the gut metagenome of patients with RMDs and investigate the bacteria strains and species associated with treatment response, similar to the work performed by Gupta et al. (2021).

These results may be considered preliminary, where the complete identification of the metabolites using fragmentation data and their validation in other related datasets was not performed in this work. Given the increasing number of publicly available datasets and the sophisticated analytical tools being developed, these results are expected to be verified soon. Doing so will ultimately help characterise the successful response to treatment on a metabolic level, and it is not unfeasible that integrating these results with other omics datasets will only increase the understanding of the mechanisms at play in the resolution of inflammation. The advancement of precision medicine in inflammatory rheumatic diseases will greatly benefit from further investment in the generation, analysis, and integration of metabolomic (and other omic) data.

8.8. Improving the Design of Future Studies

Throughout the project, it was apparent that larger study sizes would likely be of benefit in increasing the confidence that the findings could be applicable to the population represented by the cohorts. The project involved secondary analyses of data generated from studies whose cohort sizes were not selected from power

calculations. Now that effect sizes between response groups have been measured, these power calculations can be performed to determine a suitable cohort size for a future study to ensure it would be statistically powered.

From the analysis performed throughout the project, there may be important geographical effects on the metabolome of patients across regions. As such, there may be benefit in limiting enrolment of patients to geographically restricted areas to reduce variation caused by geography and lifestyle factors. For example, a future study that recruits patients from around the UK would likely increase the variation observed in the metabolome of patients in the treatment response groups. Increasing sample sizes while recruiting patients from defined regions may control for the influence of geography on the metabolome and allow for omic profiles of response to be generated without these potentially confounding effects.

Finally, the generation of omics profiles specific to each possible DMARD available would be of greatest benefit. The studies used in this project included patients being treated using various drugs, leading to a loss of potentially valuable information that may result from a treatment-specific panel of response-associated metabolites. These panels of metabolites may indicate mechanisms that contribute towards the resolution of disease in response to individual drugs, shedding light on potentially new therapeutic targets.

8.9. Impact of COVID-19

The COVID-19 pandemic struck approximately 5 months into my PhD programme. During these early months, I began my training in the laboratory, aiming to investigate the immunomodulatory effects of possible biomarkers of treatment response, including itaconate. However, the ensuing lockdown led to a change in direction, resulting in a purely bioinformatics-based project and the secondary analyses of existing datasets. A further result of the pandemic was the involvement of my primary supervisor in the Lighthouse Laboratories. As a result, I was awarded a 3-month extension which allowed me to continue my project with greater supervision and feedback.

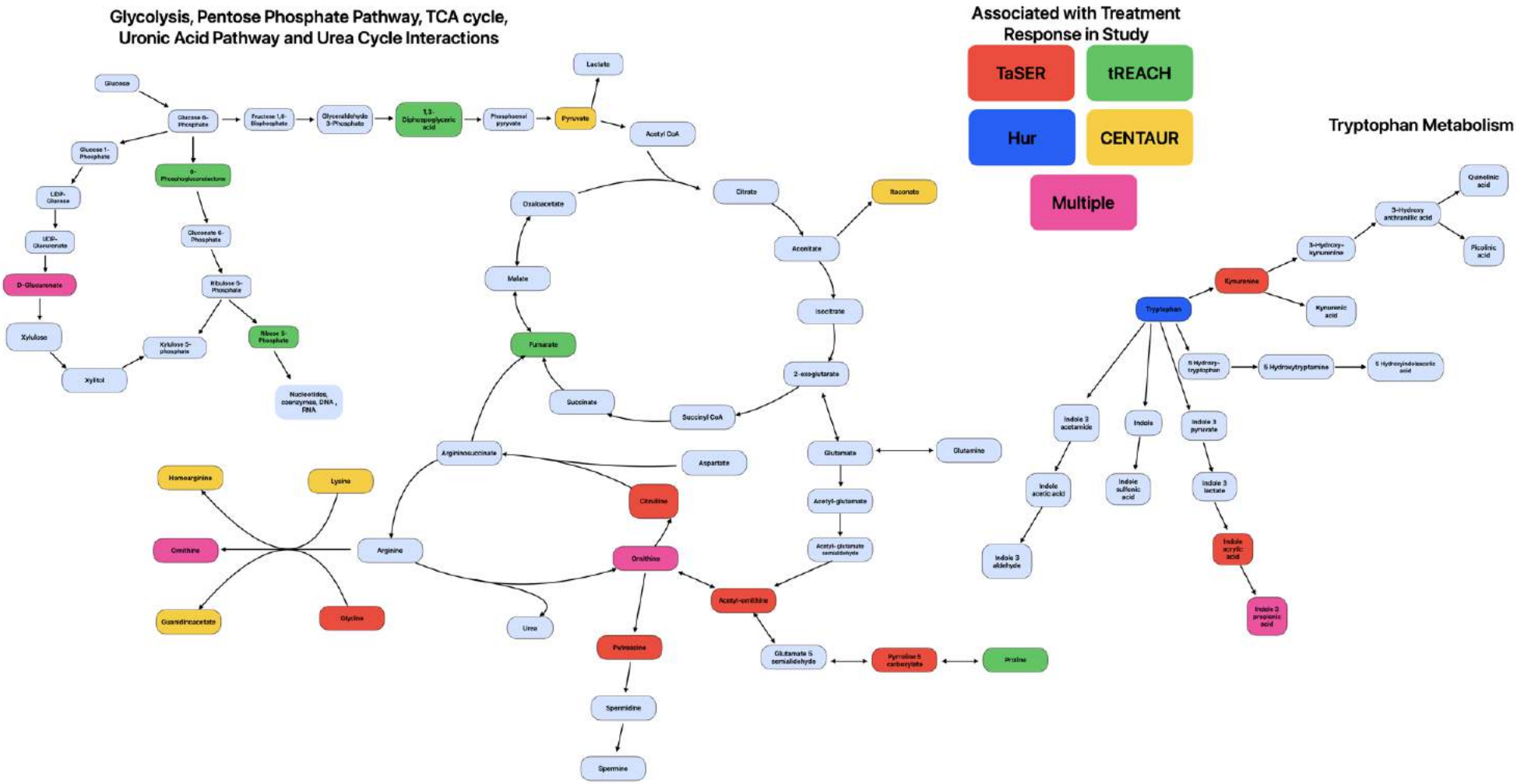

Figure 8.1. Metabolic network of connected metabolites throughout the project with colour-coded labels for the cohort from which they were derived

9. References

1. Akhtar, M. *et al.* (2021) 'Characterization of rheumatoid arthritis risk-associated snps and identification of novel therapeutic sites using an in-silico approach', *Biology*, 10(6), p. 501. Available at: https://doi.org/10.3390/biology10060501.

2. Akram, M.S. *et al.* (2021) 'Challenges for biosimilars: focus on rheumatoid arthritis', *Critical Reviews in Biotechnology*, 41(1), pp. 121–153. Available at: https://doi.org/10.1080/07388551.2020.1830746.

3. Aletaha, D. *et al.* (2010) '2010 rheumatoid arthritis classification criteria: an American College of Rheumatology/European League Against Rheumatism collaborative initiative'.

4. Aletaha, D., Alasti, F. and Smolen, J.S. (2015) 'Rheumatoid factor, not antibodies against citrullinated proteins, is associated with baseline disease activity in rheumatoid arthritis clinical trials', *Arthritis Research & Therapy*, 17(1), p. 229. Available at: https://doi.org/10.1186/s13075-015-0736-9.

5. Aletaha, D., Alasti, F. and Smolen, J.S. (2016) 'Optimisation of a treat-to-target approach in rheumatoid arthritis: strategies for the 3-month time point', *Annals of the Rheumatic Diseases*. Available at: https://doi.org/10.1136/annrheumdis-2015-208324.

6. Aletaha, D. and Smolen, J.S. (2018) 'Diagnosis and management of rheumatoid arthritis: a review', *JAMA*. Available at: https://doi.org/10.1001/jama.2018.13103.

7. Alexeev, E.E. *et al.* (2018) 'Microbiota-derived indole metabolites promote human and murine intestinal homeostasis through regulation of interleukin-10 receptor', *The American Journal of Pathology*, 188(5), pp. 1183–1194. Available at: https://doi.org/10.1016/j.ajpath.2018.01.011.

8. Alivernini, S. *et al.* (2020) 'Distinct synovial tissue macrophage subsets regulate inflammation and remission in rheumatoid arthritis', *Nature Medicine*, 26(8), pp. 1295–1306. Available at: https://doi.org/10.1038/s41591-020-0939-8.

9. Alivernini, S., Firestein, G.S. and McInnes, I.B. (2022) 'The pathogenesis of rheumatoid arthritis', *Immunity*, 55(12), pp. 2255–2270. Available at: https://doi.org/10.1016/j.immuni.2022.11.009.

10. Almoallim, H. *et al.* (2021) 'A review of the prevalence and unmet needs in the management of rheumatoid arthritis in Africa and the Middle East', *Rheumatology and Therapy*, 8(1), pp. 1–16. Available at: https://doi.org/10.1007/s40744-020-00252-1.

11. Almutairi, K. *et al.* (2021) 'The global prevalence of rheumatoid arthritis: a meta-analysis based on a systematic review', *Rheumatology International*, 41(5), pp. 863–877. Available at: https://doi.org/10.1007/s00296-020-04731-0.

12. Amar, J. *et al.* (2011) 'Involvement of tissue bacteria in the onset of diabetes in humans: evidence for a concept', *Diabetologia*, 54(12), pp. 3055–3061. Available at: https://doi.org/10.1007/s00125-011-2329-8.

13. An, G. *et al.* (2020) 'Aspects of matrix and analyte effects in clinical pharmacokinetic sample analyses using LC-ESI/MS/MS – two case examples', *Journal of pharmaceutical and biomedical analysis*, 183, p. 113135. Available at: https://doi.org/10.1016/j.jpba.2020.113135.

14. Anderson, N.M. *et al.* (2018) 'The emerging role and targetability of the TCA cycle in cancer metabolism', *Protein & cell*. Available at: https://doi.org/10.1007/s13238-017-0451-1.

15. Annese, V.F. *et al.* (2021) 'A monolithic single-chip point-of-care platform for metabolomic prostate cancer detection', *Microsystems & Nanoengineering*, 7(1), pp. 1–15. Available at: https://doi.org/10.1038/s41378-021-00243-4.

16. Antonioli, L. *et al.* (2019) 'Adenosine signaling and the immune system: When a lot could be too much', *Immunology Letters*, 205, pp. 9–15. Available at: https://doi.org/10.1016/j.imlet.2018.04.006.

17. Apalset, E.M. *et al.* (2014) 'Interferon (IFN)-γ-mediated inflammation and the kynurenine pathway in relation to bone mineral density: the Hordaland Health Study', *Clinical and Experimental Immunology*, 176(3), pp. 452–460. Available at: https://doi.org/10.1111/cei.12288.

18. Apley, D.W. and Zhu, J. (2020) 'Visualizing the effects of predictor variables in black box supervised learning models.', *Journal of the Royal Statistical Society: Series B (Statistical Methodology)*, 82.4, pp. 1059–1086.

19. Artacho, A. *et al.* (2021) 'The pretreatment gut microbiome is associated with lack of response to methotrexate in new-onset rheumatoid arthritis', *Arthritis & Rheumatology*, 73(6), pp. 931–942. Available at: https://doi.org/10.1002/art.41622.

20. Bach, E., Schymanski, E.L. and Rousu, J. (2022) 'Joint structural annotation of small molecules using liquid chromatography retention order and tandem mass spectrometry data', *Nature Machine Intelligence*, 4(12), pp. 1224–1237. Available at: https://doi.org/10.1038/s42256-022-00577-2.

21. Bajad, S.U. *et al.* (2006) 'Separation and quantitation of water soluble cellular metabolites by hydrophilic interaction chromatography-tandem mass spectrometry', *Journal of Chromatography A*, 1125(1), pp. 76–88. Available at: https://doi.org/10.1016/j.chroma.2006.05.019.

22. Baker, J.F. *et al.* (2017) 'Relationship of patient-reported outcomes with MRI measures in rheumatoid arthritis', *Annals of the Rheumatic Diseases*. Available at: https://doi.org/10.1136/annrheumdis-2016-209463.

23. Bao, X. *et al.* (2017) 'Roles of dietary amino acids and their metabolites in pathogenesis of inflammatory bowel disease', *Mediators of inflammation*. Available at: https://doi.org/10.1155/2017/6869259.

24. Bartikoski, B.J. *et al.* (2022) 'A review of metabolomic profiling in rheumatoid arthritis: bringing new insights in disease pathogenesis, treatment and comorbidities', *Metabolites*, 12(5), p. 394. Available at: https://doi.org/10.3390/metabo12050394.

25. Benasciutti, E. *et al.* (2014) 'MHC class II transactivator is an in vivo regulator of osteoclast differentiation and bone homeostasis co-opted from adaptive immunity', *Journal of Bone and Mineral Research: The Official Journal of the American Society for Bone and Mineral Research*, 29(2), pp. 290–303. Available at: https://doi.org/10.1002/jbmr.2090.

26. Bengtsson, K. *et al.* (2021) 'Incidence of extra-articular manifestations in ankylosing spondylitis, psoriatic arthritis and undifferentiated spondyloarthritis: results from a national register-based cohort study', *Rheumatology*, 60(6), pp. 2725–2734. Available at: https://doi.org/10.1093/rheumatology/keaa692.

27. Benjamini, Y. and Hochberg, Y. (1995) 'Controlling the false discovery rate: a practical and powerful approach to multiple testing', *Journal of the Royal Statistical Society. Series B (Methodological)*.

28. Berry, D.A. (2006) 'Bayesian clinical trials', *Nature Reviews Drug Discovery*, 5(1), pp. 27–37. Available at: https://doi.org/10.1038/nrd1927.

29. Beuchel, C. *et al.* (2019) 'Clinical and lifestyle related factors influencing whole blood metabolite levels – A comparative analysis of three large cohorts', *Molecular Metabolism*, 29, pp. 76–85. Available at: https://doi.org/10.1016/j.molmet.2019.08.010.

30. Biecek, P. (2018) 'DALEX: explainers for complex predictive models in R', *J. Mach. Learn. Res.*, 19(1), pp. 3245–3249.

31. Bijlsma, J.W.J. *et al.* (2016) 'Early rheumatoid arthritis treated with tocilizumab, methotrexate, or their combination (U-Act-Early): a multicentre, randomised, double-blind, double-dummy, strategy trial', *The Lancet*, 388(10042), pp. 343–355. Available at: https://doi.org/10.1016/S0140-6736(16)30363-4.

32. Bijlsma, S. *et al.* (2006) 'Large-scale human metabolomics studies: a strategy for data (pre-) processing and validation', *Analytical Chemistry*, 78(2), pp. 567–574. Available at: https://doi.org/10.1021/ac051495j.

33. Boutet, M.-A. *et al.* (2018) 'Role of the IL-23/IL-17 axis in psoriasis and psoriatic arthritis: the clinical importance of its divergence in skin and joints', *International*

Journal of Molecular Sciences, 19(2), p. 530. Available at: https://doi.org/10.3390/ijms19020530.

34. Boutet, M.-A. *et al.* (2021) 'Novel insights into macrophage diversity in rheumatoid arthritis synovium', *Autoimmunity Reviews*. Available at: https://doi.org/10.1016/j.autrev.2021.102758.

35. Brembilla, N.C., Senra, L. and Boehncke, W.-H. (2018) 'The IL-17 family of cytokines in psoriasis: IL-17A and beyond', *Frontiers in Immunology*, 9. Available at: https://www.frontiersin.org/articles/10.3389/fimmu.2018.01682 (Accessed: 14 March 2023).

36. Brenke, J.K. *et al.* (2018) 'Targeting TRAF6 E3 ligase activity with a small-molecule inhibitor combats autoimmunity', *The Journal of Biological Chemistry*, 293(34), pp. 13191–13203. Available at: https://doi.org/10.1074/jbc.RA118.002649.

37. Brenton, A.G. and Godfrey, A.R. (2010) 'Accurate mass measurement: terminology and treatment of data', *Journal of the American Society for Mass Spectrometry*, 21(11), pp. 1821–1835. Available at: https://doi.org/10.1016/j.jasms.2010.06.006.

38. Brighton, S.W. *et al.* (1988) 'The prevalence of rheumatoid arthritis in a rural African population', *The Journal of Rheumatology*, 15(3), pp. 405–408.

39. Brown, R.R. *et al.* (1991) 'Implications of interferon-induced tryptophan catabolism in cancer, auto-immune diseases and AIDS', *Advances in Experimental Medicine and Biology*, 294, pp. 425–435. Available at: https://doi.org/10.1007/978-1-4684-5952-4_39.

40. Bshesh, K. *et al.* (2002) 'The A2A receptor mediates an endogenous regulatory pathway of cytokine expression in THP-1 cells.', *Journal of leukocyte biology*, 72(5), pp. 1027–1036.

41. Bucaciuc Mracica, T. *et al.* (2020) 'MetaboAge DB: a repository of known ageing-related changes in the human metabolome', *Biogerontology*, 21(6), pp. 763–771. Available at: https://doi.org/10.1007/s10522-020-09892-w.

42. Buescher, J.M. and Driggers, E.M. (2016) 'Integration of omics: more than the sum of its parts', *Cancer & Metabolism*. Available at: https://doi.org/10.1186/s40170-016-0143-y.

43. Buleu, F. *et al.* (2019) 'Heart involvement in inflammatory rheumatic diseases: a systematic literature review', *Medicina*, 55(6), p. 249. Available at: https://doi.org/10.3390/medicina55060249.

44. Cañete, J.D. and Mease, P. (2012) 'The link between obesity and psoriatic arthritis', *Annals of the Rheumatic Diseases*, 71(8), pp. 1265–1266. Available at: https://doi.org/10.1136/annrheumdis-2012-201632.

45. Cavill, R. *et al.* (2011) 'Consensus-phenotype integration of transcriptomic and metabolomic data implies a role for metabolism in the chemosensitivity of tumour cells', *PLOS Computational Biology*, 7(3), p. e1001113. Available at: https://doi.org/10.1371/journal.pcbi.1001113.

46. Cavill, R. *et al.* (2016) 'Transcriptomic and metabolomic data integration', *Briefings in Bioinformatics*. Available at: https://doi.org/10.1093/bib/bbv090.

47. Chalecka, M. *et al.* (2021) 'P5C as an interface of proline interconvertible amino acids and its role in regulation of cell survival and apoptosis', *International Journal of Molecular Sciences*, 22(21), p. 11763. Available at: https://doi.org/10.3390/ijms222111763.

48. Chan, T.C.K. and Howell, S.B. (1990) 'Role of hypoxanthine and thymidine in determining methotrexate plus dipyridamole cytotoxicity', *European Journal of Cancer and Clinical Oncology*, 26(8), pp. 907–911. Available at: https://doi.org/10.1016/0277-5379(90)90198-3.

49. Chandrasekharan, U.M. *et al.* (2018) 'Elevated levels of plasma symmetric dimethylarginine and increased arginase activity as potential indicators of cardiovascular comorbidity in rheumatoid arthritis', *Arthritis Research & Therapy*. Available at: https://doi.org/10.1186/s13075-018-1616-x.

50. Changsirivathanathamrong, D. *et al.* (2011) 'Tryptophan metabolism to kynurenine is a potential novel contributor to hypotension in human sepsis*', *Critical Care Medicine*. Available at: https://journals.lww.com/ccmjournal/Fulltext/2011/12000/Tryptophan_metabolism_to_kynurenine_is_a_potential.13.aspx.

51. Chaussabel, D., Pascual, V. and Banchereau, J. (2010) 'Assessing the human immune system through blood transcriptomics', *BMC Biology*, 8(1), p. 84. Available at: https://doi.org/10.1186/1741-7007-8-84.

52. Chen, L. *et al.* (2020) 'Skin and gut microbiome in psoriasis: gaining insight into the pathophysiology of it and finding novel therapeutic strategies', *Frontiers in Microbiology*, 11. Available at: https://www.frontiersin.org/articles/10.3389/fmicb.2020.589726 (Accessed: 30 March 2023).

53. Chen, L. *et al.* (2021) 'Metabolite discovery through global annotation of untargeted metabolomics data', *Nature methods*, 18(11), pp. 1377–1385. Available at: https://doi.org/10.1038/s41592-021-01303-3.

54. Chen, L. *et al.* (2022) 'Influence of the microbiome, diet and genetics on inter-individual variation in the human plasma metabolome', *Nature Medicine*, 28(11), pp. 2333–2343. Available at: https://doi.org/10.1038/s41591-022-02014-8.

55. Cheung, P. *et al.* (2019) 'Single-cell technologies — studying rheumatic diseases one cell at a time', *Nature Reviews Rheumatology*, 15(6), pp. 340–354. Available at: https://doi.org/10.1038/s41584-019-0220-z.

56. Chicco, D. and Agapito, G. (2022) 'Nine quick tips for pathway enrichment analysis', *PLOS Computational Biology*, 18(8), p. e1010348. Available at: https://doi.org/10.1371/journal.pcbi.1010348.

57. Chicco, D. and Jurman, G. (2020) 'The advantages of the Matthews correlation coefficient (MCC) over F1 score and accuracy in binary classification evaluation', *BMC Genomics*. Available at: https://doi.org/10.1186/s12864-019-6413-7.

58. Choe, C. *et al.* (2013) 'Homoarginine levels are regulated by L-arginine:glycine amidinotransferase and affect stroke outcome: results from human and murine studies', *Circulation*, 128(13), pp. 1451–1461. Available at: https://doi.org/10.1161/CIRCULATIONAHA.112.000580.

59. Chong, J., Wishart, D.S. and Xia, J. (2019) 'Using MetaboAnalyst 4.0 for comprehensive and integrative metabolomics data analysis', *Current Protocols in Bioinformatics*. Available at: https://doi.org/10.1002/cpbi.86.

60. Coates, L.C. *et al.* (2020) 'Comparison of remission and low disease activity states with DAPSA, MDA and VLDA in a clinical trial setting in psoriatic arthritis patients: 2-year results from the FUTURE 2 study', *Seminars in Arthritis and Rheumatism*, 50(4), pp. 709–718. Available at: https://doi.org/10.1016/j.semarthrit.2020.03.015.

61. Coates, L.C. *et al.* (2022) 'Group for Research and Assessment of Psoriasis and Psoriatic Arthritis (GRAPPA): updated treatment recommendations for psoriatic arthritis 2021', *Nature Reviews Rheumatology*, 18(8), pp. 465–479. Available at: https://doi.org/10.1038/s41584-022-00798-0.

62. Coates, L.C., Fransen, J. and Helliwell, P.S. (2010) 'Defining minimal disease activity in psoriatic arthritis: a proposed objective target for treatment', *Annals of the Rheumatic Diseases*, 69(1), pp. 48–53. Available at: https://doi.org/10.1136/ard.2008.102053.

63. Coates, L.C. and Helliwell, P.S. (2016) 'Defining low disease activity states in psoriatic arthritis using novel composite disease instruments', *The Journal of Rheumatology*, 43(2), pp. 371–375. Available at: https://doi.org/10.3899/jrheum.150826.

64. Coates, L.C. and Helliwell, P.S. (2017) 'Psoriatic arthritis: state of the art review', *Clinical Medicine*, 17(1), pp. 65–70. Available at: https://doi.org/10.7861/clinmedicine.17-1-65.

65. Colebatch, A.N. *et al.* (2013) 'EULAR recommendations for the use of imaging of the joints in the clinical management of rheumatoid arthritis', *Annals of the Rheumatic Diseases*. Available at: https://doi.org/10.1136/annrheumdis-2012-203158.

66. Conaghan, P.G. *et al.* (2020) 'Relationship of pain and fatigue with health-related quality of life and work in patients with psoriatic arthritis on TNFi: results of a multi-national real-world study', *RMD Open*, 6(2), p. e001240. Available at: https://doi.org/10.1136/rmdopen-2020-001240.

67. Cook, T., Ma, Y. and Gamagedara, S. (2020) 'Evaluation of statistical techniques to normalize mass spectrometry-based urinary metabolomics data', *Journal of pharmaceutical and biomedical analysis*. 2019/09/03 edn, 177, pp. 112854–112854. Available at: https://doi.org/10.1016/j.jpba.2019.112854.

68. Cooles, F.A.H. *et al.* (2022) 'Interferon-α-mediated therapeutic resistance in early rheumatoid arthritis implicates epigenetic reprogramming', *Annals of the Rheumatic Diseases*, 81(9), pp. 1214–1223. Available at: https://doi.org/10.1136/annrheumdis-2022-222370.

69. Creek, D.J. *et al.* (2012) 'IDEOM: an Excel interface for analysis of LC–MS-based metabolomics data', *Bioinformatics*. Available at: https://doi.org/10.1093/bioinformatics/bts069.

70. Cronstein, B.N. and Aune, T.M. (2020) 'Methotrexate and its mechanisms of action in inflammatory arthritis', *Nature Reviews Rheumatology*. Available at: https://doi.org/10.1038/s41584-020-0373-9.

71. Cronstein, B.N. and Sitkovsky, M. (2017) 'Adenosine and adenosine receptors in the pathogenesis and treatment of rheumatic diseases', *Nature Reviews Rheumatology*. Available at: https://doi.org/10.1038/nrrheum.2016.178.

72. Cua, D.J. and Tato, C.M. (2010) 'Innate IL-17-producing cells: the sentinels of the immune system', *Nature Reviews Immunology*, 10(7), pp. 479–489. Available at: https://doi.org/10.1038/nri2800.

73. Culemann, S. *et al.* (2019) 'Locally renewing resident synovial macrophages provide a protective barrier for the joint', *Nature*, 572(7771), pp. 670–675. Available at: https://doi.org/10.1038/s41586-019-1471-1.

74. Cunnane, G. *et al.* (2000) 'Serum amyloid A in the assessment of early inflammatory arthritis', *The Journal of Rheumatology*, 27(1), pp. 58–63.

75. Cuppen, B.V.J. *et al.* (2016) 'Exploring the inflammatory metabolomic profile to predict response to TNF-α inhibitors in rheumatoid arthritis', *PLOS ONE*.

76. Cussotto, S. *et al.* (2020) 'Tryptophan metabolic pathways are altered in obesity and are associated with systemic inflammation', *Frontiers in Immunology*, 11, p. 557. Available at: https://doi.org/10.3389/fimmu.2020.00557.

77. Dale, J. *et al.* (2014) 'Tightening up? Impact of musculoskeletal ultrasound disease activity assessment on early rheumatoid arthritis patients treated using a treat to target strategy', *Arthritis Care & Research*, 66(1), pp. 19–26. Available at: https://doi.org/10.1002/acr.22218.

78. Dale, J. *et al.* (2016) 'Targeting ultrasound remission in early rheumatoid arthritis: the results of the TaSER study, a randomised clinical trial', *Annals of the Rheumatic Diseases*. Available at: https://doi.org/10.1136/annrheumdis-2015-208941.

79. Dale, J.E. (2014) *Tailoring therapy to individual patient's needs: intensive management of early rheumatoid arthritis using either clinical, laboratory or musculoskeletal ultrasound assessment of disease activity*. University of Glasgow. Available at: http://theses.gla.ac.uk/id/eprint/4991.

80. Daly, R. *et al.* (2020) 'Changes in plasma itaconate elevation in early rheumatoid arthritis patients elucidates disease activity associated macrophage activation', *Metabolites*. Available at: https://doi.org/10.3390/metabo10060241.

81. Davids, M. *et al.* (2012) 'Promiscuous activity of arginine:glycine amidinotransferase is responsible for the synthesis of the novel cardiovascular risk factor homoarginine', *FEBS Letters*, 586(20), pp. 3653–3657. Available at: https://doi.org/10.1016/j.febslet.2012.08.020.

82. Deane, K.D. *et al.* (2017) 'Genetic and environmental risk factors for rheumatoid arthritis', *Best practice & research. Clinical rheumatology*. Available at: https://doi.org/10.1016/j.berh.2017.08.003.

83. Dervieux, T. *et al.* (2006) 'Pharmacogenetic and metabolite measurements are associated with clinical status in patients with rheumatoid arthritis treated with methotrexate: results of a multicentred cross sectional observational study'.

84. Dodd, D. *et al.* (2017) 'A gut bacterial pathway metabolizes aromatic amino acids into nine circulating metabolites', *Nature*. 2017/11/22 edn, 551(7682), pp. 648–652. Available at: https://doi.org/10.1038/nature24661.

85. Domínguez-Andrés, J. *et al.* (2019) 'The itaconate pathway is a central regulatory node linking innate immune tolerance and trained immunity', *Cell Metabolism*. Available at: https://doi.org/10.1016/j.cmet.2018.09.003.

86. Drozdzik, M. *et al.* (2007) 'Reduced folate carrier-1 80G>A polymorphism affects methotrexate treatment outcome in rheumatoid arthritis', *The Pharmacogenomics Journal*, 7(6), pp. 404–407. Available at: https://doi.org/10.1038/sj.tpj.6500438.

87. Dudoit, S. *et al.* (2002) 'Statistical methods for identifying differentially expressed genes in replicated cDNA microarray experiments', *Statistica Sinica*, 12(1), pp. 111–139.

88. Dures, E. *et al.* (2020) 'Treat-to-target in PsA: methods and necessity', *RMD Open*, 6(1), p. e001083. Available at: https://doi.org/10.1136/rmdopen-2019-001083.

89. Durfee, L.A. *et al.* (2010) 'The ISG15 conjugation system broadly targets newly synthesized proteins: implications for the antiviral function of ISG15', *Molecular Cell*, 38(5), pp. 722–732. Available at: https://doi.org/10.1016/j.molcel.2010.05.002.

90. Ebbels, T.M.D. *et al.* (2023) 'Recent advances in mass spectrometry-based computational metabolomics', *Current Opinion in Chemical Biology*, 74, p. 102288. Available at: https://doi.org/10.1016/j.cbpa.2023.102288.

91. Edison, E.E. *et al.* (2007) 'Creatine synthesis: production of guanidinoacetate by the rat and human kidney in vivo', *American Journal of Physiology. Renal Physiology*, 293(6), pp. F1799-1804. Available at: https://doi.org/10.1152/ajprenal.00356.2007.

92. Ejbjerg, B.J. *et al.* (2006) 'Conventional radiography requires a MRI-estimated bone volume loss of 20% to 30% to allow certain detection of bone erosions in rheumatoid arthritis metacarpophalangeal joints', *Arthritis research & therapy*. Available at: https://doi.org/10.1186/ar1919.

93. Ejigu, B.A. *et al.* (2013) 'Evaluation of normalization methods to pave the way towards large-scale LC-MS-based metabolomics profiling experiments', *OMICS : a Journal of Integrative Biology*, 17(9), pp. 473–485. Available at: https://doi.org/10.1089/omi.2013.0010.

94. Elango, T. *et al.* (2014) 'Impact of methotrexate on oxidative stress and apoptosis markers in psoriatic patients', *Clinical and Experimental Medicine*, 14(4), pp. 431–437. Available at: https://doi.org/10.1007/s10238-013-0252-7.

95. Emery, P. *et al.* (2002) 'Early referral recommendation for newly diagnosed rheumatoid arthritis: evidence based development of a clinical guide', *Annals of the Rheumatic Diseases*. Available at: https://doi.org/10.1136/ard.61.4.290.

96. England, B.R. *et al.* (2019) '2019 Update of the American College of Rheumatology Recommended Rheumatoid Arthritis Disease Activity Measures', *Arthritis Care & Research*. Available at: https://doi.org/10.1002/acr.24042.

97. Faller, K.M.E. *et al.* (2018) 'Impaired cardiac contractile function in arginine:glycine amidinotransferase knockout mice devoid of creatine is rescued by homoarginine but not creatine', *Cardiovascular Research*, 114(3), pp. 417–430. Available at: https://doi.org/10.1093/cvr/cvx242.

98. Fan, Y. *et al.* (2022) 'Integrated multi-omics analysis model to identify biomarkers associated with prognosis of breast cancer', *Frontiers in Oncology*, 12. Available at: https://www.frontiersin.org/articles/10.3389/fonc.2022.899900 (Accessed: 4 May 2023).

99. Felson, D.T. *et al.* (2021) 'Reexamining Remission Definitions in Rheumatoid Arthritis: Considering Disease Activity Score in 28 Joints, C-Reactive Protein, and Patient Global Assessment', *ACR Open Rheumatology*, 4(2), pp. 123–127. Available at: https://doi.org/10.1002/acr2.11345.

100. Feuerman, E.J. and Nir, M.A. (1973) 'Allopurinol in psoriasis–a double-blind study', *British Journal of Dermatology*, 89(1), p. 83. Available at: https://doi.org/10.1111/j.1365-2133.1973.tb01921.x.

101. Fiehn, O. *et al.* (2007) 'The metabolomics standards initiative (MSI)', *Metabolomics*, 3(3), pp. 175–178. Available at: https://doi.org/10.1007/s11306-007-0070-6.

102. Finckh, A. *et al.* (2022) 'Global epidemiology of rheumatoid arthritis', *Nature Reviews Rheumatology*, 18(10), pp. 591–602. Available at: https://doi.org/10.1038/s41584-022-00827-y.

103. FitzGerald, O. *et al.* (2021) 'Psoriatic arthritis', *Nature Reviews Disease Primers*, 7(1), pp. 1–17. Available at: https://doi.org/10.1038/s41572-021-00293-y.

104. Flach, P.A. and Kull, M. (2015) 'Precision-Recall-Gain Curves: PR Analysis Done Right', in *Proceedings of the 28th International Conference on Neural Information Processing Systems - Volume 1*. Cambridge, MA, USA: MIT Press (NIPS'15), pp. 838–846.

105. Folkersen, L. *et al.* (2016) 'Integration of known DNA, RNA and protein biomarkers provides prediction of anti-TNF response in rheumatoid arthritis: results from the COMBINE study', *Molecular medicine (Cambridge, Mass.)*. 2016/08/15 edn, 22, pp. 322–328. Available at: https://doi.org/10.2119/molmed.2016.00078.

106. Fraga, N.A. de A. *et al.* (2012) 'Psoriasis and uveitis: a literature review', *Anais brasileiros de dermatologia*, 87(6), pp. 877–883. Available at: https://doi.org/10.1590/S0365-05962012000600009.

107. Fransen, J. and van Riel, P.L.C.M. (2005) 'The Disease Activity Score and the EULAR response criteria', *Clinical and Experimental Rheumatology*, 23(5 Suppl 39), pp. S93-99.

108. Friedman, B. and Cronstein, B. (2019) 'Methotrexate mechanism in treatment of rheumatoid arthritis', *Joint, bone, spine : revue du rhumatisme*, 86(3), pp. 301–307. Available at: https://doi.org/10.1016/j.jbspin.2018.07.004.

109. Gabay, C. *et al.* (2001) 'Leptin directly induces the secretion of interleukin 1 receptor antagonist in human monocytes1', *The Journal of Clinical Endocrinology & Metabolism*, 86(2), pp. 783–791. Available at: https://doi.org/10.1210/jcem.86.2.7245.

110. Ge, S.X., Jung, D. and Yao, R. (2020) 'ShinyGO: a graphical gene-set enrichment tool for animals and plants', *Bioinformatics*, 36(8), pp. 2628–2629. Available at: https://doi.org/10.1093/bioinformatics/btz931.

111. Ge, T. *et al.* (2020) 'The role of the pentose phosphate pathway in diabetes and cancer', *Frontiers in Endocrinology*. Available at: https://doi.org/10.3389/fendo.2020.00365.

112. van Gestel, A.M. *et al.* (1996) 'Development and validation of the european league against rheumatism response criteria for rheumatoid arthritis: Comparison with the preliminary american college of rheumatology and the world health

organization/international league against rheumatism criteria', *Arthritis & Rheumatism*. Available at: https://doi.org/doi:10.1002/art.1780390105.

113. Gibson, D.S. *et al.* (2012) 'Biomarkers in rheumatology, now and in the future', *Rheumatology*, 51(3), pp. 423–433. Available at: https://doi.org/10.1093/rheumatology/ker358.

114. Goldman, M. (1981) 'Uric acid in the etiology of psoriasis', *The American Journal of Dermatopathology*, 3(4), pp. 397–404. Available at: https://doi.org/10.1097/00000372-198100340-00014.

115. Gomez-Cabrero, D. *et al.* (2014) 'Data integration in the era of omics: current and future challenges', *BMC Systems Biology*, 8(2), p. I1. Available at: https://doi.org/10.1186/1752-0509-8-S2-I1.

116. Gossec, L. *et al.* (2016) 'European League Against Rheumatism (EULAR) recommendations for the management of psoriatic arthritis with pharmacological therapies: 2015 update', *Annals of the Rheumatic Diseases*, 75(3), pp. 499–510. Available at: https://doi.org/10.1136/annrheumdis-2015-208337.

117. Gossec, L. *et al.* (2020) 'EULAR recommendations for the management of psoriatic arthritis with pharmacological therapies: 2019 update', *Annals of the Rheumatic Diseases*, 79(6), pp. 700–712. Available at: https://doi.org/10.1136/annrheumdis-2020-217159.

118. Gosselt, H.R. *et al.* (2020) 'Identification of metabolic biomarkers in relation to methotrexate response in early rheumatoid arthritis', *Journal of Personalized Medicine*. Available at: https://doi.org/10.3390/jpm10040271.

119. Gosselt, H.R. *et al.* (2021) 'Complex machine-learning algorithms and multivariable logistic regression on par in the prediction of insufficient clinical response to methotrexate in rheumatoid arthritis', *Journal of personalized medicine*. Available at: https://doi.org/10.3390/jpm11010044.

120. Gota, C. and Calabrese, L. (2003) 'Induction of clinical autoimmune disease by therapeutic interferon-α', *Autoimmunity*, 36(8), pp. 511–518. Available at: https://doi.org/10.1080/08916930310001605873.

121. Gowda, G.A.N. and Djukovic, D. (2014) 'Overview of mass spectrometry-based metabolomics: opportunities and challenges', *Methods in molecular biology (Clifton, N.J.)*, 1198, pp. 3–12. Available at: https://doi.org/10.1007/978-1-4939-1258-2_1.

122. Grace, S. and Hudson, D. (2016) 'Processing and visualization of metabolomics data Using R'. Available at: https://doi.org/10.5772/65405.

123. Greenwell, B.M., Boehmke, B.C. and McCarthy, A.J. (2018) 'A simple and effective model-based variable importance measure'. arXiv. Available at: http://arxiv.org/abs/1805.04755 (Accessed: 22 November 2022).

124. Grenier, J.M. *et al.* (2002) 'Functional screening of five PYPAF family members identifies PYPAF5 as a novel regulator of NF-κB and caspase-1', *FEBS Letters*, 530(1–3), pp. 73–78. Available at: https://doi.org/10.1016/S0014-5793(02)03416-6.

125. Grissa, D. *et al.* (2016) 'Feature selection methods for early predictive biomarker discovery using untargeted metabolomic data', *Frontiers in molecular biosciences*. Available at: https://doi.org/10.3389/fmolb.2016.00030.

126. Gupta, S. *et al.* (2021) 'Comorbidities in psoriatic arthritis: a systematic review and meta-analysis', *Rheumatology International*, 41(2), pp. 275–284. Available at: https://doi.org/10.1007/s00296-020-04775-2.

127. Gupta, V.K. *et al.* (2021) 'Gut microbial determinants of clinically important improvement in patients with rheumatoid arthritis', *Genome Medicine*, 13, p. 149. Available at: https://doi.org/10.1186/s13073-021-00957-0.

128. Gustafsson, A. *et al.* (2020) 'Effect of IFN-γ on the kynurenine/tryptophan ratio in monolayer-cultured keratinocytes and a 3D reconstructed human epidermis model', *Journal of Dermatological Science*, 99(3), pp. 177–184. Available at: https://doi.org/10.1016/j.jdermsci.2020.07.005.

129. Guyon, I. *et al.* (2002) 'Gene selection for cancer classification using support vector machines', *Machine Learning*. Available at: https://doi.org/10.1023/A:1012487302797.

130. Halilova, K.I. *et al.* (2012) 'Markers of treatment response to methotrexate in rheumatoid arthritis: where do we stand?', *International journal of rheumatology*. Available at: https://doi.org/10.1155/2012/978396.

131. van Halm, V.P. *et al.* (2009) 'Rheumatoid arthritis versus diabetes as a risk factor for cardiovascular disease: a cross-sectional study, the CARRÉ Investigation', *Annals of the Rheumatic Diseases*, 68(9), p. 1395. Available at: https://doi.org/10.1136/ard.2008.094151.

132. Han, S. *et al.* (2021) 'A metabolomics pipeline for the mechanistic interrogation of the gut microbiome', *Nature*, 595(7867), pp. 415–420. Available at: https://doi.org/10.1038/s41586-021-03707-9.

133. Hanff, E. *et al.* (2019) 'High plasma guanidinoacetate-to-homoarginine ratio is associated with high all-cause and cardiovascular mortality rate in adult renal transplant recipients', *Amino Acids*, 51(10–12), pp. 1485–1499. Available at: https://doi.org/10.1007/s00726-019-02783-6.

134. Hao, L. *et al.* (2018) 'Comparative evaluation of MS-based metabolomics software and its application to preclinical Alzheimer's Disease', *Scientific Reports*, 8(1), p. 9291. Available at: https://doi.org/10.1038/s41598-018-27031-x.

135. Hasin, Y., Seldin, M. and Lusis, A. (2017) 'Multi-omics approaches to disease', *Genome Biology*, 18(1), p. 83. Available at: https://doi.org/10.1186/s13059-017-1215-1.

136. Haskó, G. *et al.* (2000) 'Adenosine inhibits IL-12 and TNF-α production via adenosine A(2a) receptor-dependent and independent mechanism', *FASEB Journal*, 14(13), pp. 2065–2074. Available at: https://doi.org/10.1096/fj.99-0508com.

137. Haskó, G. *et al.* (2008) 'Adenosine receptors: therapeutic aspects for inflammatory and immune diseases', *Nature reviews. Drug discovery*. Available at: https://doi.org/10.1038/nrd2638.

138. Hastie, T., Tibshirani, R. and Friedman, J. (2016) *The elements of statistical learning: data mining, inference, and prediction, second edition*. 2nd edition. New York, NY: Springer.

139. He, G. *et al.* (2022) 'Discovery of the first selective IDO2 inhibitor as novel immunotherapeutic avenues for rheumatoid arthritis', *Journal of Medicinal Chemistry*, 65(21), pp. 14348–14365. Available at: https://doi.org/10.1021/acs.jmedchem.2c00263.

140. He, J. *et al.* (2022) 'Intestinal butyrate-metabolizing species contribute to autoantibody production and bone erosion in rheumatoid arthritis', *Science Advances*, 8(6), p. eabm1511. Available at: https://doi.org/10.1126/sciadv.abm1511.

141. Helliwell, P.S. *et al.* (2020) 'Composite measures of disease activity in psoriatic arthritis: comparative instrument performance based on the efficacy of guselkumab in an interventional phase II trial', *Arthritis Care & Research*, 72(11), pp. 1579–1588. Available at: https://doi.org/10.1002/acr.24046.

142. Helliwell, P.S. and Taylor, W.J. (2005) 'Classification and diagnostic criteria for psoriatic arthritis', *Annals of the Rheumatic Diseases*, 64(suppl 2), pp. ii3–ii8. Available at: https://doi.org/10.1136/ard.2004.032318.

143. Henry, L. and Wickham, H. (2020) 'purrr: functional programming tools'. Available at: https://CRAN.R-project.org/package=purrr.

144. Heutz, J. and Jong, P.H.P. de (2021) 'Possibilities for personalised medicine in rheumatoid arthritis: hype or hope', *RMD Open*, 7(3), p. e001653. Available at: https://doi.org/10.1136/rmdopen-2021-001653.

145. Hirabayashi, Y. and Ishii, T. (2013) 'The DAS28-ESR cutoff value necessary to achieve remission under the new Boolean-based remission criteria in patients receiving tocilizumab', *Clinical Rheumatology*, 32(1), pp. 123–127. Available at: https://doi.org/10.1007/s10067-012-2103-4.

146. Ho, A. *et al.* (2019) 'Circulating glucuronic acid predicts healthspan and longevity in humans and mice', *Aging (Albany NY)*, 11(18), pp. 7694–7706. Available at: https://doi.org/10.18632/aging.102281.

147. Hodkinson, B., Tikly, M. and Adebajo, A. (2014) 'Rheumatoid arthritis in the developing world: stepping up to the challenge', *Clinical Rheumatology*, 33(9), pp. 1195–1196. Available at: https://doi.org/10.1007/s10067-014-2690-3.

148. Hoffman, G.E. and Schadt, E.E. (2016) 'variancePartition: interpreting drivers of variation in complex gene expression studies', *BMC Bioinformatics*. Available at: https://doi.org/10.1186/s12859-016-1323-z.

149. Hoffmeister, R.T. (1972) 'Methotrexate in rheumatoid arthritis', in *Arthritis and Rheumatism*. WILEY-BLACKWELL 111 RIVER ST, HOBOKEN 07030-5774, NJ USA, pp. 114-+.

150. Holman, J.D., Tabb, D.L. and Mallick, P. (2014) 'Employing ProteoWizard to Convert Raw Mass Spectrometry Data.', *Current protocols in bioinformatics*, 46, p. 13.24.1–9. Available at: https://doi.org/10.1002/0471250953.bi1324s46.

151. Honda, K. and Taniguchi, T. (2006) 'IRFs: master regulators of signalling by Toll-like receptors and cytosolic pattern-recognition receptors', *Nature Reviews Immunology*, 6(9), pp. 644–658. Available at: https://doi.org/10.1038/nri1900.

152. Hooftman, A. and O'Neill, L.A.J. (2019) 'The immunomodulatory potential of the metabolite itaconate', *Trends in Immunology*. Available at: https://doi.org/10.1016/j.it.2019.05.007.

153. Houttekiet, C. *et al.* (2022) 'Systematic review of the use of CRP in clinical trials for psoriatic arthritis: a concern for clinical practice?', *RMD Open*, 8(1), p. e001756. Available at: https://doi.org/10.1136/rmdopen-2021-001756.

154. Huang, L. *et al.* (2019) 'Dysbiosis of gut microbiota was closely associated with psoriasis', *Science China. Life Sciences*, 62(6), pp. 807–815. Available at: https://doi.org/10.1007/s11427-018-9376-6.

155. Hur, B. *et al.* (2021) 'Plasma metabolomic profiling in patients with rheumatoid arthritis identifies biochemical features predictive of quantitative disease activity', *Arthritis Research & Therapy*. Available at: https://doi.org/10.1186/s13075-021-02537-4.

156. Hwang, J. *et al.* (2021) 'The role of leptin in the association between obesity and psoriasis', *Biomolecules & Therapeutics*, 29(1), pp. 11–21. Available at: https://doi.org/10.4062/biomolther.2020.054.

157. Hwang, S.-Y. *et al.* (2004) 'IL-17 induces production of IL-6 and IL-8 in rheumatoid arthritis synovial fibroblasts via NF-κB- and PI3-kinase/Akt-dependent pathways', *Arthritis Res Ther*, 6(2), p. R120. Available at: https://doi.org/10.1186/ar1038.

158. Janke, K. *et al.* (2022) 'A systematic comparison of different composite measures (DAS 28, CDAI, SDAI, and Boolean approach) for determining treatment effects on low disease activity and remission in rheumatoid arthritis', *BMC Rheumatology*, 6, p. 82. Available at: https://doi.org/10.1186/s41927-022-00314-7.

159. Jerram, S. *et al.* (2008) 'Discrepancies between the EULAR response criteria and the NICE guidelines for continuation of anti-TNF therapy in RA: a cause for concern?',

Rheumatology, 47(2), pp. 180–182. Available at: https://doi.org/10.1093/rheumatology/kem331.

160. Jewison, T. *et al.* (2014) 'SMPDB 2.0: big improvements to the Small Molecule Pathway Database', *Nucleic Acids Research*, 42(Database issue), pp. D478-484. Available at: https://doi.org/10.1093/nar/gkt1067.

161. Jha, A.K. *et al.* (2015) 'Network integration of parallel metabolic and transcriptional data reveals metabolic modules that regulate macrophage polarization', *Immunity*. Available at: https://doi.org/10.1016/j.immuni.2015.02.005.

162. Jiang, F. *et al.* (2020) 'IRF9 affects the TNF-induced phenotype of rheumatoid-arthritis fibroblast-like synoviocytes via regulation of the SIRT-1/NF-κB signaling pathway', *Cells, Tissues, Organs*, 209(2–3), pp. 110–119. Available at: https://doi.org/10.1159/000508405.

163. Jin, S. *et al.* (2017) 'Tetherin suppresses type I interferon signaling by targeting MAVS for NDP52-mediated selective autophagic degradation in human cells', *Molecular Cell*, 68(2), pp. 308-322.e4. Available at: https://doi.org/10.1016/j.molcel.2017.09.005.

164. Johansen, C. *et al.* (2010) 'Preferential inhibition of the mRNA expression of p38 mitogen-activated protein kinase regulated cytokines in psoriatic skin by anti-TNFα therapy', *British Journal of Dermatology*, 163(6), pp. 1194–1204. Available at: https://doi.org/10.1111/j.1365-2133.2010.10036.x.

165. John, C.R. (2021) 'MLeval: machine learning model evaluation'.

166. Johnston, A. *et al.* (2013) 'Keratinocyte overexpression of IL-17C promotes psoriasiform skin inflammation', *The Journal of Immunology*, 190(5), pp. 2252–2262. Available at: https://doi.org/10.4049/jimmunol.1201505.

167. de Jong, P.H. *et al.* (2014) 'Randomised comparison of initial triple DMARD therapy with methotrexate monotherapy in combination with low-dose glucocorticoid bridging therapy; 1-year data of the tREACH trial', *Annals of the rheumatic diseases*. Available at: https://doi.org/10.1136/annrheumdis-2013-204788.

168. Kaiser, H., Parker, E. and Hamrick, M.W. (2020) 'Kynurenine signaling through the aryl hydrocarbon receptor: Implications for aging and healthspan', *Experimental Gerontology*, 130, p. 110797. Available at: https://doi.org/10.1016/j.exger.2019.110797.

169. Kanehisa, M. and Goto, S. (2000) 'KEGG: kyoto encyclopedia of genes and genomes', *Nucleic acids research*. Available at: https://doi.org/10.1093/nar/28.1.27.

170. Kanehisa, M.A.-O.X. and Sato, Y. (2020) 'KEGG Mapper for inferring cellular functions from protein sequences'.

171. Kapoor, S.R. *et al.* (2013) 'Metabolic Profiling Predicts Response to Anti–Tumor Necrosis Factor α Therapy in Patients With Rheumatoid Arthritis', *Arthritis & Rheumatism*. Available at: https://doi.org/10.1002/art.37921.

172. Karpievitch, Y.V., Dabney, A.R. and Smith, R.D. (2012) 'Normalization and missing value imputation for label-free LC-MS analysis', *BMC Bioinformatics*, 13(16), p. S5. Available at: https://doi.org/10.1186/1471-2105-13-S16-S5.

173. Kasperkovitz, P. *et al.* (2004) 'Activation of the STAT1 pathway in rheumatoid arthritis', *Annals of the Rheumatic Diseases*, 63(3), pp. 233–239. Available at: https://doi.org/10.1136/ard.2003.013276.

174. Kay, J. *et al.* (2014) 'Clinical disease activity and acute phase reactant levels are discordant among patients with active rheumatoid arthritis: acute phase reactant levels contribute separately to predicting outcome at one year', *Arthritis Research & Therapy*, 16(1), p. R40. Available at: https://doi.org/10.1186/ar4469.

175. Kelly, D., Delday, M.I. and Mulder, I. (2012) 'Microbes and microbial effector molecules in treatment of inflammatory disorders', *Immunological Reviews*, 245(1), pp. 27–44. Available at: https://doi.org/10.1111/j.1600-065X.2011.01079.x.

176. Kerrigan, S.A. and McInnes, I.B. (2020) 'Reflections on "older" drugs: learning new lessons in rheumatology', *Nature Reviews Rheumatology*. Available at: https://doi.org/10.1038/s41584-020-0375-7.

177. Kgoebane, K. *et al.* (2018) 'The role of imaging in rheumatoid arthritis', *SA Journal of Radiology*, 22(1), p. 1316. Available at: https://doi.org/10.4102/sajr.v22i1.1316.

178. Kim, J.-H. (2009) 'Estimating classification error rate: Repeated cross-validation, repeated hold-out and bootstrap', *Computational Statistics & Data Analysis*, 53(11), pp. 3735–3745. Available at: https://doi.org/10.1016/j.csda.2009.04.009.

179. Kor, A. *et al.* (2022) 'Clinical significance of plasma tryptophan, kynurenine, and kynurenine/tryptophan ratio in rheumatoid arthritis patients', *The Egyptian Rheumatologist*, 44(4), pp. 367–371. Available at: https://doi.org/10.1016/j.ejr.2022.07.005.

180. Kotake, S. *et al.* (1999) 'IL-17 in synovial fluids from patients with rheumatoid arthritis is a potent stimulator of osteoclastogenesis', *The Journal of Clinical Investigation*, 103(9), pp. 1345–1352. Available at: https://doi.org/10.1172/JCI5703.

181. Krishnan, S. *et al.* (2018) 'Gut microbiota-derived tryptophan metabolites modulate inflammatory response in hepatocytes and macrophages', *Cell Reports*, 23(4), pp. 1099–1111. Available at: https://doi.org/10.1016/j.celrep.2018.03.109.

182. Kuhn, M. (2019) 'The caret Package'.

183. Kuhn, M. and Wickham, H. (2020) 'Tidymodels: a collection of packages for modeling and machine learning using tidyverse principles'. Available at: https://www.tidymodels.org.

184. Kurowska-Stolarska, M. and Alivernini, S. (2022) 'Synovial tissue macrophages in joint homeostasis, rheumatoid arthritis and disease remission', *Nature Reviews Rheumatology*, 18(7), pp. 384–397. Available at: https://doi.org/10.1038/s41584-022-00790-8.

185. Lampropoulou, V. *et al.* (2016) 'Itaconate links inhibition of succinate dehydrogenase with macrophage metabolic remodeling and regulation of inflammation', *Cell metabolism*. Available at: https://doi.org/10.1016/j.cmet.2016.06.004.

186. Langley, R.G. *et al.* (2014) 'Secukinumab in plaque psoriasis--results of two phase 3 trials', *The New England Journal of Medicine*, 371(4), pp. 326–338. Available at: https://doi.org/10.1056/NEJMoa1314258.

187. Lanser, L. *et al.* (2020) 'Inflammation-induced tryptophan breakdown is related with anemia, fatigue, and depression in cancer', *Frontiers in Immunology*. Available at: https://doi.org/10.3389/fimmu.2020.00249.

188. Lappas, C.M., Rieger, J.M. and Linden, J. (2005) 'A2A adenosine receptor induction inhibits IFN-γ production in murine CD4+ T cells1', *The Journal of Immunology*, 174(2), pp. 1073–1080. Available at: https://doi.org/10.4049/jimmunol.174.2.1073.

189. Lebwohl, M. *et al.* (2015) 'Phase 3 studies comparing brodalumab with ustekinumab in psoriasis', *New England Journal of Medicine*, 373(14), pp. 1318–1328. Available at: https://doi.org/10.1056/NEJMoa1503824.

190. Lee, B. *et al.* (2022) 'Medulloblastoma cerebrospinal fluid reveals metabolites and lipids indicative of hypoxia and cancer-specific RNAs', *Acta Neuropathologica Communications*, 10(1), p. 25. Available at: https://doi.org/10.1186/s40478-022-01326-7.

191. Lewis, D.D. (1998) 'Naive (Bayes) at forty: The independence assumption in information retrieval', in C. Nédellec and C. Rouveirol (eds) *Machine Learning: ECML-98*. Berlin, Heidelberg: Springer (Lecture Notes in Computer Science), pp. 4–15. Available at: https://doi.org/10.1007/BFb0026666.

192. Li, B. *et al.* (2016) 'Performance evaluation and online realization of data-driven normalization methods used in LC/MS based untargeted metabolomics analysis', *Scientific Reports*. Available at: https://doi.org/10.1038/srep38881.

193. Li, X. *et al.* (2021) 'New insights into gut-bacteria-derived indole and its derivatives in intestinal and liver diseases', *Frontiers in Pharmacology*, 12. Available at: https://www.frontiersin.org/articles/10.3389/fphar.2021.769501 (Accessed: 8 February 2023).

194. Ling, S., Bluett, J. and Barton, A. (2018) 'Prediction of response to methotrexate in rheumatoid arthritis', *Expert Review of Clinical Immunology*. Available at: https://doi.org/10.1080/1744666X.2018.1465409.

195. Lionetto, L. *et al.* (2021) 'Increased kynurenine-to-tryptophan ratio in the serum of patients infected with SARS-CoV2: An observational cohort study.', *Biochimica et Biophysica Acta (BBA) - Molecular Basis of Disease*, 1867(3), p. 166042. Available at: https://doi.org/10.1016/j.bbadis.2020.166042.

196. Liu, M. *et al.* (2018) 'Targeting the IDO1 pathway in cancer: from bench to bedside', *Journal of Hematology & Oncology*, 11(1), p. 100. Available at: https://doi.org/10.1186/s13045-018-0644-y.

197. Lu, W. *et al.* (2017) 'Metabolite measurement: pitfalls to avoid and practices to follow', *Annual review of biochemistry*. Available at: https://doi.org/10.1146/annurev-biochem-061516-044952.

198. Luis-Rodríguez, D. *et al.* (2021) 'Serum urate is related to subclinical inflammation in asymptomatic hyperuricaemia', *Rheumatology (Oxford, England)*, 60(1), pp. 371–379. Available at: https://doi.org/10.1093/rheumatology/keaa425.

199. Luque-Garcia, J.L. and Neubert, T.A. (2007) 'Sample preparation for serum/plasma profiling and biomarker identification by mass spectrometry', *Journal of Chromatography. a*, 1153(1), pp. 259–276. Available at: https://doi.org/10.1016/j.chroma.2006.11.054.

200. Lynde, C.W. *et al.* (2014) 'Interleukin 17A: toward a new understanding of psoriasis pathogenesis', *Journal of the American Academy of Dermatology*, 71(1), pp. 141–150. Available at: https://doi.org/10.1016/j.jaad.2013.12.036.

201. Maciejewski, M. *et al.* (2021) 'Prediction of response of methotrexate in patients with rheumatoid arthritis using serum lipidomics', *Scientific Reports*. Available at: https://doi.org/10.1038/s41598-021-86729-7.

202. Maillefert, J.F. *et al.* (2010) 'Prediction of response to disease modifying antirheumatic drugs in rheumatoid arthritis'.

203. Martinon, F., Burns, K. and Tschopp, J. (2002) 'The inflammasome: a molecular platform triggering activation of inflammatory caspases and processing of proIL-beta', *Molecular Cell*, 10(2), pp. 417–426. Available at: https://doi.org/10.1016/s1097-2765(02)00599-3.

204. Mathai, A.J. *et al.* (2016) 'Blood levels of monoamine precursors and smoking in patients with schizophrenia', *Frontiers in Public Health*, 4. Available at: https://www.frontiersin.org/articles/10.3389/fpubh.2016.00182 (Accessed: 7 February 2023).

205. Mc Ardle, A. *et al.* (2015) 'Early biomarkers of joint damage in rheumatoid and psoriatic arthritis', *Arthritis Research & Therapy*, 17(1), p. 141. Available at: https://doi.org/10.1186/s13075-015-0652-z.

206. McGonagle, D.G. *et al.* (2019) 'The role of IL-17A in axial spondyloarthritis and psoriatic arthritis: recent advances and controversies', *Annals of the Rheumatic Diseases*, 78(9), pp. 1167–1178. Available at: https://doi.org/10.1136/annrheumdis-2019-215356.

207. McInnes, I.B. *et al.* (2013) 'Efficacy and safety of ustekinumab in patients with active psoriatic arthritis: 1 year results of the phase 3, multicentre, double-blind, placebo-controlled PSUMMIT 1 trial', *The Lancet*, 382(9894), pp. 780–789. Available at: https://doi.org/10.1016/S0140-6736(13)60594-2.

208. McInnes, I.B. and Schett, G. (2011) 'The pathogenesis of rheumatoid arthritis', *New England Journal of Medicine*. Available at: https://doi.org/10.1056/NEJMra1004965.

209. McInnes, I.B. and Schett, G. (2017) 'Pathogenetic insights from the treatment of rheumatoid arthritis', *The Lancet*. Available at: https://doi.org/10.1016/S0140-6736(17)31472-1.

210. McLaughlin, R.W. *et al.* (2002) 'Are there naturally occurring pleomorphic bacteria in the blood of healthy humans?', *Journal of Clinical Microbiology*, 40(12), pp. 4771–4775. Available at: https://doi.org/10.1128/JCM.40.12.4771-4775.2002.

211. Mease, P. *et al.* (2018) 'Secukinumab improves active psoriatic arthritis symptoms and inhibits radiographic progression: primary results from the randomised, double-blind, phase III FUTURE 5 study', *Annals of the Rheumatic Diseases*, 77(6), pp. 890–897. Available at: https://doi.org/10.1136/annrheumdis-2017-212687.

212. Mease, P.J. *et al.* (2005) 'Psoriatic arthritis assessment tools in clinical trials', *Annals of the Rheumatic Diseases*, 64(suppl 2), pp. ii49–ii54. Available at: https://doi.org/10.1136/ard.2004.034165.

213. Mease, Philip J *et al.* (2017) 'Ixekizumab, an interleukin-17A specific monoclonal antibody, for the treatment of biologic-naive patients with active psoriatic arthritis: results from the 24-week randomised, double-blind, placebo-controlled and active (adalimumab)-controlled period of the phase III trial SPIRIT-P1', *Annals of the Rheumatic Diseases*, 76(1), pp. 79–87. Available at: https://doi.org/10.1136/annrheumdis-2016-209709.

214. Mease, Philip J. *et al.* (2017) 'Ixekizumab, an interleukin-17A specific monoclonal antibody, for the treatment of biologic-naive patients with active psoriatic arthritis: results from the 24-week randomised, double-blind, placebo-controlled and active (adalimumab)-controlled period of the phase III trial SPIRIT-P1', *Annals of the Rheumatic Diseases*, 76(1), pp. 79–87. Available at: https://doi.org/10.1136/annrheumdis-2016-209709.

215. Menyhárt, O. and Győrffy, B. (2021) 'Multi-omics approaches in cancer research with applications in tumor subtyping, prognosis, and diagnosis', *Computational and Structural Biotechnology Journal*, 19, pp. 949–960. Available at: https://doi.org/10.1016/j.csbj.2021.01.009.

216. Merola, J.F., Espinoza, L.R. and Fleischmann, R. (2018) 'Distinguishing rheumatoid arthritis from psoriatic arthritis', *RMD Open*, 4(2), p. e000656. Available at: https://doi.org/10.1136/rmdopen-2018-000656.

217. Merrick, L. and Taly, A. (2020) 'The explanation game: explaining machine learning models using Shapley values'. arXiv. Available at: http://arxiv.org/abs/1909.08128 (Accessed: 22 November 2022).

218. Micheroli, R. *et al.* (2022) 'Role of synovial fibroblast subsets across synovial pathotypes in rheumatoid arthritis: a deconvolution analysis', *RMD Open*, 8(1), p. e001949. Available at: https://doi.org/10.1136/rmdopen-2021-001949.

219. Miggiels, P. *et al.* (2019) 'Novel technologies for metabolomics: More for less', *TrAC Trends in Analytical Chemistry*, 120, p. 115323. Available at: https://doi.org/10.1016/j.trac.2018.11.021.

220. Miklossy, G., Hilliard, T.S. and Turkson, J. (2013) 'Therapeutic modulators of STAT signalling for human diseases', *Nature reviews. Drug discovery*, 12(8), pp. 611–629. Available at: https://doi.org/10.1038/nrd4088.

221. Mills, E.L. *et al.* (2016) 'Succinate dehydrogenase supports metabolic repurposing of mitochondria to drive inflammatory macrophages', *Cell*. Available at: https://doi.org/10.1016/j.cell.2016.08.064.

222. Mills, E.L. *et al.* (2018) 'Itaconate is an anti-inflammatory metabolite that activates Nrf2 via alkylation of KEAP1', *Nature*. Available at: https://doi.org/10.1038/nature25986.

223. Mills, E.L. and O'Neill, L.A. (2016) 'Reprogramming mitochondrial metabolism in macrophages as an anti-inflammatory signal', *European Journal of Immunology*. Available at: https://doi.org/10.1002/eji.201445427.

224. Miyauchi, E. *et al.* (2023) 'The impact of the gut microbiome on extra-intestinal autoimmune diseases', *Nature Reviews Immunology*, 23(1), pp. 9–23. Available at: https://doi.org/10.1038/s41577-022-00727-y.

225. Moadab, F., Khorramdelazad, H. and Abbasifard, M. (2021) 'Role of CCL2/CCR2 axis in the immunopathogenesis of rheumatoid arthritis: Latest evidence and therapeutic approaches', *Life Sciences*, 269, p. 119034. Available at: https://doi.org/10.1016/j.lfs.2021.119034.

226. Moll, J.M.H. and Wright, V. (1973) 'Psoriatic arthritis', *Seminars in Arthritis and Rheumatism*, 3(1), pp. 55–78. Available at: https://doi.org/10.1016/0049-0172(73)90035-8.

227. Molnar, C. (2019) *Interpretable machine learning. A Guide for Making Black Box Models Explainable*. Available at: https://christophm.github.io/interpretable-ml-book/.

228. Molnar, C. *et al.* (2022) 'General pitfalls of model-agnostic interpretation methods for machine learning models', in A. Holzinger et al. (eds) *xxAI - Beyond Explainable AI: International Workshop, Held in Conjunction with ICML 2020, July 18, 2020, Vienna, Austria, Revised and Extended Papers*. Cham: Springer International Publishing (Lecture Notes in Computer Science), pp. 39–68. Available at: https://doi.org/10.1007/978-3-031-04083-2_4.

229. Mora, E. *et al.* (2012) 'Bindarit', *Cell Cycle*, 11(1), pp. 159–169. Available at: https://doi.org/10.4161/cc.11.1.18559.

230. Mounessa, J. *et al.* (2016) 'Role of leptin in the progression of psoriatic, rheumatoid and osteoarthritis', *World Journal of Rheumatology*, 6(1), pp. 9–15. Available at: https://doi.org/10.5499/wjr.v6.i1.9.

231. Munn, D.H. and Mellor, A.L. (2013) 'Indoleamine 2,3 dioxygenase and metabolic control of immune responses', *Trends in immunology*. Available at: https://doi.org/10.1016/j.it.2012.10.001.

232. Murakami, Y. *et al.* (2013) 'Remarkable role of indoleamine 2,3-dioxygenase and tryptophan metabolites in infectious diseases: potential role in macrophage-mediated inflammatory diseases', *Mediators of Inflammation*. Available at: https://doi.org/10.1155/2013/391984.

233. Murillo-Saich, J.D. *et al.* (2021) 'Metabolomics profiling predicts outcome of tocilizumab in rheumatoid arthritis: an exploratory study', *Metabolomics : Official journal of the Metabolomic Society*, 17(9), p. 74. Available at: https://doi.org/10.1007/s11306-021-01822-2.

234. Najm, A. *et al.* (2023) 'Phenotypic heterogeneity in psoriatic arthritis: towards tissue pathology-based therapy', *Nature Reviews Rheumatology*, 19(3), pp. 153–165. Available at: https://doi.org/10.1038/s41584-022-00874-5.

235. Nam, J.L. *et al.* (2017) 'Efficacy of biological disease-modifying antirheumatic drugs: a systematic literature review informing the 2016 update of the EULAR recommendations for the management of rheumatoid arthritis', *Annals of the Rheumatic Diseases*, 76(6), pp. 1113–1136. Available at: https://doi.org/10.1136/annrheumdis-2016-210713.

236. Narasimhan, R. *et al.* (2018) 'Serum metabolomic profiling predicts synovial gene expression in rheumatoid arthritis', *Arthritis Research & Therapy*, 20(1), p. 164. Available at: https://doi.org/10.1186/s13075-018-1655-3.

237. Narayanan, V., Arora, I. and Bhatia, A. (2013) 'Fast and accurate sentiment classification using an enhanced Naive Bayes model', in, pp. 194–201. Available at: https://doi.org/10.1007/978-3-642-41278-3_24.

238. Nash, W.J. and Dunn, W.B. (2019) 'From mass to metabolite in human untargeted metabolomics: Recent advances in annotation of metabolites applying liquid chromatography-mass spectrometry data', *TrAC Trends in Analytical Chemistry*, 120, p. 115324. Available at: https://doi.org/10.1016/j.trac.2018.11.022.

239. Negatu, D.A. *et al.* (2020) 'Indole propionic acid, an unusual antibiotic produced by the gut microbiota, with anti-inflammatory and antioxidant properties', *Frontiers in Microbiology*, 11. Available at: https://www.frontiersin.org/articles/10.3389/fmicb.2020.575586 (Accessed: 31 January 2023).

240. Negi, S. *et al.* (2019) 'Potential role of gut microbiota in induction and regulation of innate immune memory', *Frontiers in Immunology*, 10, p. 2441. Available at: https://doi.org/10.3389/fimmu.2019.02441.

241. Nestle, F.O. *et al.* (2005) 'Plasmacytoid predendritic cells initiate psoriasis through interferon-α production', *The Journal of Experimental Medicine*, 202(1), pp. 135–143. Available at: https://doi.org/10.1084/jem.20050500.

242. NICE (2015) *Technology overview | i STAT CG4+ and CHEM8+ cartridges for point-of-care testing in the emergency department | Advice | NICE*. NICE. Available at: https://www.nice.org.uk/advice/mib38/chapter/technology-overview (Accessed: 7 February 2023).

243. Nograles, K.E. *et al.* (2008) 'Th17 cytokines interleukin (IL)-17 and IL-22 modulate distinct inflammatory and keratinocyte-response pathways', *The British journal of dermatology*, 159(5), pp. 1092–1102. Available at: https://doi.org/10.1111/j.1365-2133.2008.08769.x.

244. Ogbechi, J. *et al.* (2020) 'IDO activation, inflammation and musculoskeletal disease', *Experimental Gerontology*, 131, p. 110820. Available at: https://doi.org/10.1016/j.exger.2019.110820.

245. Olde Loohuis, L.M. *et al.* (2018) 'Transcriptome analysis in whole blood reveals increased microbial diversity in schizophrenia', *Translational Psychiatry*, 8(1), pp. 1–9. Available at: https://doi.org/10.1038/s41398-018-0107-9.

246. O'Neill, L.A.J. and Artyomov, M.N. (2019) 'Itaconate: the poster child of metabolic reprogramming in macrophage function', *Nature Reviews Immunology*. Available at: https://doi.org/10.1038/s41577-019-0128-5.

247. Orr, C.K. *et al.* (2018) 'The utility and limitations of CRP, ESR and DAS28-CRP in appraising disease activity in rheumatoid arthritis', *Frontiers in Medicine*, 5. Available at: https://www.frontiersin.org/articles/10.3389/fmed.2018.00185 (Accessed: 27 April 2023).

248. Ostojic, S.M. *et al.* (2007) 'Glucosamine administration in athletes: effects on recovery of acute knee injury', *Research in Sports Medicine*, 15(2), pp. 113–124. Available at: https://doi.org/10.1080/15438620701405248.

249. Otoo, J.A. and Schlappi, T.S. (2022) 'REASSURED multiplex diagnostics: a critical review and forecast', *Biosensors*, 12(2), p. 124. Available at: https://doi.org/10.3390/bios12020124.

250. Païssé, S. *et al.* (2016) 'Comprehensive description of blood microbiome from healthy donors assessed by 16S targeted metagenomic sequencing', *Transfusion*, 56(5), pp. 1138–1147. Available at: https://doi.org/10.1111/trf.13477.

251. Pålsson-McDermott, E.M. and O'Neill, L.A.J. (2020) 'Targeting immunometabolism as an anti-inflammatory strategy', *Cell Research*. Available at: https://doi.org/10.1038/s41422-020-0291-z.

252. Patel, M.N. *et al.* (2015) 'Hematopoietic IKBKE limits the chronicity of inflammasome priming and metaflammation', *Proceedings of the National Academy of Sciences of the United States of America*, 112(2), pp. 506–511. Available at: https://doi.org/10.1073/pnas.1414536112.

253. Patil, I. (2021) 'Visualizations with statistical details: The "ggstatsplot" approach'. Journal of Open Source Software. Available at: https://doi.org/10.21105/joss.03167.

254. Pertovaara, M. *et al.* (2006) 'The activity of the immunoregulatory enzyme indoleamine 2,3-dioxygenase is decreased in smokers', *Clinical and Experimental Immunology*, 145(3), pp. 469–473. Available at: https://doi.org/10.1111/j.1365-2249.2006.03166.x.

255. Phillips, D.C., Woollard, K.J. and Griffiths, H.R. (2003) 'The anti-inflammatory actions of methotrexate are critically dependent upon the production of reactive oxygen species', *British Journal of Pharmacology*, 138(3), pp. 501–511. Available at: https://doi.org/10.1038/sj.bjp.0705054.

256. Pisaniello, H.L. *et al.* (2022) 'Using the derived 28-joint disease activity score patient-reported components (DAS28-P) index as a discriminatory measure of response to disease-modifying anti-rheumatic drug therapy in early rheumatoid arthritis', *BMC Rheumatology*, 6, p. 67. Available at: https://doi.org/10.1186/s41927-022-00299-3.

257. van der Pol, A. *et al.* (2018) 'OPLAH ablation leads to accumulation of 5-oxoproline, oxidative stress, fibrosis, and elevated fillings pressures: a murine model for heart failure with a preserved ejection fraction'.

258. Prendergast, G.C. *et al.* (2017) 'Discovery of IDO1 inhibitors: from bench to bedside', *Cancer research*. Available at: https://doi.org/10.1158/0008-5472.CAN-17-2285.

259. Pucino, V. *et al.* (2019) 'Lactate buildup at the site of chronic inflammation promotes disease by inducing CD4+ T cell metabolic rewiring', *Cell Metabolism*. Available at: https://doi.org/10.1016/j.cmet.2019.10.004.

260. Pudjihartono, N. *et al.* (2022) 'A review of feature selection methods for machine learning-based disease risk prediction', *Frontiers in Bioinformatics*, 2. Available at:

https://www.frontiersin.org/articles/10.3389/fbinf.2022.927312 (Accessed: 9 February 2023).

261. Puentes-Osorio, Y. *et al.* (2021) 'Potential clinical biomarkers in rheumatoid arthritis with an omic approach', *Autoimmunity Highlights*, 12(1), p. 9. Available at: https://doi.org/10.1186/s13317-021-00152-6.

262. Punzi, L. *et al.* (2007) 'Laboratory findings in psoriatic arthritis', *Reumatismo*, 59 Suppl 1, pp. 52–55. Available at: https://doi.org/10.4081/reumatismo.2007.1s.52.

263. Qiu, C. *et al.* (2020) 'Multi-omics data integration for identifying osteoporosis biomarkers and their biological interaction and causal mechanisms', *iScience*, 23(2), p. 100847. Available at: https://doi.org/10.1016/j.isci.2020.100847.

264. R Core Team (2022) 'R: A language and environment for statistical computing. R Foundation for Statistical Computing'. Vienna, Austria. Available at: https://www.R-project.org/.

265. Rath, M. *et al.* (2014) 'Metabolism via arginase or nitric oxide synthase: two competing arginine pathways in macrophages', *Frontiers in Immunology*. Available at: https://doi.org/10.3389/fimmu.2014.00532.

266. Rattray, N.J.W. *et al.* (2018) 'Beyond genomics: understanding exposotypes through metabolomics', *Human Genomics*, 12, p. 4. Available at: https://doi.org/10.1186/s40246-018-0134-x.

267. Raya-Cano, E. *et al.* (2022) 'Association between metabolic syndrome and uric acid: a systematic review and meta-analysis', *Scientific Reports*, 12(1), p. 18412. Available at: https://doi.org/10.1038/s41598-022-22025-2.

268. Raychaudhuri, S.P., Raychaudhuri, S.K. and Genovese, M.C. (2012) 'IL-17 receptor and its functional significance in psoriatic arthritis', *Molecular and Cellular Biochemistry*, 359(1), pp. 419–429. Available at: https://doi.org/10.1007/s11010-011-1036-6.

269. Reichelt, A. *et al.* (1994) 'Efficacy and safety of intramuscular glucosamine sulfate in osteoarthritis of the knee. A randomised, placebo-controlled, double-blind study.', *Arzneimittel-Forschung*, 44(1), pp. 75–80.

270. Ren, W. *et al.* (2019) 'Glutamine metabolism in macrophages: a novel target for obesity/type 2 diabetes', *Advances in nutrition (Bethesda, Md.)*. Available at: https://doi.org/10.1093/advances/nmy084.

271. Ribeiro, M.T., Singh, S. and Guestrin, C. (2016) 'Model-agnostic interpretability of machine learning'.

272. Rish, I. (2001) 'An empirical study of the naive Bayes classifier', p. 6.

273. Ritchie, M. *et al.* (2015) 'Limma powers differential expression analyses for RNA-sequencing and microarray studies.', *Nucleic Acids Research*.

274. Roager, H.M. and Licht, T.R. (2018) 'Microbial tryptophan catabolites in health and disease', *Nature Communications*, 9(1), p. 3294. Available at: https://doi.org/10.1038/s41467-018-05470-4.

275. Roberts, L.D. *et al.* (2012) 'Targeted metabolomics', *Current Protocols in Molecular Biology*, CHAPTER, p. Unit30.2. Available at: https://doi.org/10.1002/0471142727.mb3002s98.

276. Rohart, F. *et al.* (2017) 'mixOmics: An R package for 'omics feature selection and multiple data integration', *PLOS Computational Biology*.

277. Rubic, T. *et al.* (2008) 'Triggering the succinate receptor GPR91 on dendritic cells enhances immunity', *Nature Immunology*. Available at: https://doi.org/10.1038/ni.1657.

278. Ruiz-Ruiz, S. *et al.* (2020) 'Functional microbiome deficits associated with ageing: Chronological age threshold', *Aging Cell*, 19(1), p. e13063. Available at: https://doi.org/10.1111/acel.13063.

279. Saas, P., Toussirot, E. and Bogunia-Kubik, K. (2022) 'Editorial: Recent advances in potential biomarkers for rheumatic diseases and in cell-based therapies in the management of inflammatory rheumatic diseases', *Frontiers in Immunology*, 12. Available at: https://doi.org/10.3389/fimmu.2021.836119.

280. Sato, J. *et al.* (2014) 'Gut dysbiosis and detection of "live gut bacteria" in blood of Japanese patients with type 2 diabetes', *Diabetes Care*, 37(8), pp. 2343–2350. Available at: https://doi.org/10.2337/dc13-2817.

281. Sawant, K.V. *et al.* (2016) 'Chemokine CXCL1 mediated neutrophil recruitment: Role of glycosaminoglycan interactions', *Scientific Reports*, 6(1), p. 33123. Available at: https://doi.org/10.1038/srep33123.

282. Scher, J.U. *et al.* (2013) 'Expansion of intestinal Prevotella copri correlates with enhanced susceptibility to arthritis', *eLife*, 2, p. e01202. Available at: https://doi.org/10.7554/eLife.01202.

283. Scher, J.U. *et al.* (2019) 'Preventing psoriatic arthritis: focusing on patients with psoriasis at increased risk of transition', *Nature Reviews Rheumatology*, 15(3), pp. 153–166. Available at: https://doi.org/10.1038/s41584-019-0175-0.

284. Scher, J.U. and Abramson, S.B. (2011) 'The microbiome and rheumatoid arthritis', *Nature Reviews. Rheumatology*, 7(10), pp. 569–578. Available at: https://doi.org/10.1038/nrrheum.2011.121.

285. Schoels, M.M. *et al.* (2016) 'Disease activity in psoriatic arthritis (PsA): defining remission and treatment success using the DAPSA score', *Annals of the Rheumatic Diseases*, 75(5), pp. 811–818. Available at: https://doi.org/10.1136/annrheumdis-2015-207507.

286. Schonfeldova, B., Zec, K. and Udalova, I.A. (2022) 'Synovial single-cell heterogeneity, zonation and interactions: a patchwork of effectors in arthritis', *Rheumatology*, 61(3), pp. 913–925. Available at: https://doi.org/10.1093/rheumatology/keab721.

287. Schrimpe-Rutledge, A.C. *et al.* (2016) 'Untargeted metabolomics strategies-challenges and emerging directions', *Journal of the American Society for Mass Spectrometry*. Available at: https://doi.org/10.1007/s13361-016-1469-y.

288. Seitz, M., Zwicker, M. and Villiger, P.M. (2003) 'Pretreatment cytokine profiles of peripheral blood mononuclear cells and serum from patients with rheumatoid arthritis in different american college of rheumatology response groups to methotrexate.', *The Journal of rheumatology*, 30(1), pp. 28–35.

289. Shapiro, J. *et al.* (2019) 'Psoriatic patients have a distinct structural and functional fecal microbiota compared with controls', *The Journal of Dermatology*, 46(7), pp. 595–603. Available at: https://doi.org/10.1111/1346-8138.14933.

290. Sheehy, C. *et al.* (2014) 'Revising DAS28 scores for remission in rheumatoid arthritis', *Clinical Rheumatology*, 33(2), pp. 269–272. Available at: https://doi.org/10.1007/s10067-013-2468-z.

291. Shi, C. *et al.* (2020) 'Using functional genomics to advance the understanding of psoriatic arthritis', *Rheumatology*, 59(11), pp. 3137–3146. Available at: https://doi.org/10.1093/rheumatology/keaa283.

292. Siebert, S., Millar, N.L. and McInnes, I.B. (2019) 'Why did IL-23p19 inhibition fail in AS: a tale of tissues, trials or translation?', *Annals of the Rheumatic Diseases*, 78(8), pp. 1015–1018. Available at: https://doi.org/10.1136/annrheumdis-2018-213654.

293. Silva, M.J. *et al.* (2003) 'Glucuronidation patterns of common urinary and serum monoester phthalate metabolites', *Archives of Toxicology*, 77(10), pp. 561–567. Available at: https://doi.org/10.1007/s00204-003-0486-3.

294. da Silva, R.R., Dorrestein, P.C. and Quinn, R.A. (2015) 'Illuminating the dark matter in metabolomics', *Proceedings of the National Academy of Sciences*, 112(41), pp. 12549–12550. Available at: https://doi.org/10.1073/pnas.1516878112.

295. Singh, A. *et al.* (2018) 'DIABLO: from multi-omics assays to biomarker discovery, an integrative approach', *bioRxiv*. Available at: https://doi.org/10.1101/067611.

296. Smolen, J.S. *et al.* (2016) 'Treating rheumatoid arthritis to target: 2014 update of the recommendations of an international task force', *Annals of the Rheumatic Diseases*, 75(1), pp. 3–15. Available at: https://doi.org/10.1136/annrheumdis-2015-207524.

297. Smolen, J.S. *et al.* (2018) 'Rheumatoid arthritis', *Nature Reviews Disease Primers*. Available at: https://doi.org/10.1038/nrdp.2018.1.

298. Smolen, J.S. *et al.* (2023) 'EULAR recommendations for the management of rheumatoid arthritis with synthetic and biological disease-modifying antirheumatic

drugs: 2022 update', *Annals of the Rheumatic Diseases*, 82(1), pp. 3–18. Available at: https://doi.org/10.1136/ard-2022-223356.

299. So, A., Dumusc, A. and Nasi, S. (2017) 'The role of IL-1 in gout: from bench to bedside', *Rheumatology*, 57(suppl_1), pp. i12–i19. Available at: https://doi.org/10.1093/rheumatology/kex449.

300. Sokolove, J. *et al.* (2014) 'Rheumatoid factor as a potentiator of anti-citrullinated protein antibody mediated inflammation in rheumatoid arthritis', *Arthritis & rheumatology (Hoboken, N.J.)*, 66(4), pp. 813–821. Available at: https://doi.org/10.1002/art.38307.

301. Sorgdrager, F.J.H. *et al.* (2019) 'Tryptophan metabolism in inflammaging: from biomarker to therapeutic target', *Frontiers in Immunology*. Available at: https://doi.org/10.3389/fimmu.2019.02565.

302. Sourdon, J. *et al.* (2018) 'Death of an antioxidant brings heart failure with preserved ejection fraction to life: 5-oxoproline and post-ischaemic cardio-renal dysfunction'.

303. Steigmann, L. *et al.* (2020) 'Biosensor and lab-on-a-chip biomarker-identifying technologies for oral and periodontal diseases', *Frontiers in Pharmacology*, 11. Available at: https://www.frontiersin.org/articles/10.3389/fphar.2020.588480 (Accessed: 7 February 2023).

304. Subramanian, I. *et al.* (2020) 'Multi-omics data integration, interpretation, and its application', *Bioinformatics and Biology Insights*, 14, p. 1177932219899051. Available at: https://doi.org/10.1177/1177932219899051.

305. Swanberg, M. *et al.* (2012) 'Polymorphisms in the inflammatory genes CIITA, CLEC16A and IFNG influence BMD, bone loss and fracture in elderly women', *PLOS ONE*, 7(10), p. e47964. Available at: https://doi.org/10.1371/journal.pone.0047964.

306. Sweeney, S.R. *et al.* (2016) 'Metabolomic profiling predicts outcome of rituximab therapy in rheumatoid arthritis', *RMD Open*. Available at: https://doi.org/10.1136/rmdopen-2016-000289.

307. Sysi-Aho, M. *et al.* (2007) 'Normalization method for metabolomics data using optimal selection of multiple internal standards', *BMC Bioinformatics*, 8, p. 93. Available at: https://doi.org/10.1186/1471-2105-8-93.

308. Szklarczyk, D. *et al.* (2019) 'STRING v11: protein–protein association networks with increased coverage, supporting functional discovery in genome-wide experimental datasets', *Nucleic Acids Research*, 47(Database issue), pp. D607–D613. Available at: https://doi.org/10.1093/nar/gky1131.

309. Takahashi, Y. *et al.* (2020) 'Improved metabolomic data-based prediction of depressive symptoms using nonlinear machine learning with feature selection', *Translational Psychiatry*. Available at: https://doi.org/10.1038/s41398-020-0831-9.

310. Tannahill, G.M. *et al.* (2013) 'Succinate is an inflammatory signal that induces IL-1β through HIF-1α', *Nature*. Available at: https://doi.org/10.1038/nature11986.

311. Taylor, W. *et al.* (2006) 'Classification criteria for psoriatic arthritis: Development of new criteria from a large international study', *Arthritis & Rheumatism*, 54(8), pp. 2665–2673. Available at: https://doi.org/10.1002/art.21972.

312. Teitsma, X.M., Yang, W., *et al.* (2018) 'Baseline metabolic profiles of early rheumatoid arthritis patients achieving sustained drug-free remission after initiating treat-to-target tocilizumab, methotrexate, or the combination: insights from systems biology', *Arthritis Research & Therapy*. Available at: https://doi.org/10.1186/s13075-018-1729-2.

313. Teitsma, X.M., Jacobs, J.W.G., *et al.* (2018) 'Inadequate response to treat-to-target methotrexate therapy in patients with new-onset rheumatoid arthritis: development and validation of clinical predictors', *Annals of the Rheumatic Diseases*. Available at: https://doi.org/10.1136/annrheumdis-2018-213035.

314. Teitsma, X.M. *et al.* (2019) 'Adding baseline protein biomarkers to clinical predictors does not enhance prediction of treatment response to a methotrexate strategy in early rheumatoid arthritis', *Annals of the Rheumatic Diseases*, 78(1), pp. 142–144. Available at: https://doi.org/10.1136/annrheumdis-2018-213767.

315. Thomas, C.E. and Ganji, G. (2006) 'Integration of genomic and metabonomic data in systems biology--are we "there" yet?', *Current Opinion in Drug Discovery & Development*, 9(1), pp. 92–100.

316. Tiwari, R. *et al.* (2019) 'Beyond Tethering the Viral Particles: Immunomodulatory Functions of Tetherin (*BST-2*)', *DNA and Cell Biology*, 38(11), pp. 1170–1177. Available at: https://doi.org/10.1089/dna.2019.4777.

317. Tonel, G. *et al.* (2010) 'Cutting Edge: A Critical Functional Role for IL-23 in Psoriasis', *Journal of immunology (Baltimore, Md. : 1950)*, 185(10), pp. 5688–5691. Available at: https://doi.org/10.4049/jimmunol.1001538.

318. Tripolino, C. *et al.* (2021) 'Hyperuricemia in Psoriatic Arthritis: Epidemiology, Pathophysiology, and Clinical Implications', *Frontiers in Medicine*, 8, p. 737573. Available at: https://doi.org/10.3389/fmed.2021.737573.

319. Turesson, C. *et al.* (2003) 'Extra-articular disease manifestations in rheumatoid arthritis: incidence trends and risk factors over 46 years', *Annals of the Rheumatic Diseases*, 62(8), pp. 722–727. Available at: https://doi.org/10.1136/ard.62.8.722.

320. Turesson, C. and Matteson, E.L. (2013) 'Malignancy as a comorbidity in rheumatic diseases', *Rheumatology*, 52(1), pp. 5–14. Available at: https://doi.org/10.1093/rheumatology/kes189.

321. Turi, K.N. *et al.* (2018) 'A review of metabolomics approaches and their application in identifying causal pathways of childhood asthma', *Journal of Allergy and Clinical*

Immunology, 141(4), pp. 1191–1201. Available at: https://doi.org/10.1016/j.jaci.2017.04.021.

322. UniProt Consortium (2023) *UniProt: the universal protein knowledgebase in 2023*, *Nucleic Acids Research | Oxford Academic*. Available at: https://academic.oup.com/nar/article/51/D1/D523/6835362 (Accessed: 28 February 2023).

323. Van den Bosch, F. and Coates, L. (2018) 'Clinical management of psoriatic arthritis', *The Lancet*, 391(10136), pp. 2285–2294. Available at: https://doi.org/10.1016/S0140-6736(18)30949-8.

324. Vargas, A.J. and Harris, C.C. (2016) 'Biomarker development in the precision medicine era: lung cancer as a case study', *Nature Reviews Cancer*, 16(8), pp. 525–537. Available at: https://doi.org/10.1038/nrc.2016.56.

325. Veale, D.J. and Fearon, U. (2015) 'What makes psoriatic and rheumatoid arthritis so different?', *RMD Open*, 1(1), p. e000025. Available at: https://doi.org/10.1136/rmdopen-2014-000025.

326. Veale, D.J. and Fearon, U. (2018) 'The pathogenesis of psoriatic arthritis', *The Lancet*, 391(10136), pp. 2273–2284. Available at: https://doi.org/10.1016/S0140-6736(18)30830-4.

327. Viana, C.M. *et al.* (2021) 'Evaluation of the factors explaining the use of agricultural land: A machine learning and model-agnostic approach', *Ecological Indicators*, 131, p. 108200. Available at: https://doi.org/10.1016/j.ecolind.2021.108200.

328. Vlachogiannis, N.I. *et al.* (2020) 'Increased adenosine-to-inosine RNA editing in rheumatoid arthritis', *Journal of Autoimmunity*, 106, p. 102329. Available at: https://doi.org/10.1016/j.jaut.2019.102329.

329. Volkov, M. *et al.* (2021) 'Evolution of anti-modified protein antibody responses can be driven by consecutive exposure to different post-translational modifications', *Arthritis Research & Therapy*, 23(1), p. 298. Available at: https://doi.org/10.1186/s13075-021-02687-5.

330. de Vries, L.V. *et al.* (2017) 'The tryptophan/kynurenine pathway, systemic inflammation, and long-term outcome after kidney transplantation', *American Journal of Physiology-Renal Physiology*. Available at: https://doi.org/10.1152/ajprenal.00690.2016.

331. Wandy, J. *et al.* (2023) 'Simulated-to-real benchmarking of acquisition methods in untargeted metabolomics', *Frontiers in Molecular Biosciences*, 10. Available at: https://www.frontiersin.org/articles/10.3389/fmolb.2023.1130781 (Accessed: 28 March 2023).

332. Wandy, J. and Daly, R. (2021) 'GraphOmics: an interactive platform to explore and integrate multi-omics data', *BMC Bioinformatics*, 22(1), p. 603. Available at: https://doi.org/10.1186/s12859-021-04500-1.

333. Wang, H. *et al.* (2015) 'Tumor necrosis factor receptor-associated factor 6 promotes migration of rheumatoid arthritis fibroblast-like synoviocytes', *Molecular Medicine Reports*, 11(4), pp. 2761–2766. Available at: https://doi.org/10.3892/mmr.2014.3104.

334. Wang, J. *et al.* (2020) 'Mechanism by which TRAF6 Participates in the Immune Regulation of Autoimmune Diseases and Cancer', *BioMed Research International*, 2020, p. 4607197. Available at: https://doi.org/10.1155/2020/4607197.

335. Wang, N. *et al.* (2022) 'Altered fecal metabolomics and potential biomarkers of psoriatic arthritis differing from rheumatoid arthritis', *Frontiers in Immunology*, 13, p. 812996. Available at: https://doi.org/10.3389/fimmu.2022.812996.

336. Wang, T. *et al.* (2021) 'MOGONET integrates multi-omics data using graph convolutional networks allowing patient classification and biomarker identification', *Nature Communications*, 12(1), p. 3445. Available at: https://doi.org/10.1038/s41467-021-23774-w.

337. Wang, Y. *et al.* (2001) 'Localization of the murine reduced folate carrier as assessed by immunohistochemical analysis', *Biochimica et Biophysica Acta (BBA) - Biomembranes*, 1513(1), pp. 49–54. Available at: https://doi.org/10.1016/S0005-2736(01)00340-6.

338. Wang, Z. *et al.* (2012) '(1)H NMR-based metabolomic analysis for identifying serum biomarkers to evaluate methotrexate treatment in patients with early rheumatoid arthritis.', *Experimental and therapeutic medicine*, 4(1), pp. 165–171. Available at: https://doi.org/10.3892/etm.2012.567.

339. Wei, R. *et al.* (2018) 'Missing value imputation approach for mass spectrometry-based metabolomics data', *Scientific Reports*. Available at: https://doi.org/10.1038/s41598-017-19120-0.

340. Wei, T. and Simko, W. (2022) 'R package "corrplot": visualization of a correlation matrix'. Available at: https://github.com/taiyun/corrplot.

341. Weinblatt, M.E. (2013) 'Methotrexate in rheumatoid arthritis: a quarter century of development', *Transactions of the American Clinical and Climatological Association*.

342. Wells, G. *et al.* (2009) 'Validation of the 28-joint Disease Activity Score (DAS28) and European League Against Rheumatism response criteria based on C-reactive protein against disease progression in patients with rheumatoid arthritis, and comparison with the DAS28 based on erythrocyte sedimentation rate', *Annals of the Rheumatic Diseases*, 68(6), pp. 954–960. Available at: https://doi.org/10.1136/ard.2007.084459.

343. Wervers, K. *et al.* (2018) 'Burden of psoriatic arthritis according to different definitions of disease activity: comparing minimal disease activity and the disease activity index for psoriatic arthritis', *Arthritis Care & Research*, 70(12), pp. 1764–1770. Available at: https://doi.org/10.1002/acr.23571.

344. Widawski, L. *et al.* (2022) 'Psoriatic arthritis with hyperuricemia: more peripheral, destructive, and challenging to treat', *Clinical Rheumatology*, 41(5), pp. 1421–1429. Available at: https://doi.org/10.1007/s10067-022-06061-x.

345. Willkens, R.F. and Watson, M.A. (1982) 'Methotrexate: a perspective of its use in the treatment of rheumatic diseases.', *The Journal of laboratory and clinical medicine*, 100(3), pp. 314–321.

346. Willkens, R.F., Watson, M.A. and Paxson, C.S. (1980) 'Low dose pulse methotrexate therapy in rheumatoid arthritis.', *The Journal of rheumatology*, 7(4), pp. 501–505.

347. Winchester, R. *et al.* (2012) 'HLA associations reveal genetic heterogeneity in psoriatic arthritis and in the psoriasis phenotype', *Arthritis and Rheumatism*, 64(4), pp. 1134–1144. Available at: https://doi.org/10.1002/art.33415.

348. Wirthgen, E. *et al.* (2018) 'Kynurenic acid: the Janus-faced role of an immunomodulatory tryptophan metabolite and its link to pathological conditions', *Frontiers in Immunology*. Available at: https://doi.org/10.3389/fimmu.2017.01957.

349. Wishart, D.S. (2016) 'Emerging applications of metabolomics in drug discovery and precision medicine', *Nature Reviews Drug Discovery*, 15(7), pp. 473–484. Available at: https://doi.org/10.1038/nrd.2016.32.

350. Wishart, D.S. *et al.* (2018) 'HMDB 4.0: the human metabolome database for 2018', *Nucleic acids research*. Available at: https://doi.org/10.1093/nar/gkx1089.

351. Wlodarska, M. *et al.* (2017a) 'Indoleacrylic Acid Produced by Commensal Peptostreptococcus Species Suppresses Inflammation', *Cell Host & Microbe*. Available at: https://doi.org/10.1016/j.chom.2017.06.007.

352. Wlodarska, M. *et al.* (2017b) 'Indoleacrylic acid produced by commensal Peptostreptococcus species suppresses inflammation', *Cell host & microbe*, 22(1), pp. 25-37.e6. Available at: https://doi.org/10.1016/j.chom.2017.06.007.

353. Wright, H.L. *et al.* (2015) 'Interferon gene expression signature in rheumatoid arthritis neutrophils correlates with a good response to TNFi therapy', *Rheumatology (Oxford, England)*, 54(1), pp. 188–193. Available at: https://doi.org/10.1093/rheumatology/keu299.

354. Wu, C.-S. *et al.* (2021) 'Age-dependent remodeling of gut microbiome and host serum metabolome in mice', *Aging (Albany NY)*, 13(5), pp. 6330–6345. Available at: https://doi.org/10.18632/aging.202525.

355. Wu, J. *et al.* (2018) 'Lab-on-chip technology for chronic disease diagnosis', *npj Digital Medicine*, 1(1), pp. 1–11. Available at: https://doi.org/10.1038/s41746-017-0014-0.

356. Xia, J. and Wishart, D.S. (2010) 'MSEA: a web-based tool to identify biologically meaningful patterns in quantitative metabolomic data', *Nucleic Acids Research*, 38(Web Server issue), pp. W71–W77. Available at: https://doi.org/10.1093/nar/gkq329.

357. Xiao, Y. *et al.* (2022) 'Multi-omics approaches for biomarker discovery in early ovarian cancer diagnosis', *eBioMedicine*, 79. Available at: https://doi.org/10.1016/j.ebiom.2022.104001.

358. Xu, S. *et al.* (2019) 'Inflammasome inhibitors: promising therapeutic approaches against cancer', *Journal of Hematology & Oncology*, 12(1), p. 64. Available at: https://doi.org/10.1186/s13045-019-0755-0.

359. Yan, J. *et al.* (2017) 'Network approaches to systems biology analysis of complex disease: integrative methods for multi-omics data', *Briefings in Bioinformatics*, 19(6), pp. 1370–1381. Available at: https://doi.org/10.1093/bib/bbx066.

360. Ye, X. *et al.* (2022) 'Dual role of indoles derived from intestinal microbiota on human health', *Frontiers in Immunology*, 13. Available at: https://www.frontiersin.org/articles/10.3389/fimmu.2022.903526 (Accessed: 19 January 2023).

361. Young, A., Wang, B. and Röst, H. (2021) 'MassFormer: tandem mass spectrum prediction with graph transformers'. arXiv. Available at: https://doi.org/10.48550/arXiv.2111.04824.

362. Yu, D. *et al.* (2022) 'The gut microbiome and metabolites are altered and interrelated in patients with rheumatoid arthritis', *Frontiers in Cellular and Infection Microbiology*, 11, p. 763507. Available at: https://doi.org/10.3389/fcimb.2021.763507.

363. Yu, X.-H. *et al.* (2019) 'Itaconate: an emerging determinant of inflammation in activated macrophages', *Immunology & Cell Biology*. Available at: https://doi.org/10.1111/imcb.12218.

364. Zaba, L.C. *et al.* (2010) 'Identification of TRAIL and other molecules that distinguish inflammatory DCs from resident DCs in psoriasis', *The Journal of allergy and clinical immunology*, 125(6), pp. 1261-1268.e9. Available at: https://doi.org/10.1016/j.jaci.2010.03.018.

365. Zakharia, Y. *et al.* (2021) 'Phase II trial of the IDO pathway inhibitor indoximod plus pembrolizumab for the treatment of patients with advanced melanoma', *Journal for ImmunoTherapy of Cancer*, 9(6), p. e002057. Available at: https://doi.org/10.1136/jitc-2020-002057.

366. Zhao, L.-L. *et al.* (2019) 'NMR metabolomics and random forests models to identify potential plasma biomarkers of blood stasis syndrome with coronary heart disease patients', *Frontiers in Physiology*. Available at: https://doi.org/10.3389/fphys.2019.01109.

367. Zhao, S.S. *et al.* (2020) 'Systematic review of mental health comorbidities in psoriatic arthritis', *Clinical Rheumatology*, 39(1), pp. 217–225. Available at: https://doi.org/10.1007/s10067-019-04734-8.

368. Zhao, T. *et al.* (2022) 'Gut microbiota and rheumatoid arthritis: From pathogenesis to novel therapeutic opportunities', *Frontiers in Immunology*, 13, p. 1007165. Available at: https://doi.org/10.3389/fimmu.2022.1007165.

369. Zhao, Y., Wong, L. and Goh, W.W.B. (2020) 'How to do quantile normalization correctly for gene expression data analyses', *Scientific Reports*, 10(1), p. 15534. Available at: https://doi.org/10.1038/s41598-020-72664-6.

370. Zhao, Z.-H. *et al.* (2019) 'Indole-3-propionic acid inhibits gut dysbiosis and endotoxin leakage to attenuate steatohepatitis in rats', *Experimental & Molecular Medicine*. Available at: https://doi.org/10.1038/s12276-019-0304-5.

371. Zheng, D., Liwinski, T. and Elinav, E. (2020) 'Inflammasome activation and regulation: toward a better understanding of complex mechanisms', *Cell Discovery*, 6(1), pp. 1–22. Available at: https://doi.org/10.1038/s41421-020-0167-x.

372. Zhu, H., Liu, L. and Hassoun, S. (2020) 'Using graph neural networks for mass spectrometry prediction'. arXiv. Available at: https://doi.org/10.48550/arXiv.2010.04661.

373. Zhu, L.-J. *et al.* (2012) 'Upregulation of tumor necrosis factor receptor-associated factor 6 correlated with synovitis severity in rheumatoid arthritis', *Arthritis Research & Therapy*, 14(3), p. R133. Available at: https://doi.org/10.1186/ar3866.

374. Zhu, T.Y., Li, E.K. and Tam, L.-S. (2012) 'Cardiovascular risk in patients with psoriatic arthritis', *International Journal of Rheumatology*, 2012, p. 714321. Available at: https://doi.org/10.1155/2012/714321.

375. Ziegler, J.F. *et al.* (2019) 'Leptin induces TNFα-dependent inflammation in acquired generalized lipodystrophy and combined Crohn's disease', *Nature Communications*, 10(1), p. 5629. Available at: https://doi.org/10.1038/s41467-019-13559-7.

376. Zoppi, J. *et al.* (2021) 'MiBiOmics: an interactive web application for multi-omics data exploration and integration', *BMC Bioinformatics*, 22(1), p. 6. Available at: https://doi.org/10.1186/s12859-020-03921-8.

10. Appendix

Supplementary Figures

Feature	logFC	AveExpr	t	P.Value	adj.P.Val	B
Pyroglutamate	0.2662	20.2103	3.4339	0.0010	0.5319	-2.1012
Peak_189.131_17.096	0.4944	20.3852	3.3019	0.0015	0.5319	-2.2974
Peak_188.127_17.098	0.4742	20.5454	3.2601	0.0017	0.5319	-2.3584
Peak_109.064_10.492	0.3355	20.4523	2.9690	0.0040	0.9089	-2.7702
Peak_117.068_9.607	-0.1456	20.6621	-2.6618	0.0095	0.9089	-3.1758
Peak_180.021_10.637	-0.3570	20.2718	-2.6167	0.0108	0.9089	-3.2326
Peak_97.967_11.819	0.6017	25.0049	2.5840	0.0117	0.9089	-3.2735
Peak_122.048_6.911	0.3626	19.4063	2.5551	0.0127	0.9089	-3.3091
Peak_156.073_10.433	0.2553	20.4443	2.4556	0.0164	0.9089	-3.4297
Cytosine	0.3896	19.6993	2.3720	0.0203	0.9089	-3.5280
Peak_270.068_8.347	-1.6812	16.1610	-2.3670	0.0206	0.9089	-3.5338
Peak_149.105_8.046	-0.3772	20.1825	-2.3640	0.0207	0.9089	-3.5373
Peak_188.069_7.065	0.2556	18.4249	2.3605	0.0209	0.9089	-3.5413
Peak_157.074_7.037	0.4358	18.2465	2.3087	0.0238	0.9089	-3.6008
Peak_173.08_10.394	0.3929	20.1635	2.2939	0.0246	0.9089	-3.6175
Peak_195.053_7.083	-1.3001	20.7395	-2.2848	0.0252	0.9089	-3.6278
Peak_203.127_9.108	-0.4570	20.3569	-2.2408	0.0281	0.9089	-3.6770
Peak_232.024_7.079	-2.4247	19.1179	-2.2247	0.0292	0.9089	-3.6948
Peak_194.115_5.525	-0.2376	19.9045	-2.1797	0.0325	0.9089	-3.7440
Peak_312.078_6.947	-1.7687	19.4118	-2.1748	0.0328	0.9089	-3.7492
Peak_220.058_8.875	-0.8449	15.6428	-2.1603	0.0340	0.9089	-3.7649
Peak_105.079_13.488	-0.2582	20.8440	-2.1499	0.0348	0.9089	-3.7761
Pantothenate	0.5558	17.4762	2.1358	0.0360	0.9089	-3.7912
Peak_233.036_10.793	0.6950	18.7176	2.1325	0.0363	0.9089	-3.7947
Peak_139.1_5.384	0.4272	19.5414	2.1308	0.0364	0.9089	-3.7965
Peak_198.075_8.519	-0.7140	20.5690	-2.1118	0.0381	0.9089	-3.8167
Peak_349.077_8.545	-1.5276	20.3774	-2.0898	0.0401	0.9089	-3.8398
Peak_110.067_10.338	0.1709	20.2847	2.0646	0.0425	0.9089	-3.8661
Peak_166.041_10.639	0.4073	20.2398	2.0602	0.0429	0.9089	-3.8706
Peak_270.067_8.209	-1.2243	20.0871	-2.0508	0.0438	0.9089	-3.8803
Pyrroline	-0.1284	20.5706	-2.0372	0.0452	0.9089	-3.8942
Peak_271.178_6.894	-0.1901	20.7411	-2.0364	0.0453	0.9089	-3.8951
Peak_357.106_7.991	-1.4943	16.1603	-2.0338	0.0456	0.9089	-3.8978
Peak_256.095_8.182	0.7917	18.6458	2.0321	0.0457	0.9089	-3.8995
Peak_327.095_8.538	-1.5675	20.3687	-2.0303	0.0459	0.9089	-3.9014
Peak_285.194_5.686	-0.3497	20.6885	-2.0297	0.0460	0.9089	-3.9020
Peak_238.084_8.032	0.8118	20.0506	2.0123	0.0478	0.9089	-3.9197
Peak_195.053_7.092	-1.1991	20.6780	-2.0117	0.0479	0.9089	-3.9203
Peak_197.09_10.437	-0.1625	20.7057	-1.9974	0.0495	0.9089	-3.9347
Peak_178.998_9.017	-0.2194	20.3596	-1.9970	0.0495	0.9089	-3.9352
Peak_212.069_6.891	0.2126	18.3209	1.9774	0.0517	0.9089	-3.9549
Peak_344.122_8.539	-1.2019	20.4473	-1.9666	0.0530	0.9089	-3.9656
Peak_192.027_11.625	0.3738	22.2998	1.9648	0.0532	0.9089	-3.9674
Peak_183.036_8.347	-1.1952	15.4406	-1.9640	0.0533	0.9089	-3.9682
Peak_116.067_9.618	-0.1162	20.6199	-1.9618	0.0536	0.9089	-3.9704
Peak_345.125_8.531	-1.3355	20.2532	-1.9563	0.0542	0.9089	-3.9759
Peak_248.143_7.603	0.8695	19.9785	1.9549	0.0544	0.9089	-3.9773
Peak_203.049_10.612	-0.1290	20.6321	-1.9364	0.0567	0.9089	-3.9955
Peak_156.006_11.042	-1.0546	16.2782	-1.9355	0.0568	0.9089	-3.9963
Peak_319.162_7.588	1.0563	18.9976	1.9294	0.0575	0.9089	-4.0023
Peak_238.141_5.859	-0.1766	20.1330	-1.9273	0.0578	0.9089	-4.0043
Peak_150.109_8.021	-0.5262	19.8504	-1.9232	0.0583	0.9089	-4.0084
Peak_350.081_8.539	-1.1949	20.0636	-1.9063	0.0605	0.9089	-4.0248
Peak_194.043_10.991	-0.3231	21.5591	-1.8801	0.0640	0.9089	-4.0500
Peak_186.053_7.041	0.1874	18.3588	1.8408	0.0697	0.9089	-4.0873
N-Acetylornithine	0.3948	19.8352	1.8383	0.0700	0.9089	-4.0897
Peak_138.032_5.504	-1.1060	17.7826	-1.8321	0.0710	0.9089	-4.0954
Peak_130.082_9.439	0.2578	20.5451	1.8144	0.0737	0.9089	-4.1120
Peak_247.14_7.603	0.5571	20.7908	1.7931	0.0771	0.9089	-4.1316
Peak_116.059_10.867	-0.1403	19.7970	-1.7856	0.0783	0.9089	-4.1385
Peak_138.011_11.413	-0.2057	19.7869	-1.7842	0.0785	0.9089	-4.1398
Peak_162.053_10.34	-0.2073	20.3457	-1.7785	0.0794	0.9089	-4.1450
N-Acetylputrescine	0.2001	19.6418	1.7725	0.0804	0.9089	-4.1504
Peak_251.053_5.573	0.0975	16.9263	1.7698	0.0809	0.9089	-4.1529
Peak_198.112_12.644	0.2564	20.4516	1.7681	0.0812	0.9089	-4.1544
Peak_151.03_8.83	0.4185	20.0233	1.7626	0.0821	0.9089	-4.1594
Peak_207.111_9.755	0.1605	17.8717	1.7527	0.0838	0.9089	-4.1684
N-Acetylleucine	0.4001	20.1394	1.7306	0.0877	0.9089	-4.1882
Uric acid	0.1842	26.1543	1.7236	0.0890	0.9089	-4.1944
L-Histidine	0.1574	23.1960	1.7187	0.0899	0.9089	-4.1987
Indoleacrylic acid	0.7419	17.5803	1.7119	0.0911	0.9089	-4.2047
Peak_199.121_8.321	0.1924	20.5653	1.7014	0.0931	0.9089	-4.2140
Peak_190.069_15.437	0.1385	20.7522	1.6884	0.0956	0.9089	-4.2253
Peak_246.137_7.605	0.5771	20.7215	1.6781	0.0976	0.9089	-4.2343
Peak_156.073_10.346	0.1259	20.5396	1.6768	0.0978	0.9089	-4.2354
Peak_201.111_8.704	-0.3346	20.7414	-1.6759	0.0980	0.9089	-4.2361
3-Hydroxyquinine	-0.6796	18.0189	-1.6743	0.0983	0.9089	-4.2376
Peak_249.057_5.669	0.0679	17.4454	1.6712	0.0989	0.9089	-4.2403
Peak_248.054_9.197	-0.1745	19.9875	-1.6604	0.1011	0.9089	-4.2495
Peak_155.977_10.131	-0.2040	20.6181	-1.6543	0.1023	0.9089	-4.2547
Peak_213.935_10.002	-0.2456	20.5170	-1.6513	0.1029	0.9089	-4.2573
Peak_141.079_7.227	0.5181	20.1290	1.6483	0.1035	0.9089	-4.2598
Peak_118.057_11.084	0.1968	20.1536	1.6447	0.1043	0.9089	-4.2629
Peak_141.079_7.335	0.5164	20.1980	1.6437	0.1045	0.9089	-4.2637
Peak_116.06_9.607	-0.1019	20.6558	-1.6407	0.1051	0.9089	-4.2663
Peak_391.977_10.13	0.2920	18.5028	1.6322	0.1069	0.9089	-4.2735
Peak_115.063_7.497	0.2094	19.9358	1.6320	0.1069	0.9089	-4.2737
Peak_150.041_10.504	-0.2156	20.7013	-1.6297	0.1074	0.9089	-4.2756
Peak_389.98_10.131	0.2919	18.5100	1.6226	0.1089	0.9089	-4.2816
L-Aspartate	0.1756	19.9414	1.6202	0.1095	0.9089	-4.2837
Peak_317.184_8.026	-0.4284	20.2374	-1.6128	0.1111	0.9089	-4.2898
Peak_393.976_10.134	0.2525	18.7664	1.6121	0.1112	0.9089	-4.2904
Peak_195.053_5.838	-1.0689	16.0938	-1.6042	0.1129	0.9089	-4.2970
Peak_208.98_10.082	-0.2246	20.5476	-1.6023	0.1134	0.9089	-4.2986
Peak_109.064_10.341	0.1185	20.5142	1.6018	0.1135	0.9089	-4.2990
Peak_398.073_10.646	-0.2630	20.2456	-1.5954	0.1149	0.9089	-4.3043
Peak_159.053_10.138	0.2919	18.6567	1.5936	0.1153	0.9089	-4.3058
Peak_356.001_10.134	0.3303	18.4940	1.5890	0.1163	0.9089	-4.3096
Peak_168.979_10.638	0.0990	20.4977	1.5866	0.1169	0.9089	-4.3116
Fructosamine	-0.1066	20.2237	-1.5850	0.1172	0.9089	-4.3129

Supplementary Figure 1.. Differential abundance of peaks at baseline across 3-month DAS28 response groups.

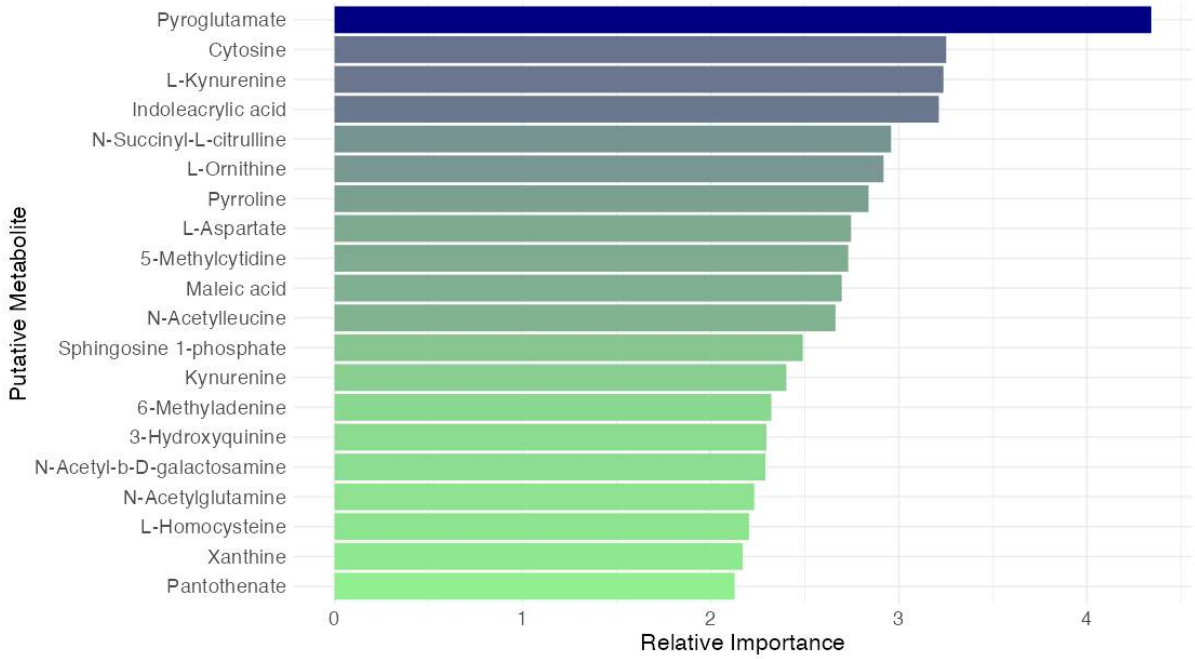

Supplementary Figure 2. Extended feature selection from metabolites model associated with 3-month DAS28 response

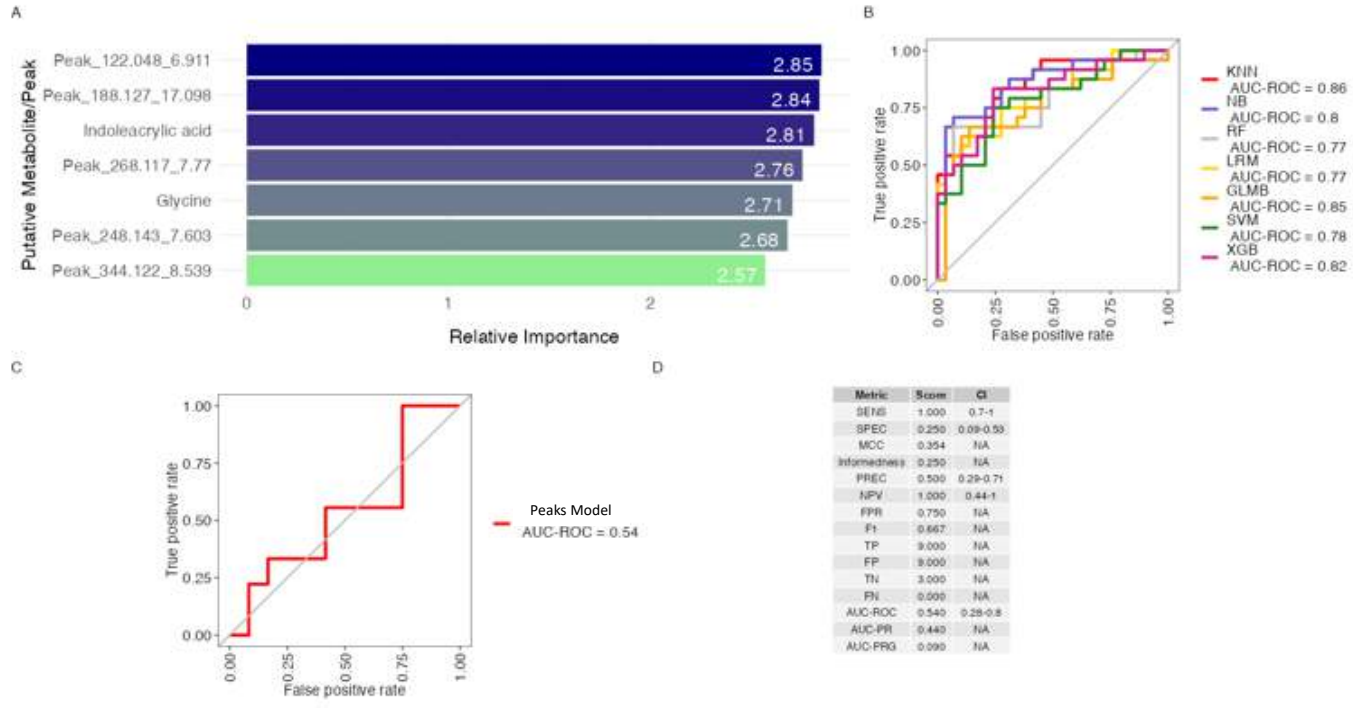

Supplementary Figure 3. Generation of a predictive model using all signals from the TaSER metabolome for comparison with the annotated-only metabolic model generated in the TaSER Metabolomic Chapter. A. Metabolites selected for inclusion in the model using RFE. B. Algorithm selection showing the KNN algorithm being the best performing. C. Final model evaluation in test subset showing poor performance. D. Performance metrics in test subset.

Gene	Gene Product	Biological Role/Function	Link with Inflammation	Potential of Targeting with Pharmacological Agents
ADAR	Adenosine deaminas	Enzyme involved in RNA editing of adenosines via deamination	Yes	
ARG1	Arginase	Enzyme involved in conversion of arginine to ornithine and urea, implicated in urea cycle and primarily expressed in the liver	Yes	Pegylated arginase 1 being tested for the treatment of diabetic retinopathy to avoid iNOS conversion of arginine to ROS - Abdelrahman et al. (2022).
BAPX1	NKX-3 Homeobox 2	Role in skeletal development	No	
BST2	bone marrow strom	Involved in regulating the interferon response following viral infection. Expression linked to IFNAR stimulation, leading to STAT1/2-IRF9 complex activity, leading to the regulation of IFN production via triggering ubiquitination of MAVS, which would normally activate IRF3-mediated IFN expression	Yes	
CCL2	C-C-motif chemokin	Involved in the recruitment of immune cells and inflammation, being largely produced by innate cells, including monocytes and macrophages. Its expression is triggered by pro-inflammatory cytokines, including IL-1β and TNF-α.	Yes	Small molecule, bindarit, tested to block CCL2 production in inflammatory mouse cell model - Mora et al. (2012)
CIITA	Class II major histoc	Protein involved in the regulation of MHC class II gene expression. Involved in mediating the immune response by supporting the presentation of antigens to T cells.	Yes	
FAM57A	Also known as TLD3	Encodes a membrane bound proten whose function is not fully characterised.	No	
IFI35	Interferon induced p	Expression induced by IFN stimulation and involved in regulating the immune response. The IFI35 protein has complex immunomodulatory effects in response to viral infection	Yes	
IKBKE	Inhibitor Of Nuclear	Involved in innate immune response against infection. IKKε contributes towards the activation of interferon regulatory factors which leads to IFNs being expressed along with other inflammatory cytokines	Yes	Small molecule -DMXD-011- being tested to inhibit TBK-1/IKKε for use in SLE and RA - Domainex UK
INDO	Indoleamine 2,3-dio	IDO1 converts tryptophan to kynurenine, the latter being a metabolite with complex immunomodulatory effects	Yes (induced by IF	1-methyltryptophan (Indoximod) currently being tested in clinical trials for various cancers - Tang et al. (2021)
IRF9	Interferon regulator	IRF9 complexes with the STAT1/2 dimer which translocates to the nucleus and induces IFN expression.	Yes	
ISG15	Interferon stimulate	Expression induced by IFN signalling. Modulates various pro-inflammatory processes involving intracellular and extracellular functions.	Yes	
OAS1	2'-5'-Oligoadenylate	Involved in immune response to infection, stimualted by IFN signalling, whereby it activates Rnase L to destroy viral RNA. Believed to have immunomodulatory effects that play a role in autoimmunity	Yes	
NCKAP1	NCK associated prot	Cytoskeletal protein involved in actin-based structure formation	No	
NLRP1	NLR family pyrin dor	Contributes to the NLRP1 inflammasome which leads to the production of pro-inflammatory cytokines, including IL-1β.	Yes	Inhibitors of caspase-1 being tested to reduce production of IL-1β and IL-18 e..g pralnacasan, VX-765 - Xu et al. (2019)
NLRP6	NLR family pyrin dor	Contributes to the NLRP6 inflammasome which leads to the production of pro-inflammatory cytokines, including IL-1β.	Yes	
PDHA2	Pyruvate dehydroger	Enzyme involved in conversion of pyruvate to acetyl coenzyme A.	Uncertain	Inhibitor pyruvate hydrogenase kinase, which blocks PDH activity, being tested as anti-diabetic agent (dichloroacetate, DCA) - Katayama et al. (2022)
RIG	Retinoic acid-inducil	Involved in immune response to infection. Can induce the production of pro-inflammatory cytokines.	Yes	Various dsRNA ligands tested *in vivo* for infection response and anti-cancer effects - Kasumba and Grandvaux (2019)
STAT1	Signal transducer an	Transcription factor that binds with STAT2 to induce the expression of interferon stimulated genes which contributes to inflammatory response	Yes	Small molecule inhibitors of STAT1 including pravastatin and ISS-840 being tested - Miklossy et al. (2013)
STAT2	Signal transducer an	Transcription factor that binds with STAT1 to induce the expression of interferon stimulated genes which contributes to inflammatory response	Yes	
TRAF6	TNF receptor associ	Signal transduction protein that mediates effects of various inflammatory cytokines, including IL-1, RANKL and TNFα. Involved in the activation of NF-κB and also required for osteoclast activation.	Yes	Small molecule inhibitor, C25-140, tested *in vivo* for interuption of TRAF6-Ubc13interaction - Brenke et al. (2018)
VAX1	Ventral anterior hon	Transcription factor involved in the development of the brain.	No	

Supplementary Figure 4. Immune-related genes from TaSER transcriptomics pathway analysis.

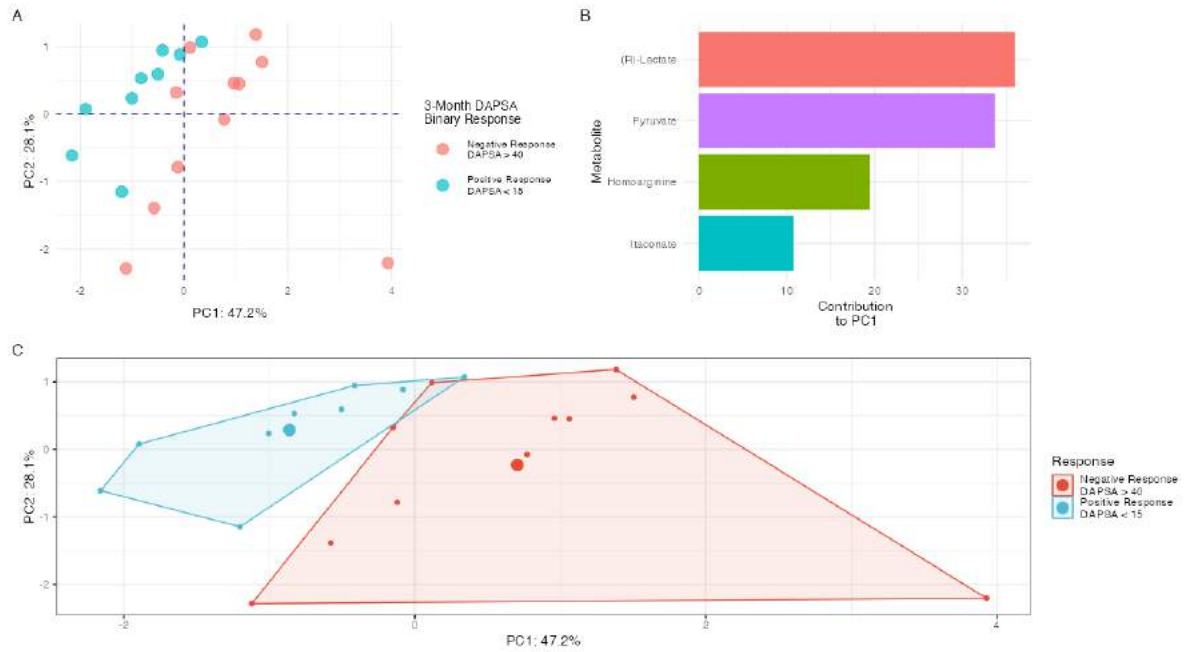

Supplementary Figure 5. Multivariate analysis of samples with features selected based on ratios with strongest correlation to DAPSA at 3 months

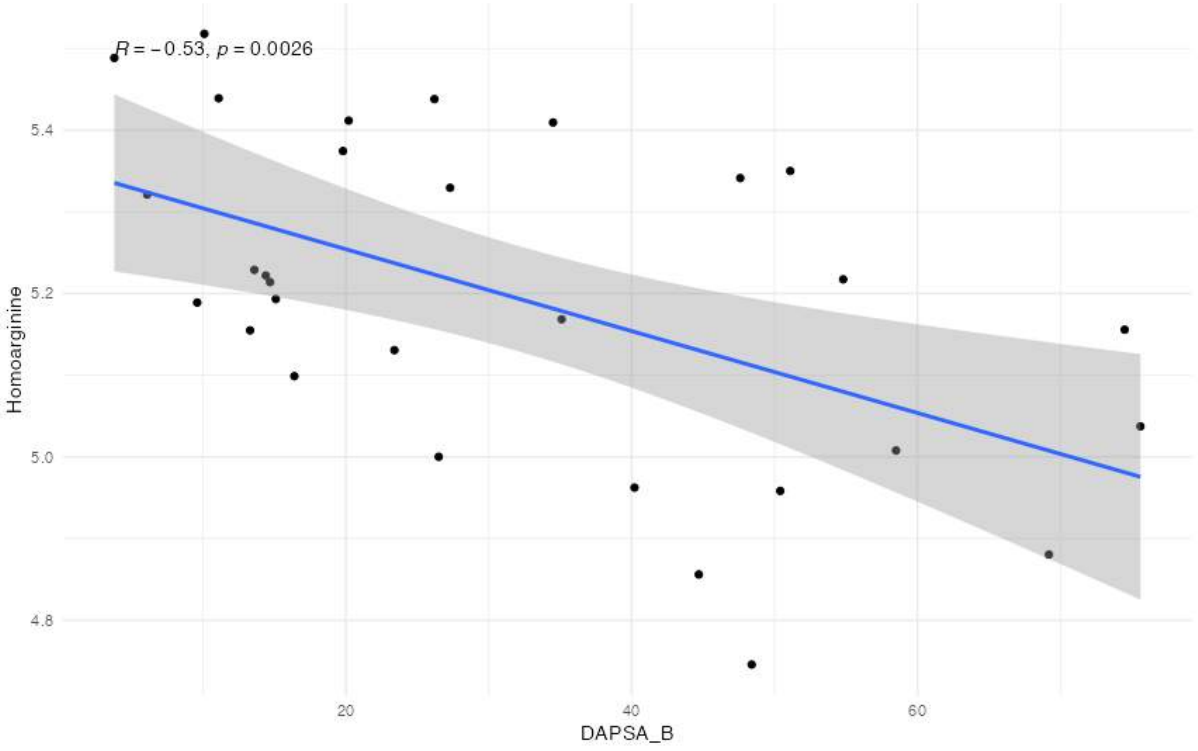

Supplementary Figure 6. Correlation of homoarginine with MTX response in a subgroup of MTX-treated patients. Spearman correlation coefficients were calculated alongside the p-value.

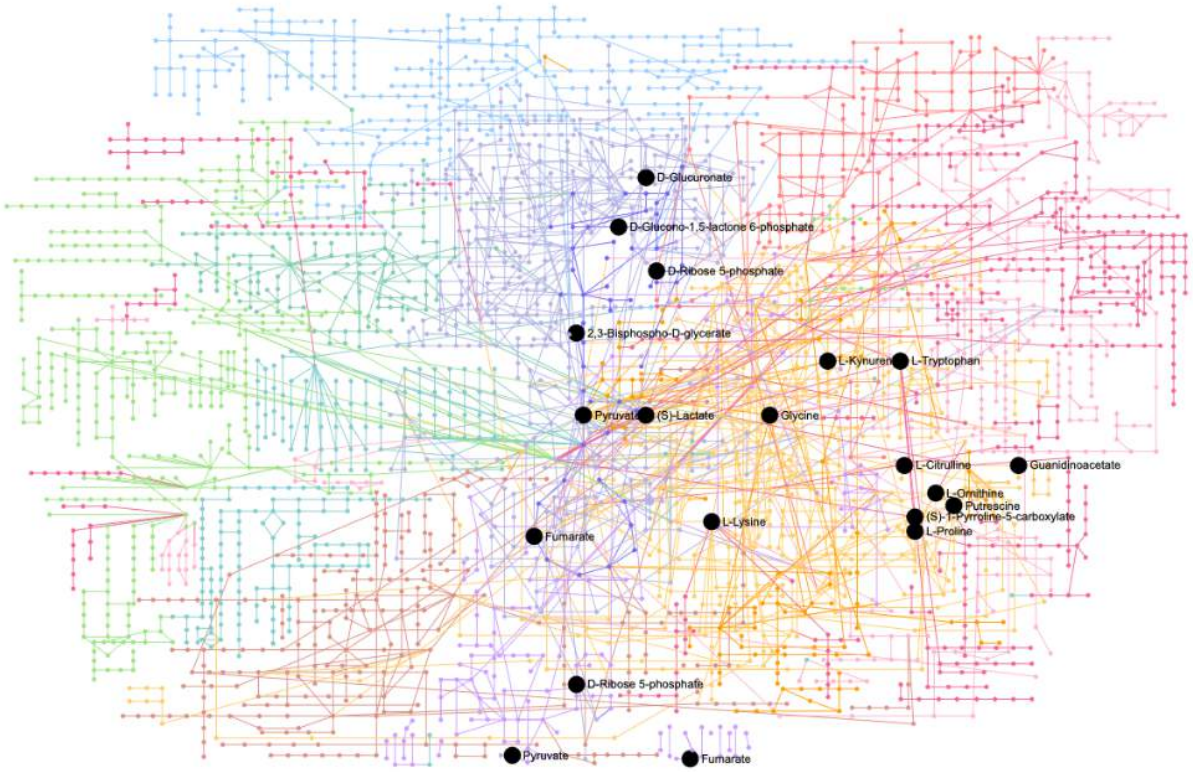

Supplementary Figure 7. Entire metabolomic network with metabolites of interest from these analyses plotted in black.

Representative Script

```
# ---------------------------------
# ---------------------------------
# The following was intended to give an overview of the steps included in the processing and analysis of the
# data across the project.

## Note the data wrangling/transformation that takes place between the following steps
## Not all wrangling steps were included to maintain clarity of the key processing and analysis steps
# ---------------------------------
# ---------------------------------

## Processing data ##
# Removing features with high proportion (80%) of samples with NAs #
number_samples <- length(omic_df$Samples)
omic_df <- as.data.frame(t(omic_df[-1]))
omic_df$Prop_Zero <- (rowSums(is.na(omic_df))/number_samples)*100

omic_df <- omic_df %>%
  filter(omic_df$Prop_Zero < 20)

## Imputing for missing values (missing not at random) using half minimum imputaion ##
# imputation function: Take the missing values for each feature
# where these are expected to be missing due to levels below quantification #
replacezero <- function(x) "[<-"(x, !x|is.na(x),
                                 min(x[x>0],
                                     na.rm=TRUE)/runif(1,min=2))

omic_df <- as.data.frame(apply(omic_df, 1, replacezero)) # apply the function to the omic dataframe

## Remove batch effects ##
batch <- samples_df$Batch
omic_df <- removeBatchEffect(omic_df, batch=batch, covariates=NULL)

## Normalise using cyclic loess function where high variation observed across features in dataset
## Metabolomic data ##
omic_df <- normalizeCyclicLoess(omic_df)

### Transcriptomic data ###
## Normalisation of transcriptomic data ##
BSData = readBeadSummaryData(dataFile = dataFile,
                             qcFile = qcFile, controlID = "ProbeID",
                             skip = 0, qc.skip = 0, qc.columns = list(exprs = "AVG_Signal",
                                                                      Detection = "Detection Pval"))
BSData.quantile = normaliseIllumina(BSData,
                                    method = "quantile",
```

```
                              transform = "log2")
omic_df = data.frame(exprs(BSData.quantile),
                type = "Quantile",
                allpositive = allpositive)

## Aggregate probes using limma's avereps function
omic_df <-avereps(omic_df, ID=omic_df$Probe_ID)

### Exploratory Data Analysis ###
## Principal Component Analysis ##
pca_omic <- omic_df # ensure numeric only
scaled_intensities <- scale(pca_omic)
scaled_intensities[do.call(cbind, lapply(scaled_intensities, is.nan))] <- 0
scaled_intensities<- as.data.frame(scaled_intensities)
pca_data <- prcomp(scaled_intensities)
pca_coord <- data.frame(pca_data$x)
var_explained <- pca_data$sdev^2/sum(pca_data$sdev^2)
var_explained[1:5] # observe amount of variance for first 5 PCs

# generate scree plot
scree <- fviz_eig(pca_data)

# generate PCA plot
ggplot() +
  geom_point(size=2, alpha=0.7,
             aes(x=PC1,y=PC2, colour= Response, fill= Response))+
  labs(x=paste0("PC1: ",round(var_explained[1]*100,1),"%"),
       y=paste0("PC2: ",round(var_explained[2]*100,1),"%"),
       colour='Response',
       fill= 'Response')+
  geom_hline(yintercept = 0,
             colour='navy',
             linetype='dashed')+
  geom_vline(xintercept = 0,
             colour='navy',
             linetype='dashed')+
  theme_minimal()+
  theme(legend.key.size = unit(01, 'cm'),
        legend.key.height = unit(1, 'cm'),
        legend.key.width = unit(1, 'cm'),
        legend.title = element_text(size=16),
        legend.text = element_text(size=12))

## Differential Analysis ##
# visualise the number of samples in each condition of interest
omic_df%>%
  ggplot(aes(x=Condition, fill=Condition)) +
  geom_bar()

# differential analysis function using the limma package
```

```
limma_fun <- function(matrix_AB, no., var1, var2){
  Group <- factor(colnames(matrix_AB), levels = c(`var1`, `var2`))
  design <- model.matrix (~Group)
  colnames(design) <- c('var1', 'var1vsvar2')
  eset <- matrix_AB
  fit <- lmFit(eset, design)
  fit <- eBayes(fit)
  toptable <- topTable(fit, coef = 'var1vsvar2', adjust = 'BH', number = no.)
  toptable <- as.data.frame(toptable)
  toptable$Feature <- rownames(toptable)
  toptable <- toptable[,c(ncol(toptable),1:(ncol(toptable)-1))]
  toptable$Sig <- ifelse(toptable$adj.P.Val <0.05, '< 0.05', '> 0.05')
  toptable$Sig_Names <- ifelse(toptable$Sig =='< 0.05' ,toptable$Feature, '')
  return(toptable)
}

# p-value histogram
qvals <- function(limma_table){
  pi0 <- 2*mean(limma_table$P.Value > 0.05)
  lfdrvals <- lfdr(limma_table$P.Value, pi0)
  qobj <- qvalue(limma_table$P.Value)
  hist(qobj)
}

number_of_features <- length(prelimma_omic[1])

limma_omic_DA <- limma_fun(prelimma_omic, number_of_features, 'Condition_1',
'Condition_2')

# volcano plot
limma_omic_DA%>%
  ggplot(aes(x=logFC, y=-log10(P.Value))) +
  geom_point (size=3,alpha=0.7,
              aes(colour=Sig,
                  group=Sig)) +
  theme_minimal() +
  labs (x='LogFC',
        y='-Log p-value',
        colour='Unadjusted \np-value')+
  geom_text_repel(aes(x = logFC, y = -log10(P.Value), label = Sig_Names_2),
                  box.padding =1,
                  size=5,
                  max.overlaps = Inf,
                  position = position_jitter(seed = 1),
                  arrow = arrow(length = unit(0.0035, "npc"))) +
  geom_vline(xintercept = c(-0.2,0.2), linetype='dashed')+
  geom_hline(yintercept = -log10(0.05), linetype='dashed')+
  geom_text(aes(x=-1.5, y= -log10(0.05)),
            label='unadjusted p-value = 0.05',
            vjust=2.1, colour='dark grey')+
```

```
  theme(plot.title = element_text(size = rel(1.5), hjust = 0.5),
        axis.title = element_text(size = rel(1.25)))+
  scale_color_brewer(palette = "Set1",direction=-1)

## Correlation analysis ##
ints_nested <- omics_df %>%
  group_by(Feature) %>%
  nest()

ints_unnested <- omics_df %>%
  unnest(cols=c())
identical(omics_df, ints_unnested)
ints_lm <- ints_nested %>%
  mutate(model = purrr::map(data, ~lm(formula = Feature_Level~Disease_Activity, data
= .x)))
model_coef_nested <- ints_lm %>%
  mutate(coef=map(model, ~tidy(.x)))
model_coef <- model_coef_nested %>%
  unnest(coef)
model_perf_nested <- ints_lm %>%
  mutate(fit=map(model, ~glance(.x)))
model_perf <- model_perf_nested%>%
  unnest(fit)
best_fit <- model_perf %>%
  top_n(n=4, wt=r.squared)
bestest_fit <- with(model_perf,model_perf[order(-r.squared),])
best_augmented <- bestest_fit %>%
  mutate(augmented = map(model, ~augment(.x))) %>%
  unnest(augmented)
best_augmented$adj_p <- p.adjust(best_augmented$p.value, method='BH')

# Plot the features that correlated with disease activity measure with adjusted p-value < 0.05
# if no features shown then use unadjusted p-value < 0.05 with caveat of non significance.
best_augmented %>%
  filter(adj_p < 0.05) %>%
  ggplot(aes(x = Disease_Activity, y=Feature_Level)) +
  geom_point(size=1, alpha=0.7) +
  stat_cor(vjust=1, hjust=0,
           size=5)+
  geom_smooth(method='lm',
              colour='red')+
  facet_wrap(~Feature, scales = "free_y")+
  theme(
    strip.text.x= element_text(#face = "bold",
      size=16),
    title=element_text(size=16),
    axis.title = element_text(size=14,face='bold'),
    axis.text = element_text(size=12))
```

```
## Supervised machine learning ##
# Generating an omic profile associated with the classification of samples across conditions
of interest

# For holdout cross validation, split omic_df into training and testing subsets
# example below uses 70:30 train:test split #
set.seed(42)
index <- createDataPartition(omic_df$Condition, p = 0.7, list = FALSE)
train_data <- omic_df[index, ]
test_data  <- omic_df[-index, ]

# Feature selection using recursive feature elimination #
# stringent function
ft_sel <- function(train_df){
  for (i in 1:10){ # run the RFE process 10 times
    profile_function <- function(Profile_number){
      options(warn=-1)
      subsets <- c(1:10)
      set.seed(42)
      # 10-fold cross validation repeated 10 times for each run
      ctrl <- rfeControl(functions = rfFuncs,
                         method = "repeatedcv",
                         number = 10,
                         repeats=10,
                         verbose = FALSE)

      profile <- rfe(x=train_df[,-1], y=train_df$Condition,
                     sizes = subsets,
                     rfeControl = ctrl)

      profile <- profile$variables
      profile <- profile %>%
        arrange(-Overall) %>%
        distinct(var, .keep_all=TRUE) %>%
        filter(Overall > 1) # filter features with relative importance > 1

      profile_df <- profile %>%
        group_by(var) %>%
        nest() %>%
        mutate(Profile=1)
    }
    profile <- profile_function(i)
    assign(paste0("profile_test", i), profile)
  }
  df <- do.call(rbind, mget(ls(pattern = "profile_test")))

  df_2 <- df %>%
    group_by(var) %>%
```

```
   filter(n() >= 5) %>% # from each of the runs, select features that are included in at least
half of the runs
   unnest()
  df_2 <- df_2 %>%
   aggregate(.~var, mean, na.rm=TRUE) %>%
   mutate(Round_overall=round(Overall,1)) %>%
   arrange(-Overall)
}

ft_sel_results <- ft_sel(train_data)

ft_sel_results %>%
  ggplot(aes(x=Overall, y=reorder(var, Overall)))+
  geom_col(aes(fill=Overall))+
  geom_text(aes(label = round(Overall, 2)),
            vjust=0.8,
            hjust=1.2,
            color="white",
            size=6) +
  #scale_color_colorblind()+
  scale_fill_continuous(low='light green', high='navy')+
  theme_minimal()+
  theme(legend.position = 'none',
        axis.title.y = element_text(size = 20),
        axis.title.x = element_text(size = 20),
        axis.text.y = element_text(size = 20),
        title=element_text(size=22)
  )+
  labs(x='Relative Importance',
       y='Feature')

# Keep only selected features
train_data_2 <- train_data %>%
  dplyr::select(Condition, ft_sel_results$var) %>%
  as.data.frame()

# Algorithm Selection
# Function for algorithm tuning and selection
multi_mods_test <- function(){
  control <- trainControl(method="repeatedcv",
                          number=10,
                          repeats=10,
                          summaryFunction=twoClassSummary,
                          savePredictions = TRUE,
                          classProbs = TRUE,
                          verboseIter = TRUE,
                          search = 'random')
  # train the SVM model
  set.seed(42)
  modelSvm <- caret::train(Condition~., data=train_data_2,
```

```
                    method='svmRadial',
                    metric='ROC',
                    tuneLength=10,
                    trControl= control)

# train the LogM model
set.seed(42)
modelglm <- caret::train(Condition~., data=train_data_2,
                    method='glm',
                    metric='ROC',
                    tuneLength=10,
                    trControl= control)
# train the LogM model
set.seed(42)
modelglm_boost <- caret::train(Condition~., data=train_data_2,
                         method='glmboost',
                         metric='ROC',
                         tuneLength=10,
                         trControl= control)
# train the RF model
set.seed(42)
model_rf <- caret::train(Condition~., data=train_data_2,
                    method='ranger',
                    metric='ROC',
                    tuneLength=10,
                    trControl= control)
# train the XGBoost model
set.seed(42)
model_xgb <- caret::train(Condition~., data=train_data_2,
                     method='xgbTree',
                     metric='ROC',
                     tuneLength=10,
                     trControl= control)
# train the KNN model
set.seed(42)
model_knn <- caret::train(Condition~., data=train_data_2,
                     method='kknn',
                     metric='ROC',
                     tuneLength=10,
                     trControl= control)
# train the naive Bayes model
set.seed(42)
model_naivebayes <- caret::train(Condition~., data=train_data_2,
                         method='naive_bayes',
                         metric='ROC',
                         tuneLength=10,
                         trControl= control)


# collect resamples
```

```
  results <- resamples(list(SVM = modelSvm, RF= model_rf, LRM=modelglm,GLMB =
modelglm_boost,
                           XGBoost =model_xgb, KNN=model_knn,
                           Naive.Bayes= model_naivebayes)) #LRM= modelLRM))


  # summarize the distributions
  summary(results)
  # boxplots of results
  plott <- bwplot(results)
  comp_roc <- evalm(list(modelSvm,
                         model_rf,
                         modelglm,
                         modelglm_boost,
                         model_xgb,
                         model_knn,
                         model_naivebayes),
                    gnames=c('KNN', 'NB', 'RF','LRM','GLMB', 'SVM', 'XGB'))

  ml_eval_output <- as.data.frame(comp_roc$stdres)
  ml_eval_output$Measure <- rownames(ml_eval_output)
  ml_eval_output <- back_2_front(ml_eval_output)
  ml_eval_output <- flextable_only(ml_eval_output)
  listt <- list(comp_roc, ml_eval_output)
  return(listt)
}

# Compare algorithms
alg_sel <- multi_mods_test()
met_table <- alg_sel[[2]]
met_roc <- alg_sel[[1]]$roc
met_prg <- alg_sel[[1]]$prg


# Select final model and increase number of repeats in cross validation to 100
# Model generation
set.seed(42)
fit_control <- trainControl(method="repeatedcv",
                            number=10,
                            repeats=100,
                            summaryFunction=twoClassSummary,
                            savePredictions = TRUE,
                            classProbs = TRUE,
                            verboseIter = TRUE,
                            search = 'random')

set.seed(42)
omic_model <- caret::train(Response~., data=train_data_2,
                           method='xgbTree',
                           metric='ROC',
```

```
                    tuneLength=15,
                    trControl= fit_control)

ggplot(omic_model) # check the trained model's initial performance

# Evaluate model's performance in the training subset using the ML_eval package
train_results <- evalm(omic_model)
train_roc <- train_results$roc
train_prg <- train_results$prg

# Evaluate final tuned model in testing subset
# testing subset
# function
model_performance <- function(model, test_df){
  predictions <- predict(model, test_df)
  confusionMatrix(predictions, test_df$Condition)
  con_matr <- confusionMatrix(predictions, test_df$Condition)
  con_stats <- con_matr$overall

  pr <- prediction(as.numeric(predictions), as.numeric(test_df$Condition))
  prf <- performance(pr, measure = "tpr", x.measure = "fpr")
  auc <- performance(pr, measure = "auc")
  auc_val <- auc@y.values[[1]]
  result.predicted.prob <- predict(model, test_df, type="prob") # Prediction
  result.roc <- roc(test_df$Good, result.predicted.prob$Good) # Apply the positive class e.g. a
'Good' response
  list_pred <- list(model, con_stats, result.roc, con_matr)
  return(list_pred)
}

test_performance <- model_performance(omic_model, test_data)
test_roc <- test_performance[[3]]
test_roc$auc

# Feature Interpretation using the DALEX and DALEXtra packages
model_explainer <- DALEX::explain(model = omic_model,
                      data = omic_df[, -1],
                      y = omic_df$Condition,
                      type='classification')

## attempt accumulated local effects plots to explain interaction of features in the plot
pdp_model <- model_profile(explainer = model_explainer,
                   type = "partial",
                   variables = names(omic_df)[2:ncol(omic_df)])
ld_model <- model_profile(explainer = model_explainer,
                   type       = "conditional",
                   variables = names(omic_df)[2:ncol(omic_df)])
ale_model <- model_profile(explainer = model_explainer,
                    type='accumulated',
                    variables = names(omic_df)[2:ncol(omic_df)])
```

```
shapleys_model <- predict_parts(explainer = model_explainer,
                        type='shap',
                        new_observation =  omic_df,
                        B=25) # the B=25 is the number of random orderings of the explanatory
variables

pdp_model$agr_profiles$`_label_` = "partial dependence"
ld_model$agr_profiles$`_label_` = "local dependence"
ale_model$agr_profiles$`_label_` = "accumulated local"

partials <- plot(pdp_model, ld_model, ale_model)

breakdown <- model_explainer %>%
  predict_parts(new_observation = omic_df) %>%
  plot()

SHAP <- plot(shapleys_rf)

# Explain the variance
# include only the selected features
omic_df_cut <- omic_df %>%
  dplyr::select(c(Sample, ft_sel_results$var))

# Select patient factors of interest
patient_factors <- patient_metadata%>%
  dplyr::select(Sample,Age, Sex, aCCP.Status, RhF.Status, Smoking.Status )

form <- ~ Age + (1|Sex) + (1|aCCP.Status) + (1|RhF.Status) + (1|Smoking.Status)

varPart <- fitExtractVarPartModel(omic_df_cut, form, patient_factors)

vp <- sortCols(varPart)
explain_each <- plotPercentBars( vp[] ) +
  theme(text=element_text(size=16))
var_plot <- plotVarPart( vp )+
  theme(text=element_text(size=16))


# Model comparison
# generate the above objects for each model of interest
test_roc_model_1$auc
test_roc_model_2$auc
test_roc_model_3$auc

roc_comp <- rbind.data.frame(test_roc_model_1,
                        test_roc_model_2,
                        test_roc_model_3)

# Plot the ROC curves for each model as a single figure
```

```
roc_comparison <- roc_comp%>%
  ggplot(aes(x = One_Minus_Spec, y = Sensitivity, group_by=Model)) +
  geom_path(aes(colour=Model), size=1)+
  geom_abline(linetype='solid', colour='grey') +
  coord_equal()+
  theme_minimal()+
  labs(x='False positive rate',
       y='True positive',
       colour='')+
  theme(panel.grid.major = element_blank(),
        panel.grid.minor = element_blank(),
        panel.border = element_rect(colour = "black", fill=NA, size=1),
        legend.text = element_text(size=16),
        axis.title = element_text(size = 16),
        axis.text = element_text(size = 16))

# Statistical testing for difference between models' performance
#delong

roc_comparison_1 <- roc.test(test_roc_model_1, test_roc_model_2)
roc_comparison_2 <- roc.test(test_roc_model_1, test_roc_model_3)
roc_comparison_3 <- roc.test(test_roc_model_2, test_roc_model_3)


roc_table_1 <- (cbind.data.frame(roc_comparison_1$roc2$auc,
                                 roc_comparison_1$roc1$auc,
                                 round(roc_comparison_1$p.value,3)))
names(roc_table_1) <- c('AUC-ROC 1', 'AUC-ROC 2', 'p-value')
roc_table_2 <- (cbind.data.frame(roc_comparison_2$roc2$auc,
                                 roc_comparison_2$roc1$auc,
                                 round(roc_comparison_2$p.value,3)))
names(roc_table_2) <- c('AUC-ROC 1', 'AUC-ROC 2', 'p-value')
roc_table_3 <- (cbind.data.frame(roc_comparison_3$roc2$auc,
                                 roc_comparison_3$roc1$auc,
                                 round(roc_comparison_3$p.value,3)))
names(roc_table_3) <- c('AUC-ROC 1', 'AUC-ROC 2', 'p-value')
roc_table_complete <- rbind.data.frame(roc_table_1, roc_table_2, roc_table_3)
rownames(roc_table_complete) <-  c('Model 1 vs Model 2',
                                   'Model 1 vs Model 3',
                                   'Model 2 vs Model 3')

plottt <- roc_table_complete %>%
  kable() %>%
  kable_styling(bootstrap_options=c("striped", "hover", "responsive"))
ggplot() +
  theme_void()+
  annotate(geom='table',
           x=1, y=1,
           label=list(roc_table_complete))
```